Reliability of Marine Structures Program

PROBABILISTIC SEISMIC DEMAND ANALYSIS OF NONLINEAR STRUCTURES

Nilesh Shome
C. Allin Cornell

March 1999
Report No. RMS-35

(Supported in Part by
NSF Grant No. CMS-94-23596)

Department of CIVIL ENGINEERING
STANFORD UNIVERSITY

Probabilistic Seismic Demand Analysis of Nonlinear Structures

Nilesh Shome
C. Allin Cornell

March 1999

Report No. RMS-35

Supported in Part by
NSF Grant No. CMS-94-23596

Reliability of Marine Structures Program

Department of Civil Engineering
Stanford University

Abstract

The objective of this study is to establish efficient, but accurate procedures for evaluation of the nonlinear seismic behavior of multi-degree-of-freedom (MDOF) structures including the probabilistic analysis of this behavior. The proposed procedures address, first, the current seismic-structure assessments that require – for a given ground-motion intensity – an estimation of in-structure demands such as global or local displacements, hysteretic energy, or damage indices. More generally, we develop procedures to estimate the annual probability of exceedance of any specified nonlinear response (demand) level due to future ground motions at a specific site. This is referred as Probabilistic Seismic Demand Analysis (PSDA). The latter procedure prepares the way for the next stage development of seismic assessment that considers the uncertainties in nonlinear response and capacity. The proposed PSDA procedures require the coupling of (1) structure-specific nonlinear analyses for a relatively small set of recorded accelerograms and (2) (either site-specific or USGS-map-like) probabilistic seismic hazard analyses (PSHA).

We have directly addressed some of the important, but not well studied, nor even well posed issues of nonlinear seismic demand analysis, which include selection of records for structural analysis, the number of records to be used, scaling of records, etc. Initially these issues are studied through nonlinear analysis of structures for a number of magnitude-distance bins containing numerous records. Subsequently we introduce regression analysis of response results against spectral acceleration, magnitude, duration, etc., which helps to study and resolve these issues more systematically. First-mode spectral acceleration proves to be an effective intensity measure for moderate period structures.

We illustrate the demand-hazard procedures and calculations through two major example problems: a moderate period 5-story and a long period 20-story special moment-resisting frame (SMRF) building. We determine that one can calculate demand hazard from an simple explicit equation if the likelihood of collapse of structures is low at the damage level of interest. Otherwise we have to either carry out a simple numerical integration, or use a complicated, but explicit equation for demand-hazard calculations. We have introduced a three-parameter distribution model for demand-hazard calculations when the likelihood of collapse of structures is high at the intensity level of our interest. In addition to the conventional regression results, we require results from binary-regression analysis to evaluate the parameters of the distribution model. Several simple, but quite accurate closed-form solutions have also been proposed to expedite the demand-hazard calculations when the likelihood of collapse of structures is high.

We also find that vector-valued (e.g., 2-D) PSDA estimates demand hazard more accurately. This procedure requires information about 2-D seismic hazard. The 2-D hazard can either be obtained from disaggregation of 1-D PSHA results, or directly from 2-D PSHA (Bazzurro, 1998). The direct 2-D PSHA calculation is a relatively new tool and so, unlike conventional 1-D PSHA, the results are not yet readily available. The comparison of results between 2-D and 1-D PSDA indicates that the difference in results may be significant even for the low-rise 5-story building.

We extend the response to the common question – "How many records must I use?" – to address it in the broader context of achieving adequate accuracy of the estimate of the seismic demand and demand-hazard. By considering different sources of uncertainties in these estimates we recommend a number of nonlinear analyses so that the change in the total uncertainty due to limited number of analyses is within an acceptable limit.

Contents

Chapter 1

Introduction

1.1 Background

The general philosophy of earthquake-resistant building design codes has been to safeguard against the collapse of structures and loss of lives (see, for example, SEAOC, 1996). As a result, we have seen little loss of life in properly engineered buildings in the past earthquakes and professionals in the area of earthquake safety were quite happy. In recent earthquakes (e.g., Loma Prieta, 1989, and Northridge, 1994), however, we have observed significant damage to buildings and their contents (although very few lost lives) leading to the loss of billions of dollars in each earthquake. This demanded from the professionals better-designed structures to minimize the damage within the constraints of resources available and the intended function of the structures. In order to fulfill this demand several new, improved guidelines have in recent years been proposed for general building structures from different organizations, notably Federal Emergency Management Agency (FEMA-273, 1996) and Structural Engineers Association of California (Vision-2000, 1996). In all these new guidelines we observe a paradigm shift in earthquake-resistant design philosophy: the introduction of performance-based design. In recent earthquakes, building owners have found that the cost of loss of functionality of their buildings is very high compared to the additional cost that required to construct buildings that have a higher performance level.

They have demanded better performance of structures, and the new guidelines have proposed a framework for performance-based seismic design. In this new design philosophy we need to calculate the seismic demand accurately and compare the demand result with the allowable demand at the desired performance level (see, for example, FEMA-273, 1996).

In the current guidelines we observe that we need to calculate the demand for a given spectrum, e.g., the uniform hazard spectrum (UHS). If we assume that the elastic demand calculation of structures is adequate then the characterization of input ground motion by spectra is sufficient. But structures are always designed to go beyond their elastic capacity under severe ground motion because elastic design for severe, but rare earthquake is unrealistic. Following elastic-design philosophy, one designs a structure elastically for a reduced elastic force. This elastic force would develop in a structure under the design-earthquake load if the structure behaved elastically. While designing a structure, one reduces this force by a factor, called response modification factor ($\mathcal{R}$). This reduction is based on the premise that well-designed and -detailed structures can sustain large deformations without collapse (ductile behavior). The failure of a number of structures in recent earthquakes, however, indicates that this assumption is questionable; to do better one needs to perform nonlinear analysis of structures.

That is why we see in the new guidelines for the first time consideration of nonlinear analysis which predicts accurately the behavior of structures under severe seismic loads. These guidelines have incorporated the nonlinear-static analysis (more popularly known as "pushover" analysis) as a tool for seismic-demand prediction. This method of analysis is relatively simple and computationally efficient. Nonlinear static analysis is definitely a step toward better understanding the behavior of structures under high lateral loads. Krawinkler and Seneviratna (1997) have observed that nonlinear-static analysis or "static-pushover" analysis can predict with reasonable accuracy the maximum global response (roof displacement) of multi-degree-of-freedom (MDOF) structures if their elastic response is dominated by a single mode. The calculation of more local demands from global demand is, however, unreliable. Only nonlinear time-history analysis can reliably predict the local demand as well as the global demand of structures. This method of analysis on the other hand is more

complex and requires significantly more computer time for analysis of a structure. With the improvements of computing power and analysis software, we can overcome these limitations in near future.

In nonlinear time-history analysis we need a suite of ground-motion records. These may be spectrum-compatible records (see Carballo and Cornell, 1998) or recorded ground-motions for a "scenario" earthquake[1]. The methods of selecting records are, however, open to question. The use of spectrum-compatible records will need a systematic study before we can accept its legitimacy for nonlinear structural analysis. Also matching the records to the full design spectrum may not be justified, as the design spectrum in general (e.g., the UHS) does not represent a particular magnitude and distance event. The design spectrum is a product of events of different magnitudes and distances that might occur at a site. Because the seismic risk of a structure is a combination of threats from earthquakes of different magnitudes and distances, consideration of a particular magnitude and distance in response calculation may not be appropriate (unless nonlinear responses are independent of the magnitude and distance of earthquakes, but this needs to be verified).

Because of the limitations of the above procedures, we find that the procedures outlined in recent guidelines to select a suite of records require the recorded ground motions to match a part of the design spectrum. It is suggested that we select a suite of ground-motion records (3 to 7 as per SEAOC Blue book, 1996 or FEMA-273) such that "on an average" the spectra of the records are equal to or greater than the design spectrum across the "range of frequencies of interest." But we are not sure how many ground-motion records are sufficient for nonlinear dynamic analysis of a particular structure. This number might vary from structure to structure. We need some explicit basis to calculate the required number of records. The "range of interesting frequencies" is also not defined. The sensitivity of structural response to frequency range needs to be studied. The guidelines also do not define the method to be adopted for matching the ground-motion spectrum to the target design

[1]This can be determined, for example, from the deterministic maximum considered earthquake (MCE) as in FEMA-273 or from a probabilistic average magnitude ($\bar{M}$) and distance ($\bar{R}$) of earthquake (e.g., Bazzurro and Cornell, 1999).

spectrum. So we find in the recent SAC-II steel project that a very reasonable mean square error minimization technique was adopted for this purpose (Somerville, et al., 1998). This technique is found at the end to be quite "inefficient" however.[2] We are also not sure how to select the records. The guidelines say that "the time histories should match the source and site characteristics and should be rich in energy across the range of frequencies of interest" (see SEAOC, 1996). As the threats to a structure at a site will usually be from many different magnitude and distance earthquakes, it is not clear whether we should consider only the most important event (e.g., the "characteristic" event) to select a small number of records. On the other hand, if we want to adopt a simulation-based approach so that we can incorporate all the threats to a structure (e.g., Wen, 1995), then we need a large number of ground-motion records that have precisely the same magnitude and distance needed for simulation and also we need records for many different magnitudes and distances. In that case we need to have a large data base of real and synthetic ground-motion records (e.g., a "juke box" as envisaged by Spudich, 1997). The guidelines are also silent about the relative importance of the parameters in nonlinear structural analysis, e.g., magnitude, distance, fault type, duration, or frequency content. This information would have helped us to select records based on the more important parameters in selecting records. We will investigate all these issues in the following chapters.

Another important issue that the guidelines ignore most of the time is how to deal with the dispersion of damage measures. We often find that two ground-motion records of virtually identical response spectra give different nonlinear responses of a structure. Recognizing this variability SEAOC Blue book (1996) suggests that "if we use three time histories we should consider the maximum damage; if seven or more are used, we should consider the

[2]It has been observed by Gupta and Krawinkler (1998) for a ductile model of steel frame structures and by Cornell and Luco (1998) for a fracture model of the same structures that the variability of response is high even after the records are scaled by the method adopted in the SAC Steel project. They observed in general three types of response results from these scaled records–mild (much lower than the mean), moderate (close to the mean), and "rogue" (much higher than the mean)–instead of mainly moderate response and low variability. We will find that because of this high variability we will get an inaccurate estimate of structural response with only the three to seven records envisaged by the FEMA and SEAOC guidelines, implying that the scaling procedure is inefficient.

average damage." The main objection to this recommendation is that it is conservative because we do not have sufficient knowledge about the variability of nonlinear response. Also, although this SEAOC ad-hoc recommendation seems conservative, in reality we might get an under-designed structure from the limited samples of data. We will investigate how efficiently we can calculate the statistics of nonlinear responses with sufficient accuracy. We will also investigate how to incorporate the variability in seismic-demand calculations, a randomness ignored by the guidelines. For certain more important structures designers also need to calculate not the median or mean but the 84% response or damage measure. Unless an "appropriate" procedure is followed, this may lead to overestimating the damage measure by "double counting" the uncertainty[3]. We will investigate the "appropriate" procedure for the 84%-demand calculation.

The guidelines suggest that we calculate the seismic demand for a given spectrum or a scenario event and then compare the demand result with the allowable limit given in different codes and guidelines. This procedure often considers the uncertainty in ground-motion spectral acceleration rigorously (e.g., using PSHA in the calculation of a uniform hazard spectrum) but ignores the uncertainty in demand estimation (or considers it inappropriately). We would like to combine (correctly) both the ground-motion and response uncertainties in demand estimation. One possible outcome of this approach would be the calculation of the probability that any damage measure exceeds an allowable limit. Note that this approach is different from the code approach, in which we calculate the nonlinear response for a target return-period intensity (spectral acceleration) of ground-motion. We cannot calculate the probability of exceedance or return period of a given damage level simply from the response results for ground-motion records at a fixed intensity level. Large response deviations at lower levels may also cause the exceeding of a given damage level. The probability of exceedance of any damage measure depends on quantities such as the slope of the hazard curve and the variability of that damage measure.

[3]One considers in general the uncertainties in ground-motion loading while recommending the target response spectrum, e.g., the uniform hazard spectrum. But for calculating the nonlinear response we may again introduce variability in input motion by scaling the ground motions inappropriately; thus we may "double count" the uncertainty.

Our primary objective is to calculate the seismic demand of nonlinear structures in a way that will consider the uncertainties both of the ground motion and of the nonlinear response. In general the seismic demand can be estimated very precisely by the Monte-Carlo simulation technique. The probability of exceeding a damage level, y, of any damage measure, Y, for any given fault i, that is $P[Y \geq y|event]_i$, can be calculated from the nonlinear dynamic results from several ground-motion records generated by that fault. The ground motion can be simulated from the joint magnitude-distance (M-R) density function of that fault. Finally the probability of exceeding a damage level y is computed by summing up the contributions from all the faults:

$$P[Y \geq y] = \sum_i \nu_i P[Y \geq y|event]_i \tag{1.1}$$

where ν_i is the mean annual rate of activity of events generated by fault i. The main drawback of this approach is that we may need to carry out literally thousands of nonlinear time-history analyses for the seismic-demand calculation. Also it will be impossible to get a sufficient number of recorded ground motions that will satisfy all the M, R characteristics of all the faults at a site. Hence we have to use simulated, synthetic ground motion in this approach. Although this approach may in the end yield very accurate probabilistic results, at least given the underlying models, we cannot apply it to individual structural problems in practice.

An improvement on the above approach is the generation of structure-specific attenuation results (similar to the approach described by Bazzurro, 1998, to study the amplification of ground motions at a soil site). In this case a structure is analyzed for a large number of as-recorded ground-motions of different magnitude and distance characteristics. The results of nonlinear analysis give us the variation of damage measures with magnitude and distance (similar to ground-motion attenuation results where we get the variation of spectral acceleration with magnitude and distance, e.g., Joyner and Boore, 1981, and Abramhamson and Silva, 1997). The probability of exceeding a damage level y can be calculated as follows

(the calculation is similar to that of the probabilistic seismic hazard analysis):

$$P[Y \geq y] = \sum_i \nu_i \int\int P[Y \geq y|m,r] f_{M,R}(m,r) dm dr \tag{1.2}$$

The drawback of this approach is that it too needs a hundred or more nonlinear-structural-analysis results for calculation of seismic demand. But the approach is more efficient than the preceding Monte-Carlo simulation. The structure-specific attenuation results can be obtained from regression analysis of relatively fewer results and from as-recorded ground motions.

In order to apply the simulation procedure more efficiently Wen and co-workers (Collins et al., 1996; Han and Wen, 1997) introduced an "equivalent" nonlinear system (ENS) model of the complete nonlinear MDOF structure. This simplification permits one to carry out thousands of nonlinear analyses more economically. The response of MDOF structures can be obtained from the response of ENS as follows:

$$Y_{MDOF} = C.Y_{ENS} \tag{1.3}$$

where, Y, C, and Y_{ENS} are all random variables. The correction factor, C, can be obtained from regression analysis of nonlinear-dynamic-analysis results of a MDOF structure and its ENS for a suite of ground-motion records (e.g., 88 records were used by Han and Wen, 1997). Hence the seismic demand of an MDOF structure can be estimated from the seismic demand of its ENS. The responses of ENS at a particular site are obtained from synthetic records that are based on the seismotectonic features of the site (e.g., magnitude and distance distribution, mean and variance of spectral accelerations from appropriate attenuation results, the recurrence models, etc.). (See Eliopoulas and Wen (1991) for details on the generation of synthetic records adopted in this approach.) Finally the probability of exceedance of a given level of damage y can be obtained from Equation 1.1 as follows:

$$P[Y \geq y] = \sum_i \nu_i \cdot P[C \cdot Y_{ENS} \geq y|event]_i \tag{1.4}$$

This approach is geared not towards practical individual structural applications, but towards calibration of design parameters in fully reliability-based seismic codes. Ellingwood et al. (1980) developed load and resistance factors for a target member-level limit state probability, whereas Wen and co-workers want to develop design parameters that will also satisfy the system-level limit state probability. The approach has several limitations in application to a structure-specific demand calculation. First a large number of nonlinear analyses of a MDOF structure must be carried out for the calculation of the correction factor, C. Second the simulations of ENS can be time consuming as well. Finally, the use of synthetic ground-motion in nonlinear structural analyses is not well accepted by the structural engineering community.

Cornell and co-workers simplified the seismic demand calculations further. Their approach couples the probabilistic seismic hazard analysis (PSHA) with the nonlinear dynamic analysis of MDOF structures. The advantage of this approach is that we can combine *independently* the developments in seismology and structural engineering. We also do not need to carry out the multitude of simulations required by the other approaches because the site-specific variability of the seismological parameters, namely spectral acceleration, magnitude, and distance (S_a, M, and R), are considered in the (conventional PSHA) spectral-acceleration hazard calculations. The remaining variability of structural responses *conditioned* on those seismological parameters is calculated by nonlinear dynamic analysis of MDOF structures from a comparatively small number of ground-motion records. Finally, the results from hazard calculations and from the nonlinear structural analysis are combined to get the seismic demand.

Previously Cornell and co-workers (Sewell and Cornell, 1987; Inoue and Cornell, 1991; Bazzurro and Cornell, 1994) calculated the variability of structural response using an "indirect" method. In this method the relative damage potential of a ground-motion record is summarized by a structure-specific "nonlinear response" factor ($F_{Y=y}$). This factor is defined as the amount by which a ground-motion record that causes incipient yield ($S_{a,ref}$) in a structure has to be scaled up to obtain a target damage level y in that structure. The approach assumes that F_Y is not dependent on M and R. So the seismic hazard results are

used directly in this approach. The probability of exceedance of a given level of damage y can be obtained as follows:

$$P(Y > y) = \sum_i P(s_{a,i} \geq F_{Y=y} . S_{a,ref}) \cdot P(S_a = s_{a,i}) \tag{1.5}$$

Lately it has been found that the variability of structural response can be calculated in a more transparent and "direct" way (see Shome et al., 1998). In this approach nonlinear structural responses are calculated directly from different ground-motion records. The variability of responses for different seismological parameters are calculated by regression analysis of structural responses against those seismological parameters. The coupling of these structural response results with the seismic hazard results are quite similar to the "indirect" approach. The seismic demand hazard is estimated as follows:

$$P(Y > y) = \sum_i P(Y > y | s_{a,i}) \cdot P(S_a = s_{a,i}) \tag{1.6}$$

This demand calculation is, however, based on several assumptions. We will discuss the validity of those assumptions in the following chapters. The advantage of this approach is its *efficiency and accuracy.* In addition we can get an *explicit* formulation for demand calculations for most of the problems. As we are coupling the seismic hazard results in the demand calculation, we need to carry out nonlinear structural analysis for only a limited number of records, approximately 5 to 10 for most of the problems[4] to calculate the conditional probability of exceedance of a given level of damage in Equation 1.6; hence this approach is efficient.

1.2 Focus of This Study

This dissertation develops a methodology to calculate the seismic demand efficiently

[4]Compare this number with 1234 used by Han and Wen (1997) in their simulation-based approach. Note that they used that many simulations only for the ENS which is very efficient computationally. They, however, used 88 records to get the mean correction factor ($\hat{C}$).

(from a relatively small number of records) and accurately. We will consider nonlinear-time-history analysis of MDOF structures for demand calculations. In time-history analysis the problems an analyst has to resolve are the number of records to be used, the records to be selected from a catalogue, how to scale the records (if at all), etc. These issues have been addressed only vaguely in recent guidelines. We will discuss them in detail. In the course of the process, we will also investigate different parameters that might influence the nonlinear responses: large versus small magnitude earthquake, close versus distant faults, duration of records, spectral shape, etc. This will help to determine which parameters we need to consider in response calculations. It will also clarify the "revered" duration effect on nonlinear response. As duration, spectral shape, and magnitude are quite well correlated, we also need to understand which is the most important with respect to observed differences in response. We will also quantify the effect of all these parameters on structural response.

In order to make the seismic demand calculation efficient, we will investigate different ways to reduce the dispersion of nonlinear response, which in the end reduces the number of ground-motion records required for a target level of accuracy of response calculations. We will investigate several approaches to reducing the dispersion and we will find the most efficient one for a particular structural type. Sometimes the engineer may also need to calculate a fractile such as the 84% demand. This calculation requires the information about the dispersion of the damage measure given an event that we cannot get directly if before analysis we scale the ground-motions records to a target intensity level. We will recover the dispersion of damage measures in two ways: from an approximate, easy approach and from a more accurate approach that needs more involved calculations.

In order to help generalize our conclusions, we will verify those observations through a large number of single-degree-of-freedom (SDOF) and multi-degree-of-freedom (MDOF) example problems with significantly different characteristics, such as frequencies, P-Δ effect, multi-mode effect, etc. This will also help us to understand the correlation between the response characteristics of SDOF and MDOF systems and to understand the limitations of

code procedures that are based mainly on the study of linear and nonlinear SDOF systems.[5]

We will show how we can combine efficiently the nonlinear-structural-analysis results and the seismic-hazard results. The demand calculation of those structures that do not collapse (or for which the likelihood of collapse is negligible) at the required intensity (which is the spectral acceleration required to induce the target damage measure) is particularly easy: it can be calculated from a simple, explicit equation. The same may not be true for those structures whose likelihood of collapse (strictly speaking non-convergence of the numerical analysis) is high at the required intensity. We will demonstrate how we can calculate the demand hazard in case of collapses of some of the nonlinear structural analyses. This calculation is particularly important when we want to calculate the performance of structures at the low-probability, high-intensity ground motion. We will also demonstrate the (conditional) demand calculations for responses that depend on the additional seismological parameters, e.g., magnitude and distance, on duration, and on spectral shape. If the nonlinear responses significantly depend on those parameters, we will demonstrate the importance of incorporating these parameters in demand-hazard estimation.

Finally we will calculate the uncertainty in the estimation of demand or demand hazard. We will consider in those estimations different sources of uncertainties which are modeling, estimation of median demand due to limited sample size, seismic hazard, and physical properties. We will determine the uncertainties in our results from each of those sources and recommend an appropriate required number of analyses so that the uncertainty of the estimation of demand or demand hazard is within the acceptable limit.

The conclusions we will be drawing at the end should be interpreted in the context of simplifications in the modeling of structures and the specific ground-motion characteristics that we will consider in this study. In the following we summarize some of the simplifications and assumptions of this study:

- We have considered only the accelerograms recorded in California at a stiff-soil site

[5]The only exception is FEMA-273 guideline which has incorporated in demand calculations additional MDOF correction factors from the study of Krawinkler and co-workers (see, e.g., Nassar, et al., 1991, Seneviratna and Krawinkler, 1994).

(site class D as per FEMA-273). In this study we have not selected any near-source-type records or subduction-zone records.

- We have considered only the 2-D center-line model for mathematical representation of the perimeter moment resisting frames. The effects of joint shear strength and deformation, additional strength and stiffness of floor girders due to floor slabs, additional stiffness from interior frames and from partition walls are neglected.
- We have neglected the effect of soil-structure interaction.
- We have selected only the 2-D steel SMRF's for this study. These structures are regular in plans and elevations. Hence we have neglected the effect of torsion, soft story, and other specific behaviors of irregular buildings.

Also the conclusions here will be based on a small number of case studies. So if we want to generalize the conclusions in this study we have to make further case studies for different types of structures, e.g., concrete structure, for different types of frames, e.g., braced frame, for improved modeling of structures, and for mass and stiffness irregularities of buildings.

1.3 Organization

The purpose of this study is to calculate the seismic demand and demand hazard *efficiently and accurately.* Before we plunge into the problems of demand prediction, we need to investigate some of the basic issues of nonlinear seismic analysis of structures. We address these issues in Chapter 2. The focus of this chapter will be on the following practical issues, which an analyst encounters while carrying out nonlinear structural analysis:

1. We will investigate how, in the face of large dispersion, one can make nonlinear seismic demand calculations efficient, i.e., how one can make confident demand predictions from a relatively small number of nonlinear analyses. This can be done by *scaling* the ground-motion records to a particular intensity level. We will address this issue of scaling with a simple stick-model representation of an MDOF structure. We will

look into different aspects of the scaling issue, e.g., the effect of scaling low-magnitude ($M \approx 5.5$) records to the intensity level of high-magnitude ($M \approx 7.0$) records and vice versa.

2. We will also investigate different *types of scaling* schemes, e.g., scaling to the spectral acceleration at the elastic, first-mode frequency of a structure, scaling to the average spectral acceleration over a range of frequencies, etc.

3. We will find out how to *select records* for nonlinear structural analysis from a data base of hundreds of records. We will show which are the parameters we should consider and which are the ones we can neglect while selecting ground-motion records. We will do this by looking into the magnitude, distance, and duration dependency of displacement- and energy-based damage measures.

4. We will investigate the effect of *frequency range* on the mean and variance of nonlinear structural response.

5. We will look into the problem of *the required number of records* in nonlinear structural analysis. Although recent guidelines recommend using 3 to 7 records (see, e.g., SEAOC, 1996), we will verify whether and when this number is sufficient.

6. It is sometimes necessary to calculate the 84^{th}*-percentile demand* at a target intensity level. We will demonstrate how one can calculate this quantity from a small number of scaled results. We will also show how this calculation can be improved if necessary.

7. We will look into the advantages and disadvantages of *direct versus alternative methods* of demand calculations.

The conclusions we will draw in Chapter 2 are based on one example problem only. We will verify the validity of those conclusions in Chapters 3 and 4 for different structural frequencies, for significant multi-frequency effects, for a predominant P-Δ effect, etc. To study the dependency of structural responses on different parameters we will in these chapters introduce regression analysis of response results against those parameters instead of

analyzing that structure for different bins of records. The other advantage of this approach is that we do not need to scale ground-motion records; the spectral accelerations of ground-motion records should be in the region of interest. The demand-hazard calculation, we will demonstrate, is an improved methodology to calculate the probability of exceedance of a damage measure (such as maximum interstory drift) from its limiting or target performance level. This approach is different from the current code procedures in which we calculate the demand for a uniform-hazard spectrum. In the proposed method we will also incorporate the record-to-record variability in the response calculations, which is neglected or not considered explicitly in the current code approach. In Chapters 3 and 4 we will demonstrate the *seismic demand* calculations for the example problems considered in those chapters. We will also calculate the seismic drift demand by the nonlinear static procedure that was introduced recently in FEMA-273 and we will compare those results with those we get from the rigorous nonlinear-MDOF-time-history analyses.

In Chapter 3 we will consider a simple example problem to demonstrate the demand calculation. In Chapter 4 the demand calculation becomes more complicated because the "collapse" (non-convergence of solution) of the structure is frequent at the spectral acceleration levels required to induce the target damage level. In Chapter 5 we will also show the demand-hazard calculations for responses dependent on spectral accelerations at frequencies higher than the elastic-first-mode frequency, on magnitude (M), on distance (R), and on duration (D). In order to carry out demand-hazard calculations by including those additional parameters we will introduce *2-D seismic demand-hazard analysis.* In this demand-hazard calculation we will require disaggregation of seismic hazard results (McGuire, 1995; Bazzurro and Cornell, 1999). If we want to incorporate the duration dependency of damage measures in demand-hazard calculations, we will require additionally the duration-attenuation results. As duration-attenuation results are not very commonly available in literature, we will show some preliminary results in Chapter 5. Sometimes the disaggregation may not be sufficient, we will require a separate 2-D PSHA results (Bazzurro, 1998). We will demonstrate the importance of considering those parameters in demand-hazard prediction. We will also show how one can improve the conventional

demand-hazard calculations to minimize the difference in results with the more accurate 2-D seismic demand-hazard calculations.

In Chapter 6 we will recommend different efficient and accurate procedures which we will develop in this study for the estimation of structural demand at a specified intensity of ground motion and also for the estimation of demand hazard. The recommended procedures are based on the results from a particular mathematical representation of structures which we will adopt in this study, from a limited number of case studies, and from the particular ground-motion types which we will select for this study. In Chapter 6 we will summarize all the simplifications in modeling, the assumptions in the estimations of demand or demand-hazard , and the limitations of this study. We will also consider in that chapter different sources of uncertainties in our estimations of demand or demand-hazard. We will determine the relative importance of each of the sources of uncertainties and based on those we will recommend the required number of analyses so that the uncertainty is within an acceptable limit.

Chapter 2

Different Issues of Seismic Analysis of Nonlinear Structures

2.1 Introduction

The objective of the present work is the establishment of accurate and efficient estimation of post-elastic damage measures to be expected in a multi-degree-of-freedom (MDOF) structure subjected to a specified earthquake event of a given magnitude, M, and distance, R. The damage measure may, for example, be interstory drift or cumulative hysteretic energy. The earthquake may be a design event, e.g., the deterministic maximum considered earthquake (MCE) of Caltrans (ATC-32, 1996, and CDMG 92-1, 1992) or of NEHRP (FEMA-273, 1996), or the probabilistic-seismic-hazard-analysis (PSHA) -based scenario event of the U.S. D.O.E. (DOE-1020, 1994) or of the U.S. NRC (NUREG 1.165, 1997). We shall demonstrate that when a structure experiences different ground-motion records representative of the same predefined earthquake event, the record-to-record variability in calculated damage measures is large; this threatens to make damage estimates from a practical number of records very unreliable. We propose here strategies to make the estimate more efficient.

In the present chapter, the primary interest is in a "best estimate" of the post-elastic

damage measure. For this purpose, we shall use the *median* value which is the geometric mean (see Appendix A for a discussion on this estimator of median). This best estimate should be unbiased with the minimum variance possible for the effort as measured by computation time. The minimum variance objective insures the narrowest possible confidence band on the median (for a given M and R) and thus reduces the number of nonlinear structural analyses required to achieve a desired level of accuracy. We also have a secondary interest in estimating a measure of dispersion. We shall adopt the "dispersion," δ, which is defined as the standard deviation of the natural logarithm of the data (see Appendix A for a discussion on this estimator of dispersion). An estimate of δ is needed in several practical cases, for example, if the relevant design basis calls for the "84^{th} percentile demand," which is usually defined as the median times the exponential of δ (i.e., $\hat{x} \cdot e^{\delta}$). It is also necessary in probabilistic or performance-based design. We shall also approach the problem from the equivalent, orthogonal perspective of the median and "dispersion" of spectral acceleration required to induce a specified damage level. This is analogous to a force-based as opposed to a displacement-based approach to nonlinear response analysis.

This chapter addresses directly several of the common issues that seismologists and structural engineers face, including the choice of the records, the number of records to be analyzed, presentation of results, etc. Their main concerns are scaling of records, sensitivity of results to M and R, accuracy of results given the limited number of records, and the broad scatter in the results. The conclusions of this study are that many of these concerns either are not as serious as feared, or can be reduced by appropriate scaling.

In this chapter, we shall first look at simple, direct results. We present nonlinear response statistics from samples of records representative of several M, R pairs. Then we introduce our proposed strategy. We begin by taking advantage of years of effort by earthquake engineers and strong-motion seismologists towards improving the estimation (for a given M and R) of the spectral acceleration, S_a, at a specified oscillator frequency and damping. Armed with this information, we can then focus on the "easier" problem of estimating the median damage measure, *given* that the record has a specified "intensity" (as measured by this S_a value). We demonstrate here that this two-step approach is both valid and more

efficient. This chapter then addresses various related issues such as scaling, magnitude dependencies, and choice of the optimal "intensity measure." (Scaling means here simply multiplying an accelerogram by a scalar factor.) We can extend the strategy to multiple levels of spectral acceleration associated with different events, and we show that doing so is advantageous in probabilistic damage hazard prediction.

The conclusions in this chapter will be based on the results of many nonlinear dynamic analyses of a representative 5-story MDOF structure subjected to multiple records, representing different M, R pairs; we shall look at several different global and local damage measures. Therefore, before looking at these results, we first describe these various elements of the study.

2.2 Ground Motion

The ground-motion records considered in the present study belong to four M, R categories or "bins":

1. Bin-I : M = 5.25-5.75 and R = 5-25km.
2. Bin-II : M = 6.5-7.0 and R = 50-70km.
3. Bin-III : M = 6.7-7.3 and R = 10-30km.
4. Bin-IV : M = 6.5-7.0 and R = 15-35km.

In this context, M is the moment magnitude of the event and R is the closest distance to the rupture zone.

For each bin, 20 accelerograms recorded in California on stiff soil (soil site type S_2 as per UBC, 1994, or site class D as per FEMA-273, 1996) have been considered to analyze the structure. While this number is larger than, and hence unrepresentative of, current practice, it insures accurate estimates and thus firm general conclusions. See the report (Shome et al., 1997) for a complete list of ground-motion records.

These records were screened to insure that they did not display any apparent coherent-pulse-like behavior. This "near-source" effect must be addressed separately (Hall et al., 1995), it is not expected to be a significant factor for 1Hz structures for the bins used. (For

the structure considered in this study, the fundamental frequency of the structure is 0.95Hz and damping, ξ, is 2%. A detailed description of the structure is to follow.) See Somerville et al. (1997) for details.

The pair Bin-I and Bin-II are considered in part because they may represent the two alternative scenario events at some site. Such scenarios are typically of two kinds: one representing closer, smaller magnitudes and the other more distant, larger magnitudes. These two bins are chosen such a way that they give, on average, about the same median S_a at the fundamental frequency of the structure, f_0. Thus the median first-mode linear responses of the structure will be very similar for both the bins. But many engineers would anticipate that the MDOF nonlinear responses will be substantially different because of the systematic differences in the ground-motion characteristics, e.g., spectral shape, duration, etc., associated with these very different magnitudes and distances. These concerns have been communicated to ground-motion specialists who carefully search for records that closely match these hypothesized scenarios. Hence, whether or not the two bins represent alternative scenarios, comparison of the results here will help to confirm or deny the commonly-held beliefs about response sensitivity to event characteristics.

Many engineers also express concern about the scaling of records. We interpret this concern here to mean that scaled records will produce different nonlinear structural response statistics than the unscaled records of the same "intensity" will produce. As part of the effort to explore this concern, two sets of records, Bin-III and Bin-IV, are considered here. The median spectral acceleration of these two bins at the fundamental frequency of the structure, $\hat{S}_a(f_0)$, are much higher (about three and two times respectively) than those of the other two bins. It is to be noted here that the stronger records in Bin-III have spectral accelerations of interest that are more than ten times those of the weaker records in Bins I and II. To be more representative of the most severe threats in, for example, UBC Zone IV of California, still stronger records would have been desirable, but it is not feasible to obtain a large enough sample of such records in a sufficiently narrow magnitude-distance bin that includes records displaying coherent-pulse-like near-source effects.

The median response spectra of ground-motion records from each bin are shown in

Figure 2.1(a). The median spectra as obtained from the Abrahamson and Silva (1997) attenuation law at the central M and R range of each bin are shown in Figure 2.1(b). They are quite similar, suggesting that our samples are representative. For our simple comparative purposes, we have obtained the median attenuation law spectra at 2% damping by multiplying the available 5% attenuation law results by the ratio of 2%- to 5%-damped median spectra values from the 20 records of each bin. Similarly, we have obtained the attenuation law spectrum at 0.95Hz by multiplying the spectrum at 1.0Hz (that is closest to the fundamental frequency of the structure available in the published attenuation laws) times the ratio of 0.95Hz and 1.0Hz bin-median spectrum value at 5% damping. Although many would say that we should use higher damping to reflect the nonlinear behavior of the structure, we choose here to use spectral acceleration corresponding to 2% damping since that value characterizes the linear response of the structure. In both Figures 2.1(a) and 2.1(b), we see first the relative intensity levels at 0.95Hz (the fundamental frequency of the structure considered in this study) as discussed above. Further we see that the smaller magnitude bin (Bin-I) produces systematically higher intensities than Bin-II at the higher frequencies, which influence the higher modes of the structure, and systematically lower intensities at the lower frequencies of concern when the structure "softens" during its nonlinear excursions. In contrast, Bin-III and Bin-IV, whose magnitude ranges are similar to that of Bin-II, show virtually the same spectral shape as Bin-II, but a systematically higher intensity at all frequencies, reflecting the closer distance.

Comparisons of selected response-spectral-ordinate statistics (median and "dispersion," δ) as obtained (1) from the 20 records in each bin and (2) from the published attenuation law regressions[1] are given in Table 2.1. The statistics of spectral acceleration from attenuation

[1]Some details follow. We predicted the ground motion that using the magnitude and distance values at the center of the bin ranges. We made no attempt, as some do, to adjust the records with relatively larger or smaller magnitudes or distances (within the bins) to reflect these central magnitude and distance values. Therefore it might be argued that the bin δ values are somewhat exaggerated. Some minor non-random selectivity of the records was involved to insure that the (small sample) median and δ were close to the target values obtained from attenuation law, specially at about 1 Hz (the fundamental frequency of the structure). Even so, we see a 20% difference at 0.95Hz in the Bin-I versus Bin-II medians.

Although it is of no particular significance in this study, it happens that the predicted spectral values were obtained for a site located on the hanging wall of a reverse fault. Some of the results used here were also

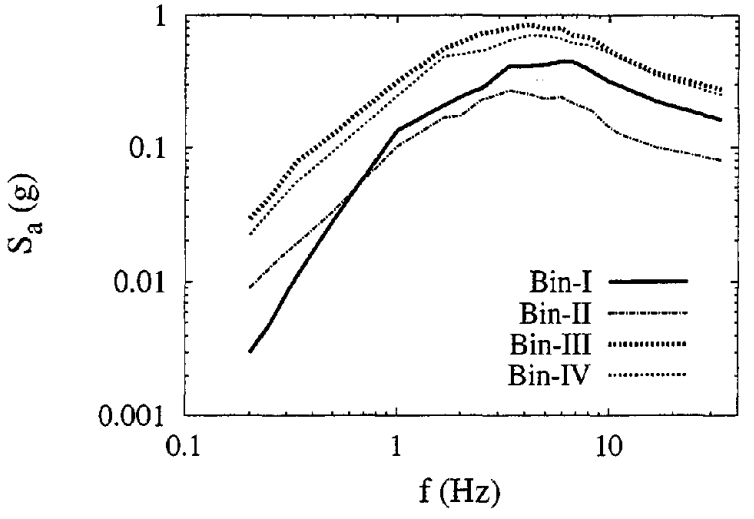

(a) Median spectra from 20 ground-motion records per bin.

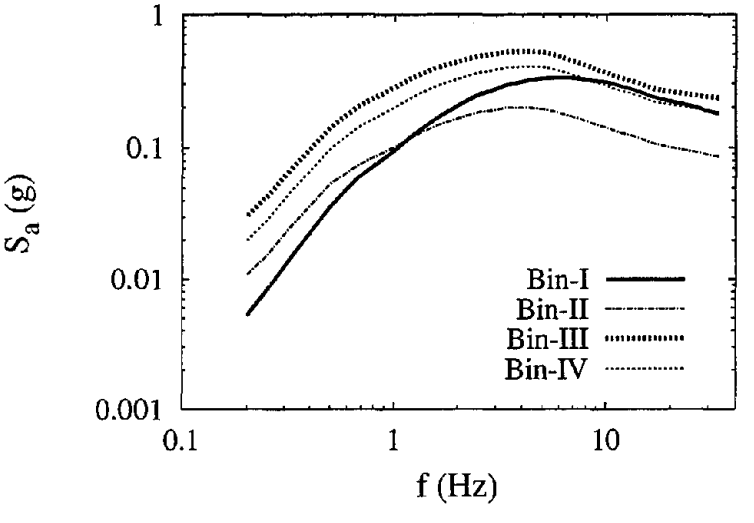

(b) Median spectra from Abrahamson and Silva (1997) attenuation law.

Figure 2.1: Median spectra of different bins for 2% damping.

Case	Source	Statistics of $S_a(g)$	Frequency (Hz)			
			0.25	**0.95**	**3.33**	**33.0**
Bin-I	Attn.	Median	0.01	0.11	0.38	0.18
M=5.25-5.75	Law	δ_{S_a}	0.83	0.77	0.71	0.63
R=5-25km	Binned	Median	0.01	0.12	0.41	0.16
	Records	δ_{S_a}	0.97	0.74	0.60	0.66
Bin-II	Attn.	Median	0.02	0.11	0.26	0.09
M=6.50-7.00	Law	δ_{S_a}	0.72	0.62	0.54	0.46
R=50-70km	Binned	Median	0.01	0.09	0.27	0.08
	Records	δ_{S_a}	0.93	0.58	0.56	0.57
Bin-III	Attn.	Median	0.05	0.34	0.70	0.23
M=6.70-7.30	Law	δ_{S_a}	0.69	0.59	0.51	0.43
R=10-30km	Binned	Median	0.05	0.31	0.78	0.27
	Records	δ_{S_a}	0.90	0.50	0.66	0.61
Bin-IV	Attn.	Median	0.03	0.24	0.53	0.18
M=6.50-7.00	Law	δ_{S_a}	0.72	0.62	0.54	0.46
R=15-35km	Binned	Median	0.03	0.24	0.65	0.25
	Records	δ_{S_a}	0.94	0.61	0.52	0.45

Table 2.1: Values of median S_a and dispersion δ_{S_a} of spectra for 2% damping as obtained from the Abrahamson and Silva (1997) attenuation law and from 20 records in each bin used in this study.

law and from the records in a bin help to confirm that the records are representative of the specified magnitude-distance ranges. Note the typical large-dispersion measures (0.5 to almost 1.0); inevitably these will be reflected in the structural responses.

2.3 Post-Elastic Damage Measures

In the structural engineering literature one can find various damage measures in experimental and theoretical studies that have been used by researchers to explain the damage observed in test structures under simulated ground motion or in actual structures subjected to real earthquakes. The purpose of the present study is not to recommend any specific

intended for a companion study (Carballo et al., 1999) where a downtown Los Angeles site is of interest. Probabilistic Seismic Hazard Analysis (PSHA) showed that for that site, the contribution to hazard was highest from this fault type and geometry.

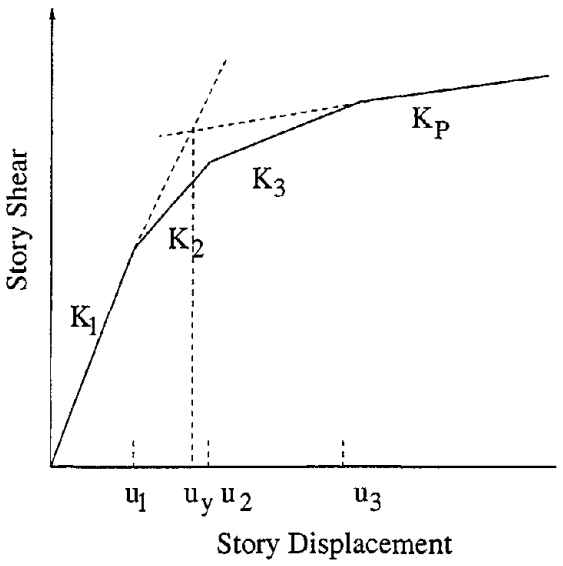

Figure 2.2: Definition of yield displacement, u_y, from a typical force-displacement curve.

damage measure to be used in predicting the state of damage of a structure after an earthquake. Rather, this study considers a number of damage indicators that are believed to be representative of the current set of state-of-the-art building damage measures.

We consider first three "local" measures, defined at the story level, and report the maximum over the five stories. The local damage measures considered in this study are the following:

1. Displacement Ductility, μ: This measure is defined here as the ratio of the *maximum* absolute interstory displacement response to the corresponding displacement at incipient yield, i.e.,

$$\mu = \frac{|u|_{max}}{u_y} \tag{2.1}$$

where u is the interstory displacement, and u_y is the yield displacement. In the present chapter, the yield force and displacement are defined at the intersection of the tangents in the elastic and strain-hardening range of the force-displacement curve (see Figure 2.2). The frequently cited "interstory drift" is the maximum story displacement divided by the story height. Commonly for steel moment-resisting frames this measure, expressed as a

percentage, is approximately equal to the interstory ductility.

2. Normalized hysteretic energy, NHE: NHE is defined here as the total hysteretic energy absorbed in all the cycles normalized by twice the yield strain energy:

$$NHE = \frac{\sum_1^N (\oint_i R_u du)}{R_y \cdot u_y} \tag{2.2}$$

where R_u is the force history at each story level, N is the number of response cycles, and R_y is the yield force. The cyclic integrals $\oint_i$ represent the areas under the force-displacement curves in each response cycle.

3. Damage index, DI: The damage index studied here is a linear combination of normalized displacement and NHE (Park and Ang, 1985):

$$DI = \frac{|u|_{max}}{u_{ult}} + \beta \cdot \frac{HE}{R_y \cdot u_{ult}} \tag{2.3}$$

where β is 0.15, HE is the total absorbed hysteretic energy, which is the same as the numerator in the preceding equation, and u_{ult} is the ultimate monotonic displacement capacity. We assumed u_{ult} is equal to $4.0 \cdot u_y$. Note that the first term in the sum would be the same if it were defined in terms of the ratio of ductility to ultimate ductility capacity. In practice the sum tends to be dominated by the first term.

In addition, we consider three "global" damage measures:

1. Global Ductility, μ: The global ductility is defined as the top-story maximum displacement (relative to the base) divided by the "global" yield displacement (see above) observed in a static force-displacement diagram ("pushover") of the entire structure.

2. Global NHE: The global normalized hysteretic energy is defined here as the sum of the (unnormalized) hysteretic energies, HE, absorbed in all the stories, normalized by the product of the global-yield displacement and the "global" force at which it occurs, where the global force is the base shear obtained from static-pushover analysis.

3. Global Damage Index: The global damage index is defined as a weighted sum of the local damage indices defined above for each story. The weighting factor for each story is the

ratio of the story's cumulative hysteretic energy, HE, to the total HE of all stories (Park, Ang, and Wen, 1985). However, given the typical dominance of the first, or displacement, term over the second, or energy, term, this recommended weighting may not be the most appropriate for future use.

2.4 Structural Model

A five-story, four-bay steel moment-resisting frame is considered in the present study (Searer, 1994). The structure was designed originally for UBC Zone 4 at a site in Los Angeles. See Appendix B for a detailed description of the geometry, structural properties, and modeling of the structure. The structure is idealized here by a simple stick model, the force-deformation values having been derived from a 2-D finite element model of the structure. (Interstory displacements will be reported here in terms of ductility; interstory drift percentages are 0.8 to 1.1 times the ductility.) The fundamental frequency of the structure, f_0, is 0.95 Hz and the modal mass participation at the fundamental frequency is 82%.

For the nonlinear dynamic analyses, however, the yield capacity of each floor has been reduced to one tenth of its original value for cases involving Bin-I, Bin-II, and Bin-IV intensity levels. This configuration is designated as *Structure-I*. For cases involving intensities of the level of Bin-III, the reduction in yield capacity is only two fifths (designated as *Structure-II*). Although the intensity of ground motion is quite high for Bin-IV, we use Structure-I in this case to study the effect of extreme levels of nonlinearity in the structure. These reductions insure nonlinear response results appropriate to the objectives of this study. Without this reduction, the structure would remain elastic for most of the selected ground motions. The lower ground motions were necessary because the objectives of the study require the availability of a significant number of records within several different, but relatively narrow, magnitude and distance ranges. It is to be noted here that Bin I and II events and intensity levels might in fact be more representative of an eastern U.S. site, but the reduced structure (Structure-I) has not especially been designed for that type of site. On the other hand, the

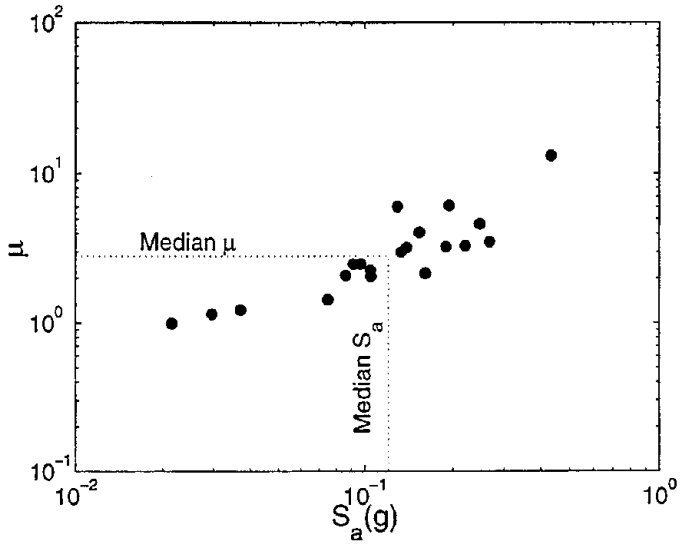

Figure 2.3: Variation of maximum interstory ductility, μ, of Structure-I versus the $S_a(f_0, 2\%)$ of the records as obtained from direct (non-normalized) results of Bin-I. Note the median values.

response measure results reported here are identical to those that would be obtained in the original UBC Zone 4 structure if the records were scaled up by factors of 10 and 2.5 for Structure I and II respectively. The appropriateness of such scaling will be studied below.

2.5 Damage Results

2.5.1 Direct Results

The results of the direct (non-normalized) calculations of nonlinear response (Structure I) to records of Bin-I (M = 5.25 to 5.75 and R = 5 to 25km) are shown in Figure 2.3. Note the broad scatter (a factor of 10). The simple statistics of these calculations of post-elastic damage measures from Bin-I and Bin-II (Structure-I) are given in Table 2.2. The question is, can we say that the results depend on the M and R of the scenario earthquake? We find that for each of the six damage measures, the two bins' median values are within about 50% or less of one another, the Bin-I results being higher. As we shall see below, most of these differences in median responses are largely explainable by the 25% difference in the

Case	Damage Measure	$\hat{\mu}$	δ_μ	$\hat{NHE}$	δ_{NHE}	$\hat{DI}$	δ_{DI}
Bin-I	Global	1.7	0.57	3.7	0.66	0.8	0.75
$\hat{S}_a(f_0, 2\%)$=0.12g	Max. Inter-St.	2.8	0.62	6.1	1.31	1.0	0.75
Bin-II	Global	1.4	0.43	2.6	0.91	0.6	0.66
$\hat{S}_a(f_0, 2\%)$=0.09g	Max. Inter-St.	1.9	0.51	3.9	1.34	0.6	0.69

Table 2.2: Damage measure results of Structure-I from Bin-I and Bin-II for direct (non-scaled) records. Medians and dispersions of six damage measures.

bins' median ground-motion "intensities," i.e., by the differences in the median spectral accelerations at the 0.95 Hz fundamental frequency of the structure, and *not* by dissimilar ground-motion characteristics implied by the differences in bins' magnitudes and distances.

The "dispersions," δ, (or more precisely, the standard deviations of the log damage measures) are large: for the global and local ductilities they approximately equal those of the S_a's in Table 2.1. For the four measures that involve hysteretic energy, they are even larger (for the interstory NHE, the δ is about twice that of the S_a's). This wide scatter in the direct nonlinear response data (given M and R) implies that even for this quite large sample size (n = 20), the estimates of the median responses are subject to significant uncertainty. The "standard errors of estimation" (as percentages of the medians) are approximately the sample "dispersions" in Table 2.2 expressed as percentages and divided by $\sqrt{n}$ or 4.5. So, for example, the "± one-sigma confidence band" on the median Bin-I maximum story ductility is 2.8 ± (62%/4.5) or 2.8±14% or 2.4 to 3.2. Clearly the use of a sample size typical of professional practice (n = 3 to 7) implies one-sigma confidence bands on median nonlinear response of 30% or more. The conventional 95% confidence bands are about twice as wide.

The large value of the standard error of estimation of damage measures makes it particularly difficult to estimate the *ratios* of the two medians, i.e., to decide in our case if magnitude and distance matter in the prediction of nonlinear response. The standard error of estimation of the ratio of the two medians in Table 2.2 is the square root of the sum of the squared "dispersions" divided by $\sqrt{n}$, e.g., $\sqrt{(0.62^2 + 0.51^2)/20}$ or 18%. So the one-sigma confidence band on the ratio of the Bin-I maximum interstory ductility to the Bin-II ductility is 2.8/1.9 ±18% or 1.47±0.26, hardly statistically significantly different from one, and

certainly not significantly different if we recognize that the intensity of ground motion in Bin-I is systematically stronger in the 1Hz frequency range by about 25%. The uncertainty in the ratio of the two estimates of the medians should be kept in mind in all that follows.

The spectral accelerations and (maximum) interstory ductilities from Bins I and II are plotted in Figures 2.4(a) and 2.4(b) (arithmetic and log scales respectively). These plots are very informative. First, they demonstrate visually what δ's of this level (0.6) imply with respect to the variation in the individual observations: the ratio of the maximum to the minimum values is typically about a factor of ten! Second, as emphasized by the regression lines (which are of the form $\mu = \beta_0 \cdot S_a^{\beta_1}$), within a bin there is an important trend suggesting that the ductility response induced by a particular record is strongly dependent on the "intensity" of that record. We will exploit this observation below. Further, the regression lines from these two bins are very similar to each other and to a common regression line run on the combined data sets. This implies that the differences between the median responses induced by the two M-R bins are due almost solely to the differences in the bins' median intensities, and not to M or R per se. If this were not the case, the two within-bin regression lines would be different from one another. Because of its predominant role in current practice, we shall focus discussion throughout the chapter on the (maximum) interstory ductility as the damage measure; if the conclusions differ for other measures, as they sometimes will for the NHE's, we shall point these differences out.

From the median and δ the response corresponding to various percentiles can be estimated provided one assumes an appropriate form for the probability distribution. We use here the common lognormal assumption, an assumption confirmed in the Appendix C. So, for example, the 84% interstory ductility (given $M \approx 5.5$ and $R \approx 15$ km, i.e., Bin-I) is $\hat{\mu} \cdot e^{\delta} = 2.8 \cdot e^{0.62}$ or 5.2. The (conditional) probability of the interstory ductility exceeding, say, four, given the Bin-I scenario event is $1 - \Phi\left[\frac{\ln(4/2.8)}{0.62}\right] = 1 - \Phi(0.575) = 0.28$, in which $\Phi(\cdot)$ is the widely tabulated standard normal cumulative distribution.

2.5.2 Normalized Results

The above observations regarding the trends in the nonlinear response with respect

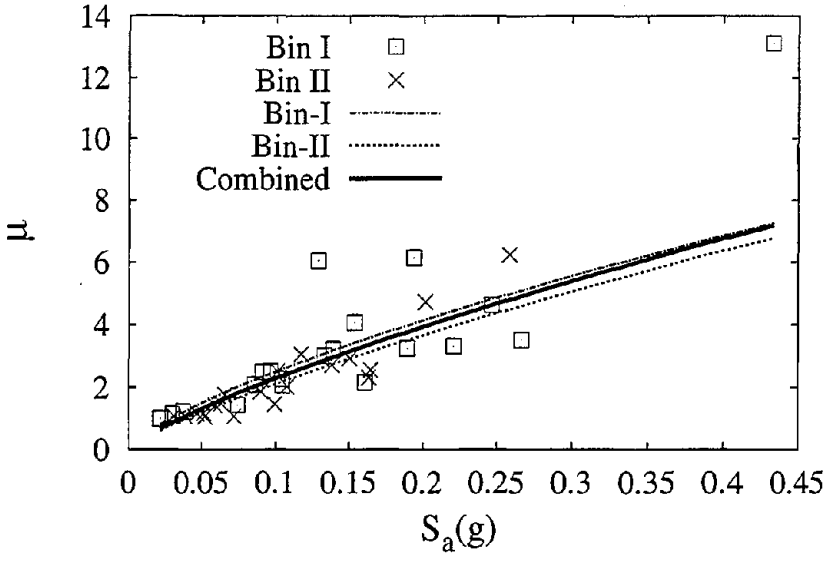

(a) Arithmetic scale.

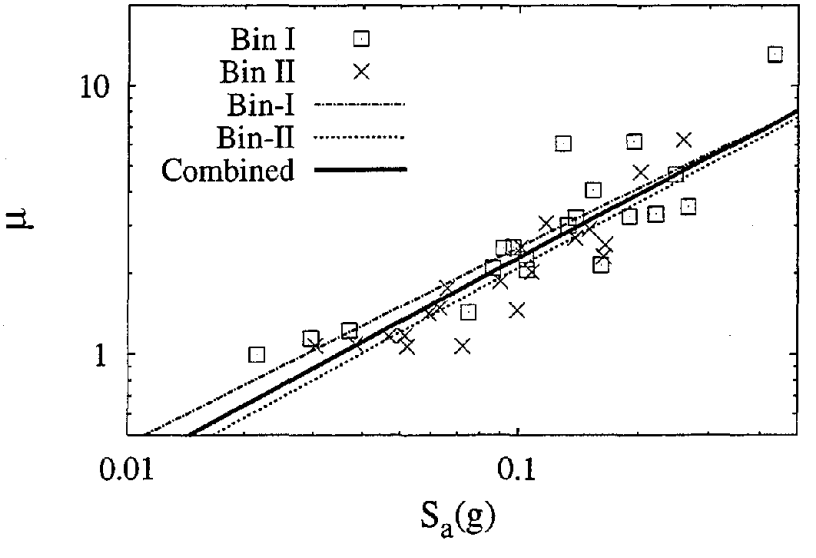

(b) Log scale.

Figure 2.4: Variation of maximum interstory ductility, μ, of Structure-I versus the $S_a(f_0, 2\%)$ of the records as obtained from the direct (non-normalized) results of Bin-I (M=5.25 to 5.75; R=5 to 25km) and Bin-II (M=6.5 to 7.0; R=50 to 70km). Linear least squares fits (on log-log data) shown on arithmetic and log scales.

Case	Damage Measure	$\hat{\mu}$	δ_μ	$\hat{NHE}$	δ_{NHE}	$\hat{DI}$	δ_{DI}
Bin-I	Global	1.6	0.18	3.1	0.40	0.7	0.26
$\hat{S}_a(f_0, 2\%)$=0.12g	Max. Inter-St.	2.6	0.28	6.3	0.44	0.9	0.28
Bin-II	Global	1.4	0.19	2.7	0.48	0.6	0.26
$\hat{S}_a(f_0, 2\%)$=0.09g	Max. Inter-St.	2.0	0.25	5.0	0.51	0.7	0.30

Table 2.3: Damage measure results of Structure-I from Bin-I and Bin-II when the records in each bin are normalized to the median $S_a(f_0)$ of that bin. Medians and dispersions of six damage measures. Medians are similar and dispersions are less than those of Table 2.2.

to the ground-motion intensity (e.g., Figure 2.4) strongly suggest that our estimation of (median) nonlinear responses may well benefit from first normalizing the records to the median "intensity" of the bin[2]. We can anticipate reduced dispersion; we see in Figure 2.4 that the variability of the responses at a given value of S_a is much less than that in the entire response data set. (Formally, we should say that the variability in nonlinear response given M, R and S_a is much less than that given only M and R.) We must confirm, however, that this normalization does not produce a biased estimate of the median.

We can compare the statistics of nonlinear responses in Table 2.3, where the records were first normalized (i.e., scaled in such a way that each record has the median intensity of the bin), with those in Table 2.2. First we observe that, for a given bin, the medians in Tables 2.2 and 2.3 are virtually identical (recalling, too, the 15% uncertainty in the estimates of the median ductility in Table 2.2 due to limited sample size). Only the Bin-II interstory NHE values (direct and normalized results are 3.9 and 5.0 respectively) "look" different, but note that the uncertainty in the Table 2.2 median value of 3.9 is about 30% because the sample δ is 1.34. On the basis of this comparison, we draw the critical conclusion that the scaling of records within a bin to the bin-median spectral acceleration produces unbiased estimates of the nonlinear response medians.

Next, let us consider the "dispersions" (δ). These values in Table 2.3 are less than half

[2]This particular normalization is suggested by the good fit of the data to the functional form of the power type (i.e., the good linear fit of log damage measure versus log spectral density). Under quite robust assumptions, the median of a damage measure will then be found to be the same function evaluated at the median spectral acceleration. The results to follow will confirm the choice.

those in Table 2.2. This is a major benefit. As we saw above, the uncertainty band on the median is the δ divided by the square root of the sample size. So the reduction in δ to half cuts the confidence band in half. Or, for a given acceptable response confidence band width, e.g., $\pm 10\%$, cutting the δ in half reduces the necessary sample size by a factor of 4. In other words, the results from one record are as effective as those from four records if the records are first scaled to the bin median spectral acceleration.

We conclude that an efficient way to predict the nonlinear response given a scenario event is (1) to use a representative ground-motion attenuation law to predict the median spectral acceleration at the fundamental frequency of the structure, (2) to select "appropriate records," and (3) to normalize them to the predicted spectral acceleration before using them to analyze the structure. For ductility or Park-Ang damage index responses, the typical numbers of records used in practice (e.g., about four) will provide an estimate of the median response with a confidence band of about $\pm 15\%$, about half the width the band would have if normalization were not used. NHE medians will have confidence intervals at least 50% wider. Although we demonstrate our conclusions only for a single MDOF structure here, they may well be valid for virtually all structures whose response is dominated by the first mode of vibration. We will discuss what we mean by "appropriate records" below.

The only negative aspect of the reduced δ provided by this normalization is its implied failure to provide an unbiased estimate of the actual δ of the response (given only M and R) when that number is needed, e.g., for a criterion that requires the 84% response. Of course, a typical sample size (of about four) will not produce a reliable estimate of this number in any case. An approximate estimate may suffice in some circumstances. For ductility and damage index measures, it is usually somewhat conservative to use as an estimate simply the square root of the sum of the square of δ of the spectral acceleration given M and R (a number provided with all attenuation laws) and the square of the δ of the damage measure obtained from the scaled records (e.g., the Table 2.3 values). For example, for Bin-I interstory ductility, this approximation yields an estimate of the δ equal to $\sqrt{0.74^2 + 0.28^2}$ or 0.79 versus the Table 2.2 value of 0.62 (a more accurate estimation of δ is given below). This error in δ would affect the estimate of the 84% ductility (given M and R) by $\exp(0.17)$

or 20%. The value 0.74 is the Bin-I observed δ value of the 2%-damped 0.95 Hz spectral acceleration that is used here (see Table 2.1). The value of 0.77 for the attenuation law in Table 2.1 is based on the 5%-damped 1 Hz value, which is readily available in the published attenuation results. Note that in this case, the δ of the nonlinear response is actually somewhat less than that of the spectral acceleration alone.

The estimation of δ can be further improved by assuming the functional dependency of μ on S_a to be of the form

$$\mu = \beta_0 \cdot S_a^{\beta_1} \cdot \varepsilon \tag{2.4}$$

where β_0 and β_1 are the regression parameters, ε is the random-error term with median = 1 and $\sigma_{\ln \varepsilon} = \delta_\varepsilon = \delta_{\mu|S_a,M,R}$. Note that an approximate method of estimation is a particular case of the expression given above by setting β_1=1. For instance, for Bin-I we derived the following results:

$$\beta_0 = 0.174 \qquad \beta_1 = 0.730 \qquad \delta_{\mu|S_a,M,R} = 0.32 \tag{2.5}$$

These values imply that, for $\hat{S}_a$=44.87 in/sec^2 (0.12g), we predict a median ductility, $\hat{\mu} = 0.174 \times (44.87)^{0.73} = 2.8$. The δ of μ given M and R can then be estimated as

$$\begin{aligned} \delta_{\mu|M,R} &= \left[(\beta_1 \cdot \delta_{S_a|M,R})^2 + (\delta_{\mu|S_a,M,R})^2 \right]^{\frac{1}{2}} \\ &= \left[(0.73 \times 0.74)^2 + 0.32^2 \right]^{\frac{1}{2}} = 0.63 \end{aligned} \tag{2.6}$$

Both the accurate and the approximate method yield a value for the median of μ that is in very good agreement with the result obtained by means of the direct calculation (i.e., $\hat{\mu} = 2.8$). The approximate procedure, however, overestimates the δ computed by the direct method (0.79 versus 0.62), while the more accurate method appears to give a result (0.63) more in tune with the "target" value computed by the direct method.

The approximate calculation of δ is consistent with the "equal displacement" rule (i.e., the nonlinear response on average grows in proportion to the spectral acceleration, or β = 1) and is based on some rather mild assumptions about correlations. Note that under this approximation the result will be dominated by the first, or "attenuation law," variability

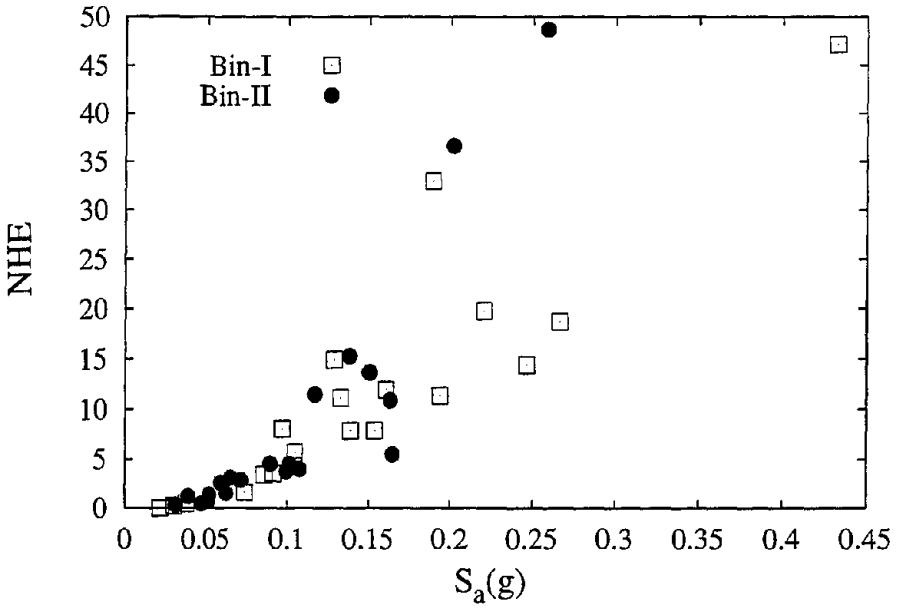

Figure 2.5: Variation of maximum interstory normalized hysteretic energy (NHE) of Structure-I versus the $S_a(f_0, 2\%)$ of the record as obtained from direct (unscaled-record) results of Bin-I and Bin-II.

term, implying that one does not need a very accurate estimate of the variability of the responses to the scaled records. This approximation may be unconservative for nonlinear responses such as NHE, which grow more rapidly than simply in proportion to "intensity." Figure 2.5 shows, for example, that for Bins I and II, the local NHE grows approximately like the square of the spectral acceleration.

2.6 Scaling of Records

We found previously that there is a benefit in the form of reduction of δ in normalizing records within a bin (i.e., given M and R) to the median spectral acceleration of the bin. We saw that this within-bin scaling did not bias the median nonlinear response estimation. There are also other benefits if more general scaling is viable. This statement is related to the question of whether or not nonlinear responses depend systematically on M and R. More

precisely, we want to know if nonlinear responses of MDOF structural systems depend on M and R *beyond* their dependence through the intensity (first-mode spectral acceleration) level. (More formally we are asking if the nonlinear MDOF response is conditionally independent of M and R, given spectral acceleration.) It should be noted that by definition the linear response of a SDOF system is independent of M and R given S_a. Based on knowledge about the effectiveness of the "equal displacement" rule and the predominant role of SDOF systems in recent guidelines (e.g, FEMA 273, Nassar and Krawinkler, 1991), and the empirical findings by Sewell (1989), Inoue and Cornell (1991), and Bazzurro and Cornell (1994a and 1994b), it is not unreasonable to pose this question. If the MDOF responses do not depend on these parameters, then the choice of records to be used in nonlinear analysis is greatly simplified. For example, one would not need to use records from a bin surrounding the M and R of interest; in principle he could use records from any bin (any M and R) provided he scaled them to the correct intensity level, e.g., to the median spectral acceleration predicted by an attenuation law for the M and R of interest. So we are addressing here the question raised above: what are the "appropriate" records to scale and then run in the structural analyses?

More generally, if this conditional M and R independence holds, and if one is given exogenously the spectral acceleration level of interest, then one need not be concerned about the M and R of the records one uses in structural analyses, provided they are scaled to this spectral acceleration. Today the exogenous source of that spectral acceleration level may very well be a Probabilistic Seismic Hazard Analysis (PSHA) of the site (or a map of such accelerations at a specified probability of exceedance, e.g., 2% in 50 years). Such hazard analyses integrate over a wide range of magnitudes and distances to accumulate the total probability of exceeding that spectral acceleration value. Therefore, there can be no single scenario M and R that fully represents the PSHA results. If we were confident that, beyond the spectral level, M and R played little systematic role in nonlinear responses, then we could remove the M and R issue from the process of selection of records. (Other issues such as site conditions, style of faulting and near-source effects may remain, of course, to be considered.)

Case	Damage measure	$\hat{\mu}$	δ_μ	$\hat{NHE}$	δ_{NHE}	$\hat{DI}$	δ_{DI}
Bin-I	Global	1.6	0.19	3.1	0.40	0.7	0.26
	Max. Inter-St.	2.6	0.28	6.3	0.44	0.9	0.28
Bin-II	Global	1.6	0.22	4.9	0.52	0.8	0.32
	Max. Inter-St.	2.5	0.28	9.2	0.57	0.9	0.36

Table 2.4: Damage measure results of Structure-I from Bin-I and Bin-II when the records from both the bins are scaled to the median $S_a(f_0)$ of Bin-I (0.12g). Medians and dispersions of six damage measures.

The question of M and R dependence and the question of whether the records can be scaled are interrelated. Many engineers are concerned that records scaled to a substantially higher intensity level will give improper response results. This is because those higher intensities may in fact be representative only of a more intense record generated by a larger magnitude or closer distance. Regarding this question, however, one should remember that, as reflected in the large "dispersions" in Tables 2.1 and 2.2, the records within one bin (one narrow M and R range) may themselves have intensity values and produce responses that differ by a factor of 10, i.e., a factor of 3 on either side of the median (see Figure 2.3, for example).

Let us consider therefore some other results of scaling. In Table 2.4, we show the statistics of response results after the records in both Bins I and II are scaled to the median spectral acceleration at 0.95Hz of Bin I, i.e., to 0.12g. This addresses the question raised previously: can the difference in Bin-I and Bin-II direct results (Table 2.2) be explained by the difference in (median) intensities between these two bins alone? Recall that the magnitudes of the records of of these two bins differ by more than one unit (a factor of about 30 in energy release) and the distances by a factor about 4. The numbers in Table 2.4 suggest that the answer is yes: once scaled to the same intensity, the records in these two bins give virtually the same nonlinear response statistics. The exception is perhaps NHE. We will return to this issue below.

In the case shown in Table 2.4, although the individual records within a bin were scaled by factors as large as 3, the scaling from one bin's median to the other was only a factor

Case	Damage measure	$\hat{\mu}$	δ_μ	$\hat{NHE}$	δ_{NHE}	$\hat{DI}$	δ_{DI}
Bin-I	Global	1.2	0.16	1.3	0.38	0.4	0.22
	Max. Inter-St.	1.6	0.26	2.3	0.50	0.5	0.27
Bin-II	Global	1.2	0.17	1.8	0.42	0.5	0.26
	Max. Inter-St.	1.7	0.24	4.1	0.53	0.6	0.31
Bin-III	Global	1.3	0.20	1.6	0.42	0.5	0.32
	Max. Inter-St.	1.9	0.32	3.8	0.51	0.6	0.36

Table 2.5: Damage measure results of Structure-II from Bin-I, Bin-II, and Bin-III when the records are scaled to the median $S_a(f_0, 2\%)$ of Bin-III (0.31g). Medians and dispersions of six damage measures.

of 1.33 (i.e., 0.09 to 0.12g). In Table 2.5, we present the results (using now Structure-II) of having scaled all the records in Bins I and II to the median spectral acceleration of Bin-III, i.e., to 0.31g. This is a factor of more than 3, bin median to bin median, implying that there are records from Bin-III whose original, unscaled spectral accelerations are a factor of 30 or more greater than some of those from the lower bins. We find that the ductility and Park-Ang damage index medians and "dispersions" are virtually identical for all the three bins. We find too that the NHE results from Bins II and III are very similar but substantially higher than those of Bin-I. Bins II and III are, of course, from higher magnitudes than Bin-I (about 7 rather than 5.5). In fact, the factor of less than 2 between these various medians is, pair by pair, hardly statistically significant (given the δ's of about 0.5), but the systematic difference over several pairs is convincing. Further the Bin-II and Bin-III durations are found to be substantially longer. The median bracketed duration, as defined by Trifunac and Brady (1975), is only 7.3 seconds for Bin-I, 17.3 seconds for Bin-II and 15.2 seconds for Bin-III. This difference suggests that duration may be a factor influencing the cumulative NHE measure (but apparently not the ductility or ductility-dominated Park-Ang damage index). See Shome et. al (1997) for a detailed discussion on duration dependency of damage measures. Suffice it to say here that any damage measure duration dependence there may be is captured implicitly and practically in our results (now, as always, conditional on knowing the intensity as measured by spectral acceleration).

Table 2.6 shows the results of scaling records down rather than up. The records of

Case	Damage measure	$\hat{\mu}$	δ_μ	$\hat{NHE}$	δ_{NHE}	$\hat{DI}$	δ_{DI}
Bin-I	Global	1.6	0.18	3.1	0.40	0.7	0.26
	Max. Inter-St.	2.6	0.28	6.3	0.44	0.9	0.28
Bin-III	Global	1.8	0.30	4.6	0.49	0.9	0.42
	Max. Inter-St.	3.0	0.40	10.6	0.56	1.1	0.44
Bin-IV	Global	1.7	0.24	4.2	0.64	0.8	0.44
	Max. Inter-St.	2.9	0.35	9.6	0.67	1.1	0.47

Table 2.6: Damage measure results of Structure-I from Bin-I, Bin-III and Bin-IV when the records are scaled to the median $S_a(f_0, 2\%)$ of Bin-I (0.12g). Medians and dispersions of six damage measures.

Case	Damage measure	$\hat{\mu}$	δ_μ	$\hat{NHE}$	δ_{NHE}	$\hat{DI}$	δ_{DI}
Bin-I	Global	2.9	0.25	11.8	0.44	2.1	0.38
	Max. Inter-St.	6.2	0.36	27.6	0.52	2.6	0.39
Bin-II	Global	3.1	0.41	21.6	0.65	2.3	0.55
	Max. Inter-St.	5.5	0.44	41.2	0.72	3.0	0.59
Bin-III	Global	3.9	0.45	20.4	0.52	2.8	0.45
	Max. Inter-St.	7.7	0.41	48.7	0.55	3.8	0.42
Bin-IV	Global	3.5	0.39	18.2	0.62	2.5	0.56
	Max. Inter-St.	6.9	0.42	43.1	0.69	3.4	0.54

Table 2.7: Damage measure results of Structure-I from Bin-I, Bin-II and Bin-III, and Bin-IV when the records are scaled to the median $S_a(f_0, 2\%)$ of Bin-IV (0.24g). Medians and dispersions of six damage measures.

Bin-III and Bin-IV are scaled to the Bin-I median spectral acceleration (0.12g) and run through Structure-I. The conclusions of the previous paragraph still hold. With the possible exception of NHE (and by extension, perhaps other strongly cumulative damage measures), M and R dependence is weak, given S_a intensity.

Table 2.7 shows the results of scaling the records in each bin to the median spectral acceleration of Bin-IV (0.24g) and applying them to Structure-I, inducing more extreme levels of nonlinearity. The general conclusions still hold. The smaller magnitude records (Bin-I) do not produce unusual ductilities or Park-Ang damage indices. The only unusual value is the comparatively low median interstory ductility produced by Bin-II, whose records are drawn, as mentioned before, from large magnitude events and whose median spectrum

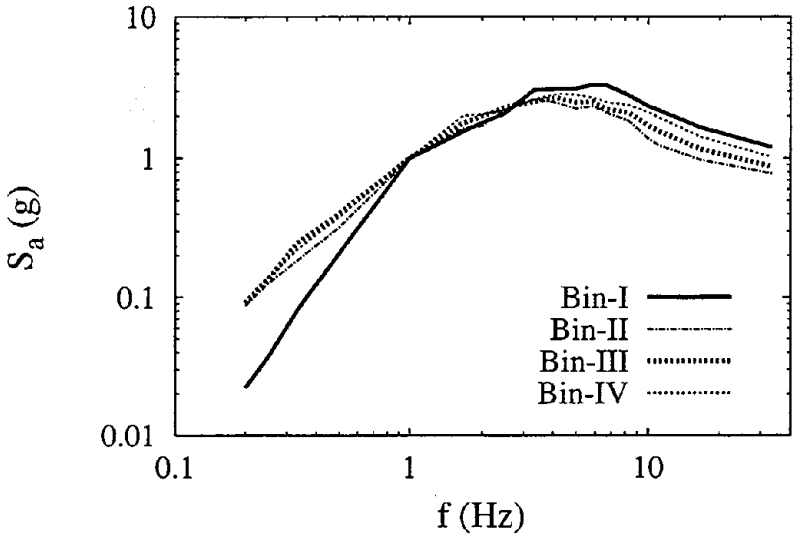

Figure 2.6: Comparison of shape of the response spectra for 2% damping, normalized to the spectral acceleration at the fundamental frequency of the structure (f_0=0.95Hz) from Bins I through IV.

is virtually identical in shape to that of Bins III and IV (Figure 2.6). Bin-II's median maximum interstory value (5.5) is, however, statistically significantly different from the average median of the other bins. A more detailed study of the subsets of records within the bin revealed no obvious generalizable explanation for this outlying result.

We conclude that major degrees of scaling apparently do not significantly bias the median estimates of the most interesting measures of MDOF nonlinear behavior, and the choice of the M and R in record selection is not an issue sensitive to the estimation of responses (extreme near-source effects aside). The demonstrations here are limited, of course, to a single MDOF structural model. We have also confirmed this conclusion for a high frequency MDOF structure (see Shome and Cornell, 1998). As will be discussed below, other evidence is available to support our conclusion. Nonetheless, we shall confirm these findings with additional realistic case studies in the following chapters. In particular, 2D and 3D structures with more significant higher mode effects and with strength-degrading characteristics are currently under consideration. It can be anticipated that very long period structures may

show a "reverse" magnitude dependence because of the stronger dependence of this portion of the spectrum on the magnitude and the comparatively higher high frequency content in smaller magnitude events. The latter will encourage greater response due to higher modes (at least in the elastic range). Such structures may demand different intensity measures to achieve low dispersion. We will investigate these issues of tall structures in Chapter 4.

2.7 Alternative, Equivalent Approaches

We have addressed the question of predicting the nonlinear damage measure demand or response (e.g., the maximum interstory ductility) given an event of magnitude, M, and distance, R. We estimated the median and δ. We also showed how to estimate the probability of exceeding any particular demand level, e.g., ductility 4, given the event. In today's practice this can be called a displacement-based approach. We call it a *direct approach.* It is currently more common to consider demands in ground-motion intensity (spectral acceleration) and/or force-related terms. This would be called a force-based approach. Here we show the parallel analysis of demand prediction given magnitude and distance.

2.7.1 Required Spectral Acceleration Basis

We define for any record, the required spectral acceleration, $S^R_{a_{\mu'}}$, as the spectral acceleration level at the fundamental frequency of the structure *required* to induce a ductility level μ'. This level defines the degree of scaling, as indexed by the spectral acceleration at the fundamental mode, that must be applied to the record in order that it causes precisely the specified nonlinear demand or response level in the structure of interest. The demand is represented by the damage measure of interest, and the maximum interstory ductility is used for illustration here. Note that the value of $S^R_{a_{\mu'}}$ is a property of the record, but it is defined relative to a particular structural property response measure in a particular structure. In this sense it is analogous to the spectral acceleration itself, which is defined relative to a particular linear SDOF "structure." Because of the nonlinear nature of the problem, $S^R_{a_{\mu'}}$ must generally be found iteratively: scaling of ground motion must be adjusted by trial and

error until the structure exhibits the specified response. (Several programs exist to do this efficiently for simple SDOF systems, e.g., Sewell, 1989.) Alternatively one can estimate the response by scaling a record to several levels and then interpolating the spectral acceleration values required to get the target damage measure of interest. See Appendix D for further discussion.

For the Bin-I records, the results of such an analysis for maximum interstory ductility equal to 4.0 produced 20 values of $S^R_{a_{\mu'}}$. The median and δ of this required spectral acceleration were found to be 0.17g and 0.28 respectively. Note the relatively narrow scatter, analogous to that observed above in responses only after the records had been scaled by the median spectral acceleration. This required spectral acceleration serves like a *capacity*. The ductility will exceed 4, if and only if the ground-motion intensity demand exceeds this (random) capacity. Therefore its distribution can be used to answer the question: if the ground motion has spectral acceleration level x, what is the likelihood that the ductility will exceed 4? The answer is simply $\Phi\left(\frac{\ln[x/0.17]}{0.28}\right)$.

If we ask, as we did above, what the likelihood is that the ductility will exceed 4, given a Bin-I scenario magnitude and distance, then we need to go to an attenuation law (e.g., Table 2.1) to find the distribution of spectral acceleration demands (here we use the Bin-I statistics for the 0.95 Hz and 2% damped spectral acceleration). The median is 0.12g and the δ is 0.74. Then, based on the argument that the ductility will exceed 4 if and only if the (random) ground-motion intensity "demand" exceeds the (random) "capacity" or spectral acceleration required, we can say that this ductility level will be exceeded if and only if the ratio of the first (demand) to the second (capacity) is greater than unity, or

$$P(\mu > 4 \mid M, R) \;=\; P(S_a/S^R_{a_{\mu'}} > 1 \mid M, R) \;=\; 1 - \Phi\left[\frac{\ln(1) - \ln(0.68)}{0.79}\right] \;=\; 0.31 \qquad (2.7)$$

Here we have taken advantage of the assumption that the ratio of these two lognormal variables is also lognormal, with a median equal to the ratio of their medians (0.12/0.17 = 0.68) and with a δ equal to the square root of the sum of the squares of the δ's of the two variables ($[(0.74)^2 + (0.28)^2]^{1/2} = 0.79$). The last calculation conservatively ignores the

typically small negative correlation between these demand and "capacity" variables. Note that the value of 0.31 is very close to the 0.28 estimated before.

As a describer of the effect of one or a sample of records on the nonlinear response of MDOF structure, the required spectral acceleration, $S^R_{a_{\mu'}}$, has the same advantages of a reduced variability as we found by scaling records before reporting response statistics. Therefore its median can be estimated reliably from a relatively small sample of records. Also its δ plays a relatively minor role in estimating the likelihood of exceeding a given ductility or other nonlinear response/demand level; hence this δ need not usually be estimated very accurately.

Unlike the direct approach discussed previously, this required spectral acceleration approach has the characteristic of being defined in ground-motion input-level terms; this may be an advantage in certain analysis and assessment formats, especially when normalized, as we shall see below. The disadvantage of this approach is that it is "indirect." Nonlinear dynamic analysis must proceed by specifying a ground-motion intensity (input) level and then the calculation of the response; in contrast this approach asks for the intensity associated with a given response. The required spectral acceleration associated with a specified (output) response measure will, therefore, always have to be found in some iterative or "equivalent" manner (see Appendix D). Depending on the application, this may or may not lead to additional calculations, but it seems to make the interpretation of the approach somewhat more difficult when it is first encountered.

2.7.2 Nonlinear Capacity Factor Basis

It is common in this force-based approach to normalize the value of the required spectral acceleration, $S^R_{a_{\mu'}}$, by the spectral acceleration required to induce incipient yield or significant nonlinearity in the structure, which we refer to here as the "reference acceleration," $S_{a,ref}$. For a simple SDOF oscillator this reference spectral acceleration is a property of the structure only. It is simply the yield force divided by the mass of the oscillator. Usually for MDOF systems, the reference acceleration varies mildly from record to record, depending on the importance of higher modes and on the variation from record to record in the *relative*

strengths and the phasing of the Fourier components at the modal frequencies (Inoue and Cornell, 1991). We, therefore, may anticipate some degree of magnitude dependence of this quantity in certain structures. Its value can usually be found from a single linear analysis of the structure. For certain systems (see, e.g., Bazzurro and Cornell, 1994a), it may be preferable to define the reference spectral acceleration relative to a selected global deformation level at which the nonlinearity becomes significant. In this study such a deformation, beyond the initial yield level, is used as discussed above (see Figure 2.2). The precise choice of the definition of this deformation is not critical because the reference deformation and spectral acceleration in effect enter both in the numerator and denominator in the calculation of the ratio, $S^R_{a_{\mu'}}/S_{a,ref}$. This ratio is denoted as F_μ in the literature (e.g., Kennedy et al., 1984, and Bazzurro and Cornell, 1994a). F_μ will be referred to here as the nonlinear "capacity" factor (see, e.g., DOE 1020, 1994) because it indicates how much stronger the ground-motion intensity must be than the yield-causing intensity (the "linear capacity" of the structure) in order to induce the specified level of ductility. For any specified value of $\mu = \mu'$, the value of F_μ for any record is a property of that record (for that structure); it varies from record to record. Its value is found iteratively or by interpolation as discussed above for $S^R_{a_{\mu'}}$.

We analyzed the records for Bin-I to estimate their reference spectral accelerations, and calculated the nonlinear "capacity" factors, F_μ, using the required spectral acceleration values discussed above. The simple statistics of the reference spectral acceleration are a median equal to 0.043g and a δ equal to 0.10 (in our experience, a comparatively large value suggesting perhaps significant higher mode effects and high variability in the record-to-record spectral shape even within this single M and R bin). The low value of the spectral acceleration required to induce incipient yield, 0.043g, is a result of the scaling down of the original (UBC Zone 4) structural capacity by a factor $\frac{1}{10}$ to accommodate the readily available record sets (refer to Searer [1994] for details of the original structure). The median of F_μ for a specified maximum interstory ductility of 4 is found to be 4.14 with a δ of 0.25. (Note that a value of 4.0 would be consistent with the "equal displacement" rule, although this is an interstory, not a global ductility.) This value of F_μ is independent of

the structural capacity scaling mentioned above. Note the small δ of F_μ, which is again analogous to the δs obtained in the direct approach only after scaling the records to a common spectral acceleration.

To estimate the likelihood of the Bin-I scenario event causing local ductility greater than 4, we must now ask, Does the ground-motion intensity (S_a) exceed F_μ times the reference spectral acceleration, or equivalently does the ground-motion intensity divided by the product $F_\mu \cdot S_{ref}$ exceed unity? We can assume that this multiple of (approximately) lognormal variables is again lognormal, with a median equal to the median of the ground-motion value (0.12g again) divided by the product of the two medians just cited, (4.14)(0.043g)=0.18g; or 0.12/0.18 = 0.67, and with δ equal to the square root of the sum of the three squared δs: $[(0.74)^2+(0.25)^2+(0.10)^2]^{\frac{1}{2}} = 0.79$. Then the probability of exceeding ductility 4 is about $1-\Phi\left[\frac{(ln[1]-ln[0.67])}{0.79}\right]$ or $1-\Phi(0.51) = 0.31$, very close to the previous estimates. Note that since again the variability of the ground motion dominates, the variability of F_μ and of the reference acceleration could virtually be ignored. Indeed, minor negative correlations have typically been ignored in the simple SRSS rule just given: they would have reduced the net δ.

Because they are interesting record properties, we could, as before, ask questions about the dependence of either $S^R_{a_{\mu'}}$, the required spectral acceleration, or F_μ on M and R. For example, for μ'=4 the medians of these two factors for Bin-II are 0.20g and 4.64 respectively; these values are close to, but somewhat larger than, those cited above for Bin-I (0.17g and 4.14). This implies that, if anything, these Bin-II records (given the same S_a) are somewhat more benign (with respect to maximum interstory ductility) in the nonlinear sense than the smaller magnitude Bin-I records, contrary to customary expectations but consistent with Table 2.7. For Bin-III records and Structure-I, the corresponding values are 0.16g and 3.60; this implies that these records are somewhat "more damaging" than Bin-I records. However, these differences are not statistically significant. Thus the effective independence of these nonlinear damage measures from M and R is confirmed.

Note that the above observations show that it is not necessary to consider further the actual observed intensity level of the original unscaled records. An advantage of both of

the indirect measures discussed here is that they overlook this recorded intensity to focus on the relative effectiveness of records, e.g., records from different magnitudes, on a specific structure with respect to inducing a given nonlinear damage type and level. The question of actual experienced intensity or intensity "demand" can be dealt with via a conventional attenuation law for a specified scenario event (or by PSHA for the spectrum of surrounding event possibilities).

Further the normalized measure F_μ is decoupled from the "linear effectiveness" of the records (which is captured in the reference spectral acceleration of a record). F_μ is a strictly "post-linear" measure of record effectiveness with respect to a particular structure and damage, or conversely, it is a measure of the capacity of the structure provided by the post-linear static and dynamic qualities of the structural system to resist earthquakes with some specified limit of damage. F_μ can be used to compare different systems or, as anticipated in the ongoing SAC Steel Project, to compare the "nonlinear" capacities of a given steel moment-resisting frame building with and without considering its limited connection fracture toughness (Luco and Cornell, 1998).

It is not surprising, therefore, that there is a growing literature about F_μ, especially for simple nonlinear SDOF systems, where it is often denoted as $\mathcal{R}$. This is because the ground-motion intensity demand *divided* by F_μ can be thought of as the "reduced" demand that the structure must be "designed for elastically" to limit damage to the level μ. This procedure is practiced in many current seismic building codes. F_μ is a more general concept as it can refer to local measures of ductility demand (or capacity, e.g., in DOE 1020, 1994) and it is used for other damage measures as well. The SDOF literature, e.g., Veletsos (1969), Sewell and Cornell (1987), Nassar and Krawinkler (1991), Miranda and Bertero (1994), Bea (1996), etc., focuses generally on structural issues, such as the shape of the force-deformation curve and more recently on soil types (e.g., Sewell, 1989, and Miranda and Bertero, 1994).

Sewell and Cornell (1987) also studied SDOF F_μ as a ground-motion property. They were perhaps the first to demonstrate its lack of important dependence on M and R, at least for damage measures other than NHE. Sewell (1989) looked at two other damage measures

in addition to ductility and NHE: he considered a pinched hysteresis model with stiffness degradation, designated as a "shear wall model," and a bilinear model. He considered many structural frequencies and more than 100 records. In all the cases, for ductilities of 2 and 4 he observed no significant dependency of F_μ on M or R. It is this SDOF study that suggest that M and R independence of F_μ, and hence of $S^R_{a_{\mu'}}$, and of the ductility given S_a, might be a very general property of strong ground motions and nonlinear structural responses. In the intervening years, the sample of larger magnitude records has increased. With these new data and larger sample sizes one can identify mild ductility dependence on magnitude in some cases, but seldom more than about 10% per magnitude unit, an amount one can typically neglect in practice (Shome and Cornell, 1998).

The study of more realistic MDOF systems is of course more difficult because there are many possible parameter variations (see, for example, Seneviratna and Krawinkler, 1996); we can only hope, as a profession, to generate empirical generalizations by collecting a body of experience with MDOF nonlinear analyses. F_μ promises to be an effective vehicle for such building-to-building comparisons. Inoue and Cornell (1991) and Bazzurro and Cornell (1994b) extended the concern for magnitude and distance dependence into MDOF studies, but we have found little dependence of damage measures other than NHE. This dependence, if any, represents the degree to which there is seismological/structural-engineering coupling *beyond* the simple ground-motion intensity variable, spectral acceleration. The practice of both the fields is simplified if any dependence on M and R is effectively negligible.

2.8 Choice of The Ground-Motion Measure

The advantage of the reduction of nonlinear response variance produced by scaling records to the same spectral acceleration was shown before, for instance in the comparison of Tables 2.2 and 2.3. Previously we have used the required spectral acceleration, $S^R_{a_{\mu'}}$, to define two other relatively low-variance measures of the nonlinear effects of records. Throughout we have used the spectral acceleration at the fundamental frequency of the structure (and at the elastic analysis damping level) as the scaling, or "pinch point," variable. It is reasonable

Case	Damage measure	$\hat{\mu}$	δ_μ	$\hat{NHE}$	δ_{NHE}	$\hat{DI}$	δ_{DI}
Normalized	Global	1.7	0.52	3.4	1.09	0.8	0.78
to $\widehat{PGA}$	Max. Inter-St.	2.8	0.58	6.9	1.26	1.0	0.79
Normalized to	Global	1.6	0.18	3.1	0.40	0.7	0.26
$\hat{S}_a(f = 0.95Hz)$	Max. Inter-St.	2.6	0.28	6.3	0.46	0.9	0.29
Normalized to	Global	1.6	0.46	3.3	0.47	0.7	0.74
$\hat{S}_a(f = 0.25Hz)$	Max. Inter-St.	2.7	0.65	6.0	0.68	0.9	0.75

Table 2.8: Damage measure results from Bin-I of Structure-I when the records are normalized to the median of PGA, $S_a(f = 0.95Hz)$ and $S_a(f = 0.25Hz)$ for 2% damping. Medians and dispersions of six damage measures.

Case	Damage measure	$\hat{\mu}$	δ_μ	$\hat{NHE}$	δ_{NHE}	$\hat{DI}$	δ_{DI}
Normalized	Global	1.4	0.36	2.7	1.08	0.6	0.76
to $\widehat{PGA}$	Max. Inter-St.	2.1	0.51	4.9	1.34	0.8	0.82
Normalized to	Global	1.4	0.19	2.7	0.48	0.6	0.26
$\hat{S}_a(f = 0.95Hz)$	Max. Inter-St.	2.0	0.25	5.0	0.51	0.7	0.30
Normalized to	Global	1.4	0.71	3.3	0.86	0.5	1.01
$\hat{S}_a(f = 0.25Hz)$	Max. Inter-St.	1.9	0.83	5.0	1.16	0.7	1.01

Table 2.9: Damage measure results from Bin-II of Structure-I when the records are normalized to the median of PGA, $S_a(f = 0.95Hz)$ and $S_a(f = 0.25Hz)$ for 2% damping. Medians and dispersions of six damage measures.

to ask if another variable might be still more effective. A logical measure of this effectiveness is now available: the δ of the nonlinear response found after the records are normalized to the same amplitude of the candidate variable. The choice of considering spectral acceleration at the fundamental frequency of a structure has the advantage that S_a is the only variable that can produce *zero* δ for the limiting case, that in which the structure is linear and dominated by one mode. MDOF nonlinear structures, however, "sample" other frequencies in the record, spectra for low dampings are "jagged," and nonlinear systems are effectively more heavily damped. These observations have led to other suggestions (e.g., Kennedy et al., 1984).

Tables 2.8 and 2.9 show the results of scaling the records to the spectral accelerations associated with frequencies higher and lower than the first-mode frequency. PGA (i.e., $f = \infty$) has often been used to scale records. It is clearly not a good choice compared to

Case	Frequency Range	$\widehat{Avg.S_a}$ (g)	δ of Avg. S_a	Story Duct.		Story NHE	
				$\hat{\mu}$	δ_μ	$\hat{NHE}$	δ_{NHE}
Bin-I Structure-I	f_0	0.12	0.74	2.6	0.28	6.3	0.44
	$f_0 \pm 12.5\%$	0.12	0.74	2.6	0.27	6.3	0.33
	$f_0 \pm 25\%$	0.12	0.74	2.7	0.27	6.3	0.43
	$f_0 \pm 50\%$	0.12	0.71	2.7	0.28	6.4	0.67
	$f_0 \pm 75\%$	0.12	0.71	2.7	0.31	6.4	0.76
Bin-II Structure-I	f_0	0.09	0.64	2.0	0.25	5.0	0.51
	$f_0 \pm 12.5\%$	0.09	0.61	2.0	0.20	4.8	0.44
	$f_0 \pm 25\%$	0.09	0.58	2.0	0.17	4.9	0.40
	$f_0 \pm 50\%$	0.09	0.57	2.0	0.19	4.9	0.58
	$f_0 \pm 75\%$	0.09	0.57	2.0	0.25	4.9	0.62
Bin-III Structure-II	f_0	0.31	0.43	1.8	0.32	3.7	0.51
	$f_0 \pm 12.5\%$	0.32	0.47	1.8	0.29	3.6	0.43
	$f_0 \pm 25\%$	0.32	0.48	1.8	0.31	3.6	0.54
	$f_0 \pm 50\%$	0.32	0.50	1.9	0.30	3.7	0.62
	$f_0 \pm 75\%$	0.32	0.51	1.9	0.33	3.8	0.63

Table 2.10: Damage measure results of local spectral averaging for different bins and structures. The records in each bin are scaled to the median of 2% damped S_a averaged over a range of frequencies.

the fundamental frequency of the structure as it results in higher δ of post-elastic damage measures. Both low- and high-frequency measures (Tables 2.8 and 2.9) suffer from the vagaries (record-to-record) of the *general* shape of spectra of records, even here where they are from the same bin.

It has been shown by Kennedy et al. (1984) for SDOF structures that there may be a reduction in the variability of nonlinear responses when each record is averaged over a range of closely spaced sets of frequencies varying from the fundamental frequency of the structure to an equivalent reduced frequency that depends on the level of nonlinearity. In order to verify whether the above conclusion is valid for MDOF structures, we analyze Structures I and II. The results of this "local spectral averaging" are given in Table 2.10. In this case, in order to incorporate the higher modes as well, the averaging of the spectral ordinates is carried out at a closely spaced set of frequencies over a range that includes and is symmetric about the fundamental frequency. The records are then scaled to the median of this

Case	$\hat{S}_a(f_0, 2\%)(g)$	Damage	$\hat{\mu}$	δ_μ	$\hat{NHE}$	δ_{NHE}	$\hat{DI}$	δ_{DI}
Normalized	0.12	Global	1.6	0.18	3.1	0.40	0.7	0.26
to $\hat{S}_a(2\%)$		Max. St.	2.6	0.28	6.3	0.44	0.9	0.28
Normalized	0.12	Global	1.6	0.13	3.1	0.43	0.7	0.21
to $\hat{S}_a(5\%)$		Max. St.	2.7	0.21	6.4	0.48	0.9	0.24
Normalized	0.12	Global	1.6	0.12	3.1	0.54	0.7	0.25
to $\hat{S}_a(10\%)$		Max. St.	2.7	0.19	6.5	0.61	0.9	0.27
Normalized	0.12	Global	1.6	0.15	3.1	0.63	0.7	0.32
to $\hat{S}_a(20\%)$		Max. St.	2.7	0.19	6.4	0.72	0.9	0.32

Table 2.11: Damage measure results from Bin-I of Structure-I when the records are normalized to the median $S_a(f_0)$ at different damping levels. Note that the median spectral acceleration at 2% damping, $\hat{S}_a(f_0, 2\%)(g)$, are same for all the cases.

"frequency-averaged spectral acceleration" before being used in the structural analyses. In all the cases, a marginal reduction is gained provided the range is not too wide. We have observed, however, a more significant reduction in dispersion for a high-frequency MDOF structure (Shome and Cornell, 1998). If these spectral accelerations were to be used widely in the future, their adoption would require developing new attenuation laws, national PSHA maps, supporting software, etc. They have been used in site-specific modern nuclear power plant practice. For low-frequency structures these additional reductions do not appear to be worth the effort.

Table 2.11 shows the results when higher damping values are used to normalize the records. In this case, the records are normalized to the median spectral acceleration at the fundamental frequency of the structure, and the analysis is carried out for 2% damping. The use of higher damping was recommended by Kennedy et al. (1984) and is implicit in current methods, such as the capacity spectrum method (e.g., Freeman, 1978). We observe that ductility prediction is improved if damping values of 5% or more are used, but for NHE the δ increases. Damping at 10% and 20% appears to produce no better results than damping at 5% in ductility prediction. Table 2.12 shows the results of a combination of 5% damping and mild frequency averaging. The results are not improved over those we obtained from 5% damping without frequency averaging.

Case	$\widehat{Avg.}$ $S_a(g)$	δ of $Avg.S_a$	Damage	$\hat{\mu}$	δ_μ	$\hat{NHE}$	δ_{NHE}	$\hat{DI}$	δ_{DI}
Norm. to $\hat{S}_a(f_0, 5\%)$	0.12	0.74	Global	1.6	0.18	3.1	0.40	0.7	0.26
			Max. St.	2.6	0.28	6.3	0.44	0.9	0.28
Norm. to $S_a(5\%)$ and Avg. over $f_0 \pm 12.5\%$	0.12	0.73	Global	1.6	0.14	3.1	0.40	0.7	0.20
			Max. St.	2.7	0.20	6.4	0.47	0.9	0.22

Table 2.12: Damage measure results from Bin-I of Structure-I when the records are normalized to the median S_a averaged over a frequency range at higher level of damping (5%). Note the median of spectral acceleration at 2% damping as obtained from normalization to the spectral acceleration averaged over the frequency range, $\hat{Avg}.S_a(g)$, is same as the median $S_a(f_0, 2\%)(g)$.

Case	Frequency Range	$\widehat{Avg.}$ $S_a(g)$	δ of avg. S_a	Story Duct.		Story NHE	
				$\hat{\mu}$	δ_μ	$\hat{NHE}$	δ_{NHE}
Bin-IV Structure-I	f_0	0.24	0.63	6.9	0.42	43.1	0.69
	$f_0 \pm 12.5\%$	0.24	0.61	6.7	0.42	43.2	0.61
	$f_0 \pm 25\%$	0.24	0.62	6.7	0.39	43.3	0.58
	$f_0 \pm 50\%$	0.24	0.60	6.7	0.37	42.6	0.54
	$f_0 \pm 75\%$	0.24	0.55	6.5	0.39	41.3	0.50

Table 2.13: Results of the maximum interstory damage measures of Structure-I when the records in Bin-IV are normalized to the median 2%-damped S_a averaged over a range of frequencies.

One of the apparent limitations of the above results is that the level of nonlinearity (measured by median ductility, which is in the range of 1.2 to 1.7 for global ductility) in the structure is not very high. This means that the structure is not softening enough to be significantly affected by the change in the shape of the response spectra. In order to investigate this, we have carried out the above procedure of normalization at "frequency-averaged" spectral acceleration and at higher damping for Structure-I and Bin-IV records. The results of local spectral averaging are given in Table 2.13 and of higher damping are given in Table 2.14. The tables show that the conclusions of the previous paragraphs still hold for this higher level of nonlinearity.

Level of $\xi(\%)$	$\hat{S}_a(f_0, 2\%)$ (g)	$\hat{\mu}$	δ_μ	$\hat{NHE}$	δ_{NHE}	$\hat{DI}$	δ_{DI}
2.0	0.24	6.9	0.42	43.1	0.69	3.4	0.54
5.0	0.24	6.8	0.40	43.5	0.71	3.4	0.54
10.0	0.24	6.9	0.37	43.5	0.68	3.4	0.49
20.0	0.25	6.8	0.34	43.1	0.66	3.4	0.45

Table 2.14: Results of the maximum interstory damage measures from Bin-IV of Structure-I when the records are normalized to the median $S_a(f_0)$ at different damping levels.

We conclude from these results that the use of the conventional (non-frequency averaged) spectral acceleration and damping level (5%) is as effective a predictor of nonlinear MDOF behavior as any other measure of ground-motion intensity yet considered. It also permits the use of widely available attenuation laws and hazard results. In the following chapters we will carry out studies of other structures to confirm this conclusion.

2.9 Conclusions

In this chapter we have addressed several issues of seismic analysis of nonlinear structures. We will briefly summarize the findings of the major issues separately.

1. Scaling of Ground-motion Records and the Most Efficient Estimation Strategy: The nonlinear response (damage) measures from a suite of records which are chosen from a narrow magnitude and distance interval (or "bin") display wide dispersion (equal to, or greater than, that of the spectral accelerations). It is observed, however, that when the records in each bin are normalized or scaled to the bin-median spectral acceleration at the fundamental frequency of the structure, we obtain the *same* median damage measures with *reduced* variability compared to those of the unscaled sets of records. These conclusions imply that the most efficient way to estimate the nonlinear response from a given event (M and R) is to first use an established attenuation law to estimate this median spectral acceleration, and then to scale the records from roughly the same magnitude to this spectral acceleration before carrying out the nonlinear analyses. This procedure can reduce the number of runs required to estimate the median response by a factor of about 4.

We also scale the records in one bin to the higher and lower median intensity levels of other bins. In these cases, too, most of the median results are generally very close to the results of the unscaled case. The NHE damage measure may be an exception. Within broad limits, scaling records does not appear to bias nonlinear response estimates.

2. Different Methods of Scaling and Relative Advantages: Of several alternative scaling measures considered in this study (e.g., the commonly used scaling to the peak ground acceleration (PGA) level, scaling to the spectral acceleration level averaged over a frequency band, scaling to the spectral acceleration at a higher level of damping, etc.), the scaling of ground-motion records to the 5%-damped spectral acceleration at the fundamental frequency of the structure is best. The uncritical use of PGA is to be discouraged. The results from the other cases show some marginal reduction in variance, but the gain is not worth the effort.

3. Number of Records for Nonlinear Structural Analysis: If one wants to obtain an estimate of the median response within a factor of X (e.g., ± 0.1) with 95% confidence, one must use approximately $n = 4.0 \cdot \delta^2/X^2$ records. Typical values of δ are given in Table 2.2. Proper scaling reduces δ by about a factor of 2 (Table 2.3), reducing the required number of records by a factor of 4.

4. Estimation of Variance of the Damage Measures from Scaled Records: This statistic is required for the criteria that call for 84^{th} percentile demand and is also necessary for the probabilistic or performance-based design. Although it is observed that the scaled results have lower dispersion than those of the unscaled results, it is shown here how an adequate estimate of the standard deviation of the post-elastic damage measures can be recovered from the results of scaled records.

5. Dependence of Damage Measures on Earthquake and Ground-motion Parameters: The parameters considered in this study are magnitude, distance and duration of records. It has already been observed for SDOF structures that the response to scaled records (whether "direct" or "indirect") is not importantly dependent on any of those ground-motion parameters. The exception is perhaps the NHE, which shows some dependency on duration of records. The results of the present study confirm this trend for MDOF

structures. It can be anticipated that this conclusion may not be valid for longer-period structures because of a significant multi-mode effect.

6. Direct and Alternative/Indirect Approaches: The direct approach is easier to understand and apply to real-life problems. The alternative approach has the advantage of yielding the nonlinear capacity factor, F_μ. This factor helps one to compare the results for different structural systems and different parameter variations. We have demonstrated here that we can calculate the annual frequency of exceedance of a target level of damage measure both from the direct and indirect approaches, and we have shown that both approaches give consistent results in terms of structural performance levels (i.e., responses and probabilities).

Finally it should be remembered that all the above conclusions are derived here strictly from the study of a single MDOF structure. Like for many such structures, the elastic response is dominated by its first mode of vibration. For some of the issues, such as practical magnitude and distance independency of most post-elastic responses, previous studies of SDOF and MDOF have produced conclusions that the present study substantiates. For some other issues (e.g., duration dependency of post-elastic response, efficient ground-motion scaling parameters, etc.), however, little work has so far been done for MDOF structures. Further study is necessary for other types of structures, e.g., different heights, frequencies, force-deformation characteristics, etc., to confirm or modify the conclusions reported here.

Chapter 3

Probabilistic Seismic Demand Analysis: Simplified Approach

3.1 Introduction

In the last chapter we have made several important observations on different issues of nonlinear structural analysis, e.g., normalization and scaling of ground-motion records do not introduce any significant bias but do reduce the dispersion of damage measures (see Section 2.9). These observations were made strictly from the results of a simplified stick model representation of a 5-story steel moment resisting frame. In Appendix E we make similar observations for two nonlinear SDOF structures of frequencies 0.95Hz, and 4Hz. We find in the appendix that these observations are also valid for stick-model representations of two nonlinear MDOF structures whose first natural frequencies are the same as those of the SDOF structures. In this chapter we will verify whether these observations are valid for a more realistic 2-D model of a 5-story steel moment frame[1]. In Chapter 2 and in Appendix E we have not considered the P-Δ effect in nonlinear dynamic analyses. Now we will check whether inclusion of this parameter changes the conclusions in Chapter 2.

In Chapter 2 we have investigated the issue of scaling by using the results of bin of

[1]The 5-story structure we will consider in this chapter is different from the 5-story structure in Chapter 2.

records. This approach is straightforward. Another, even easier way to investigate this issue is to carry out regression analysis of nonlinear response results. This regression analysis will help to verify whether, given the first-mode S_a, the nonlinear structural responses are dependent on the seismological parameters (e.g., magnitude and distance of events), or on the record parameters (e.g., duration and spectral acceleration at frequencies higher than the elastic-first-mode frequency of a structure). If we find that the responses are not dependent or mildly dependent on these additional parameters, we can conclude that scaling of ground-motion records by the first-mode S_a is legitimate.

One of the problems with the binning approach used in Chapter 2 is that the magnitude, distance, spectral shape, and duration characteristics all vary from bin to bin. In the binning approach we cannot vary only one parameter at a time to find out its effect on nonlinear response. For example, if we vary the magnitude associated with the records by keeping the distance associated with those records the same, we will find that the spectral shape and duration also vary. It is therefore difficult to determine which parameter may explain a difference in results. The regression results on the other hand will help to identify the parameter that causes the difference in results. If the responses are dependent on more than one parameter, the regression analysis will help to select the more important parameter.

We will also investigate the "best" way (i.e., the most efficient from a computational point of view) to carry out the expensive nonlinear dynamic analyses. This helps one calculate as efficiently as possible the best estimate (i.e., the median) of the structural demand for a specified ground-motion intensity (as is required by the recent guidelines, e.g., FEMA-273). In addition, we can calculate the 84^{th} percentile demand from the results of bin of records when these records are scaled to a specified intensity. We believe, however, that a more desirable way to assess the possible performance of a structure is to estimate the probability of exceedance of a damage capacity. This estimation requires one to know the (median) demand induced by a range of potential spectral accelerations. This is facilitated by the proposed regression analysis of the damage-measure results.

At the end we will show how to calculate the probability of exceedance of a specified capacity with the example of the 5-story steel frame. We will calculate the seismic demand

of a structure in two different ways: direct and alternative (or indirect). In this chapter we will focus on the demand estimation of responses dependent on only one parameter, the spectral acceleration at the first mode. The calculation of the performance of structures for responses dependent on additional parameters will be shown in Chapter 5.

3.2 Design and Description of Structure

We consider here a five story steel residential building. The building has four special moment-resisting frames (SMRF) along the perimeter. See the plan of the building in Figure 3.1(a) and the elevation of the perimeter frame in Figure 3.1(b). Since the simple bay of the perimeter frame does not provide any significant lateral support against the earthquake loads, we will consider only the SMRF part of the perimeter frame for detailed analysis. The structure is designed for a central Los Angeles site with A36 steel for beams and A50 steel for columns following LRFD specifications (LRFD, 1994) and NEHRP provisions (FEMA-222, 1994). The dead loads and live loads on the structure are shown in Figure 3.2. The equivalent lateral force on the structure for the design earthquake load is calculated according to FEMA-222 (we have assumed $k = 2$ for vertical distribution of seismic forces), and is also shown in Figure 3.2. The earthquake-load parameters of a site are defined in the FEMA guideline by the effective peak acceleration coefficient (A_a) and the effective peak velocity coefficient (A_v). The value of these parameters for the site is equal to 0.4. The Seismicity Index of the site is 4 which is equivalent to UBC Zone-4. The site coefficient is 1.2, which corresponds to soil profile type S_2 of FEMA-222. The response modification factor, $\mathcal{R}$, of the frame is equal to 8; the deflection modification factor, C_d, is equal to 5.5. The structure is designed to satisfy the requirements of special moment resisting frames as given in UBC (1994). Some of these requirements are as follows: strength of the panel zones should be more than the shear force induced by gravity and seismic loads, the strength of the columns at a joint should be more than the strength of the beams at that joint to ensure the strong-column weak-beam design philosophy, etc. Finally the story deflections must be verified to be less than 1.5% of the story height. This limiting value is applicable for the

seismic hazard exposure group-II as per FEMA-222. Note that this limiting story drift criterion governs the design of the building. The size of the members and relevant member properties are indicated in Figure 3.1.

We analyze the 2-D SMRF by using the standard nonlinear beam-column element. The structure is considered fixed at the base. Each SMRF is assumed to carry half of the mass of the whole structure; thus it resists half of the lateral load in each direction. The masses of the structure at each floor level are shown in Figure 3.2. Because the columns derive their lateral stability in each direction from the two SMRFs along that direction, the additional P-Δ loading, which is equal to half of the total gravity load, is placed on a fictitious column. The fictitious columns are connected to the main structure by a fictitious, rigid link beam. This additional P-Δ load increases the moments in the columns at each floor level as the lateral story-displacements increase.

3.3 Results

3.3.1 Static-Pushover Analysis and Elastic-Modal Properties

At first, we study the global behavior of the structure by nonlinear step-by-step static analysis, popularly known as "static-pushover analysis". We carry out the analysis by using the DRAIN-2DX (1993) program. The lateral load pattern is calculated according to FEMA-222 provisions ($k = 2$). The plots of global and story load-deformation are shown in Figure 3.3. The response of the structure at different stages of pushover analysis under the applied load pattern is shown in Figure 3.4. These results indicate that the structure has a hardening post-yield stiffness and it is true even at very large drifts. Hence although we have considered for the first time P-Δ effect in our analysis, we do not expect any significant change in response of the 5-story structure due to this effect. Figures 3.3 and 3.4 help us to identify which members or stories are critical. We find that the first three stories are critical since the nonlinearity is concentrated mainly in these stories. The yield displacement, which is used to calculate the ductility or to calculate the normalized hysteretic energy, is obtained

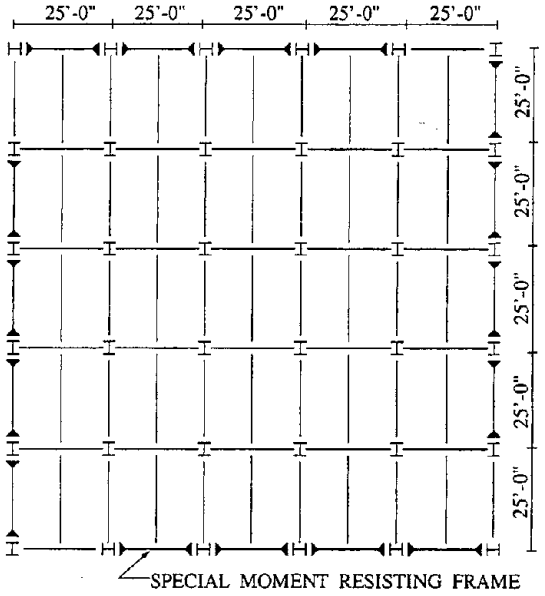

(a) Typical floor plan

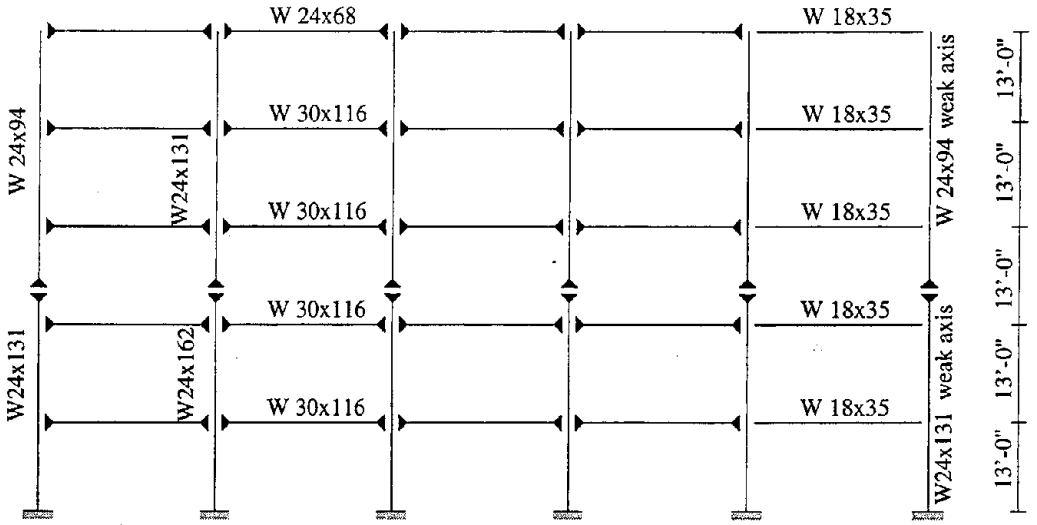

Note: Dimensions shown are centerline dimensions
Columns fixed at base
Four moment resisting bays and one simple bay
Column splice at 6'-0" above floor level

Analysis Parameters:
Beam: A36 Steel, $F_y = 49.2$ ksi
Column: A50 Steel, $F_y = 57.6$ ksi
Damping= 2%

(b) Elevation of the perimeter frame

Figure 3.1: Plan and elevation of the 5-story building.

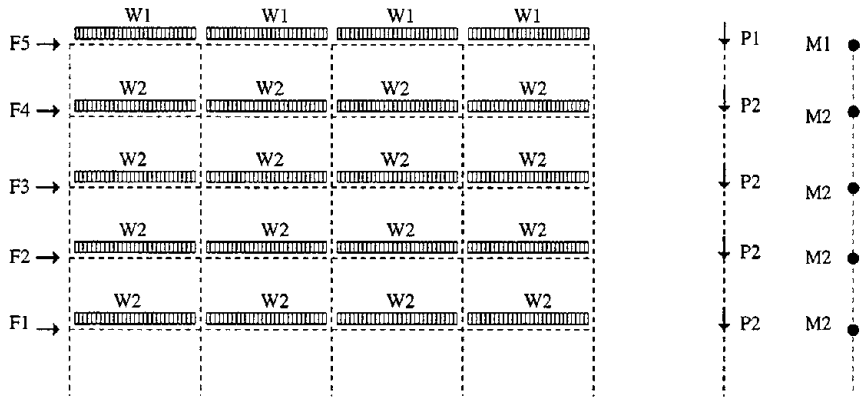

Figure 3.2: Different loads and floor mass of the 5-story building.

from the results of the pushover analysis. The frequency and modal mass participation at the first five modes are given in Table 3.1.

3.3.2 Selection of Records

The results of nonlinear dynamic analyses for earthquake loading are given below. We will use the same Bin-II and Bin-III records as before (see Chapter 2), but for Bin-I we will use 31 records, the maximum possible number of records available in the catalogue (Silva,

Mode	Period(sec)	Freq(Hz)	Mass Part(%)
1	1.09	0.92	0.81
2	0.38	2.65	0.12
3	0.21	4.65	0.04
4	0.15	6.87	0.02
5	0.11	9.09	0.01

Table 3.1: Periods, frequencies, and modal mass participations at different modes of excitation.

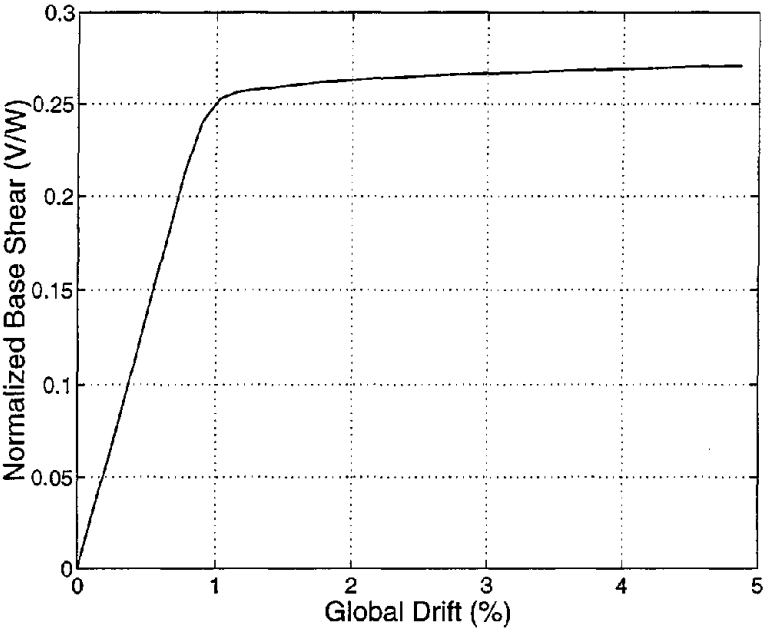

(a) Global force-displacement

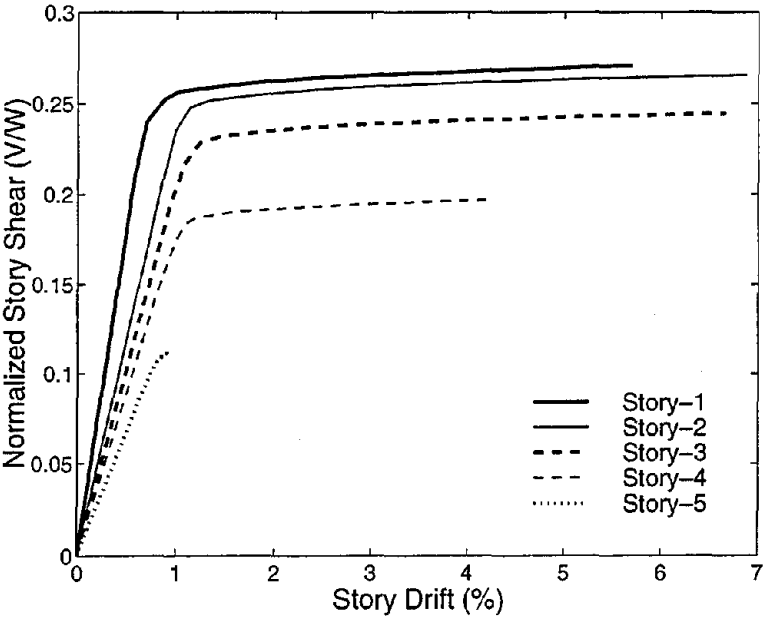

(b) Story force-displacement

Figure 3.3: Results from static pushover analysis for a 5-story building at a Los Angeles site. Here W is the seismic dead load of the structure and V is the shear force.

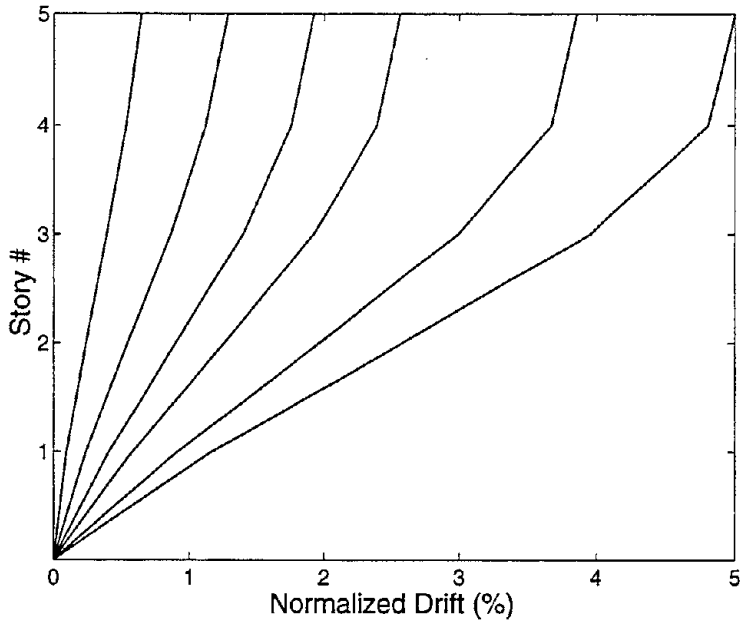

Figure 3.4: Deflected shapes at different stages of static pushover analysis of a 5-story structure at a Los Angeles site.

1995) for that bin. This increase in the number of records in Bin-I will give equal weight to the statistics of responses to high- and low-magnitude (M) events; we will thus avoid a bias to high- or low-magnitude events in our results if there is any systematic dependence of response on magnitude.

3.3.3 Direct Results

The "direct" results we will present below are not from the as-recorded accelerograms that we used to obtain the results in Chapter 2. Since the building is designed to behave elastically for strong ground-motion, we will observe inelastic behavior of the structure from only a very small number of records if we use the as-recorded accelerograms. We find in Figure 3.4 that the maximum normalized base shear or the base shear coefficient is around 0.15, whereas we find in Table 2.1 that for low-magnitude and close-distance or high-magnitude and long-distance records the median spectral acceleration at 1Hz is about

0.1g. Hence we expect nonlinear behavior of the structure mainly from high-magnitude and close-distance records. In order to get interesting results from all types of records we scaled down the structure in Chapter 2 by a constant factor by reducing the yield displacement of the members. In the present study, however, we will first scale up all the records by a common value, the ratio of a target spectral acceleration to the bin-median spectral acceleration at the first-mode frequency and 2% damping. We have defined this spectral acceleration as the *structure-specific-intensity* of ground-motion. Alternatively we can call this method "cloud-scaling" because we are scaling a cloud of data points to an intensity level that is different from the sample central level. The different approaches of nonlinear seismic analyses we have introduced so far are direct analysis, normalized analysis, scaled analysis, and "direct" (cloud-scaled) analysis. The differences among these methods are illustrated in Figure 3.5. The cloud-scaling of the records will retain the scatter of the spectral acceleration (i.e., the same δ_{S_a}). These records differ from the original records in so far as their intensity level, but retains the characteristics of the spectral shape (i.e., frequency content) and duration of the original records. We will consider a very high target spectral acceleration, 2.5g, which corresponds to a 5000-year return period, a high target spectral acceleration, 1.5g, which corresponds to a 2475-year return period (or a probability of exceedance of 2% in 50 years) level, and a low target spectral acceleration, 0.5g, which corresponds to a 75-year return period (or a probability of exceedance of 50% in 50 years). At the high-target spectral acceleration, the structure gives a highly nonlinear response, whereas at the low-target level we get on average virtually linear response. Considering the results at these target spectral accelerations will help us to verify the conclusions drawn in Chapter 2 at high as well as at low levels of nonlinearity. Also the regression analysis we will carry out later on will be valid for a wide range of spectral accelerations.

The results of the direct calculations of some important damage measures are given in Table 3.2 and the results of all the damage measures at all the three spectral acceleration levels are given in Table 3.3. We observe that the dispersion of Bin-II spectral accelerations at 0.9Hz is quite high compared to that estimated by attenuation results (0.96 for the Bin-II records versus 0.62 from the attenuation results by Abrahamson and Silva, 1997). This high

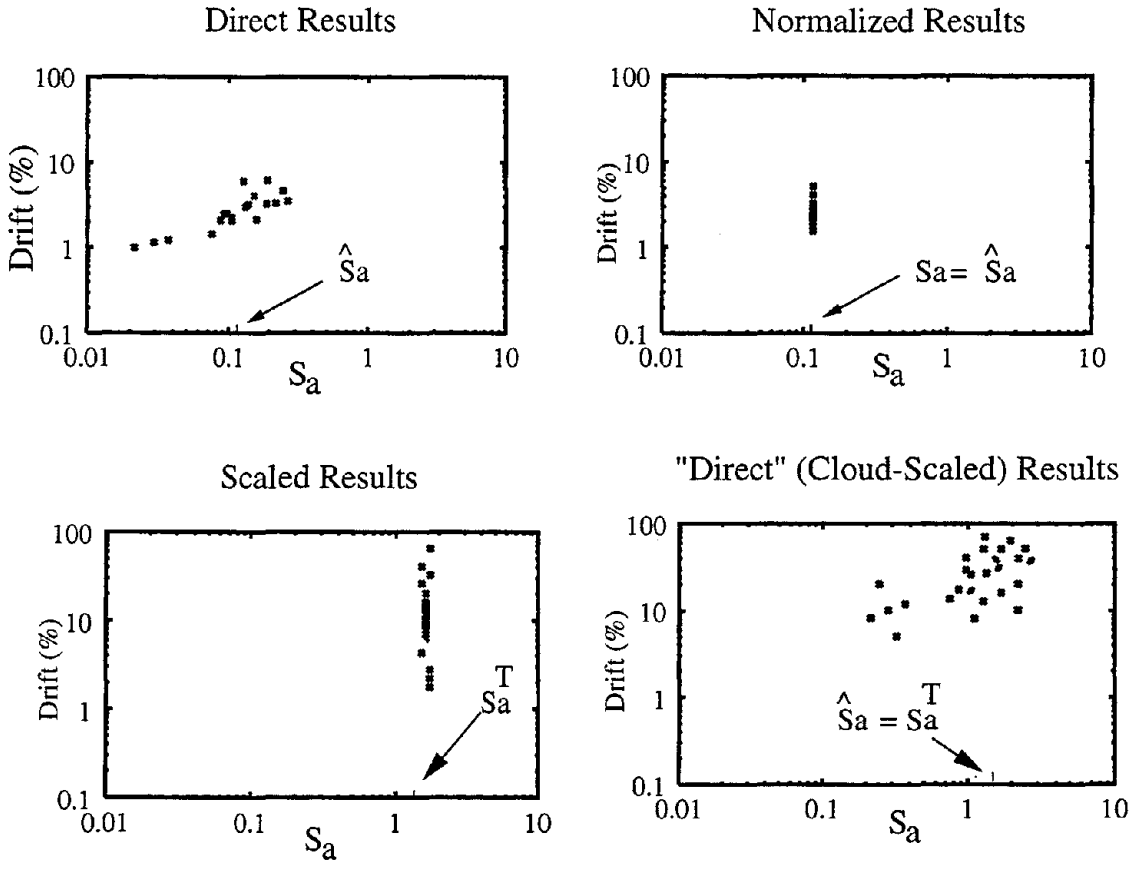

Figure 3.5: Typical results from direct, normalized, scaled, and "direct" (cloud-scaled) analysis.

Case	$\widehat{S_a}$	δ_{S_a}	Global		Story		Local	
			System Drift		Max Drift		Max Pl. Rot.	
			$\hat{D}_{sy}(\%)$	$\delta_{D_{sy}}$	$\hat{D}_{st}(\%)$	$\delta_{D_{st}}$	$\hat{\theta}_{CP}(\%)$	$\delta_{\theta_{CP}}$
Bin-I "Direct"	1.5	0.80	2.3	0.46	3.0	0.54	1.9	1.10
	0.5	0.80	1.0	0.50	1.2	0.52	-	-
Bin-II "Direct"	1.5	0.96	2.6	0.77	3.4	0.83	2.0	1.35
	0.5	0.96	1.0	0.72	1.2	0.74	-	-
Bin-III "Direct"	1.5	0.51	2.6	0.46	3.5	0.55	2.6	0.72
	0.5	0.51	1.0	0.41	1.2	0.42	-	-
Bin-I Normalized	1.5	0.00	2.4	0.30	3.0	0.36	1.8	0.43
	0.5	0.00	1.0	0.19	1.3	0.28	-	-
Bin-II Normalized	1.5	0.00	2.7	0.30	3.6	0.38	2.8	0.49
	0.5	0.00	1.0	0.17	1.2	0.23	-	-
Bin-III Normalized	1.5	0.00	2.8	0.24	3.7	0.32	2.8	0.45
	0.5	0.00	1.1	0.14	1.3	0.21	-	-

Table 3.2: "Direct" and scaled results of different damage measures from Bin-I, Bin-II, and Bin-III ground-motion records. The spectral acceleration S_a is calculated at the fundamental frequency (0.9Hz) and at 2% damping. The results of other damage measures are given in Table 3.3.

dispersion of the records is, however, local in nature as we get a close match of dispersion at 0.95Hz and at other frequencies (see Table 2.1 of Chapter 2). The damage measures we consider here are global drift, global NHE (normalized hysteretic energy), system drift (which we define here as the average of story drifts), maximum story drift (D_{st}), maximum story NHE, maximum beam plastic rotation (θ_{BP}), and maximum column plastic rotation (θ_{CP}). We define here the global drift as the maximum drift at the top of a structure relative to its base divided by the total height of that structure. The story drift is the maximum lateral displacement of a story of a structure divided by the height of that story.

We observe that the median drift results at the same spectral acceleration levels are very close to each other. The same is true for the plastic rotation damage measure except for the maximum beam plastic rotation results (compare the Bin-I to the Bin-III results). The difference in results, however, is found to be statically insignificant (in Chapter 2 we described the procedure to check whether or not the difference in results is statistically

Case	$\widehat{S}_a$ (0.9Hz,2%)	δ_{S_a}	Global Drift $\hat{D}_{gl}(\%)$	δ_D	Global NHE $\widehat{NHE}_{gl}$	δ_{NHE}	System Drift $\hat{D}_{sy}(\%)$	δ_D	Max Story Drift $\hat{D}_{st}(\%)$	δ_D	Max Story NHE $\widehat{NHE}_{st}$	δ_{NHE}	Max Plastic Rotation $\hat{\theta}_{beam}(\%)$	δ_θ	$\hat{\theta}_{column}(\%)$	δ_θ
Bin-I "Direct"	2.5	0.80	3.2	0.62	17.9	1.14	4.0	0.52	6.1	0.62	62.9	1.12	3.8	0.71	5.0	0.86
	1.5	0.80	1.8	0.51	4.2	1.55	2.3	0.46	3.0	0.54	14.1	1.56	1.1	2.95	1.9	1.10
	0.5	0.80	0.8	0.53	-	-	1.0	0.50	1.2	0.52	-	-	-	-	-	-
Bin-II "Direct"	2.5	0.96	2.8	0.78	12.5	1.76	3.7	0.64	5.1	0.71	41.1	1.78	3.2	1.03	3.8	1.07
	1.5	0.96	2.1	0.88	4.9	2.22	2.6	0.77	3.4	0.83	16.0	2.43	1.9	1.27	2.0	1.35
	0.5	0.96	0.8	0.80	-	-	1.0	0.72	1.2	0.74	-	-	-	-	-	-
Bin-III "Direct"	2.5	0.51	3.6	0.53	16.0	0.66	4.3	0.46	6.6	0.59	57.7	0.83	4.6	0.68	5.5	0.72
	1.5	0.51	2.1	0.52	5.4	0.85	2.6	0.46	3.5	0.55	20.6	0.94	2.3	0.69	2.6	0.72
	0.5	0.51	0.9	0.41	-	-	1.0	0.41	1.2	0.42	-	-	-	-	-	-
Bin-I Scaled	2.5	0	3.2	0.33	16.7	0.65	4.0	0.29	5.7	0.44	57.6	0.70	3.7	0.44	5.0	0.54
	1.5	0	1.8	0.28	5.3	0.67	2.4	0.30	3.0	0.36	16.7	0.70	1.8	0.43	2.0	0.54
	0.5	0	0.9	0.13	-	-	1.0	0.19	1.3	0.28	-	-	-	-	-	-
Bin-II Scaled	2.5	0.00	3.7	0.45	22.0	0.64	4.5	0.40	6.6	0.54	74.1	0.77	4.5	0.57	5.4	0.68
	1.5	0	2.1	0.32	7.5	0.56	2.7	0.30	3.6	0.38	27.2	0.66	2.4	0.41	2.8	0.49
	0.5	0	0.9	0.11	-	-	1.0	0.17	1.2	0.23	-	-	-	-	-	-
Bin-III Scaled	2.5	0	4.3	0.41	21.4	0.46	5.1	0.35	7.8	0.46	79.1	0.54	5.6	0.51	7.1	0.54
	1.5	0	2.3	0.30	7.1	0.47	2.8	0.24	3.7	0.32	25.7	0.54	2.4	0.45	2.8	0.45
	0.50	0	0.9	0.09	-	-	1.1	0.14	1.3	0.21	-	-	-	-	-	-

Table 3.3: "Direct" and scaled results of different damage measures from Bin-I, Bin-II, and Bin-III ground-motion records.

Case	$\widehat{S}_a$ (0.9Hz,2%)	δ_{S_a}	Global Drift $\hat{D}_{gl}(\%)$	δ_D	Global NHE $\widehat{NHE}_{gl}$	δ_{NHE}	System Drift $\hat{D}_{sy}(\%)$	δ_D	Max Story Drift $\hat{D}_{st}(\%)$	δ_D	Max Story NHE $\widehat{NHE}_{st}$	δ_{NHE}	Max Plastic Rotation $\hat{\theta}_{beam}(\%)$	δ_θ	$\hat{\theta}_{column}(\%)$	δ_θ
Bin-I																
1st Mode, $\xi = 2\%$	1.5	0	1.8	0.28	5.3	0.67	2.4	0.30	3.0	0.36	16.7	0.70	1.8	0.43	2.0	0.54
1st Mode, $\xi = 5\%$	1.5	0.11	1.9	0.26	6.9	0.61	2.6	0.24	3.4	0.30	20.8	0.71	2.2	0.37	2.7	0.51
Freq Avg($f_0 \pm 25\%$),$\xi = 2\%$	1.5	0.24	2.0	0.20	6.6	0.43	2.6	0.17	3.4	0.22	20.3	0.57	2.0	0.26	2.4	0.38
Bin-II																
1st Mode, $\xi = 2\%$	1.5	0	2.1	0.32	7.5	0.56	2.7	0.30	3.6	0.38	27.2	0.66	2.4	0.41	2.8	0.49
Freq Avg($f_0 \pm 25\%$),$\xi = 2\%$	1.5	0.16	2.1	0.27	7.4	0.44	2.7	0.25	3.6	0.32	26.8	0.57	2.3	0.35	2.8	0.42
Bin-III																
1st Mode, $\xi = 2\%$	1.5	0	2.3	0.30	7.1	0.47	2.8	0.24	3.7	0.32	25.7	0.54	2.4	0.45	2.8	0.45
Freq Avg($f_0 \pm 25\%$),$\xi = 2\%$	1.5	0.19	2.2	0.27	6.8	0.39	2.7	0.22	3.7	0.29	24.2	0.52	2.3	0.42	2.7	0.45

Table 3.4: Results of different intensity scaling schemes from different bins.

significant). The results of the NHE results are, however, statistically significantly different.

We observe that for the global and maximum story-drift calculations, the dispersions are quite similar both at high and low levels of spectral acceleration. This indicates that drift is primarily dependent on spectral acceleration. The dispersions are, however, lower than the dispersion of ground-motion spectral accelerations at the first mode. The dispersion of maximum plastic rotation at higher target levels is little higher than the dispersion of spectral acceleration at the first mode, whereas that of global and maximum story NHE are much higher. We also observe that the dispersion of drift damage measure goes up with the increase in median drift. The apparent decrease in dispersion of NHE and plastic rotation with the increase in the intensity of ground motion are due to the fact that these damage measures, unlike drift, are not a continuous function of spectral acceleration. These damage measures do not have any value below a threshold spectral acceleration level, and the logarithms of these values are $-\infty$. So with the increase in spectral acceleration level we get fewer responses of no value; thus we get less dispersion at a higher spectral acceleration level, i.e., at a higher median response. The significance of higher dispersion will be discussed below. We do not compute the statistics of NHE and plastic rotation damage measures at the lowest target level. As discussed before, since this target level is very close to the threshold level, we do not get any significant result for the NHE and plastic rotation damage measures at the low target level spectral acceleration.

The high value of the dispersion of damage measures indicates that the confidence band width of the median is quite high. For the typical number of records used in practice (n$\approx$ 5; see SEAOC, 1996 or FEMA-273, 1996) and for the Bin-I records at the higher target level ($S_a[0.9Hz, 2\%]$=1.5g), the "one-sigma" (i.e., 65% confidence) confidence band on the median maximum-story drift would be 2.4% to 3.9% (confidence band width= $\hat{D} \cdot e^{\pm \frac{\delta}{\sqrt{n}}}$), that of maximum story NHE would be 7.0 to 28.3, and that of maximum column plastic rotation 1.8% to 3.5%. As these estimates of the median are not sufficiently reliable, we would need to increase the sample size (n). Note that because of higher dispersion of plastic rotation and NHE we need larger sample size to estimate the median of those damage measures than the sample size required to estimate the median drift. But this increase of

sample size is a very expensive proposition from a computational point of view. Instead of increasing the sample size we will, as we have done before (see Chapter 2), investigate some other methods, e.g., normalization or scaling, to improve the estimation of median damage measures *without* increasing the prevailing standard of sample size (3 to 7 as per SEAOC, 1996).

3.3.4 Scaled Results

In this case, all the records in each bin are scaled to a target intensity level. The results from these scaled records are given in Table 3.2. First we observe that the medians of different damage measures from direct and scaled results are virtually the same at the same median intensity level. The small differences in the median values, moreover, are not statistically significant. As in Chapter 2, we can conclude that the scaling of ground-motion records does not introduce any bias in damage estimation. Note ,however, that in this case the perimeter moment-resisting frame is represented by a 2-D model, unlike in Chapter 2, where we considered only the simplified stick model representation. Here we have considered the P-Δ effect as well. This is one of the reasons the "second stiffness" in the approximately bilinear global static-pushover curve [Figure 3.3(a)] is only about 2% of the initial stiffness.

The advantage of using scaled rather than direct results is that scaling reduces the dispersion of damage estimations. See the Bin-II results. Initially the records in this bin had very high dispersion of spectral acceleration and so we got the highest dispersion of response, but after scaling the dispersion of response is very similar to that of the other bins. The reduction of dispersion of drift is 33% to 50%; for NHE and plastic rotation the reduction is much more than 50%. Figure 3.5 helps us understand how the median and dispersion of different damage measures vary along different stories. We observe that the median of the scaled results is the same as that of the direct results, whereas the dispersion is much lower for the scaled results. For the drift calculations, the requirement of sample size is 25% to 50% lower for the scaled results ($n_{scaled}/n_{direct} = [\delta_{scaled}/\delta_{direct}]^2$), and for the NHE and plastic rotation it is even lower than 25%. We also observe that as all the damage measures are dependent primarily on intensity or spectral acceleration (see Chapter 2), we

get a higher dispersion in response from direct analysis when the dispersion of the intensity of the ground motion is higher (compare the Bin-II with the Bin-III direct results). But in scaled analysis, the dispersions are quite constant for all the bins, e.g., the dispersion of maximum story drift is between 0.30 to 0.40 (lowest among all the damage measures), that of maximum plastic rotation is between 0.40 to 0.50, and that of maximum story NHE is between 0.60 to 0.70. Note that the dispersion of NHE is nearly double the dispersion of drift. The implication of this observation is that if we need to implement fully energy-based damage measures, we will need a higher sample size (by nearly a factor of 4) than is needed for displacement-based damage measures, even if we scale the records.

Although the scaling of records to the target spectral acceleration at the first mode reduces the dispersion significantly, we have already observed in Chapter 2 that we can further reduce the dispersion by improving the above simple scaling scheme. We found that the dispersion of damage measures can be somewhat reduced mainly in two different ways: using higher damping values and using frequency-averaged spectral acceleration. The results of scaling at higher damping, 5%, and frequency averaging ($f_0 \pm 25\%$) are given in Table 3.3. We observe that there is some reduction in dispersion and the results are not biased. Now the question is, are these procedures useful? We can answer this question from the point of view of computational gain, i.e., the reduction of sample size requirement. In order to determine this gain, we calculate the number of records required for a $\pm 10\%$ one-sigma confidence band width of the median damage measures from different scaling schemes ($n = [\delta_{scaled}/0.10]^2$); the results are given in Table 3.5. The results show that compared to the simple first-mode scaling, frequency-averaged scaling significantly reduces the sample size required for the Bin-I records but results in only a minor reduction for the other two bins. Recall that in Chapter 2 we also did *not* get any significant reduction in dispersion by using a stick model of similar structure. We have observed, however, that for high frequency structures the reduction is significant (see Shome and Cornell, 1998). We can conclude that we do get some reduction in dispersion by using these improved procedures. Because our goal is to estimate the probability of exceedance of a target response level or performance of a structure under earthquake loading, we need to find out how we can utilize these results

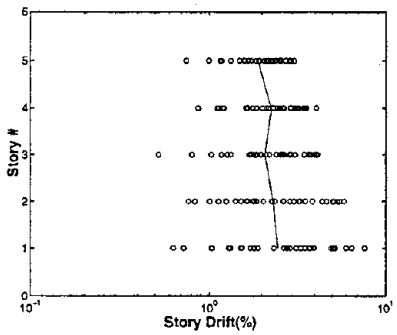

(a) Direct results: Maximum Story Drift

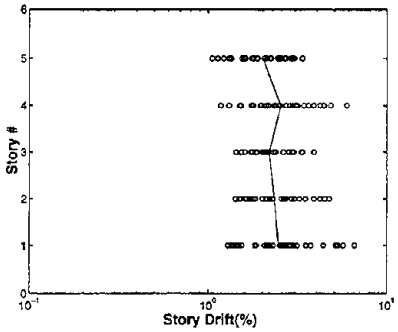

(b) Scaled Results: Maximum Story Drift

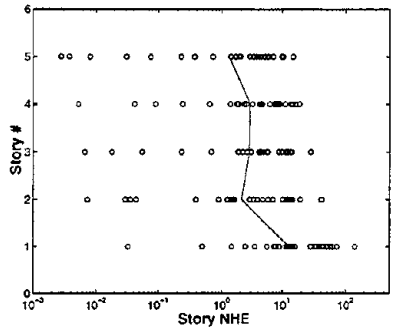

(c) Direct results: Maximum Story NHE

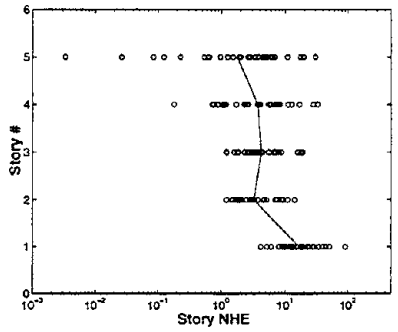

(d) Scaled Results: Maximum Story NHE

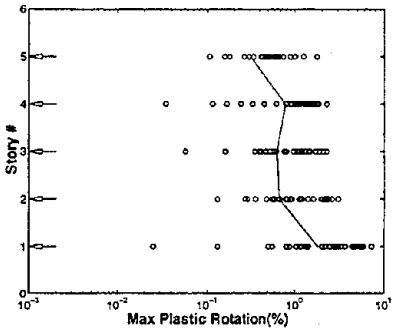

(e) Direct results: Maximum Column θ_{CP}

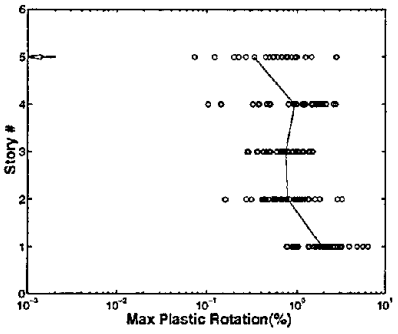

(f) Scaled Results: Maximum Column θ_{CP}

Figure 3.5: Comparison of direct and scaled results of different damage measures from Bin-I records. The arrows indicate that some plastic rotation (θ_{CP}) data points are beyond the range of the plot (i.e., they are zero).

Bin	Case	Number of records			
		Global	Story		Local
		Syst. Drift	Max St. Drift	Max St. NHE	Max Col. θ_{CP}
I	Direct	22	30	244	121
	First Mode($\xi = 2\%$) Scaling	9	13	49	29
	First Mode($\xi = 5\%$) Scaling	6	9	50	23
	Freq. Avg.($\xi = 2\%$) Scaling	3	5	33	15
II	Direct	60	69	591	183
	First Mode($\xi = 2\%$) Scaling	9	15	44	24
	Freq. Avg.($\xi = 2\%$) Scaling	6	11	30	21
III	Direct	22	31	89	52
	First Mode($\xi = 2\%$) Scaling	6	11	30	21
	Freq. Avg.($\xi = 2\%$) Scaling	5	9	27	21

Table 3.5: Number of records required for a $\pm 10\%$ one-sigma confidence bandwidth of the median damage measures for different scaling schemes.

to attain that goal *economically*. As we will discuss below, the use of higher damping in the calculation of risk is very straightforward, whereas frequency averaging is comparatively cumbersome. If the frequency band width is the same for all the structures (say $\pm 25\%$) then we would need to develop an attenuation law for frequency-averaged spectral acceleration. Otherwise we would need attenuation results specific to the frequency-band requirement of the structure. In all these cases we would need to carry out the seismic hazard analysis for these frequency-averaged attenuation results. If the nonlinear structural analysis is very expensive then this frequency-averaged spectral acceleration may be worth pursuing, otherwise we recommend using the higher-damping scaling[2] to gain this benefit of extra reduction in dispersion *at no extra effort*.

We have observed that although we can reduce the dispersion of damage measures without introducing any bias by scaling the records to the first-mode spectral acceleration at a higher damping or to a frequency-averaged spectral acceleration, the dispersions of

[2]Note that this higher damping is used solely for scaling of the records. We should use the lower 2% damping for structural analysis.

the various damage measures of the scaled results are still quite significant (see Table 3.3). We need to investigate other factors on which responses depend. This investigation may suggest a way to reduce the sample size and it will certainly give insight into the causes of the variability of response. Below, we will investigate some parameters other than the spectral acceleration at the first mode to explain the variabilities of scaled response. We will consider a particular bin so that the number of variables to look into is reduced. When we scale the records of a particular bin to the same spectral-acceleration level, the records have similar magnitude (M), distance (R), and first-mode spectral acceleration. These scaled records have different spectral accelerations at frequencies other than the scaling frequency, and have different durations. We will also investigate below the effect of including some of these parameters on the dispersion of scaled results.

Effect of Duration and Second-Mode Spectral Acceleration

We will investigate the extent which the independent parameters duration[3] D and spectral acceleration at the second mode S_{a2} can explain the differences in results scaled to a common S_{a1}. In order to investigate this issue, we assume the functional dependency of response on the independent parameters is of the form $Y = \alpha \cdot X^{\beta}.\varepsilon$ where α and β are the regression parameters and ε is the random error[4]. Next we carry out a regression analysis of the scaled results by fitting this model to the sample of results. We consider only the results obtained by scaling the records to the 1.5g spectral acceleration at the first mode. The results of regression analysis are given in Table 3.6. Note that these results are effectively the conditional dependence response on S_{a2} given, for example, the value of S_{a1}. The adjusted coefficient of determination (R_a^2) given in the table is the fraction of the total

[3] We have considered here the definition of bracketed duration as proposed by Trifunac and Brady (1975). This duration is defined as the difference in times corresponding to 95% and 5% of the total input energy carried by a record. The input energy up to a time, t_1, is calculated as the integral of the square of the acceleration time history, which is given by

$$E(t_1) = \int_0^{t_1} a^2(t)\, dt \tag{3.1}$$

where, $a(t)$ is the acceleration at a time t. Note that this duration measure is a property of a record.

[4] We will discuss the regression analysis of response results in detail in Section 3.4.

variance of damage measures explained by the independent variable duration or S_{a2}. This coefficient takes into account the number of parameters considered in the regression model. So although adding parameters in the regression model reduces the regression error or at least keeps it at the same value, the R_a^2 value in the limit starts decreasing with the increase in the number of parameters (see Neter et al., 1996, for details). The R_a^2 value is approximately related to the percentage reduction in the dispersion of response when no predictor variable, e.g., duration or S_{a2}, is considered. The reduction in dispersion is approximately equal to $1 - \sqrt{1 - R_a^2}$. So after scaling the Bin-I records to the first-mode spectral acceleration, if we consider the second-mode spectral acceleration S_{a2} to explain the variability of the scaled response, we can explain $1 - \sqrt{1 - 0.38}$ or 21% of the dispersion of the scaled response. We find that the difference of displacement-based damage measures, i.e., drift and plastic rotation, can be explained partly by the second-mode spectral acceleration, and the difference in energy-based damage measures, i.e., NHE, can be explained partly by the duration and partly by the second-mode spectral acceleration when the records are scaled to the same spectral acceleration at the first mode. Although these findings in themselves are quite interesting, we need to find out how much we gain in terms of percentage reduction of the dispersion of a damage measure relative to the dispersion from direct analysis, i.e., before conditioning on S_{a1}. We will investigate this issue formally in the following section when we carry out the regression analysis of different damage measures against various independent variables.

3.4 Magnitude, Distance, and Duration Dependency of Response

We have observed that the median drifts and plastic rotations are quite similar for all the bins when records are scaled to the same median spectral acceleration level (see Table 3.2). This suggests that the displacement response does not depend significantly on magnitude, or distance, or implicitly on duration of ground-motion. Table 3.6 confirms the general lack of duration dependency explicitly. The difference between NHE results, however, indicates

Damage Measure	Bin	S_a at 2nd mode		Duration	
		Function	R_a^2	Function	R_a^2
Max	I	$D_{st} = 0.02 \cdot S_{a2}^{0.33}$	0.38	-	≈ 0
Story	II	$D_{st} = 0.02 \cdot S_{a2}^{0.40}$	0.47	-	≈ 0
Drift(D_{st})	III	-	≈ 0	-	≈ 0
Max	I	$NHE = 6.96 \cdot S_{a2}^{0.546}$	0.23	-	≈ 0
Story	II	-	≈ 0	$NHE = 5.20 \cdot D^{0.59}$	0.16
NHE	III	-	≈ 0	$NHE = 5.20 \cdot D^{0.64}$	0.35
Max	I	$\theta_P = 0.01 \cdot S_{a2}^{0.43}$	0.27	-	≈ 0
Column	II	$\theta_P = 0.02 \cdot S_{a2}^{0.37}$	0.20	-	≈ 0
θ_P	III	-	≈ 0	-	≈ 0

Table 3.6: Results of regression analysis of different damage measures from the records *scaled to the 1.5g first-mode spectral acceleration.* R_a^2 is the adjusted coefficient of determination, which gives approximately the fraction of the total variance of the damage measure that is explained by the independent variable duration, or S_{a2}.

that there might be some dependency of NHE response on magnitude, distance, or duration. Assuming the distribution of different damage measures to be lognormal (we verify this assumption in Appendix C), we can investigate whether the difference in median damage measure from different bins is statistically significant. We consider the Bin-I and Bin-III results scaled to 1.5g spectral acceleration. For the maximum interstory drift results, we find the ratio of the medians is 1.2 (=3.7/3.0), and the standard error of estimation of this ratio is 0.10 ($= \sqrt{(\delta_1/n_1)^2 + (\delta_2/n_2)^2} = \sqrt{(0.36/31)^2 + (0.32/20)^2}$). The $\pm$ one-sigma confidence band of this ratio is $1.2e^{\pm 0.10}$ or 1.1 to 1.3; we can conclude that there is a very mild dependency of drift calculations on the magnitude of earthquakes when the records are scaled to the same intensity level (note that the difference in magnitude between the Bin-I and Bin-III records is 1.5). We have made similar observations for other structures (see Shome and Cornell, 1998). Similarly we calculate the $\pm$ one-sigma confidence band of the ratio of the medians for other damage measures. For system drift (global displacement-based damage measure), this value is between 1.1 to 1.3; for maximum column plastic rotation (local displacement-based damage measure) it is 1.2 to 1.6; for maximum story NHE (story energy-based damage measure), it is 1.3 to 1.8. Note that the

dependency of energy-based damage measures on bin parameters is much higher than the dependency of displacement-based damage measures. The other significant observation we make here is that the dependency increases progressively from global to story and from story to local damage measure. All these observations indicate that the responses depend on the characteristics of the bins, e.g., magnitude, duration, distance, etc. However, from these calculations we cannot determine which parameter can explain or make a larger contribution to these differences in results. The regression analysis of the results for different independent parameters will help us understand this issue.

We will carry out the regression analysis of different damage measures on different independent variables. These are spectral acceleration at the first and the second mode (S_{a1} and S_{a2}), magnitude (M), distance (R), and duration (D) (see Footnote 3 for a description of the duration measure adopted here). We assume the functional dependency of damage measures (Y) on different independent parameters is of the form

$$Y = \underbrace{\alpha \cdot S_{a1}^{\beta_1} \cdot S_{a2}^{\beta_2}}_{Term-1} \cdot \underbrace{e^{\beta_3 . M} \cdot R^{\beta_4}}_{Term-2} \cdot \underbrace{e^{\beta_6 \cdot D}}_{Term-3} \cdot \varepsilon \tag{3.2}$$

where

$\alpha, \beta_1, \ldots, \beta_7$ = regression parameters.

ε = random error term with median= 1, and standard deviation= $\delta_\varepsilon = \sigma_{\ln \varepsilon}$.

Term-1 represents the proportional decrease in strength ("softening") of a structure with the increase of "structure-specific-intensity" of ground motion. *Term-2* represents the primary standard variables used in attenuation studies (see Joyner and Boore, 1981). The exponent β_3 represents the magnitude dependency of the response, and the R term represents in effect a simple point-source geometric spreading. *Term-3* represents the increase in response of a structure (as expected by structural engineers) with the increase in the duration of ground motion. We have tried another form of *Term-3* which is D^{β_6}, but this form has lower correlation with the damage measures than the form adopted in Equation 3.2.

Note that an advantage of this regression model is that it is linear in log-space. The

regression results we will present now are obtained by fitting the sample of results to the logarithm of Equation 3.2 by standard linear regression analysis. We have already observed that spectral acceleration at the first mode is strongly correlated to the damage measures and explains most of the dispersion of damage measures. We will therefore first carry out the regression analysis on spectral acceleration at the first mode (S_{a1}), and then we will include the other independent variables to check for any additional significant reduction in the regression error (δ_ε). As we are interested in assessing and displaying the dependence of responses on different seismological or record parameters conditioned on the first-mode spectral acceleration (S_{a1}), we scale the records first to the same spectral acceleration level. In regression analyses we will use the results from all the bins, i.e., Bin-I, Bin-II, and Bin-III, scaled to the 0.5g, 1.5g, and 2.5g spectral acceleration levels.

The results of regression analysis are given in Table 3.7 for the three most important damage parameters: maximum story drift, maximum story NHE, and maximum column plastic rotation. The R_a^2 values indicate that most of the variability of the damage measures is explained by the first-mode spectral acceleration. This observation again confirms that scaling the ground-motion records to the first-mode spectral acceleration (what we have done in Section 3.3.4) is an efficient way to reduce the dispersion of damage measures. This will not introduce any bias in the median damage results if the damage measures are not importantly dependent on parameters other than the first-mode spectral acceleration. The variation of these three damage measures with the first-mode spectral acceleration is shown in Figure 3.6 (note that we have plotted the dependent variable, deformation, as the abscissa following the traditional "force"-deformation plots). We observe that the interstory drift varies linearly with spectral acceleration, whereas the interstory NHE varies nonlinearly (both the damage measures, however, vary linearly with spectral acceleration in log-space). Note that the other displacement-based damage measure, column plastic rotation (θ_{CP}), is linear at high S_a. We observe in Figure 3.3 that we get nonlinearity in the structure vis-a-vis plastic rotation in columns only when story drift is more than 1%, i.e., $S_a \geq 0.5g$. So θ_{CP} is nearly linear beyond 0.5g. These regression results are valid from 0.5g to 2.5g first-mode spectral acceleration or from 0.5% to 10% maximum interstory drift. The wide

Damage Measure	Independent Variable(s)	Regression Function	R_a^2	δ_ε	n_{req}
	S_{a1}	$\boldsymbol{D_{st} = 0.03 \cdot (S_{a1})^{1.00}}$	0.76	0.38	15
Maximum	S_{a1}, S_{a2}[5]	$\boldsymbol{D_{st} = 0.02 \cdot (S_{a1})^{0.75} \cdot (S_{a2})^{0.25}}$	0.80	0.35	12
Story	S_{a1}, M	$\boldsymbol{D_{st} = 0.01 \cdot (S_{a1})^{1.00} \cdot e^{0.13M}}$	0.77	0.37	14
Drift (D_{st})	S_{a1}, R	$\boldsymbol{D_{st} = 0.02 \cdot (S_{a1})^{1.00} \cdot R^{0.11}}$	0.76	0.37	14
	S_{a1}, D	$D_{st} = 0.03 \cdot (S_{a1})^{1.00} \cdot e^{0.003D}$	0.76	0.38	15
	S_{a1}	$\boldsymbol{NHE = 7.29 \cdot (S_{a1})^{2.52}}$	0.85	0.71	51
Maximum	S_{a1}, S_{a2}	$\boldsymbol{NHE = 4.58 \cdot (S_{a1})^{2.52} \cdot (S_{a2})^{0.43}}$	0.87	0.65	43
Story	S_{a1}, M	$\boldsymbol{NHE = 1.28 \cdot (S_{a1})^{2.52} \cdot e^{0.28M}}$	0.86	0.68	47
NHE	S_{a1}, R	$\boldsymbol{NHE = 3.02 \cdot (S_{a1})^{2.53} \cdot R^{0.27}}$	0.86	0.68	47
	S_{a1}, D	$\boldsymbol{NHE = 5.24 \cdot (S_{a1})^{2.52} \cdot e^{0.02D}}$	0.87	0.66	44
Maximum	S_{a1}	$\boldsymbol{\theta_{CP} = 0.013 \cdot (S_{a1})^{1.64}}$	0.80	0.55	31
Column	S_{a1}, S_{a2}	$\boldsymbol{\theta_{CP} = 0.01 \cdot (S_{a1})^{1.30} \cdot (S_{a2})^{0.34}}$	0.83	0.51	26
Plastic	S_{a1}, M	$\boldsymbol{\theta_{CP} = 0.004 \cdot (S_{a1})^{1.64} \cdot e^{0.18M}}$	0.81	0.54	30
Rotation(θ_{CP})	S_{a1}, R	$\boldsymbol{\theta_{CP} = 0.01 \cdot (S_{a1})^{1.64} \cdot R^{0.19}}$	0.81	0.54	30
	S_{a1}, D	$\theta_{CP} = 0.01 \cdot (S_{a1})^{1.62} \cdot e^{0.01D}$	0.81	0.54	30

Table 3.7: Results of regression analysis of different damage measures from the results of all the three bins scaled to the 2.5g, 1.5g, and 0.5g first-mode spectral acceleration. The sample size requirement ($n_{req} = (\delta_\varepsilon/0.10)^2$) is obtained for a target one-sigma confidence bandwidth of $\pm 10\%$. The regression results that cannot be rejected at the 1%-significance level are highlighted with bold letters.

range of validity of the regression results will help evaluate the structure at widely different performance levels, i.e., from the immediate-occupancy performance level to the collapse-prevention performance level. The median maximum interstory drift from the 0.5g scaled Bin-III records for instance, is 1.3%, and the same median from 2.5g scaled Bin-III records is 7.8%. We will discuss this issue of performance evaluation in detail below.

The results in Table 3.7 show that, given S_{a1}, the displacement-based damage measures,

[5]We can also consider S_{a1} and the ratio of S_{a1} and S_{a2} ($Z = \frac{S_{a2}}{S_{a1}}$) as independent variables. The advantage of considering this new independent variable Z is that it is not correlated with S_{a1}. Therefore we observe in the data that when the correlation between S_{a1} and S_{a2} is 0.5, the same between S_{a1} and Z is 0. When we carry out regression analysis of maximum story drift against S_{a1} and Z, we get the following:

$$\begin{aligned} Y &= \alpha(S_{a1})^{\beta_1}(S_{a2})^{\beta_2} \\ &= \alpha(S_{a1})^{\beta_1+\beta_2}(Z)^{\beta_2} \end{aligned} \tag{3.3}$$

We will discuss in Chapter 5 the usefulness of this form of regression equation in demand-hazard calculations.

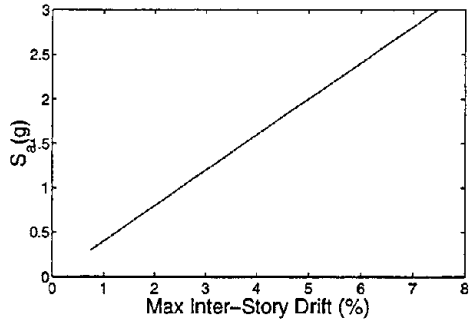

(a) Maximum interstory drift.

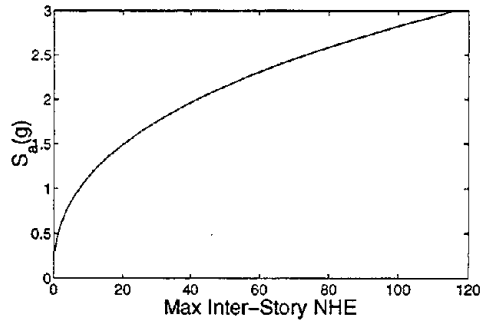

(b) Maximum interstory NHE.

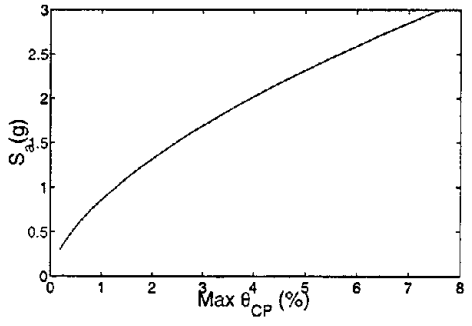

(c) Maximum column plastic rotation (θ_{CP}).

Figure 3.6: Variation of different damage measures with the first-mode spectral acceleration at 2% damping (S_a).

maximum story drift, and maximum column plastic rotation, depend, albeit very mildly, on either the magnitude, the distance, or the second-mode spectral acceleration[6], whereas the cumulative energy-based damage measures, such as maximum story NHE, depend not only on the above parameters, but also on the duration[7]. Note that from the observation of the lowest dispersion for regression analysis against S_{a2}, we can say that the conditional dependence of responses on S_{a2} is the highest among the four additional independent parameters. We have seen in Figure 2.1 that the shape of spectra changes with the magnitude of events. So the dependency of response on the magnitude (M) and the spectral acceleration at higher frequencies are somewhat interrelated. We observe that the regression coefficients for the second-mode spectral acceleration are positive and that the same is true for the magnitude even though the Figure 2.1 indicates that the high magnitude events have lower conditional median spectral acceleration at high frequencies conditioned on the S_{a1}. To understand this anomaly, we plot in Figure 3.7 the median response spectra of the

[6]From these results we can say that if 10% error in the median drift estimation is acceptable to us, we can select records from a magnitude range ($M_0 \pm \Delta M$), where M_0 is the target magnitude, which we can be any characteristic magnitude (e.g., mean magnitude, $\bar{M}$, or modal magnitude, M^* computed from the PSHA; see Bazzurro and Cornell, 1999, for details); ΔM is the magnitude difference for which the change in damage results is insignificant conditioned on S_{a1}. For example, the 5-story structure ΔM can be calculated as follows from Equation 3.2 for 10% permissible error in the median maximum story-drift results:

$$\begin{aligned} \Delta M &= \frac{1}{\beta_3} \cdot \ln(1+\varepsilon) \\ &= \frac{1}{0.13} \cdot \ln(1+0.10) \\ &= 0.73 \end{aligned} \tag{3.4}$$

Similarly, the percentage change in S_{a2} conditioned on S_{a1} for which the change in damage prediction is insignificant is the following:

$$\begin{aligned} S_{a2}(\%) &= (1+\varepsilon)^{\frac{1}{\beta_2}} - 1 \approx \frac{\varepsilon}{\beta_2} \\ &= (1+0.10)^{\frac{1}{0.25}} - 1 \\ &= 46\% \end{aligned} \tag{3.5}$$

[7]Formally this conclusion is drawn from a hypothesis test (see Neter et al., 1996, for details). If the regression coefficient of the additional parameter, e.g., magnitude, is significantly different from zero (i.e., the alternate hypothesis, H_1, is true), then we consider the damage measure to be dependent on the additional parameter. The results shown in bold letters in the table cannot be rejected at the 1% significance level. i.e., in the long run we make the mistake of considering the responses dependent on the additional parameter when this is not true only 1% of the time (note that this mistake is called *type I* error).

records used in regression analysis for the high and low-magnitude events. These records are scaled to a common value at 1.0Hz. We observe that the difference in relative spectral shape at the second mode is similar to that at 0.5Hz ($\approx \frac{1}{2}f_0$), but opposite in sense. The significance of considering the low frequency is that when a structure goes beyond its elastic limit, the effective frequency is reduced[8]. So the structure will also sample the low frequency component of the input accelerations when it goes into the nonlinear range. When we carry out regression analysis, the effect of softening most likely becomes predominant[9] and we get a positive regression coefficient for magnitude. (Although we will discuss this in detail, we should note here that the 20-story structure we will introduce in Chapter 4 has a negative regression coefficient for magnitude.) Note that the independent variable S_{a2} captures the actual shape of the spectrum of a record at the higher frequencies, whereas M only predicts the shape. So we see that the (conditional) dependency of response on S_{a2} is more than that on M (compare the δ_ε or R_a^2 values). The regression results that are statistically significant at the 1% significance level are shown in Table 3.7 by bold letters. These regression results confirm the observations drawn before from the within-bin scaling results (see Table 3.6).

The plot of residuals in Figure 3.8 shows the variation of responses with predictor variables S_{a2} and M. The residual shown in Figure 3.8 is $e_i = \ln y_i - \ln \hat{y}_i$, where y_i is the observed response and $\hat{y}_i$ is the fitted or predicted value of y_i based on the first-mode spectral acceleration. We can conclude in general that (conditional on the elastic-first-mode spectral acceleration) the responses are statistically significantly dependent on the spectral acceleration at frequencies higher than the elastic-first-mode frequency. Inclusion of the other independent variables reduces somewhat the dispersion of damage measures. The dependency is, however, mild and for most practical purposes we can neglect it. Also this

[8]This effective frequency is approximately $f_0/\sqrt{D_g\%}$ at the global drift D_g. Hence by considering the relative spectral acceleration to be $\frac{1}{2}f_0$, we are focusing here on the effect of change in spectral shape at $D_g = 4\%$.

[9]Note that the regression analysis of maximum story drift (D_{st}) against $S_a(0.5Hz)$ in addition to S_{a1} gives the following:

$$D_{st} = 0.033 \cdot S_{a1}^{0.71} \cdot [S_a(0.5Hz)]^{0.29} \qquad R_a^2 = 0.81 \tag{3.6}$$

The higher R_a^2 value (compared to 0.80 we get for S_{a2}) suggests that story drift is more strongly dependent on the predictor variable $S_a(0.5Hz)$.

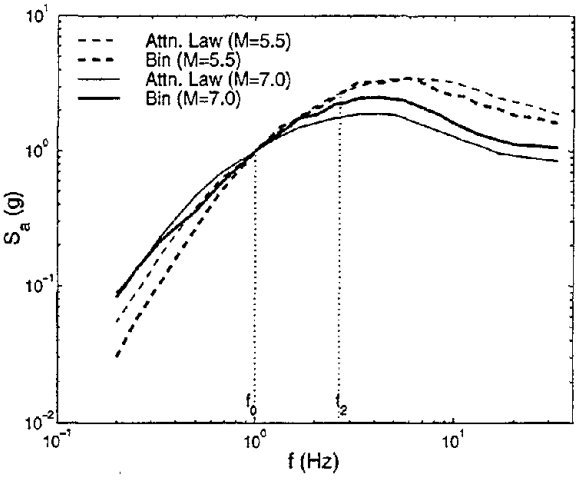

Figure 3.7: Median spectra scaled to 1.0g at 1.0Hz and 5% damping for high and low-magnitude earthquakes from the records used in regression analysis. Note that f_0 and f_1 are the first- and the second-mode frequency. Compare these results with those we get from the attenuation results (Abrahamson and Silva, 1997).

dependency does not reduce significantly the sample size requirements, and since the inclusion of additional parameters in the demand calculation also results in additional expense, considering those additional parameters is not worthwhile.

As structural engineers give significant importance to the duration of records, we plot the variation of residuals (e_i) of different damage measures with duration in Figure 3.9. As we have discussed before, the residuals are calculated by considering only the first-mode spectral acceleration as the independent variable in regression analysis. In Figure 3.9 we also show the trend of the residuals with duration conditional on the spectral acceleration at the first mode. We observe that although the maximum story drift (displacement-based story damage measure) residuals have a trend, the slope is not statistically significantly different from zero. The same is true for the maximum column plastic rotation (displacement-based local damage measure). The slope of the maximum story NHE (energy-based damage measure) residuals is, however, statistically significantly different from zero[10]. So if a damage

[10]Note that we accept the *null hypothesis*, H_0, for story drift that the slope of story drift against duration is zero at the 5% significance level. The same is true for beam plastic rotation only at the more tolerant 1% significance level. We, however, reject the null hypothesis for beam plastic rotation that the slope is greater

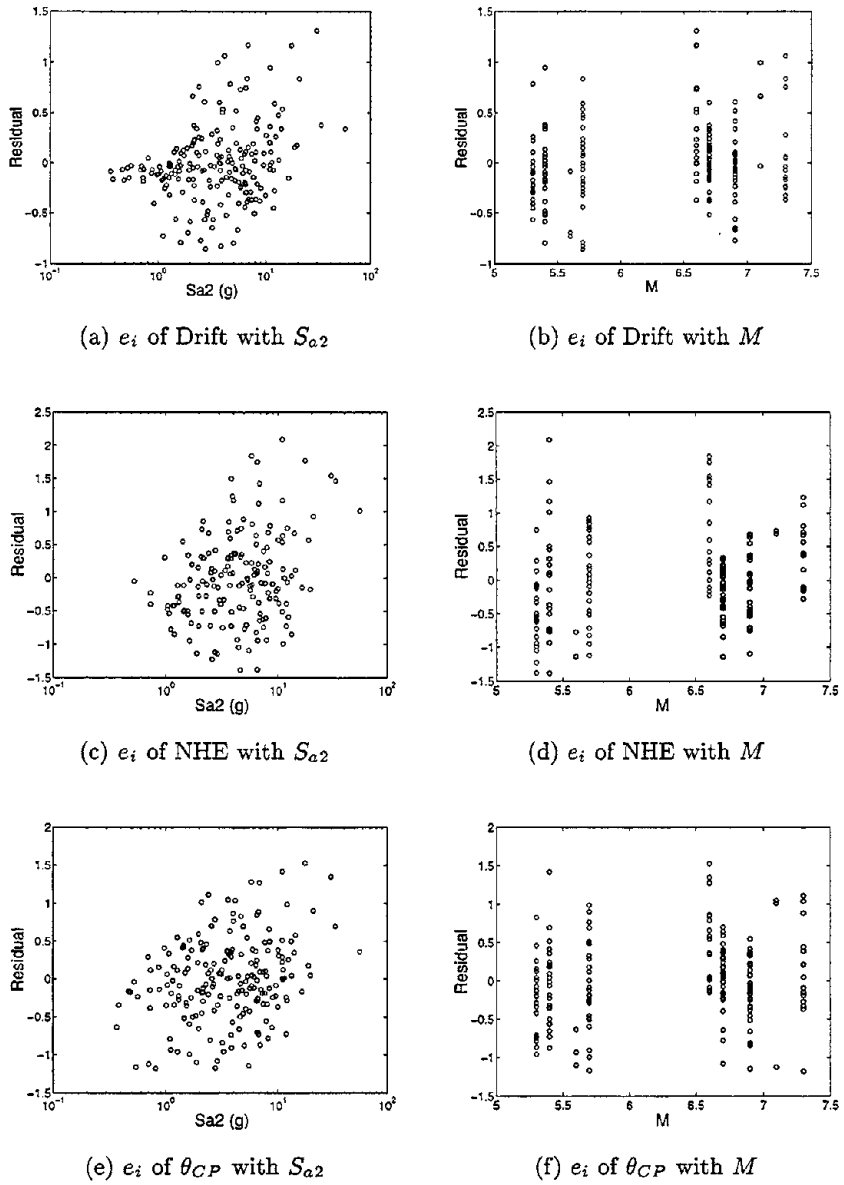

(a) e_i of Drift with S_{a2} (b) e_i of Drift with M

(c) e_i of NHE with S_{a2} (d) e_i of NHE with M

(e) e_i of θ_{CP} with S_{a2} (f) e_i of θ_{CP} with M

Figure 3.8: Variation of the residual given S_{a1} ($e_i = \ln y_i - \ln \hat{y}_i(S_{a1})$) for maximum story drift, maximum story NHE, and maximum column plastic rotation (θ_{CP}) with different additional independent variables. These are second-mode spectral acceleration (S_{a2}) and magnitude (M) of earthquake. The residuals are obtained by considering only the first-mode spectral acceleration S_{a1} as the independent variable in the regression analysis. Therefore, these plots indicate response dependence on S_{a2} and M conditioned on S_{a1}.

measure is significantly dependent on the inelastic energy dissipation, we may have to consider the effect of duration on damage measures. Figure 3.10 indicates, however, that even this dependency is not important for most practical purposes. In Chapter 5 we will check the importance of considering duration in seismic demand calculations. Although recent guidelines (see for example FEMA-273) consider only the displacement-based damage measures, in Chapter 5 we will develop a methodology to incorporate any additional duration dependency in the seismic demand calculations of structures.

We have also considered another definition of duration: response duration[11]. This definition looks promising because this duration is correlated to the strength of ground motion at the structural frequency. The previous study by Sewell (1993) on dependency of structural response on duration was confined to only nonlinear single-degree-of-freedom (SDOF) systems. Sewell was observed that for the SDOF systems the nonlinear response is better correlated to the response-duration than to the conventional duration. We have investigated here whether that observation is true for the MDOF structures, which sample frequencies over a wider range than the SDOF structures. Our conclusion is that the dependency of MDOF nonlinear responses on (1Hz oscillator frequency) response duration is not higher than the dependency on the conventional definition of duration.

In order to determine the practical effect of these additional parameters on response prediction, we plot the regression results in Figure 3.10 for the three most important parameters, which give the lowest dispersion of the regression error. The plot shows in a solid line the regression of demand given S_{a1} only. The three dashed lines show the regression of demand given S_{a1} and three values of S_{a2} (or M, or R, or D). To be consistent we make these three selected values change as S_{a1} does. These values are the conditional mean of S_{a2} given S_{a1} (i.e., the likely value of S_{a2} for each S_{a1} and the relatively unlikely high and low

than zero at the 5% significance level. We reject the null hypothesis for story NHE that the is greater than zero even at the 1% significance level.

[11] This duration measure was first proposed by Sewell (1993). It is defined as the 5% to 95% bracketed duration above a pre-defined threshold value of the absolute acceleration response of a *linear* SDOF system subjected to a ground-motion time history. The threshold value adopted here is equal to 20% of the peak acceleration response as adopted by Sewell (1993) in his study. Note that this measure of duration is not only a characteristic of the ground-motion record, but also depends on the properties of the SDOF structures (e.g., the frequency of vibration).

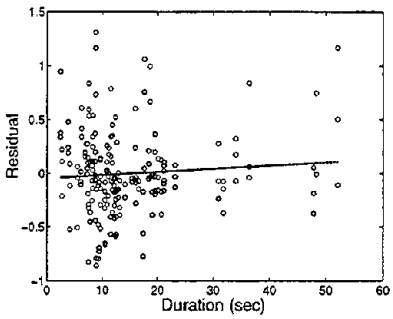

(a) Maximum interstory drift

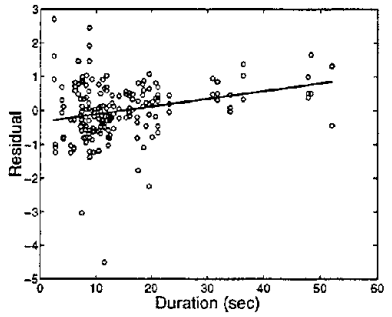

(b) Maximum interstory NHE

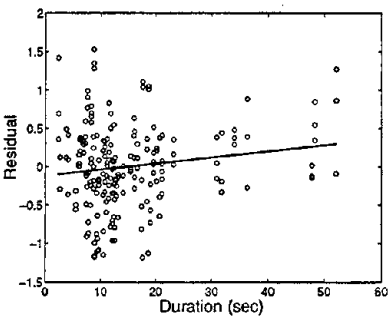

(c) Maximum column plastic rotation

Figure 3.9: Variation of the residual given S_{a1} ($e_i = \ln y_i - \ln \hat{y}_i(S_{a1})$) for maximum story drift, maximum story NHE, and maximum column plastic rotation (θ_{CP}) with the additional independent variable, duration of motion (D). The residuals are obtained by considering only the first-mode spectral acceleration S_{a1} as the independent variable in the regression analysis. Therefore these plots indicate response dependence on D conditioned on S_{a1}.

values, namely 16% and 84% (mean ± sigma values) of S_{a2} given S_{a1}[12]. Note the difference between the regression results against only the first-mode spectral acceleration and against the first-mode spectral acceleration plus an additional parameter. We observe that the difference for the case of the spectral acceleration at the elastic-second-mode frequency is substantial. Although the other parameters give statistically significantly different results, the difference between the results with and without those parameters is not substantial. Hence these differences are not important for practical purposes. Note that the inclusion of

[12] The conditional mean and the dispersion of M and R are calculated from the disaggregation results (see Section 5.3). The mean value of magnitude at a given spectral acceleration is calculated as follows:

$$\bar{M}|s_a = \int m \cdot f_{M|S_a}(m|s_a)\, dm \tag{3.7}$$

where the conditional density function, $f_{M|S_a}(.)$, is calculated from Figure 5.3. The conditional mean and dispersion of the elastic-second-mode spectral acceleration are similarly calculated from the results of the 2-D PSHA (see Section 5.5), which gives the conditional density function, $f_{S_{a2}|S_{a1}}(.)$, required for this calculation. In order to calculate the conditional mean and dispersion of duration, we first calculated the variation of duration (Trifunac and Brady, 1975) with magnitude and duration. This is obtained from the results of 100 ground-motion records of different magnitudes and distances, and the results are given in the following:

$$D = 0.29\, e^{0.49M}\, R^{0.21} \qquad \delta_{D|M,R} = 0.43 \qquad R_a^2 = 0.39 \tag{3.8}$$

From the same data similarly we get the functional dependency of spectral acceleration at 1.0Hz on magnitude and distance, and the results of regression analysis are given in the following:

$$S_a = 0.005\, e^{1.02M}\, R^{-1.03} \qquad \delta_{S_a|M,R} = 0.74 \qquad R_a^2 = 0.46 \tag{3.9}$$

Finally we calculate the conditional mean and dispersion of duration from the disaggregation results at different S_a levels as follows:

$$\bar{D}|s_a = \int d \cdot f_{D|M,R}(t|m,r)\, f_{M,R|S_a}(m,r|s_a)\, dm\, dr \tag{3.10}$$

where the conditional joint distribution, $f_{M,R|S_a}(.)$, is obtained from the disaggregation of seismic hazard results (see Figure 5.3), and the conditional distribution, $f_{D|M,R}(.)$, is obtained from Equation 3.8. Note that the correlation coefficient between duration and spectral acceleration is very low. This coefficient is calculated as follows:

$$\rho_{S_a,D} = \sum_i \frac{\varepsilon_{D|M,R}(d_i) \cdot \varepsilon_{S_a|M,R}(s_{a,i})}{\sigma_{\varepsilon_{D|M,R}}\, \sigma_{\varepsilon_{S_a|M,R}}} \tag{3.11}$$

where

Residual, $\varepsilon_{D|M,R}(d_i) = d_i - \hat{d}_i$, where d_i is the observed duration and $\hat{d}_i$ is the duration predicted from Equation 3.8.
Residual, $\varepsilon_{S_a|M,R}(s_{a,i}) = s_{a,i} - \hat{s}_{a,i}$, where $s_{a,i}$ is the observed spectral acceleration, and $\hat{s}_{a,i}$ is the spectral acceleration predicted from Equation 3.9.

The correlation coefficient from the above equation is -0.10. Hence in the calculation of conditional mean duration, $\bar{D}|s_a$, we have neglected the correlation between D and S_a in Equation 3.10.

these additional independent parameters does not change substantially either the dispersion of the residuals or the sample size requirement over the regression on only the first-mode spectral acceleration.

3.4.1 Variation of Drift over Height

The previous results for maximum story drift do not give information about the spread of nonlinear deformations over the height of the structure. The maximum story drift results do not tell us whether damage is concentrated only at a particular story or is distributed over several stories. This information is valuable in order to assess the expected cost of damage from future earthquakes. We can get some idea of the spread of damage from the regression analysis of the system drift results. But we can get more accurate results from the information about the variation of the interstory drift with spectral acceleration at each floor level. In order to get this information we carry out the regression analysis of drift for each story against spectral acceleration. The results are given in Table 3.8. The plot of variation of drifts versus height in Figure 3.11 helps to understand the results in Table 3.8. Note that the dispersion of the response results decreases at higher stories of a structure at high intensity levels. We have observed that at the lower drifts we get lower dispersions. Hence this low dispersion at the higher floors might be due to lower drifts. We also observe that the slope of the fitted curve in log-space (β) is smaller at the upper stories (close to 0.5 for the upper two stories) than at the lower stories (close to one for the lower three stories). Thus interstory drifts at the upper floors increase less than proportionately to the ground-motion intensity, whereas at the lower stories the interstory drifts will increase comparatively rapidly with spectral acceleration. The nonlinearity of the structure at the low-probability, high-intensity earthquake motions will be concentrated in these stories. The regression analyses also indicate that for the upper stories the higher-frequency spectral accelerations are important parameters (e.g., the coefficient of S_{a2} is statistically significant for regression on S_{a1} and S_{a2}). We also observe that the top-story drifts are better explained by the elastic-second-mode spectral acceleration. This indicates that although the structure is primarily single-frequency dominated, its upper stories are

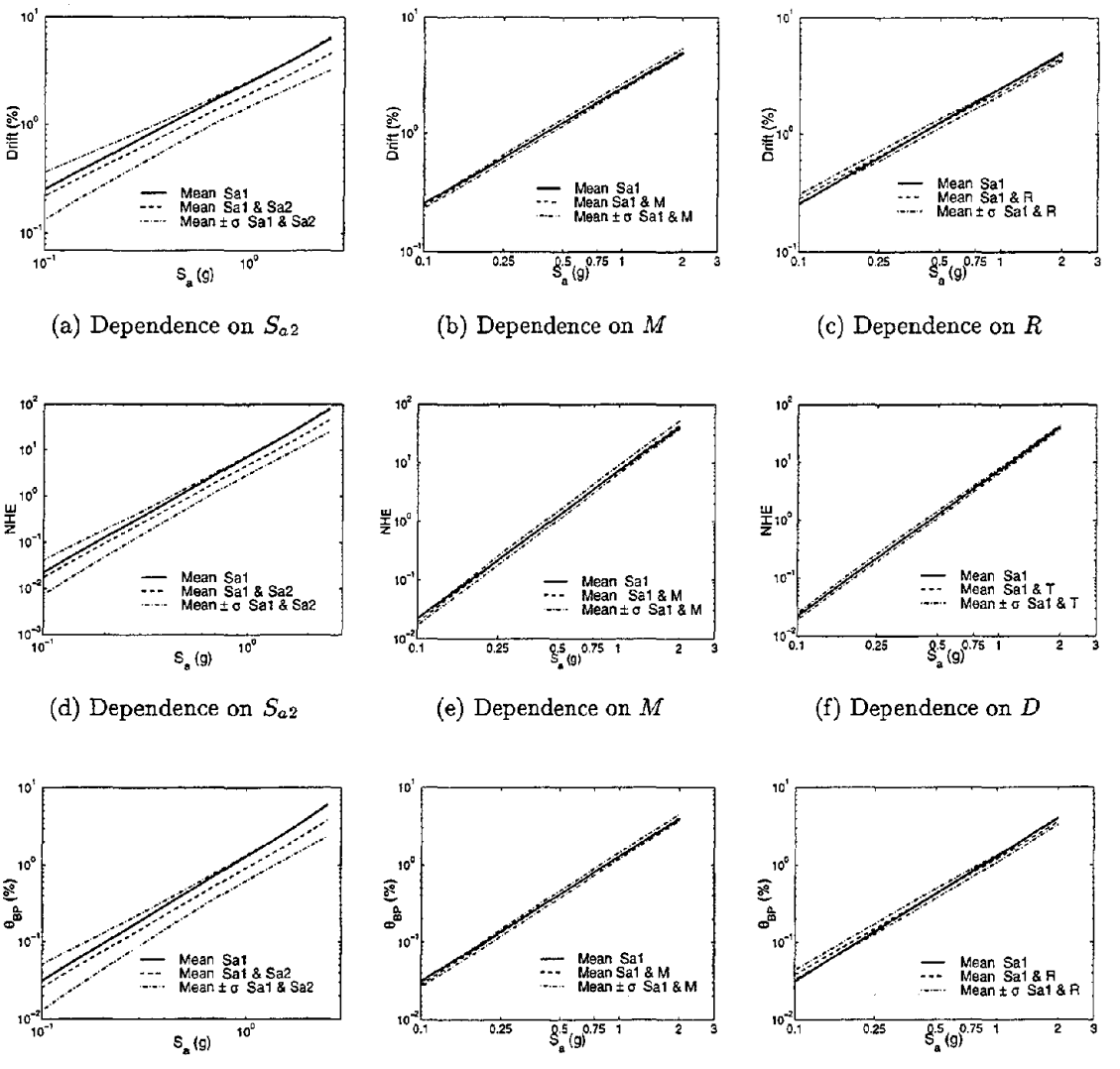

(a) Dependence on S_{a2} (b) Dependence on M (c) Dependence on R

(d) Dependence on S_{a2} (e) Dependence on M (f) Dependence on D

(g) Dependence on S_{a2} (h) Dependence on M (i) Dependence on R

Figure 3.10: Comparison of regression results of three different damage measures against only the first-mode spectral acceleration and against a second parameter *in addition to the first-mode spectral acceleration.* The values of the second parameter (e.g., S_{a2}) are the mean and the mean ± one-sigma values *conditioned* on S_{a1}. The three damage measures are the maximum interstory drift, maximum interstory NHE, and maximum beam plastic rotation (θ_{BP}).

Story	Function	δ_ε
5	$D_{st} = 0.015 \cdot S_{a1}^{0.53}$	0.31
	$D_{st} = 0.010 \cdot S_{a2}^{0.45}$	0.22
4	$D_{st} = 0.018 \cdot S_{a1}^{0.67}$	0.29
	$D_{st} = 0.011 \cdot S_{a2}^{0.48}$	0.30
3	$D_{st} = 0.019 \cdot S_{a1}^{0.81}$	0.28
2	$D_{st} = 0.020 \cdot S_{a1}^{1.01}$	0.37
1	$D_{st} = 0.020 \cdot S_{a1}^{1.13}$	0.43

Table 3.8: Results of regression analysis of interstory drifts at each floor level.

excited significantly by the higher-frequency spectral accelerations.

3.4.2 Frequency-Averaged Scaling and Scaling at Higher Damping

We have observed before that the dispersion of the damage measures is reduced when we scale the records to a higher damping level or scale to a frequency-averaged spectral acceleration. In order to validate this observation, we carry out the regression analysis on the spectral acceleration at higher damping and on the average spectral acceleration. This will help to determine by how much we reduce the regression error in this analysis compared to the error in analysis based on only the first-mode spectral acceleration. The results of the regression analysis are given in Table 3.9. We observe that there is a marginal reduction in the dispersion of maximum story drift when the independent variable in the regression analysis is the first-mode spectral acceleration at higher damping or the frequency-averaged spectral acceleration. But for the energy-based NHE damage measure, we do not get any significant reduction in dispersion when compared with the simple scaling to the first-mode spectral acceleration. These observations are similar to the results we have obtained before from the within-bin different scaling results (see Table 3.4).

3.4.3 Exploring Other Regression Models

So far, we have carried out so far linear regression analysis by fitting the logarithm of the model given in Equation 3.2. The drawback of this simplification is that for the regression

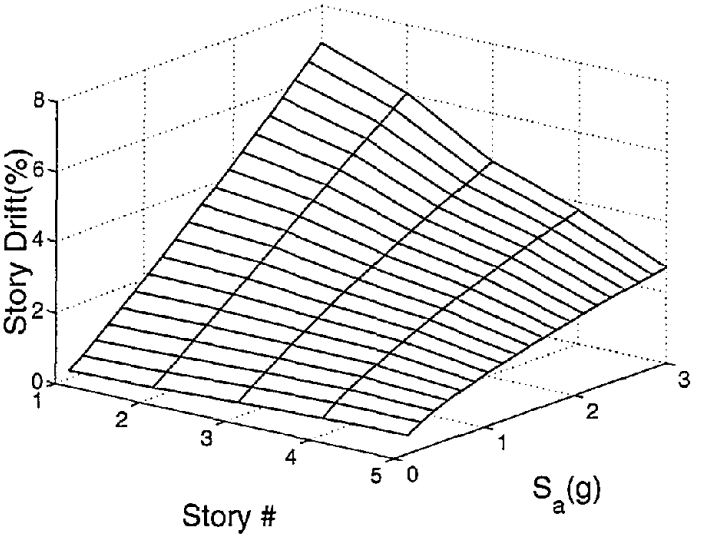

Figure 3.11: Variation of story drift over height of the structure at different first-mode spectral acceleration levels.

Damage	Scaling Method	Regression Function	δ_ε	n_{req}
Max Story Drift	Standard $S_a(0.9Hz, 2\%)$	$D_{st} = 0.025 \cdot (S_{a1})^{1.00}$	0.38	15
	High Damping $S_a(0.9Hz, 5\%)$	$D_{st} = 0.031 \cdot (S_{a1})^{1.00}$	0.36	13
	Freq Average($f_0 \pm 10\%$)	$D_{st} = 0.024 \cdot (S_a^\star)^{0.98}$	0.37	14
	Freq Average($f_0 \pm 25\%$)	$D_{st} = 0.025 \cdot (S_a^\star)^{1.00}$	0.33	11
Max Story NHE	Standard $S_a(0.9Hz, 2\%)$	$NHE = 7.29 \cdot (S_{a1})^{2.52}$	0.71	51
	High Damping $S_a(0.9Hz, 5\%)$	$NHE = 15.93 \cdot (S_{a1})^{2.11}$	0.69	48
	Freq Average($f_0 \pm 10\%$)	$NHE = 6.51 \cdot (S_a^\star)^{2.59}$	0.85	73
	Freq Average($f_0 \pm 25\%$)	$NHE = 7.16 \cdot (S_a^\star)^{2.59}$	0.77	60

Table 3.9: Results of regression analysis of different damage measures from different scaling schemes. Note that for the frequency-averaged scaling we used 2% damping. The sample size required ($n_{req} = (\delta_\varepsilon/0.10)^2$) is obtained for a target one-sigma confidence bandwidth of $\pm 10\%$. $S_a^\star$ is the average spectral acceleration over a frequency range.

analysis of the NHE and the plastic-rotation results we had to neglect the response data that were equal or close to zero. Note that these damage measures have no value at low spectral acceleration levels. The logarithm of those low response values are close to -∞, and so this information is neglected in regression analyses. The estimation of response can be improved by fitting the nonlinear regression model in Equation 3.2 directly (i.e., no transformation of the model to the log-space as was done before) to the NHE and the plastic-rotation results. In this nonlinear regression analysis we do not have to neglect the data that are close to zero. The results of nonlinear regression analyses are given in Table 3.10. The variation of maximum column plastic rotation and maximum story NHE with the spectral acceleration at the elastic-first-mode frequency as obtained from linear and nonlinear regression analysis of the same model (Equation 3.2) are shown in Figure 3.12. Note that the regression error (σ_ε) in this case is in arithmetic-space rather than in log-space where it was in the previous cases (i.e. $\sigma_{Y|S_a}$ instead of $\sigma_{\ln Y|S_a}$ or $\delta_{Y|S_a}$). See Figure 3.13 for the variation of the regression error of maximum column plastic rotation. We observe that the regression error increases with S_a, unlike before it remained constant with S_a (compare Figure 3.13 (a) and (b)). Due to this non-uniform regression error, we have also carried out weighted regression analysis by assuming the weight w_i of each data point is inversely related to the variance σ_i^2 and the σ_i is increasing with S_a (see Neter et al., 1996). We find that the result of the weighted-regression analysis is very close the results of the previous unweighted-regression analysis.

We observe in Figure 3.13 that the results of nonlinear regression analysis in arithmetic-space are not significantly different from those of the previous linear regression in log-space for plastic rotation results (θ_{CP}), whereas the same is not true for the NHE. This is due the NHE results having higher dispersion than the plastic rotation results. Note that for both the cases of linear and nonlinear regression analyses the model is same–the fitting is done in one case in arithmetic space and in the other case transformed log-space. The difference in results between the regression in log-space and arithmetic-space is due to those outcomes that are much higher than the median. These sample points are weighted differently in arithmetic-space than in log-space. An outcome that is much higher than the median gets

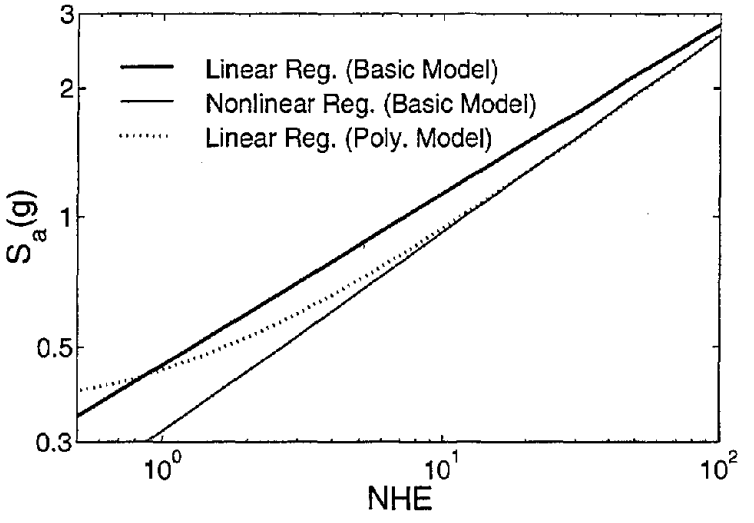

(a) Maximum interstory NHE

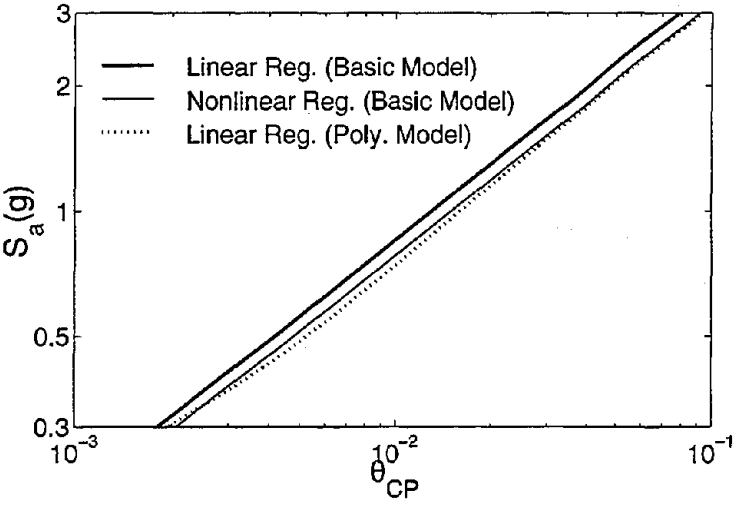

(b) Maximum column plastic rotation (θ_{CP})

Figure 3.12: Variation of different damage measures with the first-mode spectral acceleration as obtained from linear regression analysis for the basic model (Equation 3.2), which is first transformed into log-space, from nonlinear regression analysis for the basic model, and from linear regression analysis for the polynomial model (Equation 3.12).

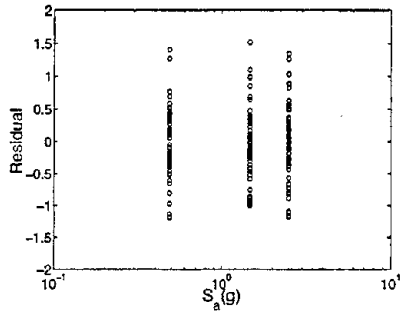

(a) Linear regression analysis of the model given in Equation 3.2 (log-space).

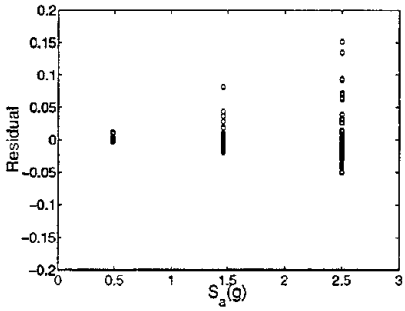

(b) Nonlinear regression analysis of the model given in Equation 3.2 (arithmetic-space).

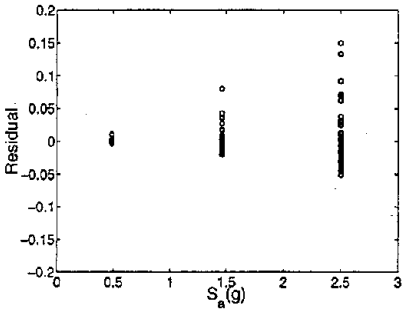

(c) Linear regression analysis of the polynomial model given in Equation 3.12 (arithmetic-space).

Figure 3.13: Variation of residual of maximum column plastic rotation (θ_{CP}) with the first-mode spectral acceleration as obtained from different regression analyses.

Damage Measure	Independent Variable	Regression Function	R_a^2	δ_ε	n_{req}
Maximum	S_{a1}	$NHE = 7.29 \cdot (S_{a1})^{2.52}$	0.85	0.71	51
Story	S_{a1}	$NHE^* = 11.93 \cdot (S_{a1})^{2.17}$	0.40	43.30[1]	58
NHE	S_{a1}	$NHE^{**} = -0.67 - 2.90S_{a1} + 15.13S_{a1}^2$	0.40	43.40[1]	66
Maximum	S_{a1}	$\theta_{CP} = 0.013 \cdot (S_{a1})^{1.64}$	0.80	0.55	31
θ_{CP} (%)	S_{a1}	$\theta^*_{CP} = 0.015 \cdot (S_{a1})^{1.65}$	0.49	0.026[1]	33
	S_{a1}	$\theta^{**}_{CP} = -0.002 + 0.011S_{a1} + 0.007S_{a1}^2$	0.48	0.026[1]	31

(*) From nonlinear regression analysis of model (Equation 3.2).
(**) From polynomial regression model.
(1) The regression error varies with S_a. See Figure 3.13. Note that these regression errors are in arithmetic space. So in this case $\delta_\varepsilon = \sigma_{Y|S_a}$, whereas previously we got $\delta_\varepsilon = \sigma_{\ln Y|S_a}$.

Table 3.10: Results of regression analysis of different damage measures from the results of all the three bins scaled to the 2.5g, 1.5g, and 0.5g first-mode spectral acceleration. The sample size required ($n_{req} = (\delta_\varepsilon/0.10)^2$) is obtained for a target one-sigma confidence bandwidth of ±10%. Note that for nonlinear regression analysis and for linear regression analysis using the polynomial model the variance of ε varies with S_a. So the sample size for these cases is calculated at 1.5g spectral acceleration.

higher weight in arithmetic-space than in log-space. So although we use the same regression model, we get different results from these two regression analyses. The difference becomes more significant for the NHE because of its high dispersion, i.e., a large number of sample points are higher than the mean. The advantages of the regression analysis in log-space are that we can carry out the conventional linear regression and that the variance of the error does not depend on the level of spectral acceleration (i.e., is homoscedastic). The advantage of this constancy of variance will be clear when we discuss the use of these regression functions in seismic demand calculations. The use of nonlinear regression, however, is preferable because we have kept all the information about the sample space instead of throwing away some of the sample points, as we did in the linear regression analysis. When the sample space of the responses does not have a large number of sample points close to zero, it is advantageous to carry out the linear regression analysis in log-space. Otherwise the nonlinear regression analysis will give us more precise results.

The nonlinear regression model helps to get rid of the problem of zero response; the other

easier alternative is the use of the polynomial regression model. The general polynomial regression model is of the following form:

$$Y = \alpha + \beta_1 \cdot S_{a1} + \beta_2 \cdot S_{a1}^2 + \ldots + \beta_n \cdot S_{a1}^n + \varepsilon \tag{3.12}$$

The advantage of this model is that it is a special case of the general linear regression model. The results of this linear regression analysis are also given in Table 3.10. The results of regression analysis for plastic rotation and NHE are shown in Figure 3.12. Note that in the case of the polynomial regression model, the variance of error is not constant, i.e.,is heteroscedastic; the variation of error with spectral acceleration is shown in Figure 3.13. We also observe that, as before, the weighted regression analysis of this polynomial model does not change the results significantly and that the results of the polynomial-regression model are very close to the results of the nonlinear regression for the model given in Equation 3.2 except in the low response region (see Figure 3.12). The difference we observe is due to the difference in the characteristics of the regression models. The model given in Equation 3.2 has a slope of either zero or ∞ at the origin, depending on the value of the exponent β, whereas the polynomial model has a finite slope at the origin. But the polynomial model is difficult to apply for seismic demand calculations of structures due to its nonuniform variance. Therefore, the polynomial regression model is preferable to the nonlinear regression model only when we have a large number of sample points close to zero.

3.5 Calculation of Seismic Demand

Our goal is to calculate the seismic demand of a structure *economically.* The recent guidelines (see, e.g., FEMA-273, 1996) require nonlinear response calculations only for the ground motion of a target return period to check whether the demand is less than the specified allowable limiting value at a target performance level. This demand calculation, however, does not take into account the uncertainty in nonlinear response results. We will see below that at a central Los Angeles site, the 2475-year return period spectral acceleration

is 1.5g at 1.0Hz and 2% damping. From Table 3.7 we find that the median maximum story drift of the 5-story structure is 4.5% at the 1.5g spectral acceleration. This drift demand result is well below the FEMA-273 5% allowable drift at the collapse prevention performance level. So the structural performance may well be deemed satisfactory. See Bazzurro et al., 1998, for a detailed comparison between the method we will discuss here and the FEMA-273 guideline. In the procedure we discuss here, we find that when we couple the uncertainty of nonlinear response calculations to the uncertainty of ground-motion, the above perception of performance of structure is changed substantially.

The methodology we will follow to compute the demand of a structure is a coupling of the conventional probabilistic seismic hazard analysis, PSHA (Cornell, 1968; McGuire, 1995; Bazzurro and Cornell, 1999) and the nonlinear structural analysis. We call this estimation of the probability of exceedance of a given level of nonlinear response of a structure *Probabilistic Seismic Demand Analysis* (PSDA). This methodology can be visualized as follows: Suppose that the threats to the 5-story building are exclusively from two faults that produce magnitudes in only two narrow ranges (characteristic magnitudes). These ranges of magnitudes and distances correspond to those of Bin-II and Bin-III. The seismologist tells us, based on the historical records and paleo-seismology, that the annual frequency of occurrence of a 6.75 magnitude earthquake 60km from the site (this event corresponds to Bin-II records) is 0.02 and that of a 7.0 magnitude earthquake 20km from the site (this event corresponds to Bin-III records) is 0.002. Thus we can calculate the annual probability of exceedance of 0.7% maximum interstory drift (the FEMA-273 immediate-occupancy-allowable-drift level for moment-frame steel structures) from the preceding information and from prior calculations of response. The direct analyses (from the as-recorded ground motion) of the structure give the median and the dispersion of maximum interstory drift as respectively 0.2% and 0.80 for Bin-II; for Bin-III those values are 0.8% and 0.47. We have observed that the response parameters are lognormally distributed (see Appendix C). So given a Bin-II-like event, the probability of exceeding 0.7% drift is $1 - \Phi\left[\frac{\ln(0.7/0.2)}{0.80}\right] = 1 - \Phi(1.57) = 0.0582$; the corresponding value for a Bin-III-like event is 0.6103. $\Phi(.)$ is the widely tabulated standard normal cumulative distribution. Then the annual probability of exceeding the 0.7%

maximum interstory drift (D_{st}) can be calculated from the theorem of total probability:

$$(0.0582)(0.02) + (0.6103)(0.002) = 0.0012 + 0.0012 = 0.0024 \quad (3.13)$$

Note that the events contribute equally to the risk. The disaggregation of seismic hazard results (see Bazzurro and Cornell, 1999) similarly helps to understand the contribution to risk of different events from the input ground motion. Formally we can write Equation 3.13 as:

$$P[D_{st} > 0.7\%] = \sum_{i,j} P[D_{st} > 0.7\% \mid M = m_i, R = r_j] \cdot P[M = m_i, R = r_i] \quad (3.14)$$

3.5.1 Direct Approach

Alternatively we can make use of the results that are conditioned on the spectral acceleration. In order to do this, we expand Equation 3.14 by conditioning further on the spectral acceleration S_a, obtaining the following form:

$$\begin{aligned} P[D_{st} > 0.7\%] = & \sum_{i,j,k} P[D_{st} > 0.7\% \mid S_a = s_{a,k}, M = m_i, R = r_j] \cdot \\ & P[S_a = s_{a,k} \mid M = m_i, R = r_j] \cdot P[M = m_i, R = r_j] \end{aligned} \quad (3.15)$$

The main advantage of this form of the equation will become apparent below when we illustrate its application.

In general, the calculation of the probability of exceedance of a level y of any damage parameter Y involves summation over all possible seismic sources of the integral of the product of the joint probability distribution of magnitude and distance times the probability distribution of the spectral acceleration conditioned on magnitude and distance times the probability that the damage parameter of interest is exceeding a target level due to an earthquake of magnitude m at a distance r, generating spectral acceleration s_a. Hence the

general form of Equation 3.15 is the following:

$$P(Y > y) = \sum_{i=1}^{N} \nu_i \left\{ \int\int\int P[Y > y \mid s_a, m, r] \cdot f_{S_a|M,R}(s_a \mid m, r) \cdot f_{M,R}(m, r)\, ds_a\, dm\, dr \right\}_i \tag{3.16}$$

where N is the number of seismic sources at a site, ν_i is the mean annual rate of occurrence of earthquakes from source i, $f_{M,R}(m,r)$ is the joint probability distribution of magnitude M and distance R of the site, $P[Y > y \mid s_a, m, r]$ is the conditional probability that the response or damage parameter Y exceeds a level y due to an earthquake of magnitude m at distance r that generates spectral acceleration s_a at the site, and $f_{S_a|M,R}(s_a|m,r)$ is the conditional probability distribution of S_a for an event of magnitude m at a distance r. We have already seen in regression results that most of the response parameters depend to good approximation on S_a alone. So the conditional probability inside the integrand will be dependent only on S_a and Equation 3.16 simplifies to:

$$\begin{aligned} P(Y > y) &= \sum_{i=1}^{N} \nu_i \left\{ \int\int\int P[Y > y \mid s_a] \cdot f_{S_a|M,R}(s_a \mid m, r) \right. \\ &= \left. f_{M,R}(m, r)\, ds_a\, dm\, dr \right\}_i \end{aligned} \tag{3.17}$$

The conventional spectral acceleration seismic hazard function $H(s_a)$ is

$$H(s_a) = \sum_{i=1}^{N} \nu_i \left\{ \int\int G_{S_a|M,R}(s_a \mid m, r)\, f_{M,R}(m, r)\, dm\, dr \right\}_i \tag{3.18}$$

where $G_{S_a|M,R}(.)$ is the complementary cumulative distribution of S_a conditioned on M and R. We can take advantage of the conditional independence of damage measures Y given S_a to write Equation 3.17 as follows:

$$P(Y > y) = \int_0^{+\infty} G_{Y|S_a}(y \mid s_a) \cdot \left| \frac{H(s_a)}{ds_a} \right| ds_a \tag{3.19}$$

We have written here $P[Y > y \mid s_a]$ as the conditional complementary cumulative distribution $G_{Y|S_a}(.)$. Alternatively, integration by parts yields:

$$P(Y > y) = \int_0^{+\infty} \frac{\partial G_{Y|S_a}}{\partial s_a}(y \mid s_a) \cdot H(s_a)\, ds_a \tag{3.20}$$

In general we can solve the above equation numerically.

We can, however, get an explicit solution of Equation 3.20 by assuming the following:

1. The damage parameter Y is conditionally lognormally distributed. We have verified this assumption in Appendix C. Hence we can get the conditional probability density function $f_{Y|S_a}(y \mid s_a)$ from the results of regression analyses as $(1/\delta_{Y|Sa}) \cdot \phi\left[\frac{\ln Y - \ln \hat{Y}}{\delta_{Y|Sa}}\right]$, where $\phi(.)$ is the unit Gaussian probability density function and $\hat{Y}$ is the median damage measure as predicted from the regression analysis (see Table 3.7).
2. The functional dependency of the damage measure Y on S_a is of the form

$$Y = \alpha \cdot S_a^{\beta} \cdot \varepsilon \tag{3.21}$$

where α and β are the regression parameters (e.g., see Table 3.7), and ε is the random error term with median equal to 1 and standard deviation equal to δ_ε. We have already observed that this form of regression model works satisfactorily for the response data [e.g., see Figure 3.13(a)]. So we will get the following:

$$\frac{\partial G}{\partial S_a} = \phi\left[\frac{\ln(y/\alpha s_a^{\beta})}{\delta_{Y|S_a}}\right] \cdot \left[\frac{\beta}{s_a \delta_{Y|S_a}}\right] \tag{3.22}$$

3. The hazard function in the region of interest is linear in log-space and can be approximated by the following expression in the range of S_a values that contribute significantly to the integral given in Equation 3.20:

$$H(s_a) = K_0 \cdot s_a^{-K_1} \tag{3.23}$$

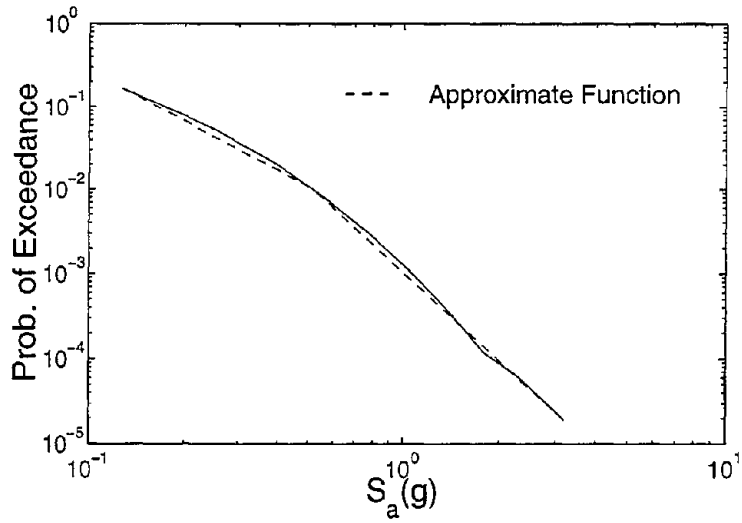

Figure 3.14: Seismic hazard curve at 2% damping for 1Hz structure at a central Los Angeles site.

where, K_0 and K_1 are the appropriate constants obtained by fitting the functional form (Equation 3.23) to the PSHA results. This approximation is also quite satisfactory over a wide range of spectral accelerations (see for example the hazard curve in Figure 3.14).

Hence all the above assumptions are satisfactory for our problem. Equation 3.20 then simplifies to (see Cornell, 1996 and Bazzurro, et al., 1998)

$$P(Y > y) = H[(y/\alpha)^{\frac{1}{\beta}}] \cdot e^{\frac{1}{2}\left(\frac{K_1 \cdot \sigma_{\ln Y|Sa}}{\beta}\right)^2} \tag{3.24}$$

$$= H[(y/\alpha)^{\frac{1}{\beta}}] \cdot C_f \tag{3.25}$$

where the exponential factor in Equation 3.25, C_f, can be considered to be the "correction factor" due to the uncertainty in the response calculation. Note that $(y/\alpha)^{\frac{1}{\beta}}$ is the value of S_a "corresponding" to y, i.e., for the value of S_a, y is the median value of the response.

Let assume, for illustration, the structure is at a central Los Angeles site. The seismic

hazard curve of the site for spectral acceleration at 1.0Hz is shown in Figure 3.14. If we adopt the allowable story-drift and plastic-rotation values of the FEMA-273 guideline at different performance levels, we can calculate the probability of exceeding those limits from Equation 3.25 (note that these allowable responses at different performance levels are applicable only for seismic rehabilitation of fully restrained steel moment frame buildings). The probability of exceedance of 5% maximum story drift (which is the allowable drift for collapse-prevention performance of a structure) is found as:

$$\begin{aligned} P(\text{max story drift} > 5\%) &= H[(0.05/0.03)^{1}] \cdot e^{\frac{1}{2}\left(\frac{3.45 \cdot 0.38}{1.0}\right)^2} \\ &= 9.45(10^{-5}) \times 2.36 = 2.23(10^{-4}) \end{aligned} \tag{3.26}$$

The values of α, β, and δ_ϵ (or $\sigma_{\ln Y|\ln Sa}$) are obtained from the first row of Table 3.7. The value of K_1 is found to be 3.45 at 1.0Hz frequency from the PSHA results (in the probability range from 10^{-3} to 10^{-5})[13]. Note that the return period of the 5% allowable drift demand is 4500 years, which is greater than the target 2500 year return period specified in the FEMA-273 guideline. We also observe in this calculation the importance of inclusion of a correction factor–this factor increases the probability of exceedance of maximum story drift by a factor of 2.4.

We have calculated similarly the seismic demand of the structure at different levels for different damage measures. The results of demand calculations of system drift (average story drift), maximum story drift, maximum story NHE, and maximum plastic rotation are shown in Figure 3.15. We can calculate the demand of the damage parameters at different performance levels, namely, at the collapse-prevention level (2475-year return period), the life-safety level (475-year return period), and the immediate-occupancy level (75-year return period) from this figure. These curves can be called the seismic demand-hazard curve of the structure. Note that as per current guideline, the drift demand of the structure at the collapse-prevention performance level ground-motion is 4.5% (median drift from the results

[13]A typical value of this slope parameter for the PGA is 3 to 4.5 for western US and 2 to 3 for eastern US. See DOE-1020, 1994.

of all the bins at the 1.5g or 2475-year return period ground motion; the the first-row results in Table 3.7), whereas the drift demand at the 2475-year return period is 4.3%, which also takes into account the record-to-record variability of drift results.

Story-by-Story Demand-Hazard Curve: We have also calculated the demand curve of each story and compared the results with those of the maximum story drift. The results are shown in Figure 3.16. We observe that at low return periods the risk is concentrated mainly at the upper stories, whereas at high return periods the risk is mainly at the lower stories. We lose this information when we look only at the maximum story drift results. The comparison of these story drift results with the maximum story drift results shows that at low drifts the maximum story drift under-predicts the probability of exceedance of the allowable drift. Figure 3.16 indicates that the slope of the demand curve for the maximum story drift is dominated by the results from lower stories, and we thus get a flatter slope of the demand curve. The results at the low return period (not very important in most cases), however, are not very accurate as the regression model (Equation 3.2), fitted over a wide range of spectral accelerations, does not work well at very low values of S_a. We need to consider the polynomial model (Equation 3.12) at low spectral accelerations and carry out the numerical integration for the performance evaluation (see Section 3.5.5 for details).

3.5.2 Alternative (Indirect) Approach

We can also use one of the indirect or alternative approaches defined in Section 2.7 to calculate the seismic demand of a structure. We will follow here the required spectral acceleration basis of the indirect approach, which is discussed in detail in Section 2.7.1 to calculate the seismic demand of a structure. The required spectral acceleration, $S_{a_y}^R$, for any record is the spectral acceleration level at the elastic-first-mode frequency of a structure required to induce a damage level y in that structure. The probability of exceedance of a damage level y of any damage parameter Y can be obtained from Equation 3.17 as follows:

$$P(Y > y) = \sum_{i=1}^{N} \nu_i \left\{ \int\int P[S_a > S_{a_y}^R | m, r] \cdot f_{M,R}(m, r)\, dm\, dr \right\}_i$$

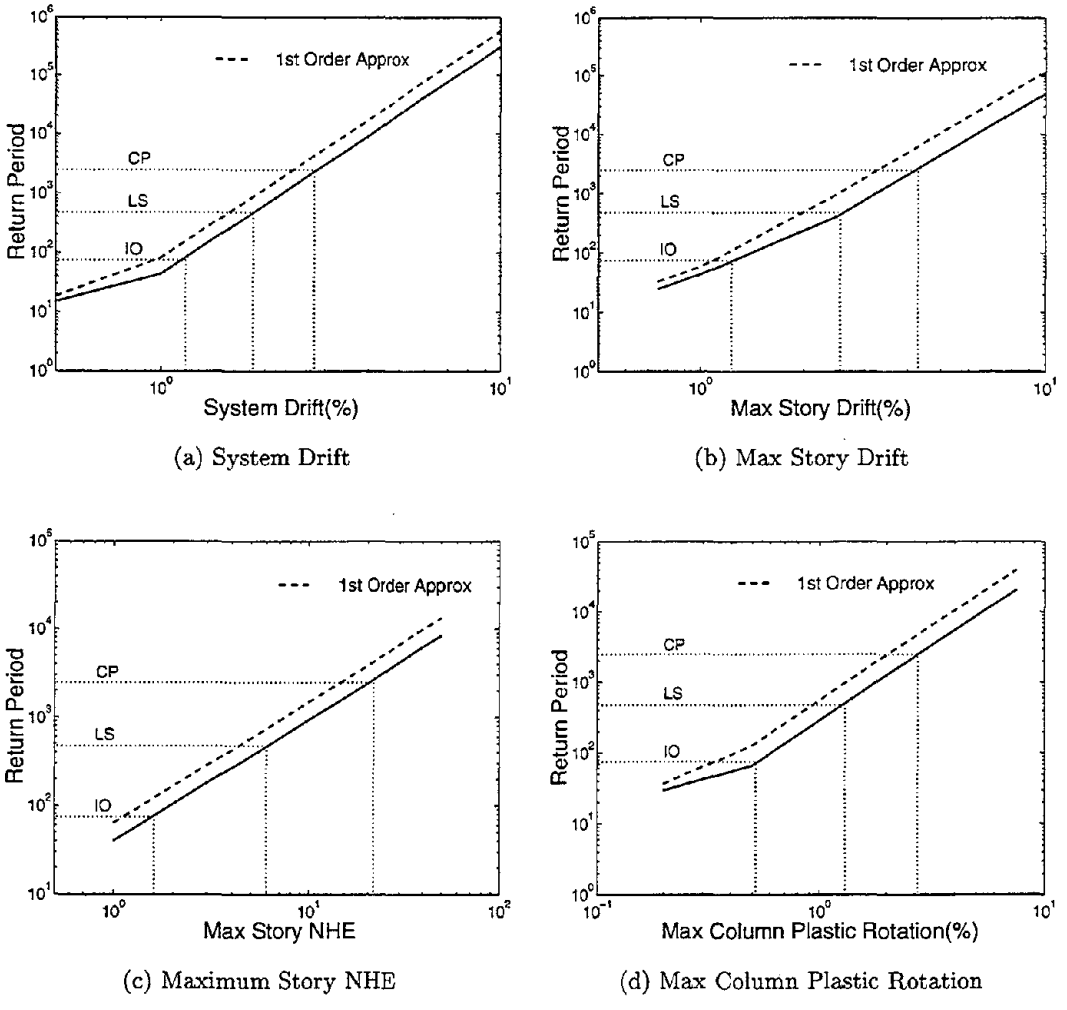

(a) System Drift

(b) Max Story Drift

(c) Maximum Story NHE

(d) Max Column Plastic Rotation

Notation: CP=Collapse Prevention, LS=Life Safety, IO=Immediate Occupancy

Figure 3.15: Seismic demand-hazard curves for a 5-story SMRF at a central Los Angeles site.

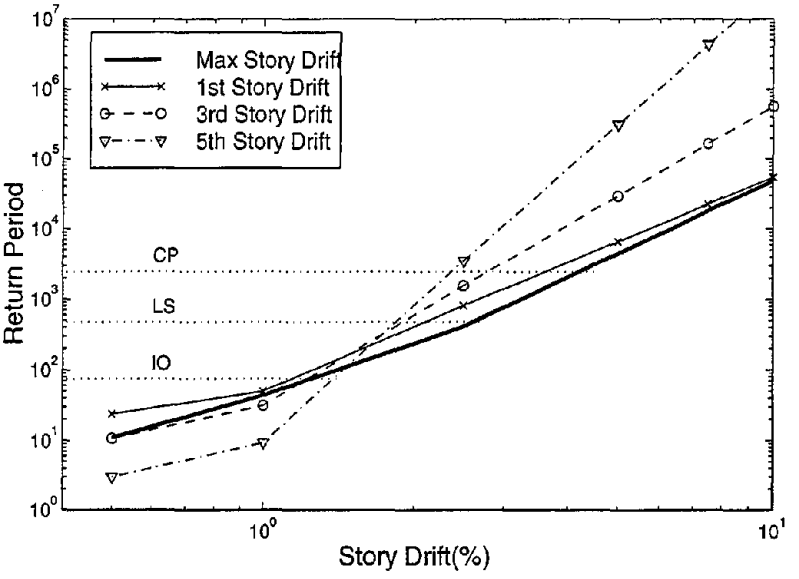

Notation: CP=Collapse Prevention, LS=Life Safety, IO=Immediate Occupancy

Figure 3.16: Seismic drift demand-hazard curves at each story for a 5-story SMRF at a central Los Angeles site.

$$= \sum_{i=1}^{N} \left\{ \nu_i \int\int\int P[S_a > s_{a_y}^R | m, r] \cdot f_{S_{a_y}^R | M,R}(s_{a_y}^R | m, r) \right. \\ \left. f_{M,R}(m, r)\, dm\, dr\, ds_{a_y}^R \right\}_i \qquad (3.27)$$

We can get an explicit solution of the above equation if we assume the following:

1. The distribution of $S_{a_y}^R$ is lognormal.
2. $S_{a_y}^R$ is not dependent on M and R.
3. The seismic hazard function $H_{S_a}(.)$ can be approximated by the Equation 3.23.

The Equation 3.27 then simplifies as follows (see Cornell, 1994, for details):

$$P(Y > y) = \int \left[\sum_{i=1}^{N} \nu_i \left\{ \int\int P[S_a > s_{a_y}^R | m, r] f_{M,R}(m, r)\, dm\, dr \right\}_i \right] f_{S_{a_y}^R}(s_{a_y}^R)\, ds_{a_y}^R$$
$$= \int H_{S_a}(s_{a_y}^R)\, f_{S_{a_y}^R}(s_{a_y}^R)\, ds_{a_y}^R$$

$$= H_{S_a}(\hat{s}^R_{a_y}) \cdot e^{\frac{(K_1 \delta_{S^R_{a_y}})^2}{2}} \tag{3.28}$$

where K_1 is the slope of the seismic hazard function in log-space in the vicinity of $\hat{s}^R_{a_y}$, and $\hat{s}^R_{a_y}$ and $\delta_{S^R_{a_y}}$ are the median and dispersion respectively of $S^R_{a_y}$ at the damage level y.

The required spectral acceleration, $S^R_{a_y}$, for maximum story drift of the 5-story building, which we get from the records of Bins I, II, and III are shown in Figure 3.17. Although one can calculate $S^R_{a_y}$ several ways, we have adopted the interpolation method for this calculation (see Appendix D for a description of different methods of calculating $S^R_{a_y}$). We also observe in the same figure the variation of dispersion of $S^R_{a_y}$ at different drift levels (shown within parenthesis). Note that the dispersion increases with the increase in drift. The probability of exceedance of 5% story drift calculated from Equation 3.28 is $2.09(10^{-4})$, which is very close to the result of calculations we did before in the direct approach ($= 2.23 \times 10^{-4}$). The calculations of seismic drift demand at other drift levels are shown in Figure 3.18. We observe that the drift demand results obtained from the direct and the indirect approaches are close to each other. Drift demand calculations based on another indirect approach, the nonlinear capacity factor basis (see Section 2.7.2 for a description of this approach), are described in Bazzurro and Cornell (1994).

3.5.3 Demand Prediction from the FEMA-273 Procedure

It is worthwhile to compare the above results above with the recently developed FEMA guidelines. If we follow the nonlinear static procedure (NSP) of the FEMA-273 guideline, we get the target displacement (δ_t) demand due to the BSE-2 earthquake (corresponds to 2475-year return period) at the top of the structure from the following relation:

$$\delta_t = C_0 \cdot C_1 \cdot C_2 \cdot S_a \cdot \frac{T_e^2}{4\pi^2} \tag{3.29}$$

where

T_e= effective fundamental period of the building= $T_i \cdot \sqrt{K_i/K_e}$= 1.1sec.

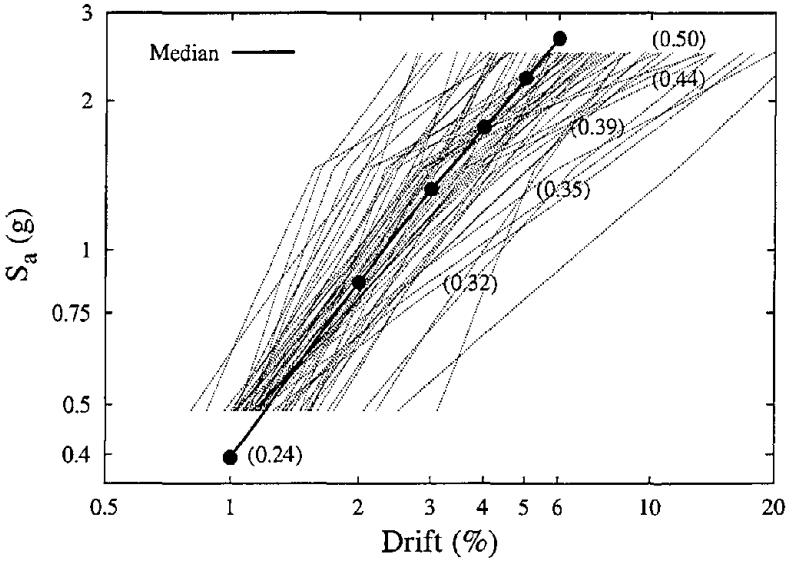

Figure 3.17: Variation of required spectral acceleration ($S_{a_y}^R$) of a 5-story SMRF at different levels of interstory drift. The median $S_{a_y}^R$ is calculated by the interpolation method. The numbers within parentheses at different levels of drift indicate the "dispersion" (as per Equation A.2) of $S_{a_y}^R$ at that level.

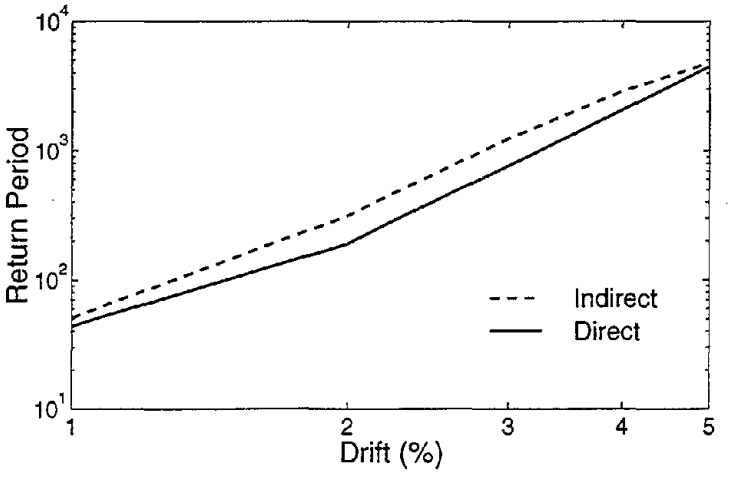

Figure 3.18: Seismic drift-demand hazard from the direct and the indirect approach for a 5-story SMRF at a central Los Angeles site.

T_i= elastic fundamental period of the structure= 1.1sec.

K_i, K_e = elastic lateral stiffness and the equivalent lateral stiffness of the building. Note that the two values are the same (see Figure 3.3).

C_0= modification factor to relate spectral displacement and likely building roof displacement= 1.4.

C_1= modification factor to relate expected inelastic displacements to displacements calculated for linear elastic response = 1.0 ($T_e > T_0$).

T_0= a characteristic period of the response spectrum, defined as the period associated with the transition from the constant acceleration segment to the constant velocity segment of the spectrum = 0.5sec (see Figure 3.19).

C_2 = modification factor to represent the effect of hysteresis shape on the maximum displacement response = 1.0

C_3= modification factor to represent increased displacement due to dynamic P-Δ effects= 1.0.

S_a= response spectrum acceleration at the effective fundamental period 1.1sec and 2% damping from Figure 3.19 = 1.4g [$S_a(2\%) = S_a(5\%)/0.8$].

So the target displacement δ_t is 23.2inch (=590mm). When we apply this displacement at the top story and carry out the nonlinear static analysis, we get the maximum story drift-demand value as 4.0%. Compare this value with the 3% drift demand, the median value we predicted from the nonlinear dynamic analysis at the 1.5g spectral acceleration (2500-year spectral acceleration at 1Hz). We have also obtained 3.4% maximum story drift for the 2500-year demand (see Figure 3.15).

3.5.4 First-Order Approximate Demand Prediction

Note that Equation 3.25 can be simplified greatly if we neglect the variability of response calculation for a given spectral acceleration (C_f= 1). Recall that we neglect this variability in demand calculations by code procedure. The equation then simplifies to

$$P(Y > y) = H[(y/\alpha)^{\frac{1}{\beta}}] \tag{3.30}$$

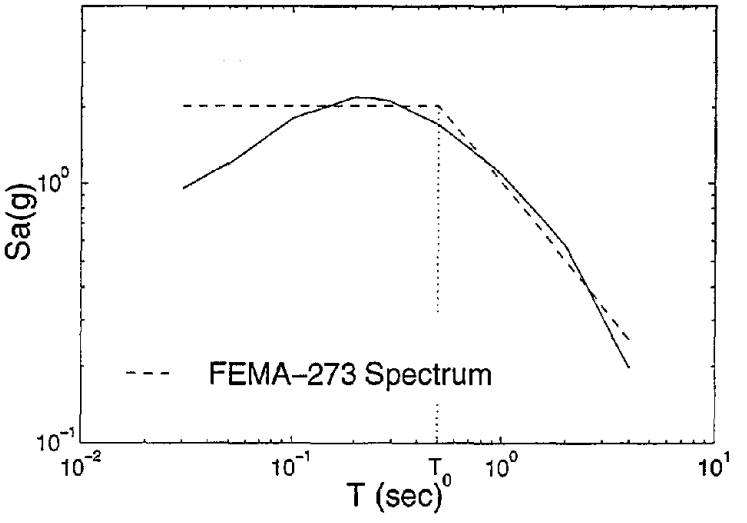

Figure 3.19: Uniform hazard curve at 5% damping for mean 2500-year return period. The FEMA-273 spectrum is the site specific ground shaking hazard spectrum as per FEMA guideline.

The first-order approximation of the probability of exceeding the 5% maximum interstory drift level (which is the limiting drift at the collapse-prevention level) is $9.45(10^{-5})$ or a 10500-year return period. Compare this result with the "exact" solution, which is a 4500-year return period. This prediction is higher by a factor of 2.4 than the exact solution because of the correction factor. Note that the advantage of this simplified method is that it gives the probability of exceeding the allowable damage unlike the FEMA-273 guideline which only calculates the damage demand at a given ground-motion level, e.g., the 2500-year level. The results of this first-order approximation for different damage measures at different damage levels are shown in Figure 3.15. Note that the 2500-year maximum story drift demand is 3.3% from this first-order approximate result, whereas it is 4.3% from the "accurate" solution in Equation 3.25. We observe that although the dispersion of plastic rotation and NHE are higher than the dispersion of drift, because of steeper slope (β) of the regression functions, the values of the correction factor for these damage parameters are lower than that of the drift. The correction factor C_f of the maximum story drift is 2.4, the maximum story NHE is 1.7, and the maximum plastic rotation is 1.9. So the difference

between the accurate solution from Equation 3.25 and the first-order approximation from Equation 3.30 is quite similar for all the damage measures.

3.5.5 Estimation of Demand for More General Regression Functions

We have seen before that the regression model (Equation 3.2) does not work well at low spectral accelerations for NHE and plastic rotation damage measures. We have improved the prediction by fitting a polynomial regression model. The major disadvantage of this model is that the calculation of performance of a structure from an explicit equation like Equation 3.25 is not possible. The other problem with this model is that the standard deviation of error σ_ε varies with the predictor variable S_a. Also note that because the regression analysis of the polynomial model is carried out in arithmetic space, this model, compared to the regression analysis in log-space, gives higher weight to these sample points that are much higher than the mean value. As a results we see in Figure 3.12 that when the linear regression model (Equation 3.2) fitted in log-space and the polynomial model (Equation 3.12) fitted in arithmetic-space, the polynomial model in general predicts higher response at a given spectral acceleration for the NHE as well as for the plastic rotation. Only at low spectral accelerations does the polynomial model predict lower response for the NHE and the plastic rotation. In order to find out the effect of incorporation of the polynomial model in predicting the seismic demand of a structure we carry out numerical integration of the following equation, which we get from Equation 3.20:

$$\begin{aligned} P(Y > y) &= \int \left| \frac{\partial G_{Y|S_a}}{\partial s_a}(y|s_a) \right| \cdot H(s_a)\, ds_a \\ &= \int \frac{1}{\sqrt{2\pi}\sigma(s_a)} e^{-\frac{1}{2}\left[\frac{y-(\alpha+\beta_1 s_a+\beta_2 s_a^2)}{\sigma(s_a)}\right]^2} \cdot |(\beta_1 + 2\beta_2 s_a)| \cdot \\ &\quad (K_0 s_a^{-K_1})\, ds_a \end{aligned} \tag{3.31}$$

where

$H(s_a)$ = hazard function, which is approximated by Equation 3.23. We could

have included the PSHA results in the numerical integration, but we are interested here in determining the effect of different regression models. We therefore use here the same approximation in hazard estimation.

$G_{Y|S_a}(y, s_a)$ = conditional complementary cumulative distribution of damage Y given S_a. We assume the distribution is normal. The mean of the distribution is $\alpha + \beta_1 s_a + \beta_2 s_a^2$ and the standard deviation is $\sigma(s_a)$, which increases with the increase in spectral acceleration. In Figure 3.13 we have observed the dependency of σ on S_a. In numerical integration we will use directly the standard deviation results obtained from fitting the polynomial model to the data. This gives us three standard deviation values at three different S_a levels; the standard deviation at the intermediate S_a levels is obtained by linear interpolation.

The results of numerical integration (Equation 3.31) and the results obtained from Equation 3.25 for maximum story NHE and for maximum plastic rotation are shown in Figure 3.20. In general we observe that the numerical integration results and the closed form results are very close to each other except at the low return-period levels (e.g., the immediate-occupancy level). Since the polynomial model does not have any constraint on the slope of the function at the origin and also does not neglect the sample points close to zero, the results from numerical integration at the region of low return periods may be more precise than the closed-form solution.

3.6 Summary

We have seen that the observations made before in Chapter 2 and in Appendix E are also valid for a realistic 2-D model of a 5-story steel moment frame. In this chapter we have considered for first time the P-Δ effect in nonlinear dynamic analyses. Although the pushover results in Figure 3.3 indicate that this effect is not very important for this structure. The most important observations are

1. Scaling introduces mild bias in the displacement-based damage measures when the

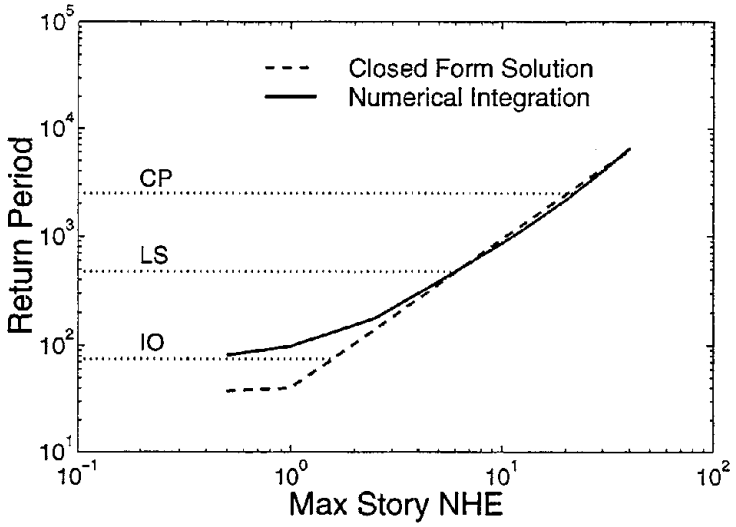

(a) Maximum Story NHE

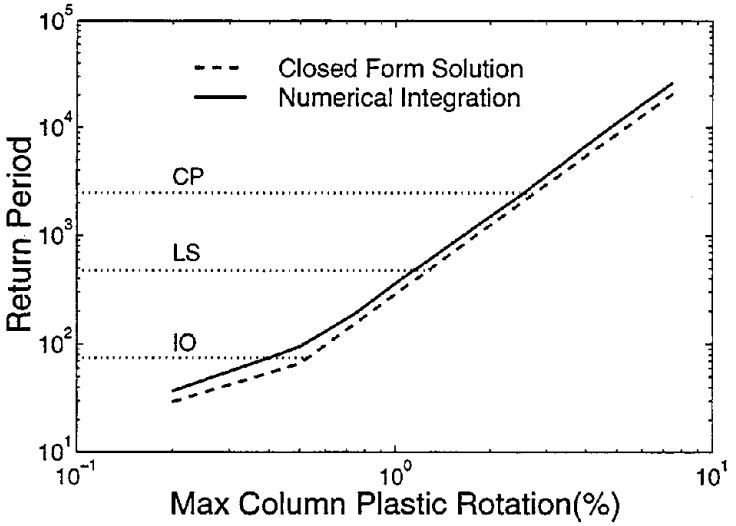

(b) Maximum Column Plastic Rotation

Notation: CP=Collapse Prevention, LS=Life Safety, IO=Immediate Occupancy

Figure 3.20: Comparison of results from the closed-form solution (Equation 3.25) and from numerical integration (Equation 3.31). Note that both in numerical integration and the closed-form solution the hazard curve is approximated by Equation 3.23.

results are compared across the bins, i.e., the scaled results of a bin are compared to the results of another bin scaled to the same intensity level; the bias in the energy-based damage measures is, however, substantial.

2. Scaling reduces the dispersion of the results significantly.

From the regression results we make the following observations:

Given S_a the dependency of the displacement-based and the energy-based damage measures on the additional parameter higher-frequency spectral acceleration (here we have used spectral acceleration at the elastic-second-mode frequency), magnitude, and distance are statistically significant. The energy-based damage measure depends additionally on duration. The dependency of damage measures on the higher-mode spectral accelerations is the most significant of all the parameters. This conditional dependence, while statistically significant, is however not of great practical importance, since the incorporation of these parameters does not reduce the dispersion or change the sample size requirement significantly. But the dependencies of the responses on different parameters may explain why we get somewhat different results from different bins. The mild dependency of damage measures on parameters in addition to the first-mode-frequency spectral acceleration confirms that scaling of records seldom introduces an important bias in damage estimation (Figure 3.10).

Finally we have used the regression analysis results to calculate the probability of exceedance of allowable damage, i.e., the performance of a structure. We have found that we can calculate very easily the seismic demand of a structure from an explicit equation with some assumptions that are valid for typical structural engineering problems. In all the demand calculations we have assumed that the structural responses are dependent only on the spectral acceleration at the lowest frequency of the structure (which we have found is valid for most of the problems we have studied for a typical California site and also for the problem considered for illustration of the methodology). The calculation of seismic demands

for responses dependent on the additional parameters will be discussed in Chapter 5. We have also found that the demand calculations from the indirect (or alternative) approach matches quite well with those of the direct approach. We have also compared these results with the approximate results from the nonlinear static procedure (NSP) described in FEMA-273 (1996). We have observed that the results of the performance calculations from the rigorous procedure developed in this chapter for a single-frequency dominated 5-story structure matches quite well with the approximate FEMA results.

We have observed that the convenient regression model that is proposed in this chapter does not work very well at the low-demand levels (e.g., at the immediate occupancy or 75-year demand level). We have also studied the impact of a more general polynomial regression model in demand calculation, and we have found that the convenient regression model overpredicts the seismic demand only at low-demand levels, and the effect is marginal.

Chapter 4

Probabilistic Seismic Demand Analysis: "Collapse" Case

4.1 Introduction

We have observed so far that the normalization and scaling do not introduce any significant bias in damage estimation for single-frequency dominated structures and also that these methods reduce the dispersion of damage measures significantly (around 50%) over the direct method. We have also observed both in regression results and in bin-to-bin results that the damage measures conditioned on the first-mode spectral acceleration do not depend significantly on the event parameters (magnitude and distance of earthquake), or the record parameters (duration and spectral ordinates at frequencies higher than the first-mode frequency of a structure). We will verify all these observations for tall structures. In general the elastic maximum-story responses of tall structures have significant higher mode effects. To study the characteristics of nonlinear response of a tall structure and its performance evaluation, we will consider In this chapter a 20-story steel-moment-resisting-frame building. This building was designed for the SAC-project. See Gupta (1999) for a detailed description of this structure. It is observed in general that the response of tall flexible

structures has a significant P-Δ effect. By considering this additional effect on nonlinear-response calculations along with the likely multi-frequency effects, we will establish whether the conclusions in the previous chapters are more universal.

We will observe from the center-line representation of the 20-story structure that because of the significant P-Δ effect the probability of "collapse" of the structure is high even at the 2500-year intensity level. We will develop a new procedure to incorporate these "collapse" results in seismic demand calculations. Finally, we will compare the results of demand calculations from the direct approach with the results from the indirect approach.

The responses of this tall structure may also be dependent on several other parameters in addition to the first-mode spectral acceleration. If so, the consideration of these parameters in demand calculations will not only reduce the number of expensive nonlinear analyses, but may also improve the accuracy of demand calculations. We will develop a procedure in Chapter 5 to take into account these additional parameters in demand calculations.

4.2 Results

4.2.1 Static-Pushover Analysis and Elastic-Modal Properties

At first we will look into the results from "static pushover" analysis, which is a nonlinear step-by-step static analysis. This analysis has become a popular tool in recent years to predict the demand of a structure under earthquake loading (e.g., FEMA-273, 1996; ATC-40, 1996; Vision-2000, 1997; etc). Static pushover analysis was developed initially to evaluate the performance of a structural system by estimating the demand from a "simple intermediate solution" instead of solving the complex and time-consuming problem of demand prediction when the deformation capacities are not known with great precision, e.g., at the design stage of a structure (see Krawinkler, 1996). It has been observed that the prediction of nonlinear global seismic demand by static-pushover analysis is quite satisfactory for a single-frequency dominated MDOF structure (see Krawinkler and Seneviratna, 1997). We have also made a similar observation in Chapter 3 for a 5-story steel-moment-resisting

frame. Recall that this structure is primarily a single-frequency dominated structure. We will check below how well the demand results from pushover analysis match those from nonlinear dynamic analyses for the (expected) multi-frequency dominated structure we consider in this chapter. The plot of static pushover analysis results for global deformation is shown in Figure 4.1 and the same plot for story deformations are shown in Figure 4.2. We carried out the step-by-step nonlinear static analysis is carried out by using the DRAIN-2DX (1993) program. In the analysis we have adopted the displacement controlled analysis procedure. The lateral load pattern on the structure is calculated according to the FEMA-273 provisions ($k = 2$). We observe that the P-Δ effect in the structure is so significant that the plateau of the load-deformation curve in the post-elastic range is quite narrow. See Figure 4.1, where the negative slope of the global-force curve starts at only 1.5% global drift. At the end of this plateau we observe a steep negative slope of the load-deformation curve leading to collapse of the structure. In Figure 4.2 we find that the upper stories (higher than nine) are, however, within their elastic range when the structure starts unloading. That is why the load-deformation plot of these higher stories is linear. The plot of deflected shape of structure in Figure 4.3 at different stages of static-pushover analysis confirms that when the structure attains a negative post-yield stiffness, displacements at the lower stories increase rapidly leading to collapse of structure, whereas the upper stories remain elastic without any appreciable increase in displacements. The force-deformation plots of different stories help to predict that the deformation demand under severe earthquake loads will be concentrated only at the lower stories. We will additionally use these pushover results to calculate the story yield displacement, which is used to calculate the story ductility or story normalized hysteretic energy (NHE).

In order to try to understand the dynamic behavior of the structure, we look into the frequencies and modal mass participations at the lowest five modes. These are given in Table 4.1. We find that this is a low-frequency structure of 0.25Hz first-mode frequency. The modal mass participations, however, do not indicate that the structure is a multi-mode dominated structure. Compare these values with those of a single-mode dominated structure in Table 3.1. We will discuss this issue of single- versus multi-mode dominated

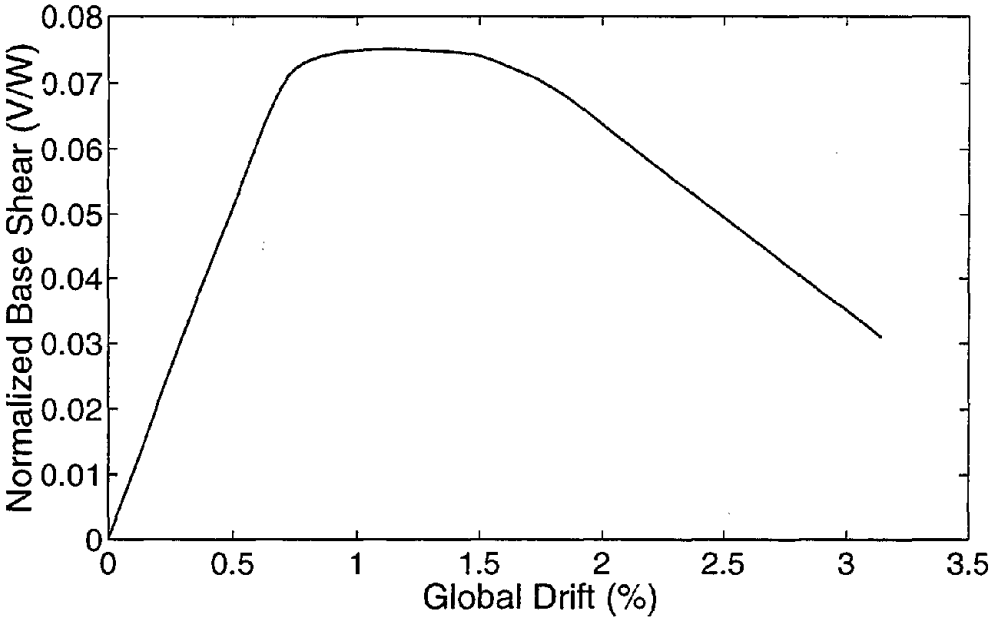

Figure 4.1: Global force-displacement results from static pushover analysis for a 20-story SMRF building. Here W is the seismic dead load of the structure and V is the shear force.

response in Section 4.2.4. Note that up to the last chapter we have considered only single-mode dominated structures. When structural responses go beyond a structure's elastic limit, the notion of "mode" in explaining the difference in responses is questionable. Mode is, however, a good indicator to understand the effect of accelerations at frequencies higher than the elastic first-mode frequency of a structure.

Next we will look into the results of nonlinear dynamic analyses. First we will consider only the results from a bin of records to verify whether scaling is a legitimate method for this tall, P-Δ sensitive structure. Subsequently we will carry out regression analysis to verify whether responses of this tall structure are, given S_{a1}, dependent on magnitude, distance, duration, or spectral shape of ground-motion records.

4.2.2 Selection of Records

We will consider only the Bin-III records for the bin-to-bin analysis. We find that most of the low-magnitude records (Bin-I) and high-magnitude, long-distance records (Bin-II) do

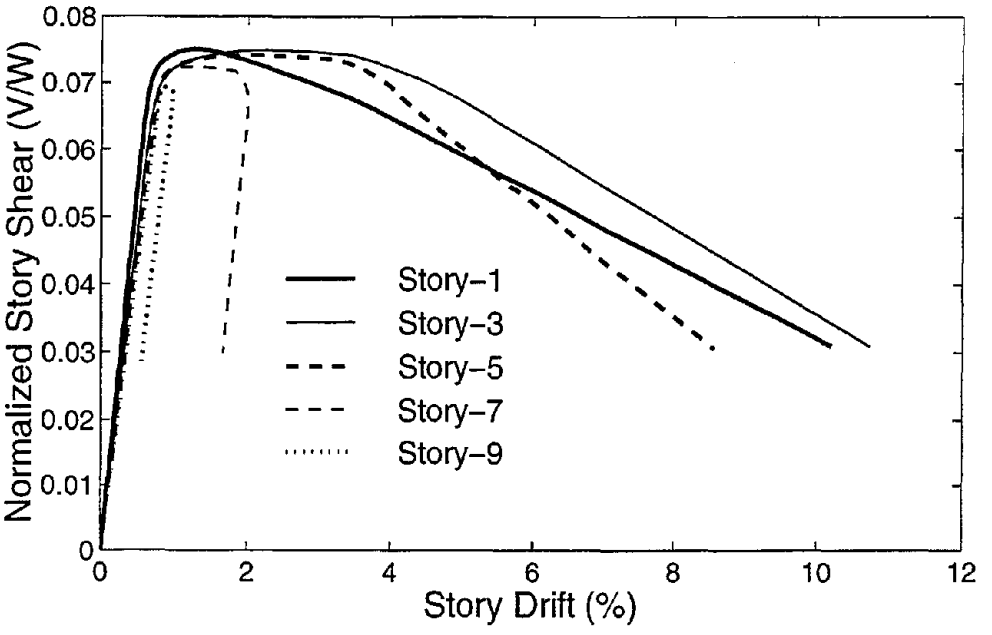

(a) Story force displacement

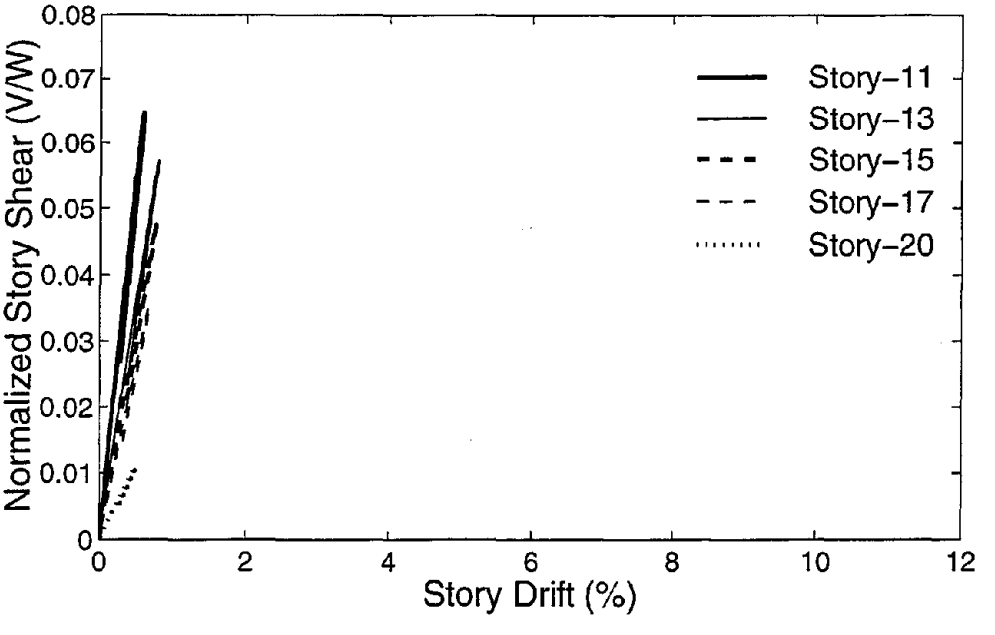

(b) Story force-displacement

Figure 4.2: Results of story force-displacement from static pushover analysis for a 20-story SMRF building. Here W is the seismic dead load of the structure and V is the shear force.

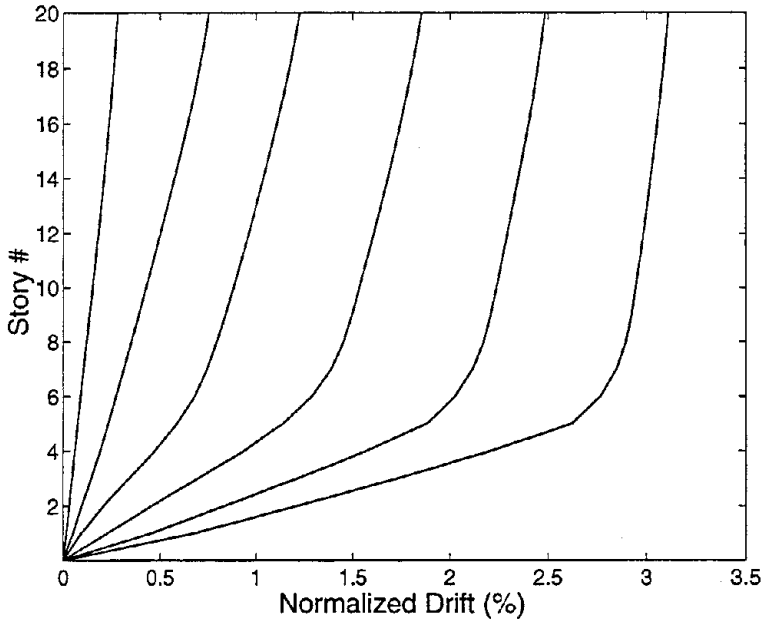

Figure 4.3: Deflected shapes at different stages of static pushover analysis of a 20-story SMRF building at a Los Angeles site.

Mode	Period(sec)	Freq(Hz)	Mass Part(%)
1	3.99	0.25	0.80
2	1.37	0.73	0.12
3	0.79	1.27	0.03
4	0.56	1.79	0.02
5	0.43	2.35	0.01

Table 4.1: Periods, frequencies, and modal mass participations at different modes of excitation.

not have any significant signal at low frequencies. We use a low-cut filter to process these records to remove the noise from the signal, and for most of these records the low-corner frequency of the filter is higher than 0.25Hz (the lowest elastic frequency of the structure and normally the most important one). Therefore these records do not contain the low-frequency power to excite the structure at the first mode. Note that the signal-to-noise ratio of the records is in general too high at the 0.25Hz frequency to give a reliable result. So we are left only with the high-magnitude and short-distance Bin-III records (M = 6.7-7.3; R= 10-30km). For the purpose of analysis of this structure we consider only those records in the catalogue (Silva, 1995) whose low-corner filter frequency (f_{LC}) is equal to or less than 0.10Hz[1]. As a structure undergoes nonlinear deformations, the "effective" frequency of that structure becomes lower than that of its elastic counterpart. Hence while selecting the records we considered a low-corner frequency that is lower than the lowest elastic frequency of the 20-story structure. The maximum value of the low-corner frequency is based on the assumption that the effective lowest frequency of the structure is 0.10Hz ($= f_0/\sqrt{D\%}$ for drift D equal to 6%; see Kennedy et al., 1984, for details). Thus we use only 44 records out of 63 from Bin-III (for Bin-I we can use only 4 records out of 36). The change of shape of the response spectra that this selection process results in is shown in Figure 4.4. We

[1]In Appendix E the "direct" results indicate that the average nonlinear response of a tall MDOF structure (0.25Hz first-mode frequency) from a bin of low-magnitude records is significantly higher than that from a bin of high-magnitude records. Note that the capacity of the tall structure in the appendix has been reduced so that we do not need to scale the low-magnitude records substantially. In this chapter we have to scale these records significantly to get the nonlinear response of this 20-story building. The response spectra of these records indicate that the relative (scaled to the same first-mode spectral acceleration) spectral ordinates of the low-magnitude records are much higher than those of the high-magnitude records at frequencies higher than 0.25 Hz (the lowest elastic frequency of the tall structure). See Figure E.3(a). This explains the significant difference in nonlinear responses in Appendix E we observe in these two bins of records and this is difference is observed also in the scaled results. On the other hand, if a record has low signal-to-noise ratio at low frequencies, we cannot get any reliable result at low frequencies. We have chosen a low-corner frequency ($f_{LC} \leq 0.10Hz$) so that the signal up to that frequency is not overly contaminated by the low-frequency noise. If we assume that the records that do not have adequate signal (hence are "weak") at low frequencies cannot cause any significant response in the structure (this is true for any properly designed structures), we can neglect those records in structural analysis. We find in the appendix that the scaled results from these "qualified" (i.e., $f_{LC} \leq 0.10Hz$) low-magnitude records are quite close to those of the high-magnitude records. The close match of the relative spectral ordinates between the high- and the low-magnitude records may explain this similarity of results. Although we are neglecting the "weak" records in response calculations, at the end we can consider the contribution of those records in demand calculations when we would combine these response results with the "corrected" seismic hazard results (see Chapter 5 for a further discussion on this issue).

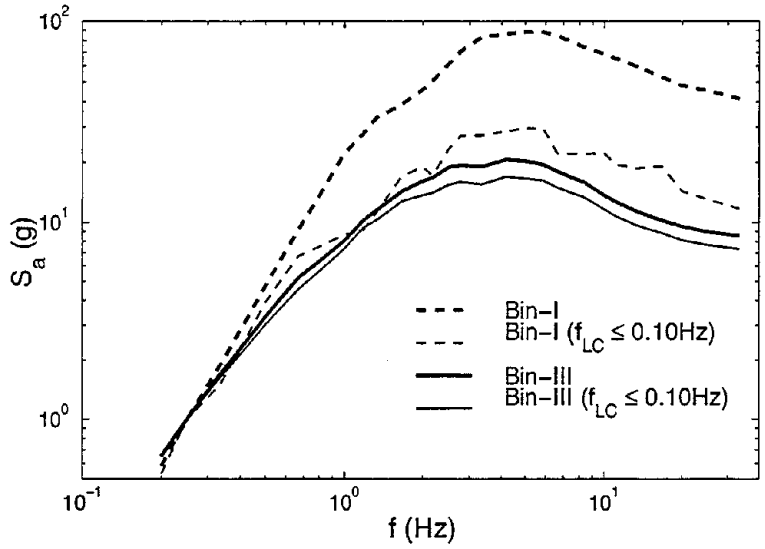

Figure 4.4: Median response spectra at 5% damping from different bins of records that are scaled to the 1.0g spectral acceleration at the 0.25Hz frequency. The thick lines indicate the original shape of the response spectrum of each bin of records and the thin lines indicate the shape we get from the records that have the effective low-corner frequency ($f_{LC} \leq 0.10Hz$).

find that the change for Bin-III records is minimal whereas that for the Bin-I records is substantial. Note that the average response spectrum of the Bin-I records, which have the effective low-corner frequency, is not very reliable as it is based on only 4 records.

4.2.3 "Direct" Results

The "direct" results we will present now are from the records pre-scaled by a common value (hence the quotes on "direct"). As described in Chapter 3 this value is the ratio of the target intensity to the median intensity of a bin. Hence these "direct" results are in fact what we have called "cloud-scaled" results (see Section 3.3.3 for details). We have scaled these records because the building's design ground motion is so strong that the structure behaves elastically for most of the as-recorded ground motion (see Table 2.1 for the intensity of records of different bins). We find in Figure 4.1 that the maximum normalized base shear or the base shear coefficient is around 0.075, whereas we find in Table 2.1 that even for high-magnitude and short-distance records the median spectral acceleration at 0.25Hz is

about 0.05g. Hence for most of those high-magnitude records we do expect any nonlinear behavior of the structure. We could have scaled down the structure, but scaling up the ground motion will give finally the performance of the original structure. Also we have seen so far that scaling has not introduced any significant bias in damage estimation. We consider here two intensity levels. We will first look into the "direct" results from records that are "cloud scaled" to a (low) intensity level of 0.05g (spectral acceleration at the first-mode 0.25Hz frequency and 2% damping). This corresponds to the 75-year intensity level (or a probability of exceedance of 50% in 50 years). We will then cloud scale those records to a (high) intensity level of 0.32g. This corresponds to approximately the 5000-year intensity level[2]. The results at the low and high intensity levels will help to verify the observations in Chapter 2 and Chapter 3 at a low and a high level of nonlinearity. The damage measures we consider are the global drift, global normalized hysteretic energy (NHE), system drift (average of all the story drifts), maximum story drift, maximum story NHE, maximum beam plastic rotation, and maximum column plastic rotation.

When we look into the results, we observe for the first time numerical instability in the solution scheme for some records at the high-intensity level. This numerical instability can be attributed to the non-convergence at a high level of nonlinearity. We will refer to this numerical instability as the "failure" or "collapse" of the structure[3]. This non-convergence implies excessive deformations in structures. The response of the structure for these "collapse" cases can be assumed to be infinitely large. So we cannot calculate the "median" and the "dispersion" from Equations A.1 and A.2 respectively as we have done in the previous chapters. In order to understand how the nonlinear response results are scattered about the central value, we plot the cumulative frequency distribution of maximum story drift in Figure 4.5. From the plot we see that only about 61% of the 44 cases converged. The median value of this damage measure is indicated to be 5.9%. We can

[2]We will find afterwards that the 2500-year intensity of ground motion is 0.25g. But Equation 3.25 indicates that for demand-hazard at 2500-year return period we need spectral acceleration of $S_{a,2500} \cdot e^{(K_1 \sigma_{\ln Y|Sa})/(2\beta_1^2)}$ which assumed here to be the intensity at 5000-year return period.

[3]Some researchers in this area also suggest including the high-drift results (e.g., $\geq$ 20% maximum inter-story drift) as "collapse" cases. The limiting drift beyond which a structure can be considered collapsed needs further research.

similarly calculate the median of other damage measures. We refer to this median estimation as the "counted median" ($\hat{y}$) because it is estimated from the middle of the ordered response results. In the present case we have estimated the median from the average of the 22^{nd} and the 23^{rd} ordered responses out of 44 results.

We need additionally information about the confidence band of this "counted median" in order to calculate the sample size requirements for a target confidence band width. We will calculate this confidence band width by *bootstrap replication* of the median damage[4]. An equivalent dispersion of the median-damage results is from the following:

$$\delta_{\hat{y}}^{eq} = \frac{1}{2} \ln \left[\frac{\hat{y}_{84\%}}{\hat{y}_{16\%}} \right] \tag{4.1}$$

where $\hat{y}_{16\%}$ is the 16^{th}-percentile of the estimator of the median response and $\hat{y}_{84\%}$ is the 84^{th} percentile. If the distribution of the estimator of the median is lognormal, then we will get the exact dispersion from this approach. We will find below that the distribution, however, is not lognormal at the high intensities when the structure collapses. Hence we refer to this estimation as "equivalent dispersion". A problem with this sample statistic is that it is a function of the sample size: it will be small for larger samples. We can finally get an equivalent dispersion of a damage measure itself as follows:

$$\delta_{eq} = \frac{1}{2} \sqrt{n_B} \cdot \ln \left[\frac{\hat{y}_{84\%}}{\hat{y}_{16\%}} \right] \tag{4.2}$$

where n_B is the size of the bootstrap sample. We are assuming here that the dispersion of the estimator of the median drift decreases by $1/\sqrt{n_B}$. We will verify this assumption in the following section. Note that δ_{eq} is not a function of the sample size. Note also that because there were no collapses, one can calculate the statistics of damage measures as before at the low-intensity level. For consistency, however, we will present now only the sample statistics

[4]Bootstrap is a data-based simulation technique for statistical inference. In this method a *bootstrap sample* is drawn with replacement from the original population. Here we repeated this process 1000 times for each of the damage measures to get the *bootstrap replication* of the median, and we finally calculated different statistics of the estimator of the median from the 1000 bootstrap replications of the median. See Efron and Tibshirani (1993) for details.

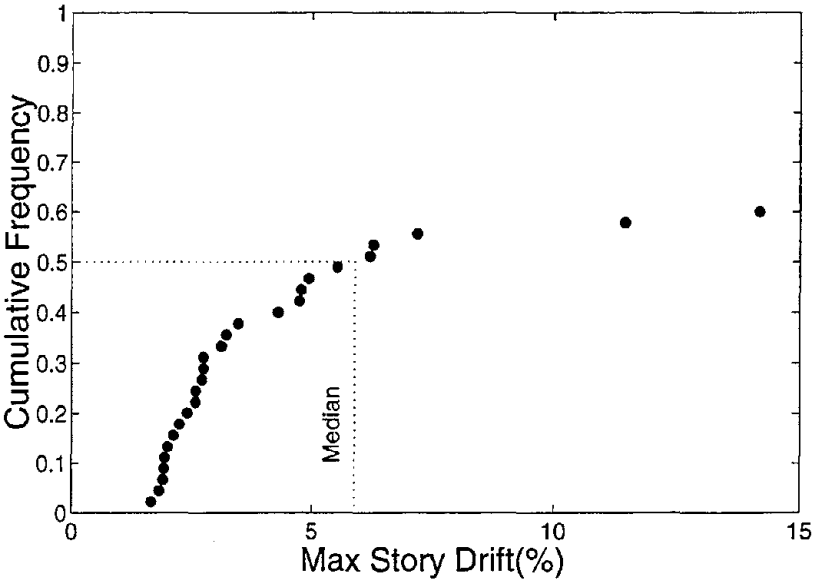

Figure 4.5: Cumulative frequency distribution of maximum interstory drift from "direct" results ("cloud" scaled to a median of 0.32g spectral acceleration at 0.25Hz and at 2% damping).

described here.

The results of the "direct" analyses are given in Table 4.2. Note that we have not provided any statistics of the NHE and plastic rotation at the 0.05g intensity level because these damage measures generally do not have any significant value at low intensities. We find that at the 0.32g intensity level the probability of "collapse" of the structure is 39%, whereas at the 0.05g intensity level it is insignificant. We observe that with the increase in the intensity of ground motion, the (counted) median damage measures also increase. The (equivalent) dispersions of all the damage measures are very high at the high-intensity level (0.32g). We observed in Chapter 3 that the dispersion of global drift and story drift were comparable to or slightly lower than the dispersion of S_a at the high intensity levels, whereas the dispersion of plastic rotation was higher. In this case we observe that although plastic rotation has relatively higher dispersion than the other displacement-based damage measures, the dispersion of all the damage measures at the high intensity level is much

Parameter	Direct				Scaled				Weighted Average			
	$\hat{y}_0$	δ_{eq}	$\hat{y}_0$	δ_{eq}	$\hat{y}_0$	δ_{eq}	$\hat{y}_0$	δ_{eq}	$\hat{y}_0$	δ_{eq}	$\hat{y}_0$	δ_{eq}
Failure (%)	0		39		0		29		0		27	
$S_a(0.25Hz)$	0.05	0.7	0.32	0.7	0.05	0	0.32	0	0.05	0.4	0.32	0.4
$S_a^\star$	–	–	–	–	–	–	–	–	0.12	0	0.73	0
Global Drift (%)	0.4	0.73	1.8	2.71	0.4	0.14	2.9	1.64	0.4	0.26	2.11	1.32
Global NHE	–	–	9.8	2.63	–	–	10.4	1.29	–	–	7.9	0.54
System Drift (%)	0.7	0.57	2.6	1.92	0.7	0.68	3.3	1.47	0.7	0.18	2.7	0.74
Story Drift (%)	1.1	0.72	5.9	2.70	0.8	0.92	7.5	1.85	0.8	0.16	5.3	1.61
Story NHE	–	–	39.8	1.99	–	–	42.3	1.71	–	–	36.7	1.12
Max. θ_{BP} (%)	–	–	5.1	2.97	–	–	6.7	2.00	–	–	4.6	1.80
Max. θ_{CP} (%)	–	–	3.1	4.50	–	–	4.3	2.73	–	–	2.3	3.23

Notation: $\hat{y}_0$= "counted" median; δ_{eq}= "equivalent" dispersion (Equation 4.2); θ_{BP}= beam plastic rotation; θ_{CP}= column plastic rotation.

Table 4.2: "Direct", scaled (to the first-mode spectral acceleration), and scaled to the weighted-average spectral acceleration, $S_a^\star$ (of the first three modes), results of different damage measures from the 44 (qualifying) Bin-III ground motion records. The spectral accelerations (S_a) are calculated at 2% damping. The two intensity levels shown are 0.05g and 0.32g.

higher than the dispersion of spectral acceleration. This high dispersion of damage measures indicates that the small sample size (three to seven) proposed by the guidelines is not sufficient. We will investigate in the following section how to reduce the sample size requirements to a practicable level.

4.2.4 Scaled Results

In this case all the records in a bin are scaled to the same target spectral acceleration at the lowest elastic frequency (0.25Hz) of the structure. The results of this analysis are given in Table 4.2. We observe that this structure collapses in 29% of the cases at the 0.32g intensity level. The median damage measures of the "direct" and the scaled results are quite close to each other at the same intensity level. (One must remember that even with 44 samples, the standard error of estimations are very high, e.g., in the direct case typically about $3/\sqrt{44}$ or 0.4, which is more than $\pm 40\%$.) We also observe that we get around 40% reduction in (equivalent) dispersion of maximum story drift by scaling these records; the system and the story drifts at the low level are exceptions (we will explain

below why these results are exceptions). Even after this reduction, the dispersion at the high intensity is still very large compared to what we have seen in the previous chapters. In order to make a visual comparison between the "shape" (or distribution) of the direct and the scaled results, we plot the cumulative frequency distribution of maximum story drift and maximum story NHE in Figure 4.6. We observe that the cumulative distribution shapes of the direct and scaled results are quite similar for the NHE, indicating little or no benefit from scaling the records. The median drift (at the 0.50-cumulative-frequency level) on the other hand looks somewhat different, but the median drift from scaled results is within the 16^{th}- to 84^{th}-percentile confidence bands on the median drift from direct results which is 4.7%-12.1%.[5]

We observe that the dispersion of maximum story drift, of maximum story NHE, and of the maximum beam plastic rotation are very high even after scaling and are also of the same order. In the previous chapters, conversely, we have observed that the dispersion of maximum story drift is in general the lowest among those three. The high dispersion observed for the 20-story building is due to large interstory drifts concentrated only at the first five stories. So this maximum story drift is, somewhat, "local" in nature. It has high dispersion similar to the local damage measures (compare the dispersion of maximum story drift and maximum beam plastic rotation). This may also explain the comparable dispersion of the story NHE. The localization of drift is due to the characteristic "bulging" of the bottom stories at high intensities (this will be obvious below when we will show the deformation plots). This shape is a characteristic of tall buildings with significant P-Δ effect at high-intensity ground motions.

We have observed before that generally at a low drift the dispersion of the maximum story drift from scaled results is around 0.1 to 0.2 (see Table 2.3 and Table 3.2), whereas for this structure the same is around 0.5, which is calculated as before in Chapter 2 or 3 for a fair comparison. Now the question is: why is the dispersion so high for these scaled

[5]Note that this is a somewhat conservative approach to check whether the *difference* in the median results is statistically significant. In this approach we have neglected the variability in the median-drift estimation of the scaled results.

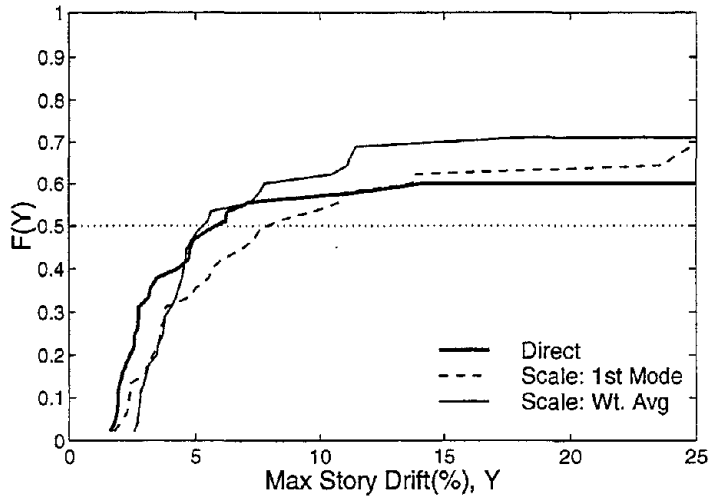

(a) Maximum interstory drift

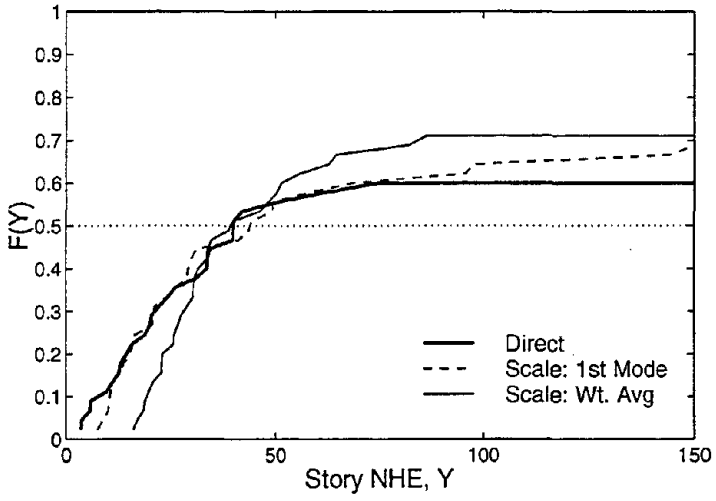

(b) Maximum interstory NHE

Figure 4.6: Cumulative frequency distribution of different damage measures from direct, first-mode scaled, and weighted-average scaled results.

results even at this low-drift level? An answer that intuitively comes to mind is the higher mode effect, but we have seen in Table 4.1 that the modal participations do not support this answer. Recall that the 5-story and the 20-story structure have very similar modal participation factors, but they have completely different elastic response statistics of the scaled results. This indicates that the difference in the elastic results may be due to the difference in spectral ordinates at higher modes relative to that at the first-mode. The ratio of the second- and the third-mode spectral ordinates to the first-mode spectral ordinate of the Bin-III records are 4.6 and 9.2 respectively for the 20-story structure and 2.7 and 2.8 respectively for the 5-story structure. The dispersions of this ratio for the 20-story structure at the second and third modes are 0.6 and 0.7 respectively and for 5-story structure at the same modes are 0.5 and 0.6 respectively. Due to these significantly higher relative spectral ordinates, we would expect that the higher modes would contribute significantly to the overall elastic response of the 20-story building even though the modal participation factors are not very high. To verify this hypothesis, we plot the variation of the scaled results of the maximum story drifts with the second- and third-mode spectral accelerations in Figure 4.7. First consider the results at the low-intensity level. We observe that there is a trend: the drifts increase with the increase in higher-mode spectral accelerations. Because the record-to-record variability of the spectral shapes (ratios) is high and the contribution of higher modes to the response results is also high, the dispersion of the maximum story drift of this 20-story structure is larger than what we have observed for the 5-story structure.

4.2.5 Weighted-Average Scaling

We have observed in Figure 4.7 that the spectral accelerations at higher modes are important at low drifts. In that figure we observe the same also at the high-drift levels. Since the contribution of spectral accelerations at higher modes (or frequencies) is significant in the overall response of this structure, we need to give an "appropriate" weight to the spectral ordinates at higher modes (or frequencies) to get a lower dispersion of response. In order to do this we calculate an average spectral acceleration from the spectral accelerations

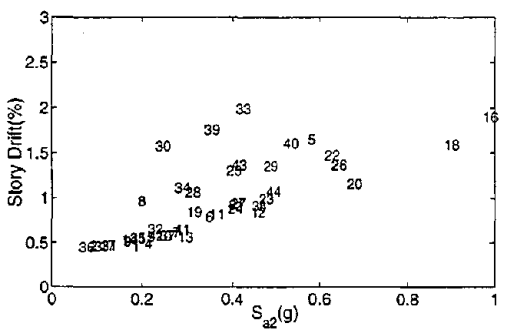

(a) At 0.05g with S_{a2}

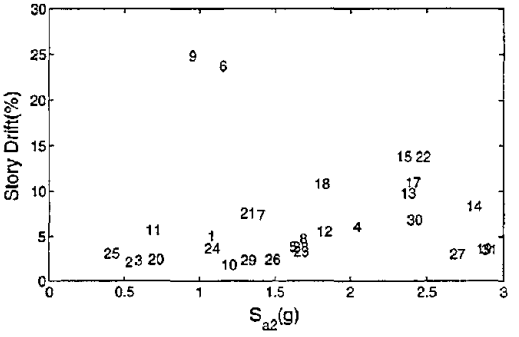

(b) At 0.32g with S_{a2}

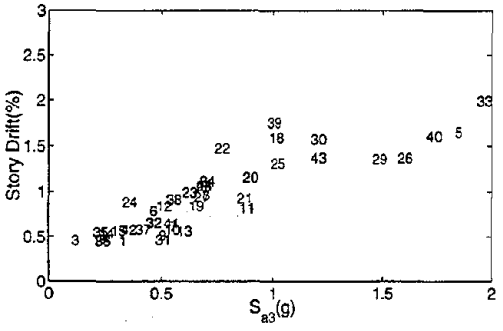

(c) At 0.05g with S_{a3}

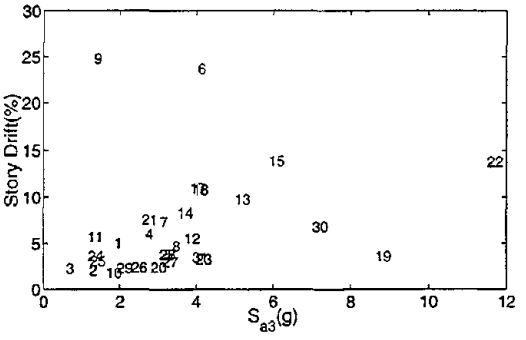

(d) At 0.32g with S_{a3}

Figure 4.7: Variation of maximum story drifts with the second-mode and the third-mode spectral accelerations (S_{a2} and S_{a3}). The results are obtained from the records scaled to 0.05g and 0.32g at the first-mode frequency and 2% damping. The numbers in the plot indicate serial numbers of the records that are the same *only* at the same intensity level. Note that at the 0.05g intensity level, we have 44 records and at the 0.32g intensity level we have 31 records.

at the first three modes weighted by 0.80, 0.15, and 0.05 to the first-, second-, and third-mode spectral accelerations respectively. These weights are calculated from the modal-mass participation factors (see Table 4.1). In this method the records in a bin are scaled to the same bin-median (weighted) average of the three spectral accelerations. The results of this weighted-average scaling are given in Table 4.2. We observe that we get approximately the same median we get from the direct results and also get a more than 50% reduction in the (equivalent) dispersion of the maximum story drift and the maximum plastic rotation damage measures. The steeper cumulative frequency curves in Figure 4.6 indicate the lower dispersion of the weighted-average scaled results. We also observe in these plots that the median damage results are close to the direct results, indicating no bias in damage estimation. As this weighted-average scaling gives consistently lower dispersion for all the damage measures, we can conclude that for multi-frequency dominated structures, it is preferable to use such a weighted-average scaling scheme in nonlinear structural analyses.

Sample Size: We have seen that the (equivalent) dispersion of the damage measures is reduced when we adopt the weighted-average scaling. We would also like to know the sample size required for each of the analysis procedures. In the previous chapters the dispersion of the estimated median decreased like $1/\sqrt{n}$ ($\delta_{\hat{y}} = \frac{\delta}{\sqrt{n}}$). This helped us to calculate the sample size. We need to find out how the equivalent dispersion of the estimator of the median (Equation 4.2) decreases with the increase in sample size. We have shown in Figure 4.8 the change of dispersion with the increase of sample size at the 0.32g intensity level. We have obtained these reductions by bootstrap replication of response results for different sample sizes. We have also shown in the same figure the change of dispersion if the sample size had decreased like $1/\sqrt{n}$ (this result matches the results from the original sample size, which is 44). We observe that the 84^{th}-percentile value decreases more rapidly than the decrease with $\sqrt{n}$. Figure 4.8 also indicates that we need much larger sample sizes than what we needed in the analyses of the previous chapters if we are to limit the 16-84% confidence band width of the median estimation of maximum story drift to $\pm 10\%$. This is the result of a large fraction of collapses.

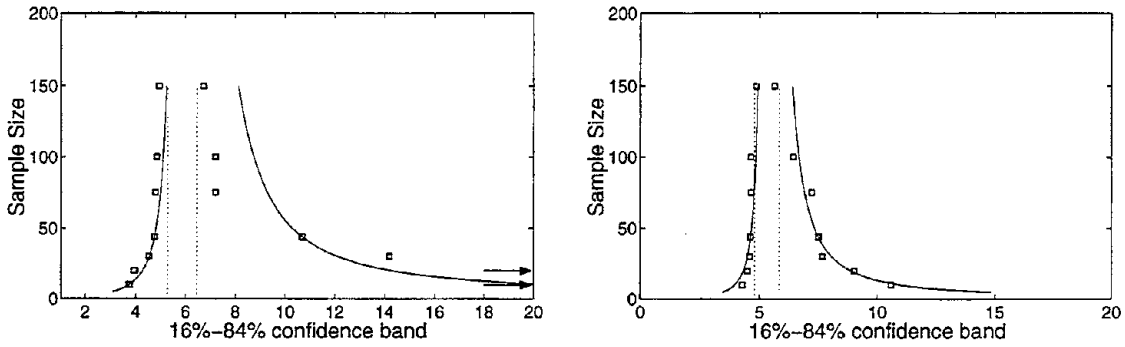

(a) Direct results

(b) Weighted-average scaled results

Figure 4.8: Variation of 16^{th}- and 84^{th}-percentile of the estimator of the median story drift with sample size. The corresponding values obtained by assuming that the dispersion of median drift decreases with $\sqrt{n}$ are also shown by solid lines. This line is drawn by assuming that the hypothetical results from the latter case match the actual results for a sample size of 44. The arrows indicate that the 84% upper confidence bands on the median drift are infinitely large. The $\pm 10\%$ confidence band is shown by the dotted lines.

4.2.6 Three-Parameter Distribution Model

So far we have considered the counted median and the equivalent dispersion for the calculation of sample statistics. Our objective is to use these results for demand calculations of structures. Now we have to develop ways to deal with in integrating these damage results with the seismic hazard results. A typical frequency distribution of the damage results at a high intensity level is shown in Figure 4.9. We can no longer afford to characterize this distribution of results by the median and δ alone as we have done in the previous chapters. We choose to use here three parameters to characterize the distribution. These parameters are the probability of no collapse (P_{NC}), and the median ($\hat{y}$) and dispersion (δ) of the no-collapse results. The median and dispersion of the no-collapse results can be calculated from Equations A.1 and A.2 respectively as we have done in the previous chapters. We can calculate conveniently the probability of exceedance of a level of damage y for any damage measure Y from the following:

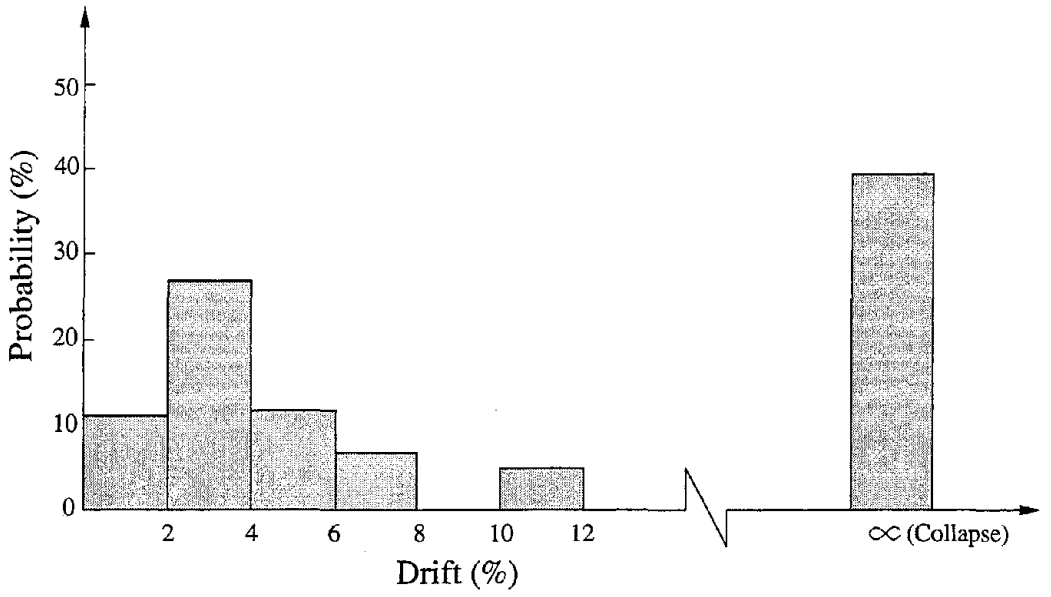

Figure 4.9: Frequency distribution of maximum story drifts from "direct" analysis of 44 (qualifying) Bin-III records at the 0.32g intensity level ($\approx$ 5000-year intensity level).

$$\begin{aligned} G_Y(y) &= G_{Y|C}(y) \cdot (1 - P_{NC}) + G_{Y|NC}(y) \cdot P_{NC} \\ &= (1 - P_{NC}) + G_{Y|NC}(y) \cdot P_{NC} \end{aligned} \tag{4.3}$$

where $G_{Y|NC}(.)$ is the complementary cumulative distribution function of Y conditioned on no collapse. If we assume the distribution of the no-collapse results is lognormal, then the above equation becomes:

$$G_Y(y) = (1 - P_{NC}) + P_{NC} \cdot \Phi^C_{Y|NC}\left(\frac{\ln(y/\hat{y})}{\delta}\right) \tag{4.4}$$

where, $\Phi^C(.)$ is the standardized complementary cumulative normal distribution.[6]

[6]Song (1998) has used a two-parameter lognormal distribution model to fit similar data by assuming that the damage measures of the collapse data (he referred to it as "censored" data) are equal to the maximum of all the observed cases. The parameters of the fitted model have been estimated from the following likelihood

The sample results of the probability of collapse (P_C), and the median $\hat{y}$ and the dispersion δ now conditioned on no collapse for the Bin-III records are given in Table 4.3. We find that the median damage measures at the low-intensity level are similar to the medians in Table 4.2. The dispersions are also quite similar, except those of the scaled results. On the other hand, the medians at the higher-drift level conditioned on no collapse are lower than what we have seen in Table 4.2. The dispersions conditioned on no collapse are also in general much lower than the dispersions in Table 4.2. This difference, however, becomes significantly smaller when we consider below the collapses.

We can calculate the median of the damage measures ($\hat{y}_M$) from the model given in Equation 4.4 as follows:

$$0.50 = P_{NC} \cdot \Phi_{Y|NC}\left(\frac{\ln(\hat{y}_M/\hat{y})}{\delta}\right) \tag{4.6}$$

Note that the median estimated from the above equation is better than the "counted median." This result will be less sensitive to the sample-to-sample variability for limited sample size. The results of the median estimated this way are given in Table 4.3. We observe that these medians are much higher than those conditioned on no collapse. Comparison of these medians with the previously estimated counted medians in Table 4.2 indicates that the results are quite close to each other. We have calculated the equivalent dispersion (δ_{eq}) from Equation 4.2 by bootstrap replication. The results of this calculation, too, are given in Table 4.3. Again, these results are not much different from those we have seen in Table 4.2. Hence the conclusions we have reached before from Table 4.2 are still valid.

Model Verification: We have seen in the preceding paragraph that the three-parameter model, which we have defined by Equation 4.4, predicts quite well the damage measures. Now we want to test the validity of this model. We plot in Figure 4.9 on lognormal-probability paper the cumulative distribution function of the data and that predicted by

---

function:

$$L(\hat{y},\delta) = \prod_{i=1}^{n_{NC}} \frac{1}{y_i\,\delta} \cdot \phi\left(\frac{y_i - \hat{y}}{\delta}\right) \prod_{j=1}^{n_C} \Phi^C\left(\frac{y_j - \hat{y}}{\delta}\right) \tag{4.5}$$

where n_{NC} is the number of non-collapsing results, n_C is the number of collapse results, and $y_j = max(y_i)$.

	Direct				Scaled				Weighted Average			
	Spectral Accelerations											
Parameter	$\hat{y}$	δ	$\hat{y}$	δ	$\hat{y}$	δ	$\hat{y}$	δ	$\hat{y}$	δ	$\hat{y}$	δ
$S_a(0.25Hz)$ | all	**0.05**	0.70	**0.32**	0.70	**0.05**	0	**0.32**	0	**0.05**	0.38	**0.32**	0.38
$S_a(0.73Hz)$ | all	0.29	0.75	1.72	0.75	0.29	0.61	1.72	0.61	0.29	0.29	1.72	0.29
$S_a(1.23Hz)$ | all	0.58	0.76	3.44	0.76	0.58	0.73	3.44	0.73	0.58	0.39	3.44	0.39
$S_a(0.25Hz)$ | NC	0.05	0.70	0.24	0.67	0.05	0	0.32	0	0.05	0.38	0.31	0.41
$S_a(0.73Hz)$ | NC	0.29	0.75	1.22	0.64	0.29	0.61	1.46	0.57	0.29	0.29	1.75	0.29
$S_a(1.23Hz)$ | NC	0.58	0.76	2.51	0.70	0.58	0.73	2.93	0.68	0.58	0.39	3.57	0.40
$S_a(0.25Hz)$ | C	0	0	0.54	0.41	0	0	0.32	0	0	0	0.37	0.27
$S_a(0.73Hz)$ | C	0	0	3.17	0.49	0	0	2.54	0.55	0	0	1.66	0.28
$S_a(1.23Hz)$ | C	0	0	5.98	0.54	0	0	5.03	0.73	0	0	3.12	0.38
Parameter	Probability of Collapse											
P_C	0		0.39		0		0.29		0		0.27	
	Damage Statistics Conditioned on No Collapse											
Parameter	$\hat{y}$	δ	$\hat{y}$	δ	$\hat{y}$	δ	$\hat{y}$	δ	$\hat{y}$	δ	$\hat{y}$	δ
Global Drift (%) | NC	0.4	0.58	1.3	0.49	0.4	0.12	1.9	0.62	0.4	0.29	2.1	0.57
Global NHE | NC	–	–	4.3	0.94	–	–	7.4	0.77	–	–	7.8	0.33
System Drift (%) | NC	0.6	0.53	1.9	0.43	0.6	0.32	2.7	0.51	0.7	0.09	2.5	0.29
Max. Story Drift (%) | NC	0.9	0.58	3.4	0.57	0.9	0.46	5.7	0.84	0.9	0.20	4.8	0.51
Max. Story NHE | NC	–	–	19.9	0.82	–	–	28.3	0.92	–	–	32.7	0.45
Max. θ_{BP} (%) | NC	–	–	2.5	0.57	–	–	4.8	0.94	–	–	4.0	0.57
Max. θ_{CP} (%) | NC	–	–	0.6	1.67	–	–	1.5	1.90	–	–	1.7	1.12
	Damage Statistics Based on Three-Parameter Distribution Model											
Parameter	$\hat{y}_M$	δ_{eq}	$\hat{y}_M$	δ_{eq}	$\hat{y}_M$	δ_{eq}	$\hat{y}_M$	δ_{eq}	$\hat{y}_M$	δ_{eq}	$\hat{y}_M$	δ_{eq}
Global Drift (%)	0.4	0.57	2.6	2.08	0.4	0.12	2.6	1.19	0.4	0.31	2.1	0.74
Global NHE	–	–	10.4	2.81	–	–	10.6	1.49	–	–	9.0	0.56
System Drift (%)	0.6	0.52	3.8	2.10	0.6	0.33	3.4	1.01	0.7	0.09	2.9	0.50
Max. Story Drift (%)	0.9	0.58	5.9	1.94	0.8	0.48	7.9	1.44	0.9	0.20	6.2	0.90
Max. Story NHE	–	–	42.9	2.40	–	–	37.9	1.54	–	–	39.9	0.75
Max. θ_{BP} (%)	–	–	5.1	2.38	–	–	6.9	1.61	–	–	5.4	1.01
Max. θ_{CP} (%)	–	–	2.8	5.21	–	–	3.7	3.25	–	–	2.9	1.83

Notation: all= all the records in the bin; C=only the records that cause failure of the structure; NC= only the records that do not cause failure of the structure; PC= fracion collapsed; $\hat{y}_M$= median; δ_{eq}= dispersion; θ_{BP}= beam plastic rotation; θ_{CP}= column plastic rotation; $\hat{y}$= median (Equation 2.1); δ= dispersion (Equation 2.2).

Table 4.3: "Direct", scaled (to the first-mode spectral acceleration), and weighted-average scaled results of different damage measures from the 44 (qualifying) Bin-III records. The spectral accelerations (S_a) are calculated at 0.25Hz and 2% damping. Note that the median and dispersion of the no-collapse (NC) results and spectral accelerations are calculated similarly to how they were calculated in Chapters 2 and 3, whereas the median and the dispersion based on a three-parameter model are calculated as in Section 4.2.2. The weighted average spectral acceleration at the 0.32g intensity level are $\hat{s}_a^*|$all = 0.73g, $\hat{s}_a^*|$NC = 0.70g, $\hat{s}_a^*|$C = 0.75g.

the model. This helps to visually compare the proximity of the observed and the predicted results. We observe that the distribution shape predicted by the model matches quite well that of the data for the direct as well as the weighted-average scaled results. This figure additionally helps us to understand how different these results are from the lognormal distribution we have assumed in the previous chapters. The plot of a lognormal distribution on the lognormal-probability paper is a straight line, but we observe that the new model deviates significantly from a line. Formally the quantification of the acceptability of a model is carried out by checking how closely the cumulative frequency curve of the data points fall within reasonable sampling variation about a line fitted by the model on the probability paper. This is done by the hypothesis test technique. One of the popular goodness-of-fit tests is the Kolmogorov-Smirnov test. We briefly describe this test in Appendix C. See Benjamin and Cornell (1970) for details on this test. The Kolmogorov-Smirnov test statistics of the maximum story drifts and the maximum story NHEs are 0.10 for direct story-drift results, 0.11 for (weighted-average) scaled story-drift results, 0.05 for direct story-NHE results, and 0.07 for scaled story-NHE results. The critical statistic of this test is 0.21 at the 0.05 significance level. So we cannot reject this hypothesized model at the 5% or lower significance level.

Distribution of Damage Over Height

The no-collapse results of maximum story drifts, maximum story NHEs, and maximum beam plastic rotations from the direct and the weighted-average-scaling analysis are plotted against story number in Figure 4.10. This figure demonstrates that from weighted-average scaling we get reduced dispersion of responses over all the stories and that the median responses are virtually the same for all the stories. Also we understand that because the dispersion is reduced for all the stories, the dispersion of estimation of economic loss (from the damage over the entire structure) will be reduced substantially. We therefore find that the reduction in dispersion of system drift conditioned on no collapse is 40% at the high intensity level (see Table 4.3). The reduced dispersions are, however, much higher than what we have obtained in most of the cases in the previous chapters.

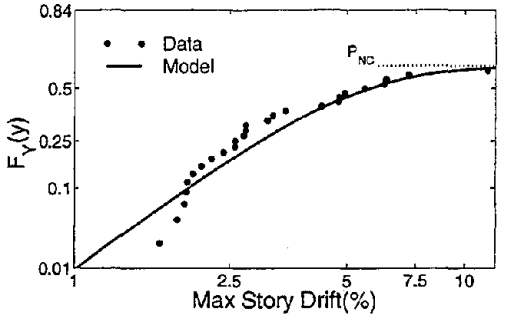

(a) "Direct" results for maximum story drift

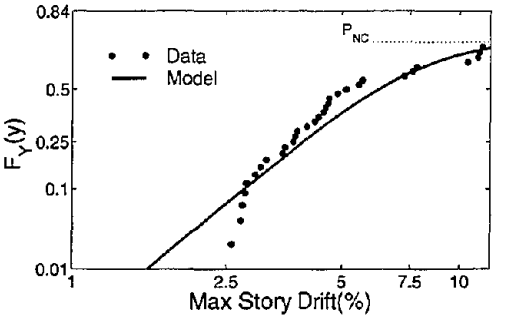

(b) Weighted-average scaled results for maximum story drift

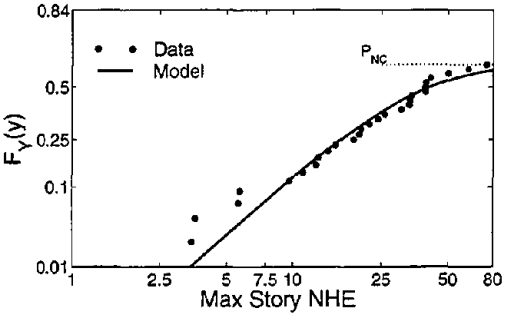

(c) "Direct" results for maximum story NHE

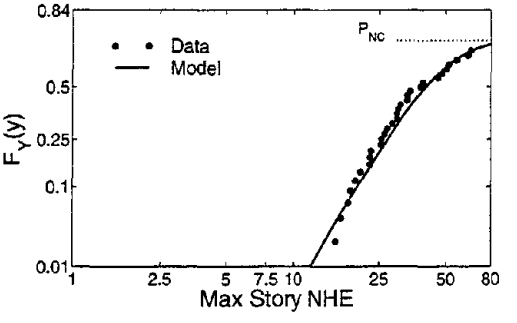

(d) Weighted-average scaled results for maximum story NHE

Figure 4.9: Cumulative distribution of different damage-measures of data and the fitted model (Equation 4.4) on lognormal probability paper. The sample fraction of no collapse is indicated by P_{NC}.

We pointed out before that the maximum story drift results of this tall structure have characteristics similar to the local drift results, e.g., maximum beam plastic rotation. The local bulging of story drifts at the high-intensity level that we observe in Figure 4.10 is the characteristic-displacement shape of tall buildings at larger drifts. This gives us higher dispersion of this displacement-damage measure. Nonlinear analysis of this tall structure is more expensive than the nonlinear analysis of the single-frequency dominated low-rise structures, and the number of analyses required to achieve a target accuracy of median response is also more for this tall structure because of higher dispersion of response even after scaling. This makes the demand calculation of tall structures computationally very expensive. Hence while calculating the performance of this structure, we will try to incorporate some of the seismological and record parameters in Chapter 5 to further reduce the number of analyses.

4.2.7 Other Scaling Schemes

Although they are not reported here, we have also investigated two other scaling schemes: scaling at a higher damping, and frequency-averaged scaling. In the first case the records are scaled to the elastic first-mode spectral acceleration at 5% damping, and in the second case the records are scaled to the spectral acceleration averaged over a range of frequencies (0.25Hz $\pm$25%). Although we got some reduction in dispersion by using these schemes for single-frequency dominated structures, we do not get any significant reduction in (equivalent) dispersion for the multi-frequency dominated structure.

4.3 Dependency of Response on Magnitude, Distance, Duration, and Spectral Accelerations at Higher Frequencies

We have seen for this 20-story structure that within M-R bin (weighted-average) scaling has not introduced any significant bias in damage estimation. We have seen before that a more general scaling scheme, which is scaling of ground-motion records from a particular M-R bin to the intensity level of other bins, is also viable for single-frequency dominated

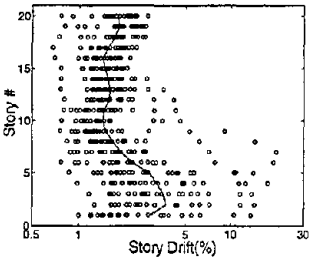

(a) Direct results: Maximum Story Drift

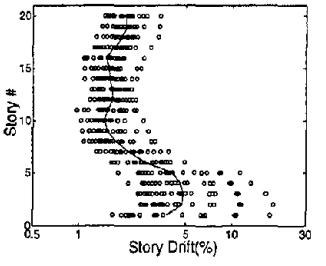

(b) Weighted-average results: Maximum Story Drift

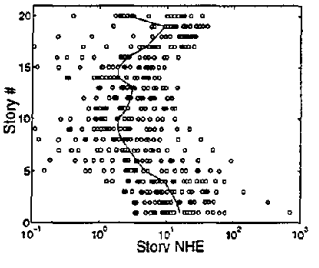

(c) Direct results: Maximum Story NHE

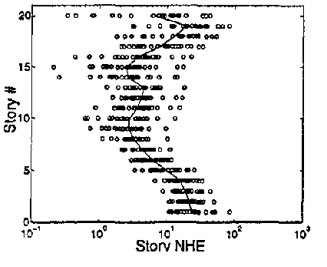

(d) Weighted-average results: Maximum Story NHE

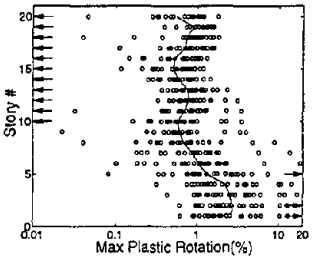

(e) Direct results: Maximum Beam θ_{CP}

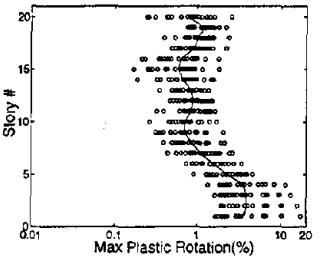

(f) Weighted-average results: Maximum Beam θ_{CP}

Figure 4.10: Comparison of "direct" and weighted-average results of different damage measures versus story number from Bin-III records at the 0.32g intensity level. The results shown here are only from the records that do not introduce numerical instability or "collapse" in the structure. The arrows indicate that some plastic rotation data points are beyond the range of the plot.

structures. We want to verify the same for the multi-frequency dominated 20-story structure. This can be done more directly as in Chapter 3 by calculating the nonlinear response dependence on M and R beyond (conditional on) their dependence on the intensity. In order to investigate the possible (conditional) magnitude dependency of responses we need to have a sufficient number of records (so that the confidence band of the median response is narrow, e.g., $\pm 10\%$) over a wide range of magnitudes. We have already observed in Section 4.2 that the number of "qualifying" records, those that have a low-corner filter frequency less than or equal to 0.10Hz, is very small at the low-magnitude ranges. From the catalogue (Silva, 1995) we have selected 50 records that satisfy this constraint on the low-corner filter frequency. In this set 23 records are from a low-magnitude range (5.2 to 6.3). We have seen before that the damage measures are mainly dependent on the first-mode spectral acceleration[7]. We will investigate now the dependency of responses on the other parameters, e.g., magnitude, when conditioned on the first-mode spectral acceleration. Hence similar to what we did in Chapter 3 we will first scale the records to three different first-mode spectral acceleration levels. These intensity levels are 0.05g, 0.15g, and 0.30g, which are are approximately 75-year, 1000-year, and 5000-year intensity levels respectively at a central Los Angeles site. In order to understand the range of different independent parameters for which the regression results will be valid and also to understand how frequently they occur in that range, we plot in Figure 4.11 the frequency distribution of the magnitude, duration, and second- and third-mode spectral accelerations of the records scaled to those intensity levels.

The regression analysis we carry out in the following sections will be used at the end in seismic demand calculations. But the attenuation results that we use in ground-motion hazard calculations are in general available at only a limited number of discrete frequencies and at 5% damping. Although for the present structure the first-mode frequency (0.25Hz) matches the frequency in the attenuation results (Abrahamson and Silva, 1997) that we have used in the PSHA, it is in general very unlikely that the frequencies in attenuation results will match the structural frequency. So we will use the regression results for spectral

[7]We observed in Section 4.2.3 that the damage measures increase with increase in the first-mode spectral accelerations.

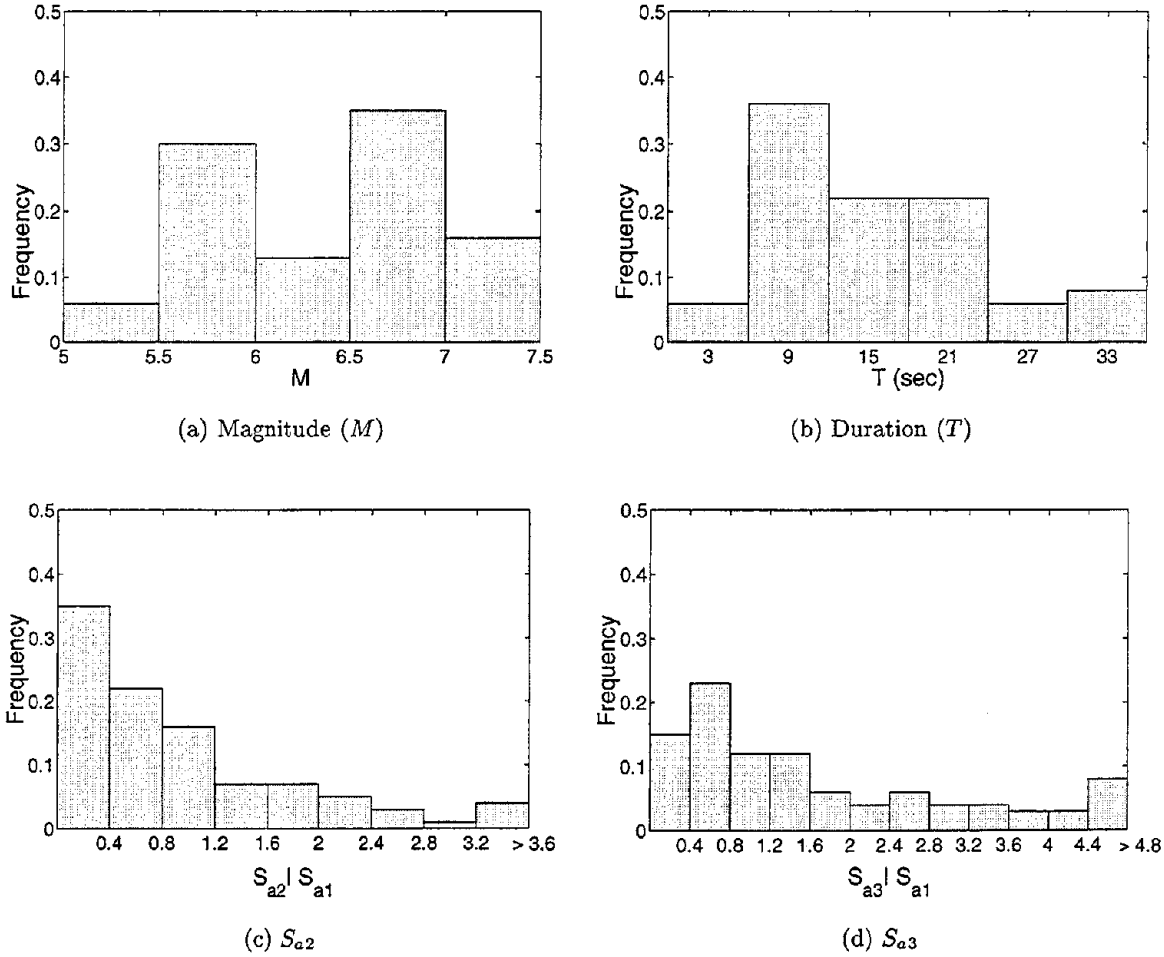

(a) Magnitude (M)

(b) Duration (T)

(c) S_{a2}

(d) S_{a3}

Figure 4.11: Frequency distribution of magnitude, duration, second-mode spectral acceleration (S_{a2}), and third-mode spectral acceleration (S_{a3}) of the records used in the regression analysis. These records are *scaled* to three different intensity levels as will be done in regression analyses. Hence we get three times the original sample points for the calculation of these conditional distributions. This makes the range of S_{a2} and S_{a3} (conditional on being scaled to three different S_{a1} levels) much wider than the original unscaled sample.

accelerations at 0.25, 0.67 and 1.33Hz and at 5% damping. There is also an additional advantage of carrying out regression at higher damping. The regression error in general is somewhat lower than the error based on spectral acceleration at 5% damping (compare the dispersions with those in Table 3.3).

4.3.1 Results Conditioned on No Collapse of the Structure

First we will look into the regression results only for the no-collapse case. We will use the same regression model given in Equation 3.2 for fitting the data. This model is linear in log-space, so the regression results we will present now are from the conventional linear regression analysis of the logarithm of the data. Although in Chapter 3 we explored the nonlinear regression analysis of the same model and also a polynomial regression model, we will not do any such exercise in this chapter. Recall that nonlinear-regression analysis and linear-regression analysis of the polynomial regression model are worthwhile only if the data have lots of zeros, e.g., for the results of plastic rotation at a low-intensity level (see Section 3.4.3 for details). The results of regression analysis against the first-mode spectral acceleration of the three most important damage measures, which are maximum story drift, maximum story NHE, and maximum beam plastic rotation, are given in the first row of each of the damage measures in Table 4.4. In order to understand the variation of these damage measures with the first-mode spectral acceleration, we have plotted the regression curves in Figure 4.12 (in keeping with traditional "force"-deformation plots, we plot the dependent variable, deformation, as the abscissa). We observe that the increase in maximum story drift with the first-mode spectral acceleration is virtually linear in our range of interest, i.e., from the 75-year intensity level to the 5000-year intensity level (in other words from the immediate-occupancy performance level to a much higher than the collapse-prevention performance level). The variation of the maximum beam plastic rotation with the first-mode spectral acceleration is slightly nonlinear in our range of interest, whereas the variation of the maximum story NHE with spectral acceleration is highly nonlinear. The dispersions of residuals conditioned on S_{a1} are about the same as the dispersions of scaled results from Bin-III records in Table 4.3 for the results conditioned on no collapse. Note in Table 4.4 the

sample size requirements (n_{req}) of different damage measures: the sample size requirement of maximum story drift is the lowest. So if the profession were to recommend an energy-based damage measure (e.g., maximum story NHE), we would need to ask for four times more nonlinear analyses than in the case of the currently used displacement-based damage measure in order to provide comparably "confident" predictions.

In order to understand the conditional dependency of the response on additional independent parameters, we plot the residuals of the responses (given S_{a1}) versus alternate second explanatory variables. These are second-mode spectral acceleration (S_{a2}), magnitude (M), and duration (T)[8]. The plots are shown in Figure 4.13. The residuals (e_i) shown in the figure are calculated by fitting only the first-mode spectral acceleration (S_{a1}) to the data. Thus the residual is equal to $(\ln Y_i - \ln \hat{Y}_i)$ where Y_i is the observed response and $\hat{Y}_i$ is the predicted response from one-dimensional regression analysis. These plots visually suggest that *conditional on* S_{a1} all the responses are dependent on the second-mode spectral acceleration, whereas these responses are apparently not dependent on the other parameters we have considered. The 2-D regression analysis can describe these observations quantitatively. If the incorporation of an additional parameter gives statistically significantly different results at the 1%-significance level compared to the result without the additional parameter, we highlight those regression results with bold letters[9] in Table 4.4.

We observe that in regression analysis when we include the second-mode spectral acceleration (S_{a2}) in addition to the first-mode spectral acceleration (S_{a1}), we get a substantial reduction in dispersion ($\delta_\varepsilon = \delta_{\ln Y|S_{a1},S_{a2}}$) compared to the dispersion of response conditioned only on S_{a1} ($\delta_\varepsilon = \delta_{\ln Y|S_{a1}}$). For the displacement-based damage measures (maximum story drift and maximum beam plastic rotation), this reduction is around 20%, and for the energy-based damage measure (maximum story NHE), it is 30%. Recall that for the single-frequency-dominated structure the reduction was only around 10% for all the damage measures (see Table 3.7). Note that the explanatory variables S_{a2} and S_{a3} in Table 4.4 are

[8]See Footnote 3 in Chapter 3 for a definition of this duration measure.

[9]Formally this is carried out by hypothesis test on a slope parameter at the 1%-significance level. See Section 3.4 for a discussion on this test.

Damage Measure	Independent Variable	Regression Function	R_a^2	δ_ε	n_{req}
	S_{a1}	$\boldsymbol{D = 0.16 \cdot (S_{a1})^{0.95}}$	0.70	0.44	20
	$S_a^\star$	$\boldsymbol{D = 0.09 \cdot (S_a^\star)^{0.92}}$	0.80	0.36	13
Maximum	S_{a1}, S_{a2}	$\boldsymbol{D = 0.09 \cdot (S_{a1})^{0.56} \cdot (S_{a2})^{0.40}}$	0.80	0.36	13
Story (D)	S_{a1}, S_{a2}, S_{a3}	$\boldsymbol{D = 0.07 \cdot (S_{a1})^{0.53} \cdot (S_{a2})^{0.23} \cdot (S_{a3})^{0.21}}$	0.82	0.34	12
Drift	S_{a1}, M	$D = 0.28 \cdot (S_{a1})^{0.95} \cdot e^{-0.08M}$	0.71	0.44	20
	S_{a1}, R	$\boldsymbol{D = 0.32 \cdot (S_{a1})^{0.95} \cdot R^{-0.22}}$	0.72	0.43	19
	S_{a1}, T	$D = 0.19 \cdot (S_{a1})^{0.95} \cdot e^{-0.01T}$	0.71	0.43	19
	S_{a1}	$\boldsymbol{NHE = 1042.1 \cdot (S_{a1})^{2.46}}$	0.71	1.13	127
Maximum	S_{a1}, S_{a2}	$\boldsymbol{NHE = 222.7 \cdot (S_{a1})^{1.47} \cdot (S_{a2})^{1.02}}$	0.81	0.92	84
Story	S_{a1}, S_{a2}, S_{a3}	$\boldsymbol{NHE = 103.4 \cdot (S_{a1})^{1.34} \cdot (S_{a2})^{0.37} \cdot (S_{a3})^{0.79}}$	0.83	0.83	69
NHE	S_{a1}, M	$NHE = 1298.5 \cdot (S_{a1})^{2.46} \cdot e^{-0.04M}$	0.71	1.13	127
NHE	S_{a1}, R	$NHE = 4402.8 \cdot (S_{a1})^{2.46} \cdot R^{-0.48}$	0.72	1.11	123
	S_{a1}, T	$NHE = 1320.8 \cdot (S_{a1})^{2.46} \cdot e^{-0.02T}$	0.71	1.12	126
Maximum	S_{a1}	$\boldsymbol{\theta_{CP} = 0.29 \cdot (S_{a1})^{1.46}}$	0.67	0.66	43
Column	S_{a1}, S_{a2}	$\boldsymbol{\theta_{CP} = 0.16 \cdot (S_{a1})^{1.05} \cdot (S_{a2})^{0.55}}$	0.76	0.56	32
Plastic	S_{a1}, S_{a2}, S_{a3}	$\boldsymbol{\theta_{CP} = 0.11 \cdot (S_{a1})^{1.00} \cdot (S_{a2})^{0.29} \cdot (S_{a3})^{0.34}}$	0.78	0.54	30
Rotation	S_{a1}, M	$\theta_{CP} = 0.39 \cdot (S_{a1})^{1.46} \cdot e^{-0.05M}$	0.67	0.66	43
Rotation	S_{a1}, R	$\theta_{CP} = 0.66 \cdot (S_{a1})^{1.48} \cdot R^{-0.26}$	0.68	0.65	42
(θ_{CP})	S_{a1}, T	$\theta_{CP} = 0.36 \cdot (S_{a1})^{1.46} \cdot e^{-0.01T}$	0.68	0.65	42

Table 4.4: Results of regression analysis of different damage measures for a 20-story building from the records scaled to the 0.30g, 0.15g, and 0.05g first-mode spectral accelerations. The independent variables S_{a1}, S_{a2}, and S_{a3} are calculated at 0.25, 0.67, and 1.33Hz frequencies respectively and at 5% damping. The other independent variable $S_a^\star$ is the weighted average spectral acceleration at 5% damping ($S_a^\star = 0.8 \times S_{a1} + 0.2 \times S_{a2}$). The sample size requirement ($n_{req} = [\delta_\varepsilon/0.10]^2$) is obtained for a target one-sigma confidence bandwidth of $\pm 10\%$. *Note that the results we have used here are conditioned on no failure of the structure.* The bold letters indicate that the addition of an independent variable makes the result statistically significantly different from the result without that independent variable at the 1%-significance level.

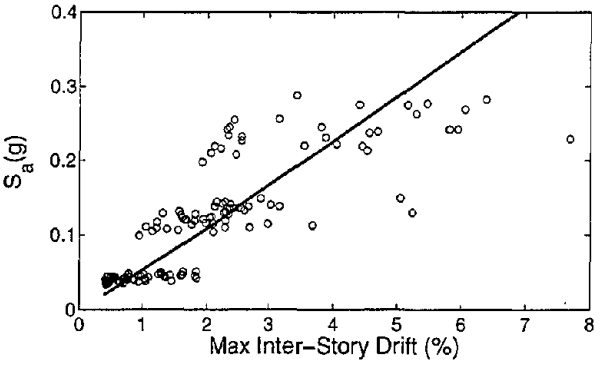

(a) Maximum inter-story drift

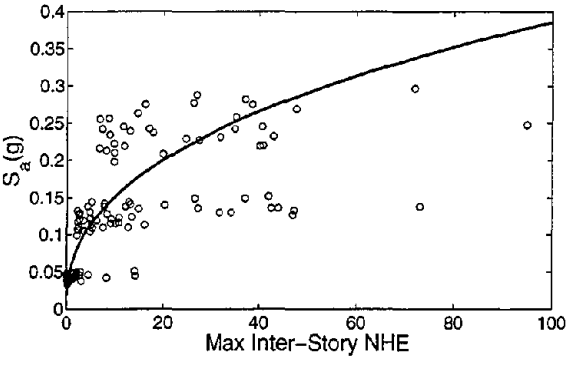

(b) Maximum inter-story NHE

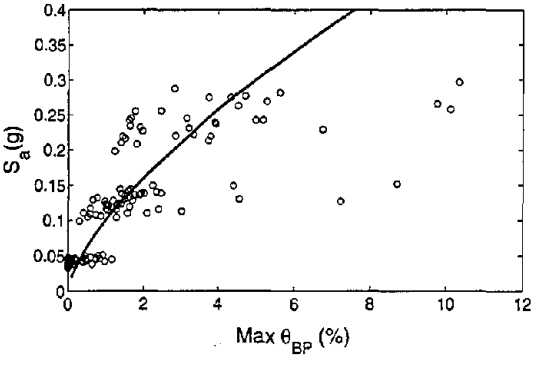

(c) Maximum beam plastic rotation (θ_{BP})

Figure 4.12: Variation of different damage measures with the first-mode spectral acceleration at 5% damping from regression results. Note that we have carried out regression analysis against S_a. But in plotting we use here the independent variable S_a as the ordinate following the traditional force-deformation plot.

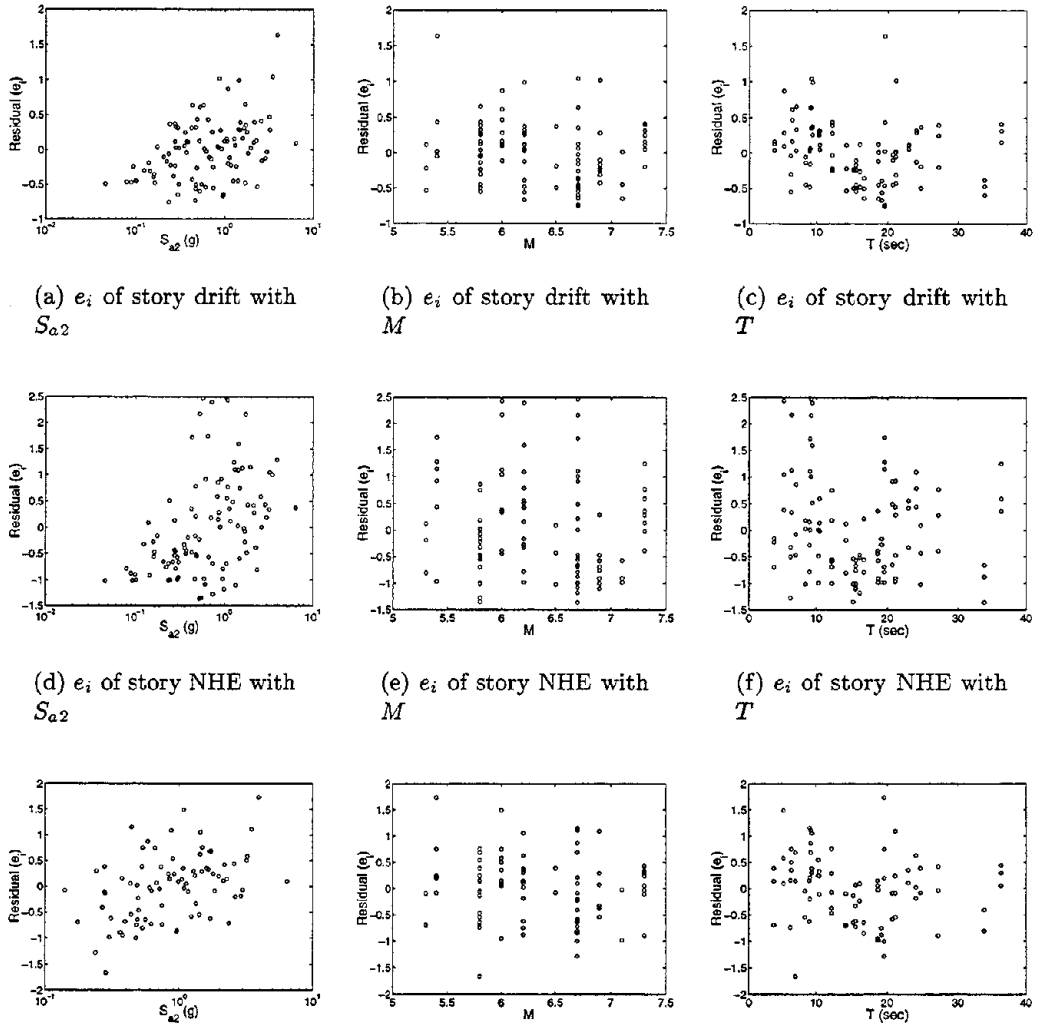

(a) e_i of story drift with S_{a2}

(b) e_i of story drift with M

(c) e_i of story drift with T

(d) e_i of story NHE with S_{a2}

(e) e_i of story NHE with M

(f) e_i of story NHE with T

(g) e_i of θ_{BP} with S_{a2}

(h) e_i of θ_{BP} with M

(i) e_i of θ_{BP} with T

Figure 4.13: Variation of residual ($e_i = \ln Y_i - \ln \hat{Y}_i$) of maximum story drift, maximum story NHE, and maximum beam plastic rotation (θ_{BP}) with second-mode spectral acceleration (S_{a2}), magnitude (M), and duration (T). The residual is obtained by considering only the first-mode spectral acceleration, S_{a1}, as the independent variable in the regression analysis. Therefore these plots indicate response dependence on S_{a2}, M, and T conditioned on S_{a1}.

considered to be the second-mode and the third-mode spectral acceleration, but in fact they are representative of spectral accelerations at higher frequencies. This substantial reduction in dispersion with the inclusion of a higher-frequency spectral acceleration indicates again that the structure is a higher-frequency-dominated structure. Hence by including the two dependent variables S_{a1} and S_{a2}, we can get around 30% reduction ($n_{req} \propto \delta^2$) in required sample size (even if we consider only the displacement-based damage measure suggested by, for example, FEMA-273). We observe further that qualitatively the regression results conditioned on no collapse are very similar to the results of the single-frequency dominated structure in Chapter 3: the responses are mostly *not* dependent on the magnitude or the duration (even for the NHE), but are dependent to a greater or lesser extent on only the second-mode spectral acceleration in addition to the first-mode spectral acceleration. Note that the dispersions of the damage measures conditioned on no collapse after inclusion of the second-mode spectral acceleration ($\delta_{\ln Y|S_{a1},S_{a2}}$) are very close to the results in Chapter 3 for the single-frequency-dominated structure (see Table 3.7). Figure 4.14 illustrates the dependency of the maximum story drift with the first- and the second-mode spectral accelerations. We notice here that, as expected, the increase in maximum story drifts with S_{a1} is significantly higher than it is with S_{a2}. It should be emphasized, however, that S_{a2} tends to increase as S_{a1} does, implying that both the basis for the prediction and its ultimate application are for S_{a1}-S_{a2} pairs on a diagonal band; the net dependence of drift is approximately linearly proportional to the intensity, as in the 1-D regression (against S_{a1} only).

We have observed that conditioned on the first-mode spectral acceleration all the damage measures are statistically significantly dependent on the elastic second-mode spectral acceleration as well and that the drift damage measure is dependent on the distance. We want to investigate here how important those additional parameters are in predicting the response. We will consider here only the no-collapse results of the three most important damage measures: maximum story drift, maximum story NHE, and maximum beam plastic rotation, and we will consider only the three most important additional parameters: second-mode spectral acceleration, distance, and duration. As we did in Section 3.4, we will first

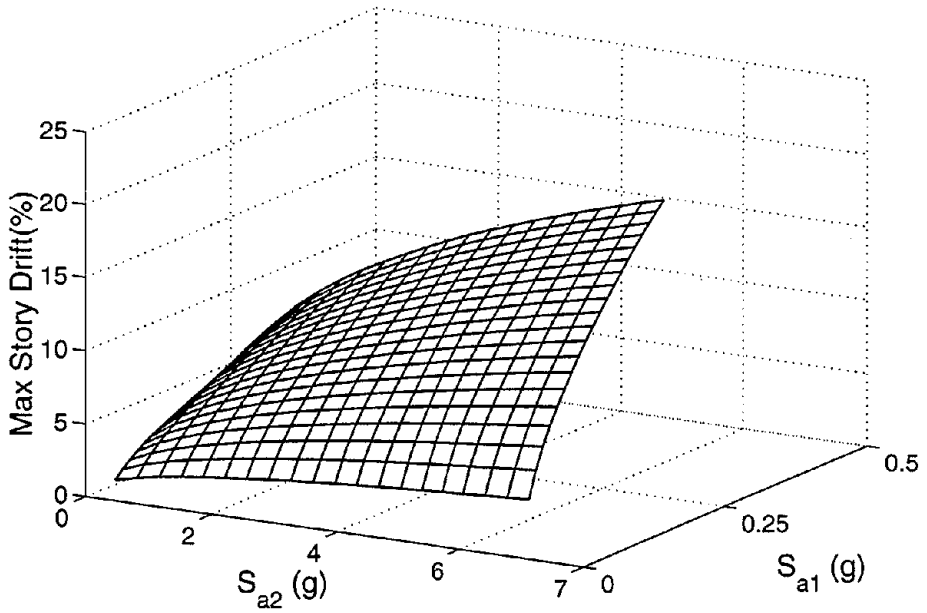

Figure 4.14: Variation of maximum inter-story drift with the first-mode and the second-mode spectral accelerations.

calculate the median damage measure conditioned on S_{a1} only. Then we will compare this result with the median damage conditioned on both the first-mode spectral acceleration and the additional parameter at the conditional median and median $\pm$ one-sigma levels of the additional parameter (given the value of the first). We described the calculation of these conditional medians and dispersions in Footnote 12 of Chapter 3. The results are shown in Figure 4.15. We observe that when we include the second-mode spectral acceleration in response prediction, the difference in results is substantial. Hence this additional parameter is important in response prediction. Although the other parameter, R, gave us statistically significantly different results for story drift, is not important in response prediction for all practical purposes.

4.3.2 Comparison Between the 5-Story and the 20-Story Regression Results

We will compare now the dependency of damage measures on the different additional

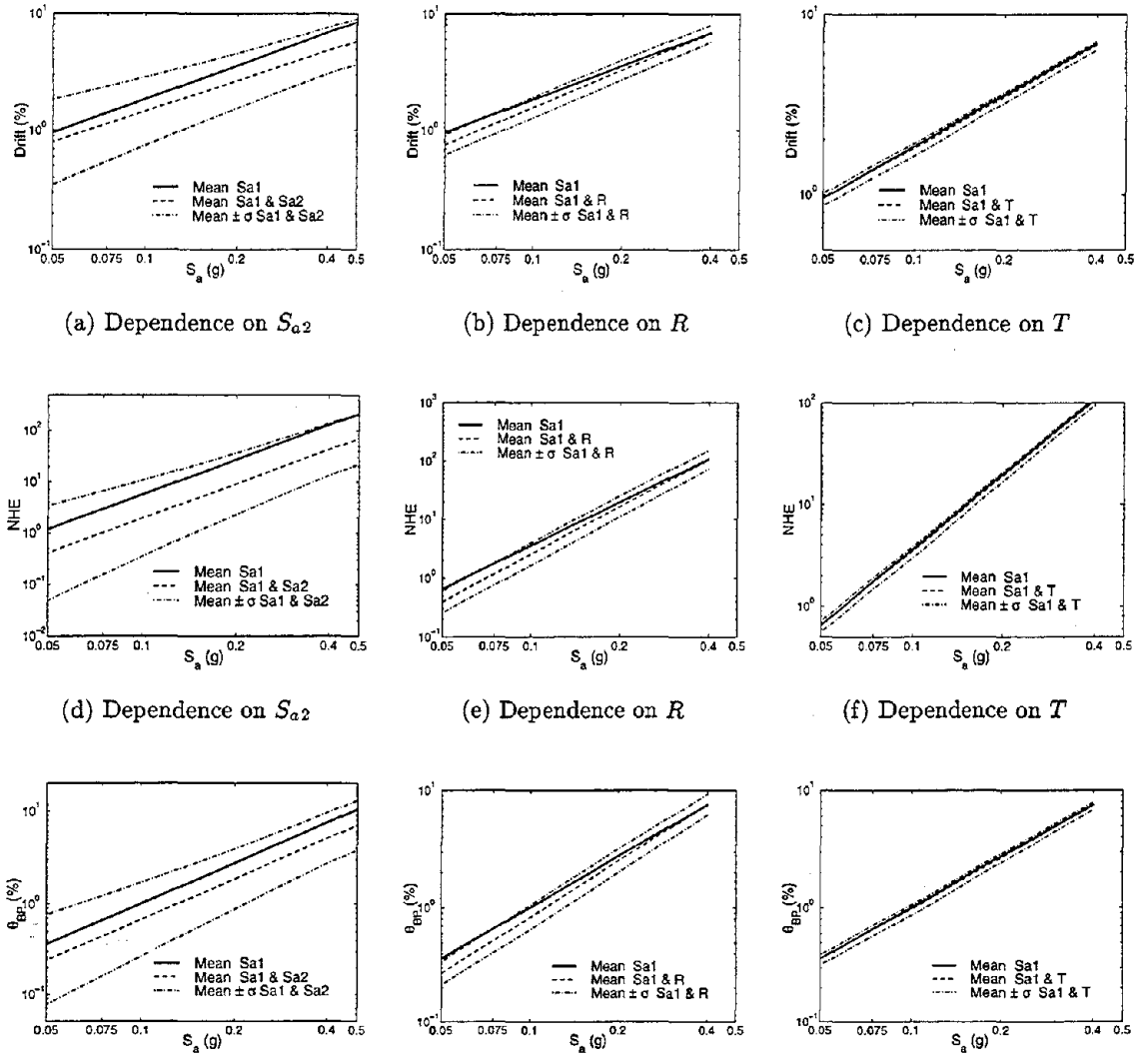

(a) Dependence on S_{a2} (b) Dependence on R (c) Dependence on T

(d) Dependence on S_{a2} (e) Dependence on R (f) Dependence on T

(g) Dependence on S_{a2} (h) Dependence on R (i) Dependence on T

Figure 4.15: Comparison of regression results of three different damage measures against only the first-mode spectral acceleration and against a parameter in addition to the first-mode spectral acceleration. The three damage measures are the maximum interstory drift, maximum interstory NHE, and maximum beam plastic rotation (θ_{BP}). The conditional mean and dispersion are calculated following the procedure described in Footnote 12 of Chapter 3.

parameters conditioned on the first-mode spectral acceleration for the 5-story and the 20-story buildings. We will consider here the regression results in Table 3.7 for the 5-story building and the results in Table 4.4 for the 20-story building, which are *conditioned on no collapse.*

Spectral Acceleration at Higher Frequency: We observe that (conditioned on the first-mode spectral acceleration) both the 5-story and the 20-story buildings are positively dependent (the regression coefficients are positive) on the elastic second-mode spectral acceleration (S_{a2}). Figures 3.10 and 4.15 indicate that the dependency of the tall 20-story structure on S_{a2} is much higher than that dependency is in the case of the 5-story building. On average the spectral shape of the records is such that S_{a2} conditioned on S_{a1} is proportionately much higher for the 20-story building than for the 5-story one. Therefore in the elastic regime the second mode is much more important for the 20-story building than for the 5-story one even through their second-mode modal participation factors are not greatly different. This is one of the reasons why we find higher dependence on S_{a2} for the 20-story building.

Magnitude (M): We have seen for the 5-story building that the damage measures are positively dependent on M. We have seen also in Figure 2.1 that relative S_{a1}, all the high-frequency spectral ordinates of high-magnitude events are lower than those of low-magnitude events. The damage measures, on the other hand, are positively dependent on the higher-frequency spectral accelerations. Hence we would expect a negative coefficient on M. In order to explain this anomalous result, we also carry out regression analysis of story drift against spectral acceleration at a frequency (of 0.25Hz) lower than the first-mode frequency in addition to S_{a1}. The regression results indicate that the story drifts are more strongly dependent on the spectral acceleration at that low frequency than they are on the higher frequency S_{a2} and that the regression coefficient is also *positive.* Because the high-magnitude events have higher relative spectral ordinate at lower frequencies (see Figure 2.1) and the regression coefficient is positive, we get a positive coefficient for M. We conclude that because of the relative flat spectral shape on either side of its 1Hz first-mode frequency, the 5-story building's nonlinear response is more sensitive to the phenomenon

of "softening" response to lower (than the first-mode) frequencies that one sees in SDOF systems than it is to the higher frequency ("higher mode") we see in the 20-story structure.

Tall structures are expected to be more strongly dependent on the magnitude of events than the single-frequency dominated shorter structures. We have seen in Figure 2.1 that the low-magnitude events are relatively poorer in low-frequency content, and hence comparatively richer in high-frequency content. Since responses of tall structures depend significantly on the higher-frequency spectral accelerations, one expects to observe *conditioned on* S_{a1} higher response from *low-magnitude* events, i.e., a high negative coefficient of M. Regression results conditioned on no collapse conversely show a mild negative slope of M, but this slope is not statistically significantly different from zero. Because the mild-negative slope is contrary to our intuition, we need to investigate carefully the spectral shape of the no-collapse records used in regression analysis. We select the records that do not cause collapse of the structure from two magnitude and distance bins: M = 5.0 - 6.0, R = 5 - 25km and M = 6.5 - 7.5, R = 10 - 30km. The spectral ordinates we get from these records are adjusted by the ratio of the spectral ordinates from attenuation results (Abrahamson and Silva, 1997) at the central magnitude and distance of a bin to the spectral ordinates from the attenuation results at the M-R of the record. Thus the spectral ordinate, s_a, of a record of magnitude, m and distance, r, is adjusted to the central magnitude and central distance of a bin (say, $m = 5.5$, $r = 15km$) as follows:

$$s_{a_{\text{adjusted}}} = s_a \cdot \frac{(s_{a_{\text{attenuation}}})_{m=5.5,r=15}}{(s_{a_{\text{attenuation}}})_{m,r}} \tag{4.7}$$

The adjusted median spectra at 5% damping at the central magnitude and distance of the bins and the same from the attenuation results are shown in Figure 4.16(a). We observe that the spectra from the bin of records appear to match well those from the attenuation results. However in order to understand the relative shape of the spectra, we scale the records to the same unit value at the first-mode frequency (0.25Hz). The results are shown in Figure 4.16(b). We observe that it is true that the 5.5 magnitude-bin spectra are higher than the 7.0 magnitude-bin spectra at the second-mode frequency, but the difference is not

very great (7.9 for M=5.5 versus 5.7 for M=7). The lower regression coefficient of S_{a2} also suggests that a large value of S_{a2} is required for a small change in drift.

It is important here to remember that we have used here only the "qualified" records, those which have a minimum low-corner frequency. We have seen in Figure 4.4 that because of this preselection of records, the reduction of relative spectral ordinates of the low-magnitude records is very large; the ordinates of these qualifying records are closer to the high-magnitude records. Hence we find practically no dependence of our regression results on M.[10] Further these regression results are also conditioned on no collapse. Hence in this regression analysis, we have neglected the stronger records, which cause failures. The comparison of relative spectral ordinates in Figure 4.4 of the non-failing records at higher frequencies also suggests that these are lower than those predicted by the attenuation results. The bin records that have higher spectral ordinates have caused collapse of the structure in a significant number of cases. By taking into account all these factors, we can infer that the lack of dependence of damage results of the 20-story building on M predicted by the regression results from this subset of records may not be correct: the dependence in reality may be much greater. It may not be possible to confirm this dependency, however, until the instrumentation improves to such an extent that the low-frequency signal in low-magnitude records is more reliably recorded, permitting us to "qualify" for these records.

Distance (R): We have seen in Table 3.7 for the 5-story structure that the damage measures (conditioned on S_{a1}) are statistically significantly dependent on R. But we find

[10]If we do not restrict ourselves to the small subset of low-magnitude records that qualify based on their low-corner frequency, we find in Table E.9 that the damage measures from the low-magnitude records are significantly higher than the high-magnitude records (e.g., the "direct" as well as the scaled results indicate that the median story drift from the low-magnitude records is 2.6 times higher than the high magnitude-records. The capacity of the 0.25Hz structure in the appendix has been reduced substantially. Hence we cannot neglect these records because of their low spectral accelerations to start with. For the low-magnitude records, the damage measures of the 5-story building do increase somewhat due to higher relative spectral accelerations at higher frequencies. On the other hand, the effect of lower relative spectral accelerations at low frequencies is to reduce the damage measures when the structure softens in its nonlinear deformations. These two counter effects, somewhat, reduce the dependence on M. For the 20-story structure, the relative spectral accelerations at the high frequencies are much larger for the low-magnitude events and there is little difference of spectral accelerations at the low frequencies. This makes the effect of higher-frequency spectral accelerations more significant for the low-frequency structures.

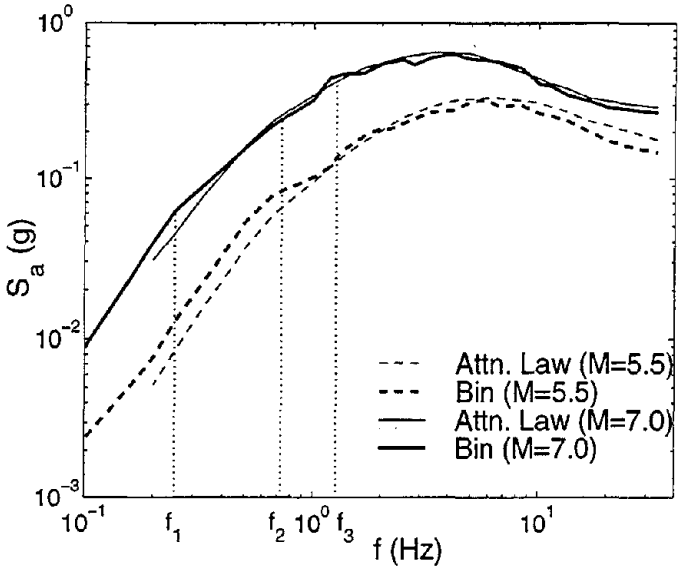

(a) Median spectra

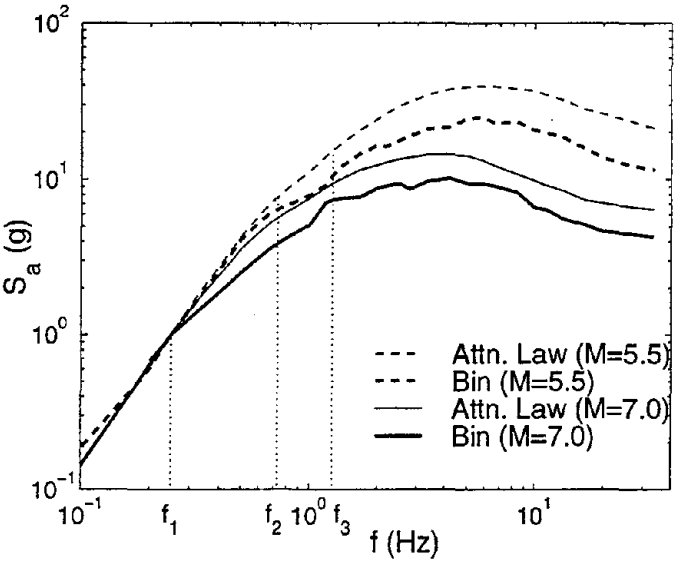

(b) Median spectra scaled to 1.0g at 0.25Hz

Figure 4.16: Median spectra at 5% damping for high and low magnitude earthquakes as obtained from the attenuation results (Abrahamson and Silva, 1997) and from the records used in regression analyses. Recall that the frequencies at the first three modes (f_1, f_2, f_3) of the 20-story building are 0.25, 0.73, and 1.27Hz respectively, as shown.

that if jointly conditioned on S_{a1} and M, the damage measures are not statistically significantly dependent on R. This indicates that R, when taken without M in effect "stands in for," or represents, the M dependency of the response. This is perhaps true because the large-distance records that we have used in regression analysis are associated only with high magnitudes. We cannot consider any low-magnitude, large-distance records because their very low spectral accelerations imply a low signal-to-noise ratio prohibiting effective processing even if the instrument is triggered. So although we observe some apparent R dependency of the response, we can ignore it for all practical purposes.

On the other hand, for the 20-story structure we observe only the R dependency of the response. Again we can neglect this observation because it is based on a subset of data that does not properly represent events of low magnitude and a range of distances. We have observed in Figure 4.4(b) that the relative spectral shape of the subset of the low-magnitude and short-distance events is substantially different from the original shape. Also we have no record at a larger distance for the low-magnitude events. So when we carried out regression analysis of damage measures *for only the large-magnitude records* against S_{a1} and R, we observed that, conditioned on S_{a1}, the dependence of the damage measures on R is not statistically significant *even* at the 5%-significance level.

4.3.3 Variation of Drift over Height

Although the regression results of maximum story drift can give us an idea about the expected collapse of the structure, we lose the information of the location of collapse. The information about maximum story drift also can not us if the damage is concentrated at a particular story or distributed over several stories. This information is needed to estimate the expected damage cost of a structure and is also useful for retrofitting the stories that are most vulnerable to earthquakes. In order to get this information, we carry out regression analysis of each story separately. The results of this regression analysis are illustrated in Figure 4.17. We observe that the drifts at the first few stories increase with spectral acceleration much more rapidly than those at the higher stories. Indeed the rate of increase of the upper story drifts becomes smaller as the lower story drifts become large. This may

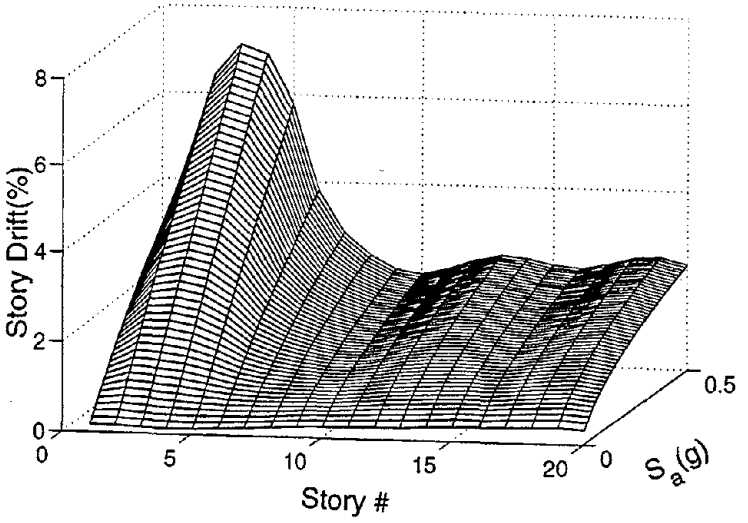

Figure 4.17: Variation of story drift over height of the structure with the first-mode spectral acceleration. Results of 20 story-by-story regressions of story drift versus S_a at the first-mode frequency (no-collapse cases only).

be an "isolation" effect, and it indicates that the damage at a high intensity level is expected to be concentrated in the first six stories.

4.3.4 Collapse of Structures: Regression Analysis of Binary Data

We turn our attention next to the "collapse" or non-converging cases and to the procedures of this outcome. The response data in this case are represented through a binary variable, Y. This variable is defined to be 1 when a structure does not collapse and is 0 when it collapses. The independent or explanatory variables ($\boldsymbol{X}$) are the record's spectral accelerations at different frequencies of the structure and the magnitude of the earthquake. The objective is to get the probability of no collapse of a structure, $P_{NC}(\boldsymbol{X})$, as a function of the independent variables. Because Y is an "indicator variable," the probability that $Y=1$ for a given $\boldsymbol{X}$ is also the expected value of Y given $\boldsymbol{X}$, i.e., $P_{NC}(\boldsymbol{X})$ is the regression of Y on $\boldsymbol{X}$:

$$P_{NC}(\boldsymbol{X}) = P(Y = 1|\boldsymbol{X}) = E(Y|\boldsymbol{X}) \tag{4.8}$$

Note that the dependent function, the regression, $E(Y|\boldsymbol{X})$, is $P_{NC}(\boldsymbol{X})$ which can vary only from 0 to 1 ($0 \leq P_{NC}(\boldsymbol{X}) \leq 1$), but observed values of Y can be only 0 or 1. If we use a simple linear model for this purpose as we have done before, we might not satisfy the constraint on $P_{NC}(\boldsymbol{X})$ even for very small-scale extrapolation. We will transform $P_{NC}(\boldsymbol{X})$ so that the transformed variable will vary monotonically from $-\infty$ to $+\infty$ and thus the constraint on $P_{NC}(\boldsymbol{X})$ will be satisfied automatically. There are several ways one can accomplish this; the most popular ones are called "probit" and "logit". In probit the dependent variable Y is transformed as follows:

$$probit[P_{NC}(\boldsymbol{X})] = \Phi^{-1}[P_{NC}(\boldsymbol{X})] \tag{4.9}$$

where Φ^{-1} is the inverse of the standardized normal cumulative distribution function. In logit the dependent variable $P_{NC}(\boldsymbol{X})$ is transformed to logistic units as:

$$logit[P_{NC}(\boldsymbol{X})] = \ln \frac{P_{NC}(\boldsymbol{X})}{1 - P_{NC}(\boldsymbol{X})} \tag{4.10}$$

Note that as $P_{NC}(\boldsymbol{X})$ varies from 0 to 1, the $logit(.)$ and $probit(.)$ vary monotonically from $-\infty$ to $+\infty$. The regression analysis by logit transformation is popularly known as "logistic" regression. If we assume that the $logit(Y)$ depends linearly on $\boldsymbol{X}$, then we get the probability of no collapse in terms of the independent variables $\boldsymbol{X}$ as follows:

$$logit[P_{NC}(\boldsymbol{X})] = \alpha + \sum \beta \boldsymbol{X} \tag{4.11}$$

Which implies,

$$P_{NC}(\boldsymbol{X}) = \frac{1}{1 + \exp[-(\alpha + \sum \beta \boldsymbol{X})]} \tag{4.12}$$

where α and β are the regression coefficients. The above function is called logistic cumulative distribution. See Cox (1983) for details. Logistic regression analysis has been popular among civil engineers in solving various types of problems in which one encounters binary response

data, e.g., for liquefaction of soils (Liao, et al., 1988), for damage assessment of bridges (Huang, et al., 1998), etc.

The objective of this binary regression analysis is to use the results to calculate the seismic demand of a structure. The use of the function given in Equation 4.12 to develop an explicit equation, like Equation 3.25 for demand calculation, will be comparatively inconvenient. In order to get a convenient expression for the demand calculation, we assume the following form of $P_{NC}(\boldsymbol{X})$:

$$P_{NC}(\boldsymbol{X}) = \alpha \prod_i X_i^{-\beta_i} \qquad 0 \leq P_{NC}(\boldsymbol{X}) \leq 1 \tag{4.13}$$

where α and β_i are the regression coefficients. Different methods are available for the calculation of these regression coefficients. We adopt here the method of maximum likelihood for this purpose.

Likelihood Function

From Equation 4.13 the probability of no collapse of the structure for the i^{th} observation is calculated as

$$P_{NC}(\boldsymbol{X}_i) = \alpha \prod_{j=1}^{m} x_{i,j}^{-\beta_j} \tag{4.14}$$

where m is the number of explanatory variables considered in the binary regression analysis. The likelihood l_i of observing either collapse, y_i= 0, or no collapse, y_i= 1, for the i^{th} case is:

$$l_i = [P_{NC}(\boldsymbol{X}_i)]^{y_i} \cdot [1 - P_{NC}(\boldsymbol{X}_i)]^{(1-y_i)} \tag{4.15}$$

Note that since observed values y_i= 0 or 1, $l_i = P_{NC}(\boldsymbol{X}_i)$ in the case of no collapse and $l_i = 1 - P_{NC}(\boldsymbol{X}_i)$ in the case of collapse. If there are n independent observations, the joint probability of occurrence of all the binary sequences that generate the particular values $y_1, y_2, \ldots, y_n$ is

$$l_1 \cdot l_2 \cdots l_n \;=\; \prod_{i=1}^{n} [P_{NC}(\boldsymbol{X}_i)]^{y_i} \cdot [1 - P_{NC}(\boldsymbol{X}_i)]^{(1-y_i)} \tag{4.16}$$

$$= l(\alpha, \beta_1, \ldots, \beta_m | x_1, \ldots, x_n) \tag{4.17}$$

The objective of the maximum likelihood method is to maximize the function given in Equation 4.17 with respect to the regression parameters $(\alpha, \beta_1, \ldots, \beta_m)$.

Observe that the likelihood function of the popular logistic model given in Equation 4.12 is a continuous function; the optimization of this function is fairly easy. The contour plot of this likelihood function in Figure 4.18(a) describes how the function is varying with different values of regression coefficients. We get the plot from the scaled results of the 20-story building for $\boldsymbol{X} = S_{a1}$. The same plot for the convenient model in Equation 4.13 is shown in Figure 4.18(b). We observe that this likelihood function has sharp ridges because the model is not a continuous function. Hence one has to be careful in providing a proper initial value of the regression parameters in order to get the correct solution of the problem.

Statistics for Model Fitting

Several statistics are available to evaluate the adequacy of model fitting of binary data (see Liao, 1988, for details). Here we will consider only two statistics, which have been found particularly useful in this study.

Modified Likelihood Ratio Index (MLRI): This ratio was proposed by Harowitz (1982) to compare the "non-nested" models, i.e., the models that cannot be obtained from one another by eliminating one or more explanatory variables. This ratio is defined as

$$MLRI = 1 - \frac{L(\alpha, \beta) - (m+1)/2}{L(0)} \tag{4.18}$$

where $L(\alpha, \beta)$ denotes the log-likelihood function evaluated using the regression coefficients α and β; $L(0)$ is the log-likelihood function for $\alpha = \beta_1 = \ldots \beta_m = 0$; m is the number of explanatory variables. The value of $MLRI$ lies between 0 and 1. The higher values indicate a better fit of the data. Note that this ratio is analogous to the adjusted coefficient

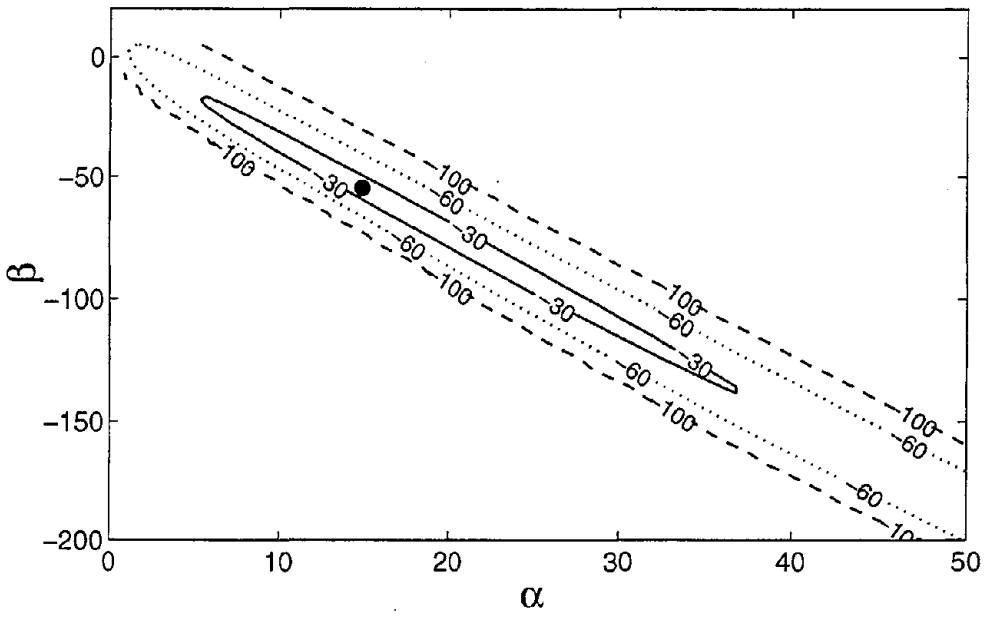

(a) Logistic regression model (Equation 4.12)

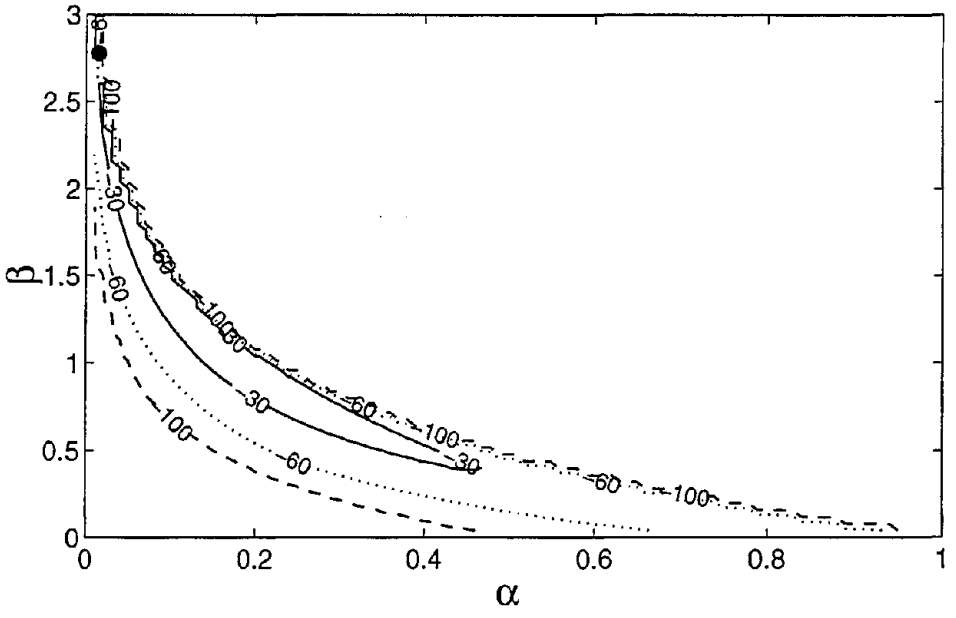

(b) Convenient regression model (Equation 4.13)

Figure 4.18: Contour plot of the logarithm of the likelihood function (Equation 4.17) for different regression models as obtained from the 20-story scaled results for $\boldsymbol{X} = S_{a1}$. The symbol • indicates the optimized values of α and β.

of multiple determination R_a^2 (see Section 3.3.4 for details) of linear regression, but unlike R_a^2 in linear regression where an R_a^2 value close to 0.8 can be considered to be a good fit, a good fit of binary regression results does not give a high value of $MLRI$ (see Liao, et al., 1988). An $MLRI$ value close to 0.4 has been considered to be a good fit by Liao, et al. (1988) in their soil liquefaction study and also by Hensher and Johnson (1981) in a transportation data analysis.

Log-Likelihood Ratio (LLR): As we have to consider several explanatory variables apart from the first-mode spectral acceleration, we need to select a few from these candidate variables for the seismic demand calculation of structures. This can be done by following the "step-wise" regression procedure. In each step this procedure either adds the most statistically significant variable not already included in the current model or deletes the least significant variable from the current model. In this procedure the log-likelihood ratio (LLR) is calculated from the following equation:

$$LLR = -2 \ln \frac{l_{m+1}}{l_m} \tag{4.19}$$

where m and $m+1$ denote the number of explanatory variables considered in the two "nested" models under consideration. Under the null hypothesis (H_0) which is that the $m+1$ variable is not important, i.e., is conditionally independent of $E(Y|X_1 \ldots X_n)$, LLR is a χ^2 distributed random variable with one degree of freedom. If $LLR \geq \chi^2_{\nu,1}$, then the addition of the candidate variable makes the prediction statistically significantly different from the prediction without the candidate variable. The significance level, ν, in this study is taken to be 0.05, and $\chi^2_{\nu,1}$ denotes the $(1-\nu)$ fractile of the χ^2 distribution with 1 degree of freedom.

Results of Binary Regression

The results of binary regression analysis of the scaled results for the 20-story structure are given in Table 4.5. It is observed that the probability of no collapse $[P_{NC}(\boldsymbol{X})]$ is mainly

Explanatory Variable	Regression Function $[P_{NC}(X) \leq 1]$	$L(\alpha, \beta)$	$MLRI$
S_{a1}	$P_{NC} = 0.02 \cdot (S_{a1})^{-2.78}$	23.7	0.76
S_{a1}, S_{a2}	$P_{NC} = 0.01 \cdot (S_{a1})^{-3.33} \cdot (S_{a2})^{-0.57}$	19.7	0.79

Table 4.5: Results of regression analysis of the probability of no collapse (P_{NC}) against spectral accelerations from the records scaled to the 0.30g, 0.15g, and 0.05g first-mode spectral accelerations. $L(\alpha, \beta)$ is the optimized log-likelihood value. $MLRI$ is the modified log-likelihood ratio (see Equation 4.18).

dependent on the first-mode spectral acceleration. The LLR for the first-mode and the second-mode spectral accelerations is calculated from Equation 4.19 as follows:

$$\begin{aligned} LLR &= -2 \ln \left[\frac{l_{S_{a1}, S_{a2}}}{l_{S_{a1}}} \right] \\ &= -2 \cdot (19.7 - 23.7) = 8 > \chi^2_{0.05,1} = 3.84 \end{aligned}$$

The LLR value indicates that the dependence of $P_{NC}(\boldsymbol{X})$ on the second-mode spectral acceleration (S_{a2}) is statistically significant. Note that because the likelihood function is not a continuous function, we find that the optimization routine does not converge when we include M, or R, or T in addition to S_a. We will show the binary-regression results against S_{a1} and M, or R, or T in Chapter 5 by adopting the logistic regression model. The variation of probability of no collapse with the first-mode spectral acceleration, $P_{NC}(S_{a1})$, and with the first- and second-mode spectral accelerations, $P_{NC}(S_{a1}, S_{a2})$, are shown in Figure 4.19.

4.3.5 Variation of Damage Measures with Spectral Acceleration including Collapses

The regression results we have seen in Figure 4.12 are conditioned on no collapse of the structure. If we calculate the median demand when collapses are included, the medians (conditioned on S_a) will differ significantly at high intensities from those in Figure 4.12. We can calculate the conditional median of a damage measure at different S_a levels from

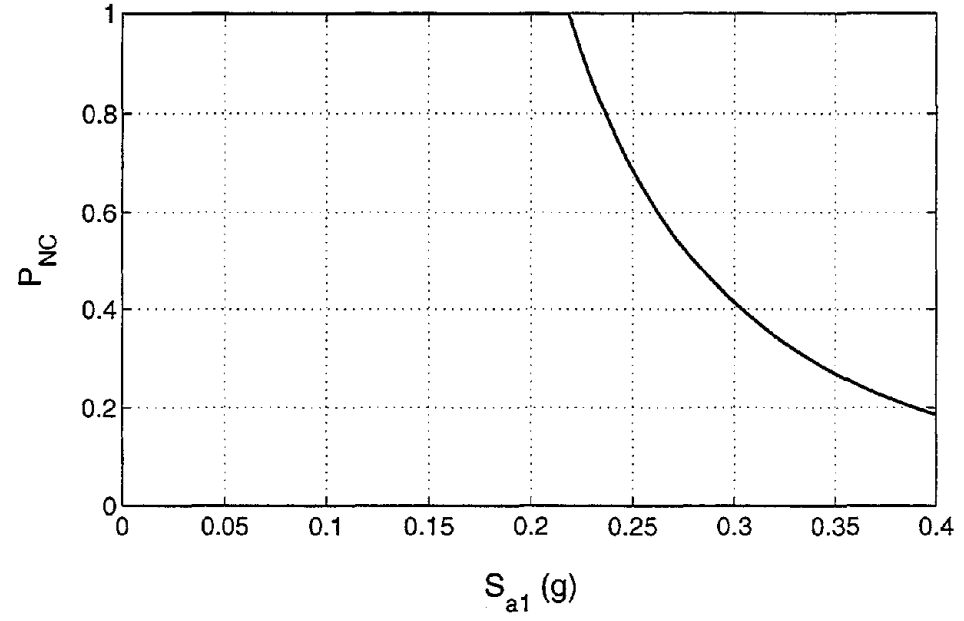

(a) First-mode spectral acceleration (S_{a1})

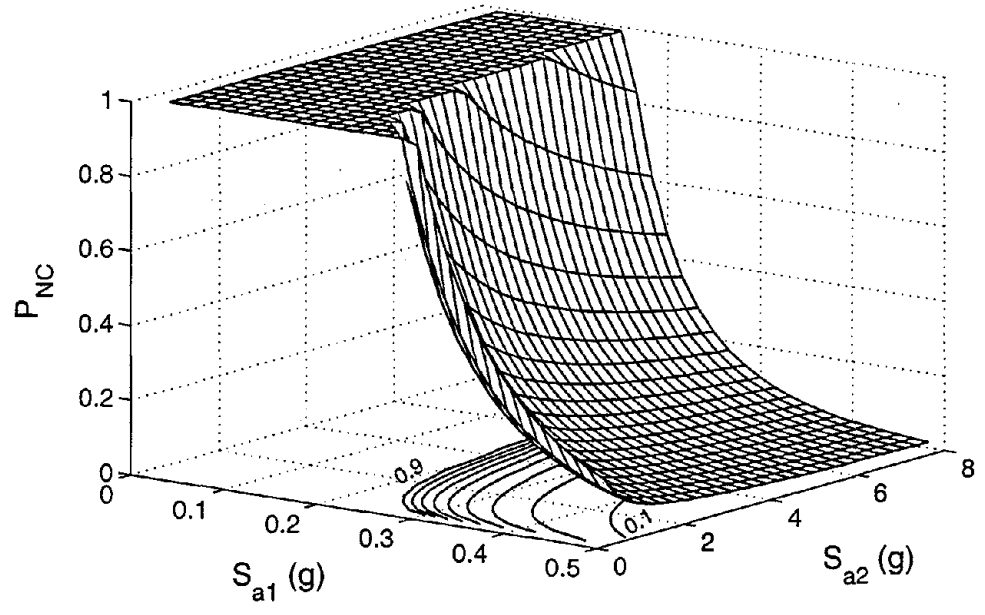

(b) First-mode and second-mode spectral accelerations (S_{a1}, S_{a2})

Figure 4.19: Variation of the probability of no collapse, $P_{NC}(\boldsymbol{X})$, of the 20-story structure with different explanatory variables.

Equation 4.6. We need for this calculation both the distribution parameters of damage measures conditioned on no collapse, which are given in Table 4.4, and the probability of no collapse, which is given in Table 4.5 as a function of S_a. Let us consider, for illustration, the maximum story-drift results. We use the regression results against S_a only. The plot of the cumulative distribution function (CDF) of this damage measure in Figure 4.20 at each of several spectral acceleration levels illustrates the damage measure's variability at that intensity level. We observe that as the spectral acceleration increases the distribution curve median increases and the shape becomes flatter, indicating higher standard deviation at higher spectral accelerations. We can also calculate the conditional median drift from this figure. The median drift results are shown in Figure 4.21. We observe that when the spectral acceleration is greater than s_{a0} (which is 0.22g), the median drift increases rapidly with small increase in S_a, indicating softening of the structure at the high intensity level. Note that the slope (in log-log space) of the regression line of the median drift is 1.15 over a wide range of S_a ($0 \leq s_a \leq 0.27g$), whereas the slope is 1.8 for $0.2g \leq s_a \leq 0.27g$. On the other hand, the median drift results conditioned on no collapse (NC) suggest a slight hardening ($\beta < 1$) of the structure even at high spectral accelerations (see Table 4.4).

4.4 Calculation of Seismic Demand

In Section 3.5 we have calculated the seismic demand of a 5-story building frame. We will use a similar approach to calculate the seismic demand of the 20-story structure. The main difference between the demand calculations of the 5-story and the 20-story structures is that the likelihood of the collapse of the latter structure is significant ($\approx 40\%$) at the 0.30g first-mode spectral acceleration or 5000-year intensity level. We therefore need to incorporate this likelihood of "collapse", or the likelihood of infinite demand in Equation 3.20 for the demand prediction of this structure. We have seen in Figure 4.9 that the sample space of all damage-measure results consists of two types of events: one is the collection of sample points of the collapse or infinite-damage results (C) and the other is is the collection of sample points of no-collapse results (NC). Hence the probability of exceedance of a level y

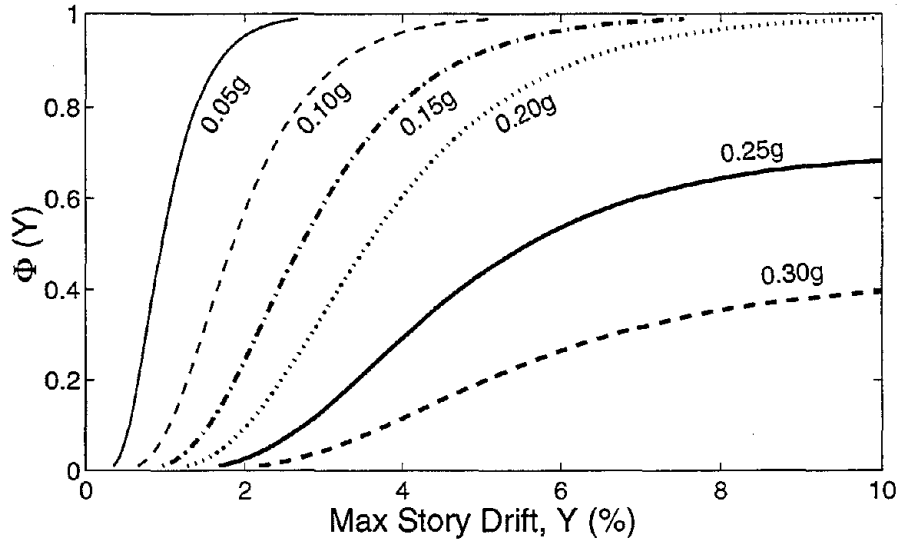

Figure 4.20: Cumulative distribution function of maximum story drift at different first-mode spectral accelerations.

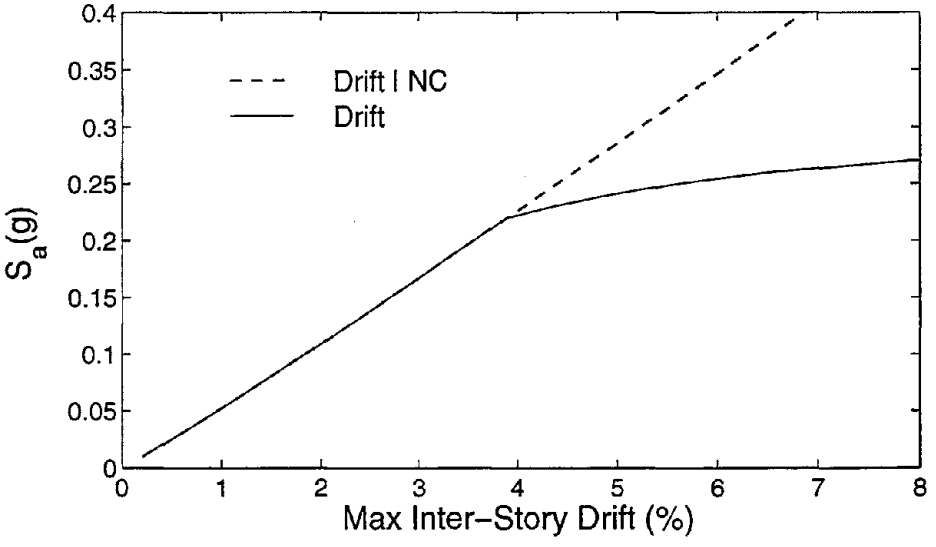

Notation: NC=no collapse

Figure 4.21: Variation of the median maximum story drift with the first-mode spectral acceleration. Note that the median drift conditioned on no collapse is obtained from Table 4.4.

of damage parameter Y can be calculated from the following:

$$\begin{aligned} P(Y > y) &= P(Y > y|C) \cdot P(C) + P(Y > y \,|\, NC) \cdot P(NC) \\ &= 1.0 \cdot P(C) + P(Y > y \,|\, NC) \cdot P(NC) \end{aligned} \tag{4.20}$$

Conditioning on S_a and applying the theorem of total probabilities, we get the following:

$$\begin{aligned} P(Y > y) = \int_0^\infty P_{C|S_a}(s_a)\, \lambda_{S_a}(s_a)\, ds_a + \int_0^\infty G_{Y|NC,S_a}(y|s_a) \\ P_{NC|S_a}(s_a)\, \lambda_{S_a}(s_a)\, ds_a \end{aligned} \tag{4.21}$$

where

$P_{NC|S_a}(s_a)$ is the probability of no collapse of a structure, which can be obtained from binary regression analysis of response results as described in Section 4.3.4.

$P_{C|S_a}(s_a) = 1.0 - P_{NC|S_a}(s_a)$

$G_{Y|NC,S_a}(y|s_a)$ is the complementary cumulative distribution function of any damage measure Y conditioned on S_a from the no-collapse results.

$\lambda_{S_a}(s_a) = \left|\frac{dH(s_a)}{dS_a}\right|$, where $H(s_a)$ is the spectral-acceleration, seismic-hazard function.

This equation can be solved by numerical integration for any arbitrary hazard function, $H(s_a)$, for any binary regression results, e.g., $logit[P_{NC|S_a}(.)]$, and for any complementary cumulative conditional distribution function, $G_{Y|NC,S_a}(.)$.

Here, we will carry out numerical integration of Equation 4.21 with the following assumptions:

1. The conditional complementary cumulative distribution, $G_{Y|NC,S_a}(.)$, conditioned on S_a and no collapse is lognormally distributed. We get the parameters of this distribution function from the regression results of the no-collapse data (see Table 4.4).
2. The hazard function, $H(s_a)$, is approximately linear in log-space, and this

can be approximated in the region of interest by Equation 3.23. Although we could have incorporated any non-analytical tabulated hazard results from PSHA in numerical integration, we will compare below the numerical integration results with the results from a simpler approach which will require the analytical representation of the hazard function (see, for example, Equation 3.23).

3. The probability of no collapse of a structure, $P_{NC}(s_a)$, is a function of the first-mode acceleration. We consider the following functional dependency of P_{NC} on S_a as per Equation 4.13:

$$P_{NC}(s_a) = \alpha_C \cdot s_a^{-\beta_C}; \qquad 0 \leq P_{NC}(s_a) \leq 1 \tag{4.22}$$

The coefficients α_C and β_C can be obtained from Table 4.5. Alternatively the above equation can be written as:

$$P_{NC}(s_a) = \left[\frac{s_a}{s_{a0}}\right]^{-\beta_C} \qquad s_a \geq s_{a0} \tag{4.23}$$

where s_{a0} is the minimum first-mode spectral acceleration required to induce "collapse" in the structure. This is equal to $\alpha_C^{\frac{1}{\beta_C}}$.

For the convenience of the demand calculation, the closed-form solution of Equation 4.21 is given in Appendix F. In the closed-form solution, a lower bound of probability of exceedance (P_{LB}) of demand calculations or an upper bound of the return period ($RP_{UB} = 1/P_{LB}$) is given by the first term in Equation 4.21 (or *Term-C* in Equation F.1). We will refer to this term frequently in describing demand results. It is given in the following:

$$1/RP_{UB} = \int_0^{+\infty} P_C(s_a) \cdot \lambda_{S_a}(s_a)\, ds_a \tag{4.24}$$

$$= H^1(s_{a0}) \cdot \frac{\beta_C}{K_1^1 + \beta_C} \tag{4.25}$$

where

$H^1(s_{a0})$ = spectral acceleration hazard function as per Equation 3.23 at s_{a0} =

$K_0^1 \cdot (s_{a0})^{-K_1^1}$. We have defined s_{a0} in Equation 4.23. K_0^1 and K_1^1 are respectively the intercept and slope of the approximate hazard function in log-log space in the region from $s_a = s_{a0}$ to $s_a = \infty$.

β_C = exponent in Equation 4.23.

We assume here that the 20-story structure is located at a central Los Angeles site. The seismic hazard curve of the site at 0.25Hz is shown in Figure 4.22. The approximate hazard function from Equation 3.23 is also shown in the figure. We observe that this approximation works quite well over a wide range of spectral accelerations. The probability of exceedance of 5% maximum interstory drift, calculated from Equation 4.21 by numerical integration, is 3.72×10^{-4} (or 2700-year return period). The 5% limiting drift is the "collapse-prevention" allowable drift as suggested in FEMA-273 (1996) for seismic rehabilitation of fully restrained steel-moment-frame buildings. If we consider only the results conditioned on no collapse (i.e., the second term in Equation 4.21), the probability of exceedance of 5% maximum story drift can be obtained from the explicit Equation 3.25. This probability is 3.34×10^{-4} (or 3000-year return period). We find that at this 5% drift level the difference in results is not significant because of negligible likelihood of collapse at this performance level.

Seismic Drift-Demand Hazard Curves: We have calculated similarly the probability of exceedance of maximum story drift at different drift levels by numerical integration. The results are plotted in Figure 4.23(b). This is the seismic demand hazard curve of the structure for maximum story drift. In the same figure we also show the results of demand hazard calculations conditioned on no collapse of the structure (from the approach described in Section 3.5). We observe that the inclusion of the collapse results in demand predictions, as expected, is important only at the high seismic demand levels. The return period of drift at high drift-demand levels reaches its upper-bound value, whereas we find that the return period keeps on increasing when conditioned on no collapse. We can calculate this upper bound of the return period (R_{UB}) from Equation 4.25. This upper bound is due to the high likelihood of collapse of the structure at the high-intensity ground motions which are required to produce that high a demand in the structure. Note that this upper-bound return

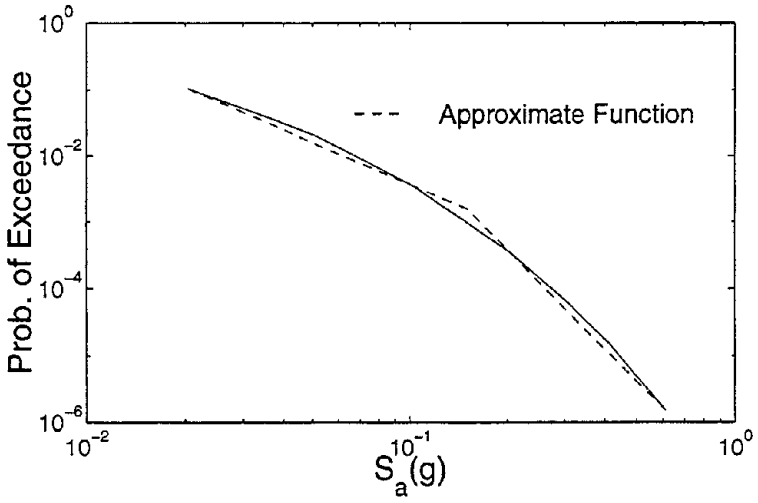

Figure 4.22: Seismic hazard curve at 5% damping for 0.25Hz frequency.

period is the same for all the damage measures but is specific to a particular structure at that site. We observe in Figure 4.23 that the R_{UB} coupled with the simple demand results conditioned on no collapse (from Equation 3.25), will be close to the results we have obtained before from Equation 4.21. Hence the demand calculation of this 20-structure simplifies to the following:

$$P(Y > y) = H[(y/\alpha)^{\frac{1}{\beta}}] \cdot e^{\frac{1}{2}\left(\frac{K_1 \cdot \sigma_{\ln Y|\ln Sa}}{\beta}\right)^2} \geq H^1(s_{a0}) \cdot \frac{\beta_C}{K_1^1 + \beta_C} \qquad (4.26)$$

We observe that the demand calculation is essentially the same as that in Chapter 3 but has only a lower-bound value. This combination simplifies the demand calculations and always gives us a somewhat conservative estimation of the return period. The simplified procedure can be useful in the development of guidelines for seismic demand calculations.

Note that the intersection of R_{UB} and the seismic demand conditioned on no collapse can be considered as a conservative estimation of the *capacity* of the structure. This can be

calculated from Equations 3.25 and 4.25 as follows:

$$\begin{aligned} P_{LB} &= H[(\hat{y}_{capacity}/\alpha)^{1/\beta}] \cdot C_f \\ \text{or,} \quad \hat{y}_{capacity} &= \alpha \cdot \left[\frac{K_0 C_f}{H^1(s_{a0})} \cdot \frac{K_1^1 + \beta_C}{\beta_C}\right]^{\frac{\beta}{K_1}} \qquad (4.27) \\ &= \hat{y}_0 \cdot \left[C_f \cdot \frac{K_1^1 + \beta_C}{\beta_C}\right]^{\frac{\beta}{K_1}} \qquad (4.28) \end{aligned}$$

where $\hat{y}_0 = \alpha(s_{a0})^\beta$ is the median story drift for spectral acceleration, s_{a0}, at which the probability of collapse is zero. This is 3.9% for the 20-story structure. We find that here the implied maximum median story-drift capacity is 7.2%. The spectral acceleration capacity of this structure can be obtained from Equation 4.28 as follows:

$$\begin{aligned} P_{LB} &= H[s_{a,capacity}] \cdot C_f \\ s_{a,capacity} &= s_{a0} \cdot \left[C_f \cdot \frac{K_1^1 + \beta_C}{\beta_C}\right]^{\frac{1}{K_1}} \qquad (4.29) \end{aligned}$$

For this 20-story structure s_{a0} is 0.22g. The spectral acceleration capacity is found to be 0.42g at 0.25Hz and 5% damping.

We have also calculated the demand of the structure for three other important damage measures: system drift (average of all the story drifts), maximum interstory NHE, and maximum beam plastic rotation. The results of these damage measures are also shown in Figure 4.23. These demand curves are quite similar to the maximum story drift. From the definition of NHE (Equation 2.2 we get the following relationship for NHE:

$$\begin{aligned} \text{NHE} &= 4 \cdot n_{eq} \cdot [\text{drift}(\%) - 1] \qquad (4.30) \\ \text{or,} \quad n_{eq} &= \frac{\text{NHE}}{4 \cdot [\text{drift}(\%) - 1]} \qquad (4.31) \end{aligned}$$

where n_{eq} is the "equivalent" number of cycles, which are calculated for the maximum drift associated with a given NHE. From Figure 4.23 we find that the 75-year, 475-year and 2475-year demands are 1.4%, 2.8%, and 4.8% respectively for story drift, and are 1.7, 10.7,

and 42.5 respectively for story NHE. Applying Equation 4.31, the equivalent number of full nonlinear cycles are 1, 1.5, and 2.8 at the 75-, 475-, and 2475-year demands respectively. These results show that the number of (equivalent) nonlinear full cycles increases nonlinearly with the increase in demand levels. This is due to the nonlinear increase in NHE with S_a as we have seen in Figure 4.12. Note that the number of equivalent full cycles at the structural capacity of 7.2% is 4.7.

Story-by-Story Drift Hazard Curves: In order to understand the risk associated with each story separately, which is needed, for example, to identify the stories in need of retrofitting for seismic rehabilitation of a building, we plot the seismic demand curve of each story in Figure 4.24. We assume here that if the structure collapses, i.e., if the algorithm does not converge, the damage measures at *all the stories are infinite.* We observe that the risk is mainly concentrated at the first few stories, e.g., the drifts of the first story and the third story are much higher than those of the other stories at the life-safety (475-year return period) or the collapse-prevention (2475-year return period) demand level. The risk at very high drift levels for all the stories, however, merges to a common value, indicating a high probability of collapse of the structure, i.e., collapse of all the stories at the ground-motion intensity level required to induce that drift. This observation is at variance with the results we have seen before in Figure 3.16, where the differences among the seismic drift demands of different stories grow wider at higher demand levels. Note that the probability of "collapse" of the 5-story building is assumed to be insignificant at the demand levels shown in Figure 3.16.

4.4.1 Simplified Explicit Seismic Demand-Hazard Relationships

The above procedure for demand-hazard calculation requires numerical integration of Equation 4.21 or application of the cumbersome, though explicit, relationships shown in Appendix F. In order to avoid this we will use here the simple explicit Equation 3.25 for the demand calculation:

$$P(Y > y) = H[(y/\alpha)^{\frac{1}{\beta}}] \cdot e^{\frac{1}{2}\left(\frac{K_1 \cdot \sigma_{\ln Y|Sa}}{\beta}\right)^2} \tag{4.32}$$

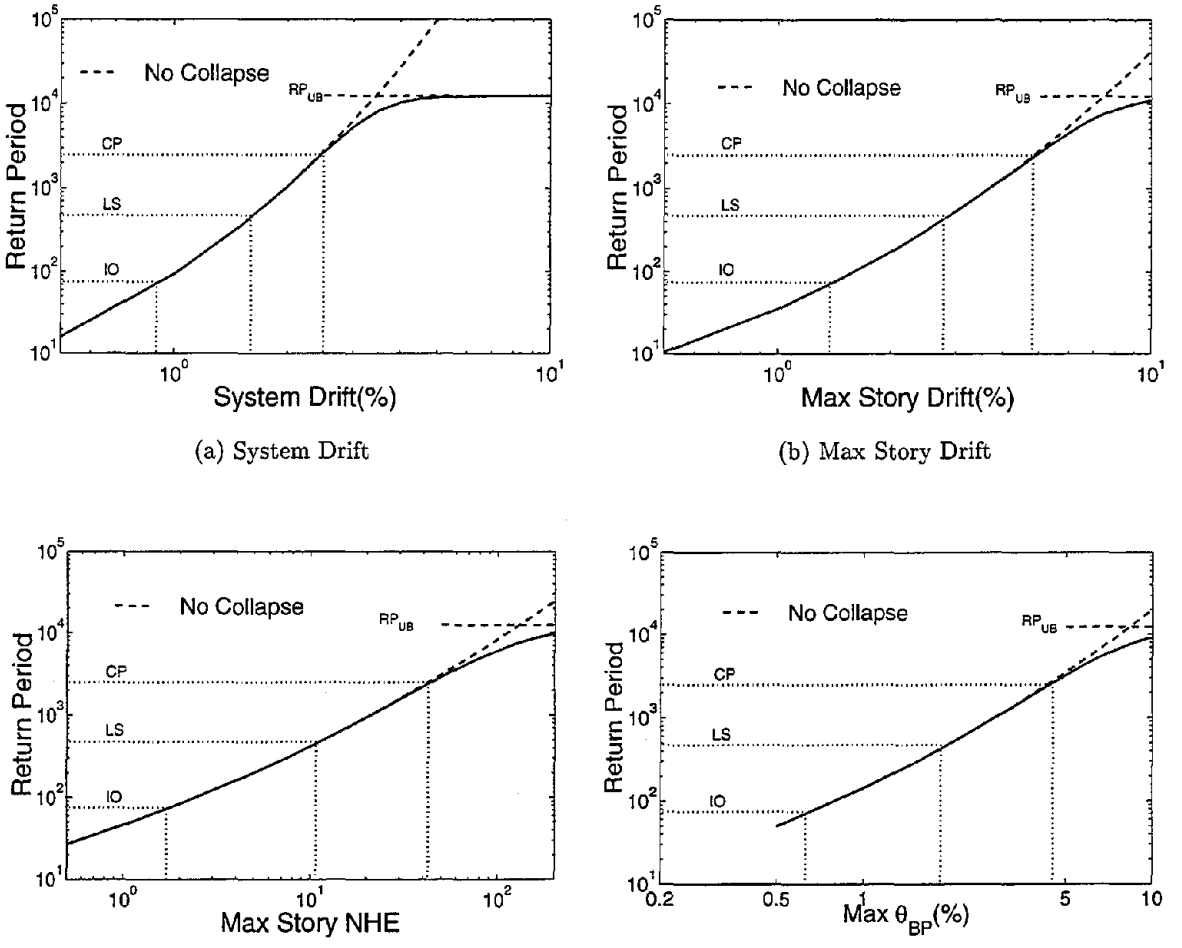

(a) System Drift

(b) Max Story Drift

(c) Maximum Story NHE

(d) Max Beam Plastic Rotation

Notation: CP=Collapse Prevention, LS=Life Safety, IO=Immediate Occupancy
RP_{UP}= Upper-bound return period (see Equation 4.25)

Figure 4.23: Seismic demand-hazard curves for a 20-story SMRF at a central Los Angeles site.

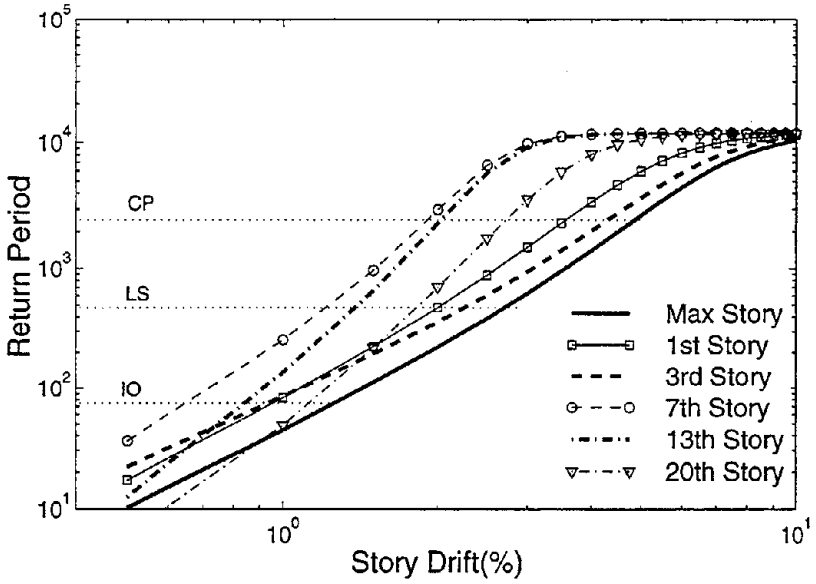

Notation: CP=Collapse Prevention, LS=Life Safety, IO=Immediate Occupancy

Figure 4.24: Seismic demand-hazard curves of different stories for a 20-story SMRF at a central Los Angeles site.

We have seen in Figure 4.23 (dotted lines) that when we use the results conditioned on no collapse, we get a good estimation of the seismic demand at the low demand levels. Now we will use the median drift results including collapses, which we have obtained from Section 4.3.4 and which are given in Figure 4.21. We use directly the spectral acceleration required for a target median drift from Figure 4.21 and the equivalent dispersions in Equation 4.32 to calculate the seismic demand. The β in the equation is calculated locally by fitting the median damage results against S_a. The results of this simplified demand calculation for maximum story drift are shown in Figure 4.25. The comparison of the results with those of the numerical-integration indicates that the simplified procedure works quite well at high demand levels; the drift-demand return period instead of increasing indefinitely, plateaus at its characteristic upper bound (Equation 4.25).

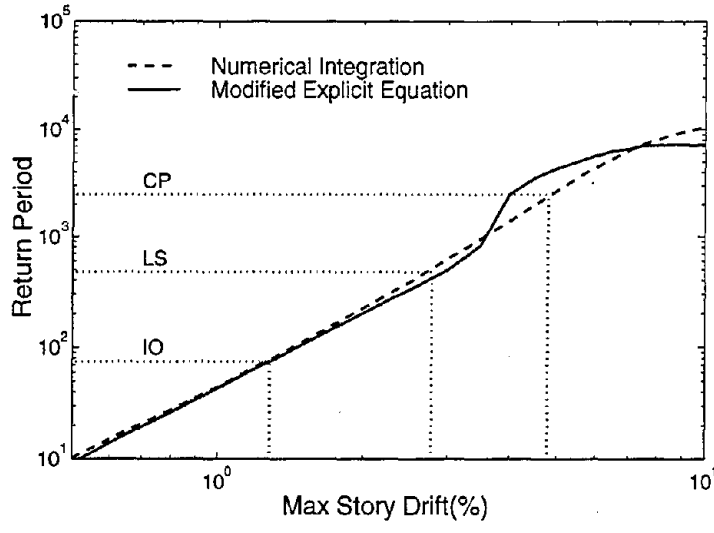

Figure 4.25: Seismic story-drift-demand curve estimated from the explicit Equation 3.25 using the median drift from Figure 4.21 for a 20-story SMRF at a central Los Angeles site. Compare the results with those from the numerical integration. The approximate calculation of the parameters of the explicit equation is described in the text.

4.4.2 Seismic Demand Analysis from Weighted-Average Spectral Acceleration

We have observed in Table 4.2 that for the 20-story building the scaling of records to the weighted-average spectral acceleration gives a significantly higher reduction in dispersion than scaling to only the first-mode spectral acceleration gives. This effect is significant because of large higher-frequency contribution to the response of this structure. So when we carry out regression analysis against an average acceleration ($S_a^\star = 0.8S_{a1} + 0.2S_{a2}$), we observe in Table 4.4 a significant reduction in regression error compared to the error obtained from the regression analysis against the first-mode spectral acceleration. If we can use these regression results for $S_a^\star$ in the drift-demand calculation, as per Table 4.4, we will need only 65% as many nonlinear runs as we need for the results against the first-mode spectral acceleration to estimate the regression parameters with a specified accuracy. The only problem in using these $S_a^\star$ regression results is that we need a structure-specific hazard

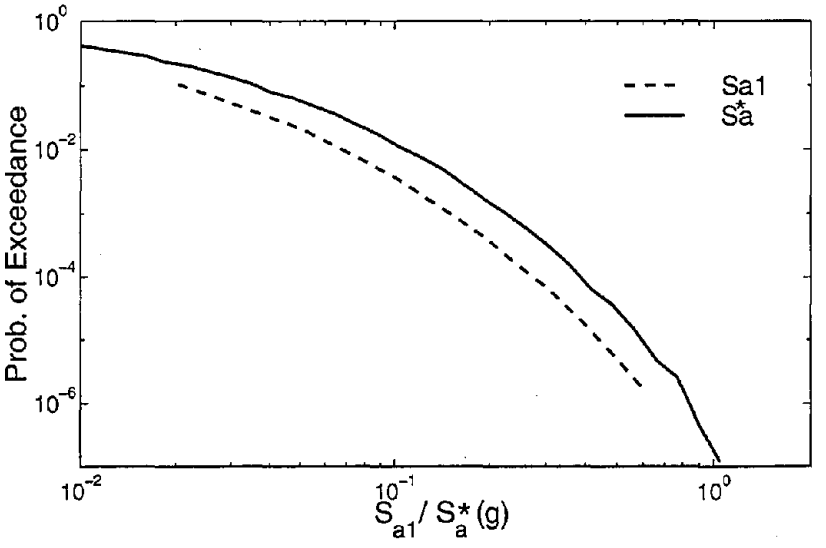

Figure 4.26: Seismic hazard curve at 5% damping for the weighted-average spectral acceleration ($S_a^\star$) at a central Los Angeles site. Also shown is that for S_{a1}.

curve (i.e., a seismic hazard curve for the weighted-average spectral acceleration, $S_a^\star$; the weights and the important higher-frequency spectral acceleration will vary from structure to structure). The hazard curve[11] for the weighted-average spectral acceleration is shown in Figure 4.26. The maximum story-drift demand of this 20-story building (conditioned on no collapse) from the weighted-average spectral acceleration is shown in Figure 4.27. Note that we do not present here the results beyond 5% drift, as we have seen before that beyond that drift level the "collapse" results are important. At high-drift levels, the difference between the results from the first-mode and the weighted-average spectral accelerations is quite significant (a factor of 2 or more). We will explain in Chapter 5 why we see this difference and why the results of weighted-average spectral acceleration are in fact more accurate.

[11] This structure-specific hazard curve can be obtained comparatively easily by constructing an attenuation law (versus M and R) from those available in the literature for S_{a1} and S_{a2}, and then by using this new attenuation result in the conventional PSHA program in place of that for S_{a1}.

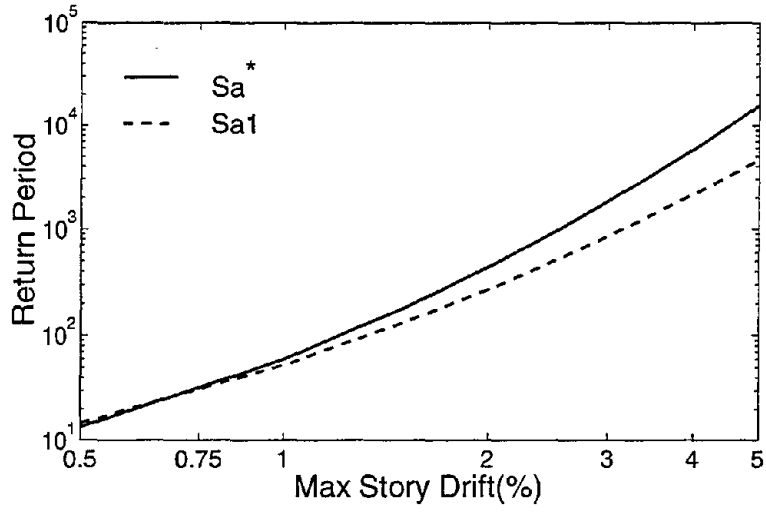

Figure 4.27: Seismic story-drift demand hazard curve from the weighted-average spectral acceleration ($S_a^\star$) hazard and the regression of maximum story drift on $S_a^\star$ for a 20-story SMRF at a central Los Angeles site. The same curve based on first-mode spectral acceleration (S_{a1}) is also shown. Here both cases are *conditioned on no collapse* for simplicity.

4.4.3 Indirect (Alternative) Method

We will now calculate the seismic demand of this structure by the indirect method, described in detail in Section 3.5.2. In this section we will follow the same "required spectral acceleration" (S_a^R) basis for the demand calculations. The main advantage of this method is that we can continue to use the same equation (Equation 3.28) for the demand calculations unlike in the direct approach where we had to modify the demand calculations to incorporate the "collapse" results. The collapse results are reflected in the statistics of S_a^R, however (see Figure 4.28). Note that, in our implementation here, the demand calculation from the indirect approach does not assume any functional variation of the median damage measures with spectral acceleration unlike in the direct approach (see the regression model in Equation 3.2). In the direct method we have also assumed (although not necessarily inaccurately) that the dispersion of damage measures conditioned on spectral acceleration is constant. We made this assumption in order to get an explicit solution for the demand calculation. These simplifying assumptions might introduce some inaccuracy in the demand

predictions obtained by the direct approach.

The variation of required spectral acceleration, $S_{a_y}^R$, at different interstory drifts, y, is shown in Figure 4.28. We observe here that at the 5% story drift the structure appears to have almost reached its capacity level, as measured by the median of S_a^R. The dispersion of $S_{a_y}^R$ at different drift levels is also indicated in the figure. We observe that the dispersion appears to increase somewhat with drift. The return period for 5% limiting story drift is 2050 year whereas the same from the direct approach is 2700 year. The results of demand calculations at other drift levels are shown in Figure 4.29. We observe that at the low-demand levels the results from these two approaches are very close to each other, whereas at the high-demand levels the results deviate. Here the calculations of S_a^R are *not* very accurate; S_a^R's calculated by interpolation of the direct results at the low-drift levels, whereas in a large number of cases the calculations are by extrapolation at large drifts. If we calculated S_a^R more accurately, we would be getting a closer match of the results of these two approaches.

4.4.4 Simplified Nonlinear Static FEMA-273 Procedure

We have seen in Section 3.5.3 that the nonlinear static procedure (NSP) of FEMA-273 predicted quite well the seismic demand of a single-frequency dominated 5-story steel moment resisting frame. Now we will verify how well the simplified NSP results predict the drift demand for the multi-mode dominated 20-story structure. The first step in this procedure is to calculate the target displacement (δ_t), which is a characteristic displacement to estimate the global displacement at a target seismic hazard level. FEMA-273 has defined the target displacement as the roof displacement that is estimated from an equivalent SDOF system transformed to the MDOF domain through the use of the modal participation factor and other modification factors. The target displacement is calculated from Equation 3.29. The calculation of δ_t of this 20-story building is given below (see FEMA-273, 1996, for details):

$T_e = 4sec; \quad T_0 = 0.5sec$ (From Figure 3.19)

$C_0 = 1.5; \quad C_1 = 1.0\ (T_e > T_0); \quad C_2 = 1.0$

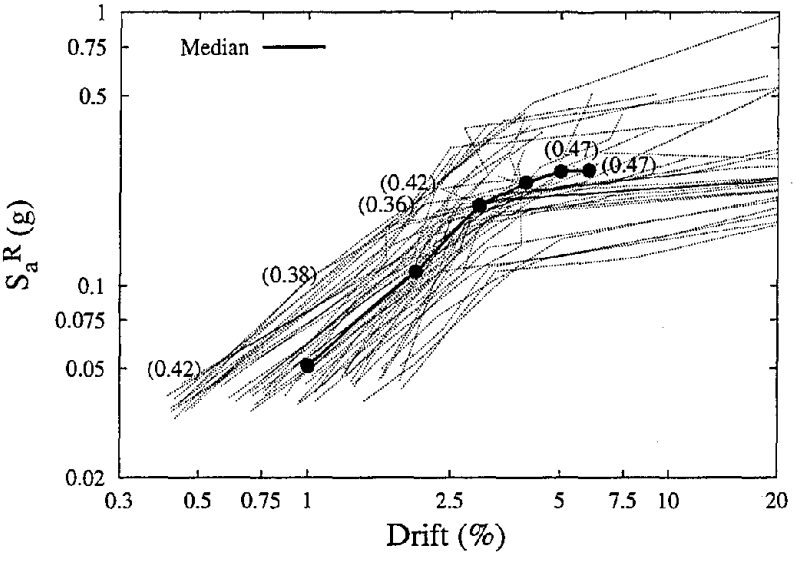

Figure 4.28: Variation of the required first-mode spectral acceleration (S_a^R) for a 20-story SMRF at different maximum interstory-drift levels. Each curve corresponds to drifts found from a different record scaled to different S_{a1} levels (i.e., each is a "dynamic pushover" curve). At each drift level the median $S_{a_y}^R$ is calculated by the interpolation method. The numbers within parenthesis at different drift levels indicate the "dispersion" (as per Equation A.2) of $S_{a_y}^R$ at that level.

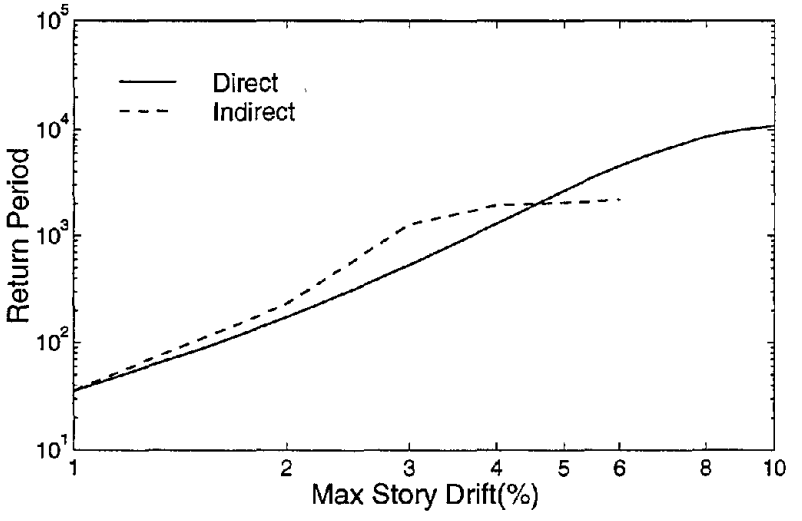

Figure 4.29: Seismic drift demand from the direct and the indirect approach for a 20-story SMRF at a central Los Angeles site.

The strength ratio $R = \frac{S_a}{V_y/W} \cdot \frac{1}{C_0} = \frac{0.24}{917/12211} \cdot \frac{1}{1.5} = 2.1$

$[S_a(0.25Hz, 2\%) = 0.24g$ at 2500 year return period. See Figure 3.19.]

$C_3 = 1.0 + \frac{|\alpha|(R-1)^{1.5}}{T_e} = 1.0 + \frac{0.27(2.1-1)^{1.5}}{4} = 1.08$

(α is calculated from Figure 4.1.)

$\delta_t = 1.5 \times 1.0 \times 1.0 \times 1.08 \times (0.24 \times 981) \times \frac{4^2}{4\pi^2} = 155cm\ (= 61inch)$

In nonlinear static procedure (NSP) the target displacement (δ_t) is applied at the top story, and the internal forces and deformations are calculated by the nonlinear step-by-step static analysis. The maximum story drift derived demand from this approach at the collapse-prevention level is 5.2%, whereas the median maximum story drift demand we have predicted given the 2500-year intensity level [$S_a(0.25Hz, 2\%) = 0.24g$] is 3.2% (see Table 4.4). Hence the FEMA-273 procedure appears to overpredict the seismic drift demand by 60%. When, however, we take into account the variability in demand prediction conditioned on no collapse (e.g., $\delta_\varepsilon = 0.39$, in Table 4.4) and also the likelihood of "collapse" (as reflected in Table 4.5), we observe in Figure 4.23(b) that the 2500-year seismic demand of the maximum story drift is 4.8%. Note that in Equation 3.29 there is no explicit factor to take

into account the uncertainty in demand prediction and the "collapse" of a structure. So Equation 3.29 should have an additional factor to incorporate explicitly these uncertainties, a factor that will help a designer to focus more on the accuracy of the demand prediction. Luco and Cornell (1998) have shown how to incorporate the variabilities of different parameters in demand calculations (although their calculation neglects the possibility of collapse of a structure at the target-demand level).

4.5 Summary

In this chapter we have considered a multi-frequency dominated structure, whereas in the previous chapters we considered only single-frequency dominated structures. One important characteristic of this structure is that the P-Δ effect is very high at large responses. We have observed for the first time "collapse" (non-convergence of the numerical integration scheme) of a structure. The collapse is due to the high negative stiffness at high drift levels (as we have seen in the pushover analysis results) due largely to the P-Δ effect. This phenomenon makes it impossible to calculate the sample statistics we calculated in the previous chapters. We have therefore introduced here (Section 4.2.3) the "counted median" and an "equivalent dispersion," the latter obtained by a bootstrap resampling technique. We have also proposed a better, but more involved, three-parameter distribution model to fit the damage results (Equation 4.4). These calculations show that scaling of ground-motion records for relatively the same M and R characteristics does not introduce any bias in damage estimations (Table 4.3). Because the 20-story building is a multi-frequency dominated structure, scaling the records to the same first-mode spectral accelerations results in an around 40% reduction in dispersion of the story-drift damage measure compared to the direct results. We can, however, get a greater than 50% reduction if in the scaling we consider also the spectral accelerations at higher frequencies. This is done by carrying out "weighted" scaling of the ground-motion records to the same average spectral acceleration, $S_a^\star$ (Section 4.2.5). Note that because of collapse (or infinite drift) the sample size required to produce accurate drift predictions is high for this structure compared to that required in

the previous chapters.

In regression analysis of the no-collapse results, we have observed that the responses are dependent mainly on the second-mode spectral acceleration in addition to the first mode spectral acceleration, S_{a1}. Once conditioned on S_{a1} the response of this tall structure (conditioned on no collapse) does not depend further on the magnitude of events or duration of records. Although we could not verify the bin-to-bin scaling scheme for this multi-frequency dominated structure, the dependency of response on higher-frequency spectral accelerations suggests that like for the previous single-frequency dominated structures we will not get an unbiased response from the records of a bin scaled via S_{a1} to the intensity level (median intensity) of another bin $(M - R)$, unless the median-spectrum shape of the records is close to that of the other bin's records. Scaling by $S_a^\star$ that reflects the high frequency effects will, however, probably avoid this problem.

We have introduced in this chapter binary regression analysis to analyze the collapse results (Section 4.3.4). Binary regression analysis also indicates that the probability of "collapse" of the 20-story structure is mainly dependent on the first-mode spectral acceleration and to some extent on a higher-frequency (e.g., the second-mode) spectral acceleration. This observation is similar to what we have seen in the no-collapse results for different damage measures.

In probabilistic seismic demand calculations for this structure, we have incorporated the collapses because the likelihood of collapse is significant at high demand levels. We have observed that due to the increase in the likelihood collapse with the increase in spectral acceleration, the seismic demand curve reaches its saturation point at high demand levels. In Chapter 3, conversely we did not observe this characteristic in the demand-hazard curve. We found that incorporation of collapse results is important only at higher demand levels.

We have found that the demand calculation of the 20-story building becomes complicated because of "collapse" of the structure at higher intensity levels, but it is still feasible. We can alternatively use an approximate but simple procedure to calculate the seismic demand (Section 4.4.1). In this procedure we have used the simple and explicit Equation 3.25 of Chapter 3 to calculate the seismic demand. We have calculated the conditional median

damage conditioned on S_a and its dispersion in that equation from Equations 4.6 and 4.2 (Section 4.3.5) respectively. The seismic demand results from this simplified approach match very closely those from rigorous numerical integration of Equation 4.21 (Figure 4.25).

We find that the demand calculation for the weighted-average spectral acceleration is "economical" compared to that based on the conventional first-mode spectral acceleration. This demand calculation needs additionally, however, structure-specific seismic hazard calculations for the site. We observe that the demand calculations from the weighted-average spectral acceleration do not match perfectly those from the first-mode spectral acceleration. In Chapter 5 we will explain these differences and show why the former is preferable to the latter.

Chapter 5

Probabilistic Seismic Demand Analysis: Based on Vector of Parameters

5.1 Introduction

We have seen in Table 3.7 and Table 4.4 that in addition to the first-mode spectral acceleration nonlinear seismic building responses may be somewhat dependent on other parameters, such as, high-frequency spectral acceleration. In probabilistic demand hazard calculations we have considered only the dependence on the first-mode spectral acceleration. Because the nonlinear response calculations are expensive from a computational point of view, especially for tall buildings, we should consider these additional parameters in demand calculations in order to reduce the number of nonlinear analyses. Compare, for example, the required number of records in the last column of Table 4.4. Besides our aim to reduce the number of analyses or improve the "efficiency" of seismic demand prediction, we need to consider whether the additional dependencies improve the accuracy of demand prediction, i.e., reduce the bias (see Bazzurro, 1998). Structural engineers also believe from the observed damage patterns that the response of structures is dependent on magnitude and duration,

the higher response being associated with higher magnitude and longer duration. We have observed so far only a mild dependency of responses on these additional parameters[1]. It is possible that a stronger dependency of response may exists for some other structures, for some other damage measures, or for improved representation of structures by more realistic modeling (see Gupta and Krawinkler, 1998, for a description of improved modeling of the 20-story structure discussed in Chapter 4). Hence in this chapter we will describe procedures for probabilistic demand calculations of structures for responses dependent on the following four parameters: magnitude, distance, spectral acceleration at higher frequencies, and duration, *in addition to the first-mode spectral acceleration.*

In this chapter we will demonstrate a procedure for demand-hazard calculations when we include the first-mode spectral acceleration and one of the above mentioned four parameters in those calculations. These calculations require 2-D hazard results which we can generate in some cases from the conventional hazard results and in the other cases we require a separate 2-D hazard calculations. We will demonstrate how we can calculate the 2-D demand hazard of a structure when we consider the first-mode spectral acceleration and an additional parameter in those calculations. If we find any statistically significantly different demand-hazard results by including the additional parameter from the results in the previous chapters without that parameter, we will investigate further to explain those differences.

5.2 General Formulation

We will introduce here a general procedure for demand calculations when a damage measure depends on a vector of parameters. We have calculated in the previous chapters

[1]Sewell (1987) did not observe any significant magnitude and duration dependency of nonlinear SDOF responses. In 1993, he, however, observed dependency of SDOF responses on response duration (we have defined this duration measure in Footnote 11 of Chapter 3). Bazzurro and Cornell (1994) also did not observe any magnitude dependency of displacement response for a jacket-type offshore-platform MDOF structure. Note that all these observations were made via the indirect method of calculation (see Section 2.7 for a description of this method). In the direct method we have, however, observed dependency of some damage measures, notably NHE, on the bin parameters (see sections 2.6, 3.5.1, and 4.3.2; Shome and Cornell, 1998).

the seismic demand hazard based on a scalar parameter that we have usually taken as spectral acceleration at the first-mode frequency, or at a frequency close to the first-mode frequency. When a damage measure Y depends on a vector of parameters, $\boldsymbol{X}$, then the mean annual frequency[2] of exceedance of the damage measure Y of level y can be written from Equation 3.19 as follows:

$$\lambda_{Y>y} = \int\int G_{Y|\boldsymbol{X}}(y|\boldsymbol{x}) \cdot \lambda_{\boldsymbol{X}}(\boldsymbol{x})\, d\boldsymbol{x} \tag{5.2}$$

where

$G_{Y|\boldsymbol{X}}(y|\boldsymbol{x})$ is the complementary cumulative distribution function of Y conditioned on the vector of parameters $\boldsymbol{X}$. We have already found that the distribution of Y conditioned on the first-mode spectral acceleration is lognormal[3]. We shall continue to assume here that lognormality also holds for the conditional distribution of Y when conditioned on several independent variables. The distribution parameters can be calculated from the regression results of a damage measure Y against a vector of parameters, $\boldsymbol{X}$ (see, e.g., Table 4.4).

$\lambda_{\boldsymbol{X}}(\boldsymbol{x})$ is the joint-mean-rate (or frequency) density of events for which $\boldsymbol{X} = \boldsymbol{x}$.

For most practical purposes we can consider only two parameters in demand calculations. We have found in Tables 3.7 and 4.4 that the variability of any damage measure is explained mainly by the elastic first-mode spectral acceleration. Hence we shall consider only one parameter in addition to the first-mode spectral acceleration to calculate the seismic demand ($\boldsymbol{X} = S_{a1}, X_1$). This additional parameter (X_1) can be, for example, magnitude, distance,

[2] Note that for all practical purposes the annual frequency of exceedance is same as the probability of exceedance at least once a year, which we have calculated before in the PSHA calculations. We have assumed in the PSHA calculations that the arrival of earthquakes is a Poisson process. Hence the probability of exceeding a level y of damage Y at least once in a unit time interval (usually one year) for a mean rate of exceedance λ can be calculated as follows:

$$\begin{aligned} P(Y>y) &= 1 - e^{\lambda_{Y>y}} \\ &\approx \lambda_{Y>y} \quad \text{at low values of } \lambda_{Y>y} \end{aligned} \tag{5.1}$$

[3] This assumption is verified in Appendix C.

duration, or spectral acceleration at a higher frequency.

This procedure requires results from 2-D or "vector"-valued PSHA to get the information on $\lambda_{S_{a1},X_1}(s_{a1},x_1)$. When presented in a discretized form, this 2-D PSHA is the joint annual probability (strictly the mean-annual frequency; see Footnote 2) that the first-mode spectral acceleration and the additional parameter equal specific levels at a site (e.g., $S_{a1} = s_{a1}$ and $X_1 = x_1$). Below when we will explain the procedure for demand-hazard calculation for each of the additional parameter X_1, we will describe the procedure for the calculation of the joint mean-annual-frequency function, $\lambda_{S_{a1},X_1}(s_{a1},x_1)$, for those additional parameters. Figures 5.1 and 5.2 show several joint mean rate mass functions ($\tilde{\lambda}_{S_{a1},X_1}$) for two S_{a1} cases ($f_1 = 1Hz$ for the 5-story building and $f_1 = 0.25Hz$ for the 20-story building) for a central Los Angeles site. We observe in Figure 5.2 that three of the four functions are quite smooth, a property we will exploit in what follows. The fourth and also the function in Figure 5.1 (the $\tilde{\lambda}_{S_{a1},S_{a2}}$) expectedly display strong positive correlation between S_{a1} and S_{a2}. Instead of working with S_{a1} and S_{a2}, below we choose to work with S_{a1} and the ratio $Z = S_{a2}/S_{a1}$. This spectral shape measure has weaker correlation and we will exploit this to simplify the 2-D demand-hazard calculations. Note that the limits of the various M, R, D, and S_a intervals of the mass functions in Figures 5.1 and 5.2 are indicated by the corresponding lines. We have used fine intervals for joint mean rate-mass function of S_{a1} and S_{a2} [as indicated in Figures 5.1 and 5.2(d)] because of their strong correlation, but in other cases we have used wider intervals as in Figure 5.2(a)-(c) because the joint mean rate mass functions do not change significantly with small change of those parameters. The calculation of seismic demand from the coupling of 2-D PSHA and 2-D demand analysis (i.e., $G_{Y|S_{a1},X_1}$) can be called *2-D probabilistic seismic demand analysis* (2-D PSDA).

5.3 Additional Magnitude or Distance Dependency

5.3.1 2-D Demand-Hazard Computation

We have seen in Tables 3.7 and 4.4 that *in addition to being dependent on the first-mode spectral acceleration*, the response of the 5-story structure is dependent on the magnitude

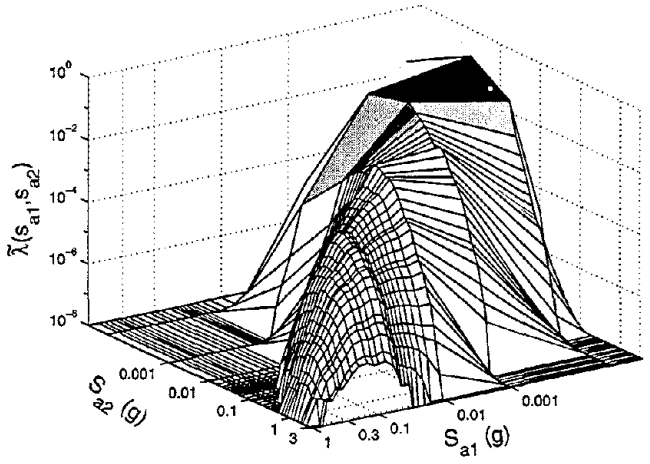

Figure 5.1: Mean rate mass of events, $\tilde{\lambda}_{[S_{a1},S_{a2}]}(s_{a1},s_{a2})$, for $S_a(1.0Hz,5\%) = s_a$ and $S_{a2}(2.67Hz,5\%) = s_{a2}$ at a central Los Angeles site.

and distance of events, whereas that of the 20-story structure is dependent only on distance. As mentioned in Section 4.3.2, the distance dependency of response that we have seen in Chapters 3 and 4 represents, somewhat, the magnitude dependency (as explained in Chapter 4 for the 20-story building the independence of response on magnitude may be misleading because of preselection of low-magnitude records based on low-corner frequency). We will demonstrate here how we can incorporate the distance parameter in demand calculations for the sake of completeness. Although these dependencies are formally statistically significant for some damage measures, Figures 3.10 and 4.15 suggest that the median predicted by the additional magnitude or distance parameter (for the site-specific range of the parameters) is not substantially different from the median predicted by only S_a. We will investigate whether these statistically significantly different results make any change in probabilistic seismic-demand estimations.

When the additional parameter is magnitude and distance, the joint mean rate density, $\lambda_{\dot{S}_a,\boldsymbol{X}}(s_a,\boldsymbol{x})$, is obtained *directly* from conventional disaggregation of seismic hazard results (see Bazzurro, 1998; Bazzurro and Cornell, 1999). The disaggregation results give us the conditional probability mass function of M and R given S_a. This mass function at the i^{th} magnitude range m_i and j^{th} distance range r_j given S_a is denoted here as $p_{m_i,r_j|S_a}(\cdot)$.

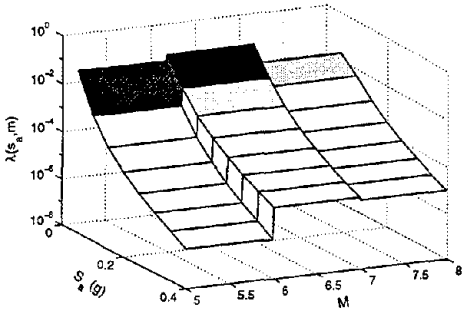

(a) Mean rate of events, $\tilde{\lambda}_{[Sa,M]}(s_a, m)$

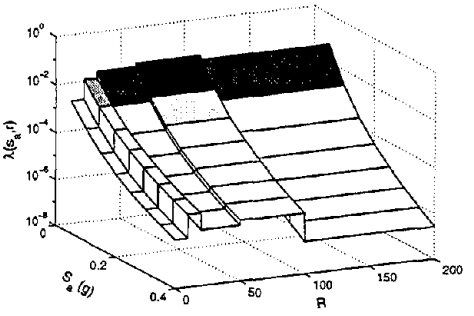

(b) Mean rate of events, $\tilde{\lambda}_{[Sa,R]}(s_a, r)$

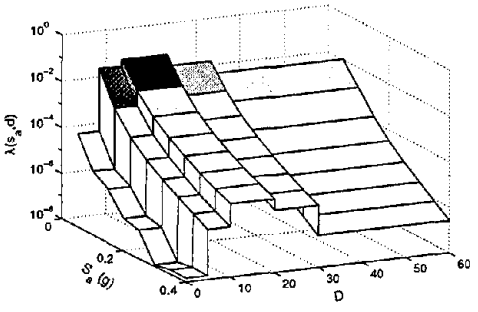

(c) Mean rate of events, $\tilde{\lambda}_{[Sa,D]}(s_a, d)$

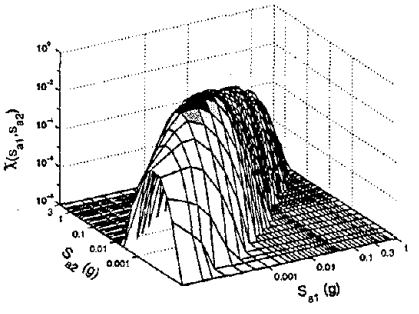

(d) Mean rate of events, $\tilde{\lambda}_{[S_{a1},S_{a2}]}(s_{a1}, s_{a2})$

Figure 5.2: Mean rate mass of events, $\tilde{\lambda}_{[Sa,X_1]}(s_a, x_1)$, for $S_a(0.25Hz, 5\%) = s_a$ and $X_1 = x_1$ at a central Los Angeles site. The additional parameter (X_1) is magnitude (M), or distance (R), or duration (D), or spectral acceleration at a higher frequency [$S_{a2}(0.67Hz, 5\%)$].

Hence the joint mean rate mass function of m_i and r_j at the k^{th} spectral acceleration range $\Delta s_{a,k}$ can be calculated from the following:

$$\tilde{\lambda}_{M,R,S_a}(m_i, r_j, s_{a,k}) = p_{m_i,r_j|S_a}(m_i, r_j|s_{a,k}) \cdot \lambda_{S_a}(s_{a,k}) \cdot \Delta s_{a,k} \tag{5.3}$$

Hence the additional vector of parameters is $\boldsymbol{X} = [M, R]$, then Equation 5.2 becomes

$$\lambda_{Y>y} = \int \sum_{i=1}^{N_M} \sum_{j=1}^{N_R} G_{[Y|S_a,M,R]}(y|s_a, m_i, r_j) \cdot p_{[m_i,r_j|S_a]}(m_i, r_j|s_a) \cdot \lambda_{S_a}(s_a)\, ds_a \tag{5.4}$$

where N_M is the number of magnitude ranges used in the discrete representation, m_i is the average magnitude at the i^{th} magnitude range, N_R is the number of distance ranges,and r_j is the average distance at the j^{th} distance range. We use this discrete (rather than continuous) representation of M and R because (in contrast to S_a) the conditional sensitivity to M and R is mild. Therefore in practice only a very small number (three to five) of ranges is necessary. This is emphasized by the discrete representation here. (In any case in the numerical integration, computations are discrete.)

The conditional joint PMF of M and R conditioned on S_a for a central Los Angeles site is obtained from the disaggregation of the seismic hazard results. The joint PMF at the 0.05g, 0.15g, and 0.25g spectral acceleration levels (of the 0.25Hz-frequency S_a at 5% damping) are shown in Figure 5.3. We observe that the contribution of the high-magnitude events is high at the higher spectral acceleration levels, whereas the contribution of the low magnitude events is high at the low spectral acceleration levels. The converse is true for R. The plot displays, too, the relatively high concentration of high-magnitude seismicity from a distance of 50-100km representing the San Andreas fault. See Bazzurro (1998) for a further discussion of this site.

If the response of a structure conditionally depends only on earthquake magnitude, then Equation 5.4 simplifies as follows:

$$\lambda_{Y>y} = \int \sum_{i=1}^{N_M} G_{[Y|S_a,M]}(y|s_a, m_i) \cdot p_{[M|S_a]}(m_i|s_a) \cdot \lambda_{S_a}(s_a)\, ds_a \tag{5.5}$$

where the conditional PMF of M at any spectral acceleration level, $p_{[M|S_a]}(m_i|s_{a,j})$, at a particular magnitude range (m_i) and spectral acceleration ($s_{a,j}$) is $\sum_k p_{[M,R|S_a]}(m_i, r_k|s_{a,j})$. The conditional PMFs at different spectral acceleration levels are shown in Figure 5.4. Note that when we observe, in contrast, only (conditional) distance dependency, we need to calculate the conditional PMF of R conditioned on the spectral acceleration, $p_{[R|S_a]}(r_i|s_{a,j})$. This also can be calculated from the results shown in Figure 5.3 by adding the PMFs for all the three different magnitude ranges at a particular distance range, r_i, and spectral acceleration, $s_{a,j}$. We show these results in Figure 5.4. Note again the changing role of larger and smaller distances and magnitudes as S_{a1} grows. The smoothness of these functions (coupled with the comparatively weak conditional dependence of the response) explains why the coarse discretization of M and R is still accurate.

We can always compute Equation 5.5 by numerical integration. A closed-form estimate of the above equation can be obtained exploiting the smoothness of $p_{M|S_a}$ as a function of S_a. We assume that $p_{M|S_a}(m_i|s_a)$ is a constant, *independent* of S_a, in the range of S_a where the integrand in Equation 5.5 is significant. This range is centered on $s_{ay,i}$, defined below, which is roughly the S_a value "most likely" to cause damage level y if the magnitude is level m_i. Then we get the following:

$$\lambda_{Y>y} = \sum_{i=1}^{N_M} p_{[M|S_a]}(m_i|s_a) \int G_{[Y|S_a,M]}(y|s_a, m_i) \cdot \lambda_{S_a}(s_a) ds_a \tag{5.6}$$

$$= \left[\sum_{i=1}^{N_M} p_{[M|S_a]}(m_i|s_{a,i} = s_{ay,i}) \cdot H(s_{ay,i})\right] \cdot e^{\frac{1}{2}\left[\frac{K_1 \cdot \sigma_{(\ln Y|S_a,M)}}{\beta_1}\right]^2} \tag{5.7}$$

where

$s_{ay,i}$ = spectral acceleration required to induce a median damage $\hat{y} = y$ in a structure at magnitude m_i.

$= [y/(\alpha e^{\beta_2 \cdot m_i})]^{\frac{1}{\beta_1}}$.

Note that we have adopted the demand-prediction regression model from Equation 3.2, which is of the form $Y = \alpha \cdot S_{a1}^{\beta_1} \cdot e^{\beta_2 \cdot M} \cdot \varepsilon$, implying $\hat{y} = \alpha \cdot S_{a1}^{\beta_1} \cdot e^{\beta_2 \cdot M}$. Then $s_{ay,i}$ is

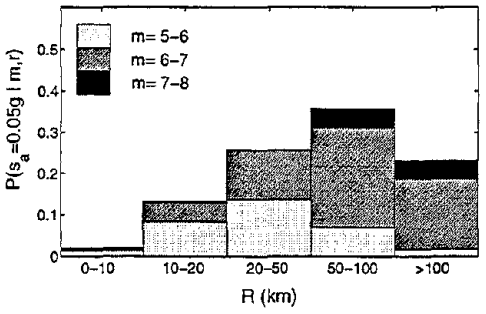

(a) $S_a = 0.05$g

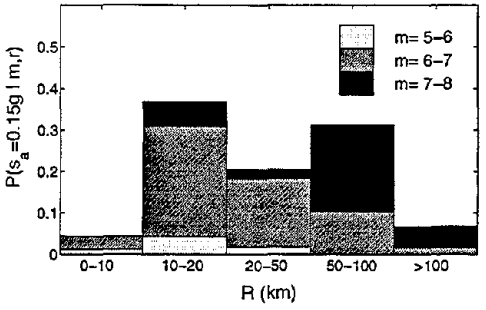

(b) $S_a = 0.15$g

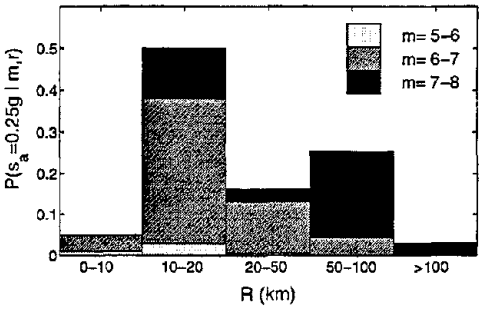

(c) $S_a = 0.25$g

Figure 5.3: Joint probability mass function of magnitude and distance conditioned on spectral acceleration, $p_{[M,R|S_a]}(m_i, r_j|s_a)$, at three different spectral acceleration levels for a central Los Angeles site. Note that the spectral accelerations are calculated at the 0.25Hz frequency and 5% damping.

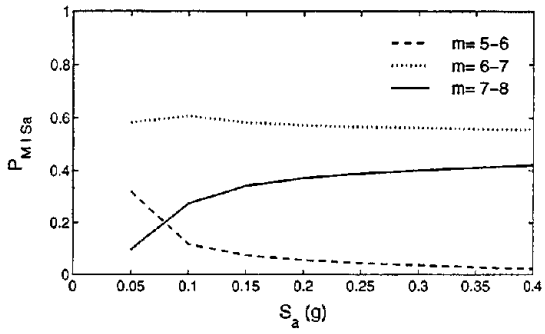

(a) Conditional probability mass function of magnitude, $p_{[M|S_{a1}]}(m_i|s_{a1})$

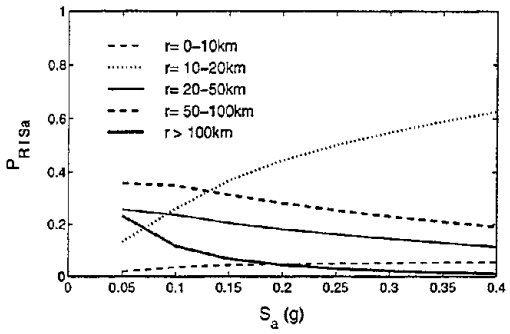

(b) Conditional probability mass function of distance, $p_{[R|S_{a1}]}(r_i|s_{a1})$

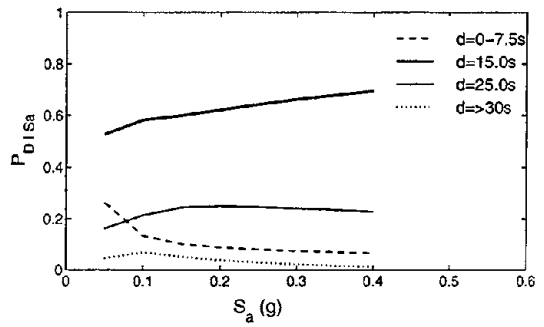

(c) Conditional probability mass function of duration, $p_{[D|S_{a1}]}(d_i|s_{a1})$

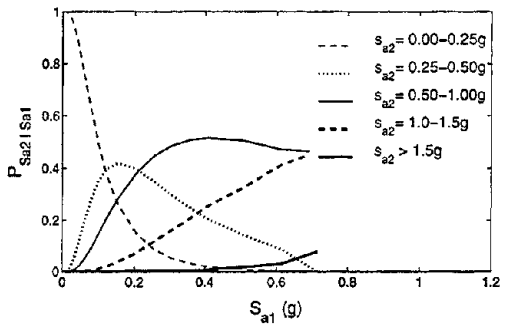

(d) Conditional probability mass function of S_{a2}, $p_{[S_{a2}|S_{a1}]}(s_{a,2}|s_{a,1})$

Figure 5.4: Conditional probability mass functions as a function of S_a for a central Los Angeles site. Note that the spectral accelerations are calculated at the 0.25Hz frequency and 5% damping.

simply the inverse of this function for $M = m_i$ and $\hat{y} = y$ In this case the complementary cumulative lognormal distribution of a damage measure Y conditioned on S_a and M can be calculated from the following:

$$G_{[Y|S_a,M]}(y \mid s_a, m_i) = \Phi^C \left[\frac{\ln(y/(\alpha \cdot s_a^{\beta_1} \cdot e^{\beta_2 \cdot m_i}))}{\sigma_{(\ln Y|S_a,M)}} \right] \tag{5.8}$$

where $\Phi^C(\cdot)$ is the standard normal complementary cumulative distribution function.

As described in Equation 3.23, in order to express the above integration in closed form we have also assumed that in the neighborhood of $s_{ay,i}$, the hazard curve for S_a, $H(s_a)$, can be represented by a power function, $K_0 \cdot s_a^{-K_1}$. We point out that (within the usual approximation of Footnote 2) $\lambda(s_a) = |dH(s_a)/ds_a|$. Equation 5.7 says that, computationally, for a damage level y, one finds the N_M (which is three here) "likely levels" of S_a for the N_M magnitude levels, finds for each the product of the hazard curve, $H(s_a)$, finds something like a weight, $p_{M|S_a}$, sums all the products, and multiplies the sum by the exponential term in Equation 5.7 which reflects the increment of probability of exceedance due to the variability of response, $\sigma_{(\ln Y|S_a,M)}$. Similarly we can calculate the demand of a structure when structural responses are dependent on the distance of events.

We can use the above equation directly to calculate the demand of the 5-story building in Chapter 3, or that of the 20-story building in Chapter 4, at least at the lower demand levels, e.g., the immediate-occupancy level in FEMA-273. Let us consider, for illustration, the 20-story building at a central Los Angeles site. We want to calculate the mean annual frequency of exceedance of 2.5% maximum story drift (life safety allowable drift of FEMA-273). We get the conditional probability mass function $p_{[M|S_a]}(m_i|s_{ay,i})$ at the required spectral acceleration, $s_{ay,i}$, from Figure 5.4. We observe in Figure 5.4 that the conditional distribution is fairly constant over a wide range of spectral accelerations at high intensity levels. Hence the assumption of independence of $p_{[M|S_a]}(m_i|s_a)$ on S_a is justified. The calculation of the probability of exceedance of 2.5% maximum story drift as per Equation 5.7 is given below:

$s_{ay,m=5.5} = [0.025/(0.28e^{-0.08\times5.5})]^{\frac{1}{0.95}} = 0.13$g (The regression coefficients α

and β are obtained from Table 4.4.)

$s_{ay,m=6.5} = 0.14g$

$s_{ay,m=7.5} = 0.15g$

(Note the mild sensitivity to M. We have observed in Table 4.4 that conditioned on S_a the dependence of story drift of the 20-story structure on M is mild. Therefore we observe that the spectral acceleration required to induce a certain drift in the structure is mildly dependent on M.)

$p_{[M|S_a]}(m = 5.5|s_{ay} = 0.13) = 0.09$ (see Figure 5.4).

$p_{[M|S_a]}(m = 6.5|s_{ay} = 0.14) = 0.59$; $p_{[M|S_a]}(m = 7.5|s_{ay} = 0.15) = 0.34$

(Note that $\sum p_{[M|S_a]}(m_i|s_{ay,i}) \neq 1$ exactly)

Correction factor, $C_f = e^{\frac{1}{2}\left(\frac{K_1 \cdot \sigma_{(\ln Y|Sa,M)}}{\beta_1}\right)^2}$

$= e^{\frac{1}{2}\left(\frac{2.1 \times 0.44}{0.95}\right)^2} = 1.62$

$\lambda_{D_{st}>2.5\%} = 1.62 \times [0.09 \times 2.122(10^{-3}) + 0.59 \times 1.815(10^{-3}) +$

$0.34 \times 1.569(10^{-3})] = 2.9(10^{-3})$

In Chapter 4 we calculated seismic demand based on only S_{a1} from Equation 3.30, and this gave $\lambda_{D_{st}>2.5\%} = 3.2(10^{-3})$. Note that the numerical integration of Equation 5.5 by considering the variation of $p_{M|S_a}$ with spectral acceleration improves the results insignificantly $[\lambda_{D_{st}>2.5\%} = 3.1(10^{-3})]$. The difference between this result and the previous approximate solution is due to the assumption of independence of $p_{M|S_a}$ on S_a in the latter solution. We observe in Figure 5.4 that this approximation is not very appropriate for low- and high-magnitude events at the spectral acceleration required for 2.5% drift (i.e., around 0.14g); this explains the difference between the numerical integration results and the results from the closed-form approximation. As we expected, demand calculations based on regression results for S_{a1} and M do not significantly change from the results based on regression results for S_{a1} only. We make this observation because magnitude dependency of response of this structure is not statistically significant. (Note, however, the reservations and discussions in Section 4.3.2 associated with the subset of smaller-magnitude records with adequate signal-to-noise ratios in the 0.25Hz frequency range.)

We can similarly calculate the seismic demand of a structure if the response conditioned on S_{a1} is dependent on the distance of the events. Recall that the maximum story drift is statistically significantly dependent on the distance (R) of events (see Table 4.4). The probability of exceedance of 2.5% story drift obtained by numerical integration of the 2-D PSDA equation is $2.2(10^{-3})$. This is somewhat different from $3.2(10^{-3})$, that we obtained by 1-D PSDA in Chapter 4. So although we have observed in Figure 4.15 that R does not change the median drift prediction substantially, we get a quite different drift-demand result when we additionally include R in demand calculations. We will find in Section 5.5.2 that the difference may be due to the inconsistency in the distribution of R in data and those predicted by PSHA at the site. We will first verify whether this difference in demand-hazard results is statistically significant. The drift-demand-hazard results at 2.5% drift by including the additional parameter M or R in demand-hazard calculations are given in Table 5.1. We have calculated similarly the demand-hazard results for the 5-story building at different interstory drift levels. The results are also given in Table 5.1. Note that we can use this approach in seismic demand-hazard calculations of any structure if the structure shows significant M or R dependency of response (conditioned on S_a) when the likelihood of "collapse" of a structure is not significant at the target demand level.

5.3.2 2-D Demand Calculation When the Likelihood of Collapse of Structures is Significant

For the 20-story building we have observed that at the high damage levels, e.g., the collapse prevention performance level in FEMA-273, the difference between the demand-hazard results and the results conditioned on no collapse is significant (see Figure 4.23). So we have to consider additionally the likelihood of "collapse" of structures in Equation 5.5. This means that the closed-form approximation in Equation 5.7 is no longer valid for this structure at high demands. If the likelihood of collapse of structures is significant, then as per Equation 4.21 the mean frequency of exceedance of damage Y of a level y when the

Parameters	Drift of the 5-story Building		Drift of the 20-story Building	
	2.5%	5%	2.5%	5%
S_{a1}	440	4500	320	2700
	–	–	–	(2800*)
S_{a1}, M	380	3850	320	2500*
S_{a1}, R	280	2750	450	2900*
S_{a1}, T	430	4640	332	2580*
S_{a1}, S_{a2}	700	10000	690	7700

Table 5.1: Interstory drift demand hazard results by including different parameters in demand-hazard calculations at the 2.5% and 5% drift levels of the 5-story and the 20-story structures at a central Los Angeles site. Here $\star$ indicates that in demand-hazard calculations of the 20-story building we have considered the binary-regression results for the logistic model in Equation 4.10. In other cases we have considered the convenient model in Equation 4.13 for demand-hazard calculations of the 20-story building. Note that these different binary-regression models are important only when the likelihood of collapse of a structure is significant, i.e., in the case of 5% drift level.

damage measure is dependent on magnitude (conditional on S_a) is the following:

$$\begin{aligned}\lambda_{Y>y} &= \sum_{i=1}^{N_M} \int_0^{+\infty} P_{[C|S_a,M]}(s_a, m_i) \cdot p_{[M|S_a]}(m_i|s_a) \cdot \lambda_{S_a}(s_a)\, ds_a + \\ &\quad \sum_{i=1}^{N_M} \int_0^{+\infty} G_{[Y|NC,S_a,M]}(y \mid s_a, m_i) \cdot P_{[NC|S_a,M]}(s_a, m_i) \cdot p_{[M|S_a]}(m_i|s_a) \cdot \\ &\quad \lambda_{S_a}(s_a)\, ds_a \end{aligned} \tag{5.9}$$

where $P_{NC|S_a,M}(\cdot)$ is the probability of no collapse (Equation 4.10), P_C is the probability of collapse which is equal to $1.0 - P_{NC|S_a,M}(\cdot)$, $G_{Y|NC,S_a,M}(\cdot)$ is the complementary cumulative distribution function of any damage measure Y conditioned on S_a and M from the no-collapse results, and the other terms are defined in Equation 5.5.

We get $P_{[NC|S_a,M]}(s_a, m)$ from binary regression results as described in Section 4.3.4. As we mentioned in Section 4.3.4, the convenient model in Equation 4.13 is a discontinuous function. Figure 4.18 reflects the discontinuity: the likelihood function has sharp ridges. The optimization of that function may not converge (unless, of course, the initial condition is close to the right solution) when we include M or R in addition to S_a. Because of this

Explanatory Variable	Regression Function	$L(\alpha, \beta)$
S_{a1}	$logit(P_{NC}) = 14.94 - 54.67S_a$	23.3
S_{a1}, S_{a2}	$logit(P_{NC}) = 13.43 - 46.10S_a - 0.42S_{a2}$	22.7
S_{a1}, M	$logit(P_{NC}) = 22.17 - 56.22S_a - 1.05M$	21.9
S_{a1}, R	$logit(P_{NC}) = 14.55 - 54.33S_a + 0.01R$	23.2
S_{a1}, D	$logit(P_{NC}) = 17.44 - 61.57S_a - 0.05D$	22.8

Table 5.2: Logistic regression results for the probability of no collapse (P_{NC}) from the records scaled to the 0.30g, 0.15g, and 0.05g first-mode spectral accelerations. $L(\alpha, \beta)$ is the optimized log-likelihood value. The regression coefficients of these additional parameters, however, are not statistically significantly different from zero at the 5% significance level. Note that $logit(P_{NC}) = \ln\left[\frac{P_{NC}}{1-P_{NC}}\right]$.

we adopt here in binary regression analysis the logistic model which is continuous at all values of S_a. The contour plot of the log-likelihood function (Equation 4.15) when the independent variables are S_a and M is shown in Figure 5.5 for $\alpha = 22.17$. (The likelihood function for only S_a has already been described in Figure 4.18.) Figure 5.5 also shows the optimized solution of this likelihood function. The binary regression results against S_a and an additional parameter (M or R) for the logistic regression model are shown in Table 5.2. Because the log-likelihood ratio (LLR) given by Equation 4.19 is less than $\chi^2_{0.05,1} = 3.84$, the conditional dependence of $P_{NC}(.)$ on M or R is not statistically significant at the 5%-significance level. The variation of $P_{NC}(.)$ with S_a and an additional variable, M or R is shown in Figure 5.6. This figure shows that the decrease in $P_{NC}(.)$ is more significant with M than with R (also compare the optimized log-likelihood value in Table 5.2). Below we will determine the effect of these additional parameters in demand hazard calculations.

We solve Equation 5.9 by numerical integration. The solution of the equation for the mean frequency of exceedance of 5% maximum story drift based on S_{a1} and M is found to be 4.0×10^{-4} (or 2500-year return period) and that based on S_{a1} and R is 3.4×10^{-4} (or 2900-year return period). Compare these numbers with 3.6×10^{-4} (or 2800-year return period) that we get based on S_{a1} only. (Note that the latter result is different from the 2700-year return period, we obtained in Chapter 4, as we have used here a different binary-regression

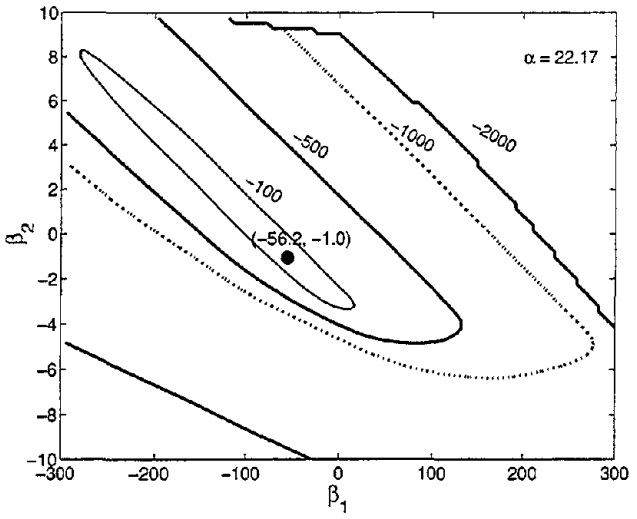

Figure 5.5: Contour of two dimensions of the 3-D log-likelihood function (Equation 4.15) of the logistic regression model for the scaled results of the 20-story building. The explanatory variables are S_a and M. The α value used in this plot is the optimized value from logistic regression analysis. Here the symbol • indicates the optimized solution of β_1 and β_2.

model.) See Table 5.1 for a comparison of drift-demand-hazard results by including different parameters in the calculation. See Figure 5.7(b) for story drift demands at various levels. We observe that as the story drift demand conditioned on no collapse and the probability of no collapse (P_{NC}) are not statistically significantly dependent on magnitude, we do not observe any significant difference between these results and those of the demand-hazard calculations based on S_a only. Conversely, when we calculate the seismic-demand hazard based on S_a and R, we observe a difference in results at the low drift-demand levels. Recall that the story drift conditioned on no collapse is statistically significantly dependent on R, but P_{NC} does not depend on R.[4] This explains, perhaps, why the difference between the 1-D and 2-D demand results is lower at high drifts.

We also calculated the seismic drift demand hazard of the 5-story building in Chapter 3 and these results are shown in Figure 5.7(a). Drift-demand-hazard results at two different levels are also given in Table 5.1 by including different parameters in the calculation. In

[4]We explained in Chapter 4 that because the available data have long-distance records only for the high-magnitude events, the R dependency of the response somewhat represents the magnitude dependency.

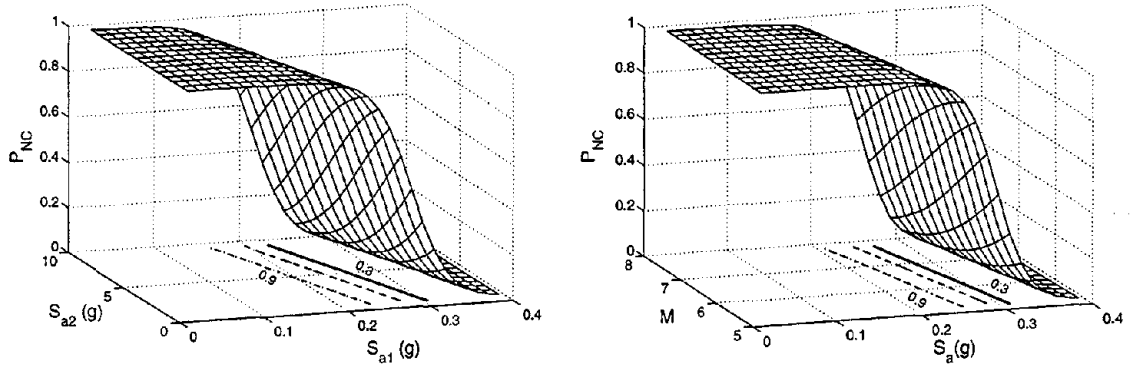

(a) $X_1 = S_{a2}$

(b) $X_1 = M$

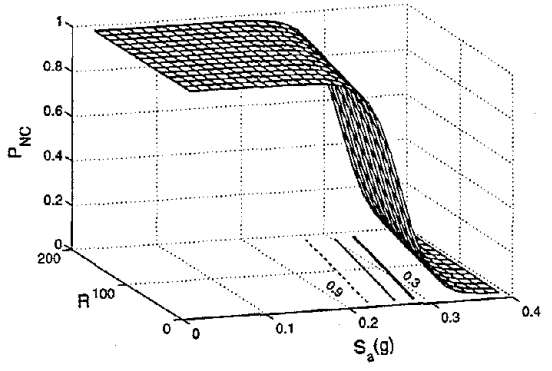

(c) $X_1 = R$

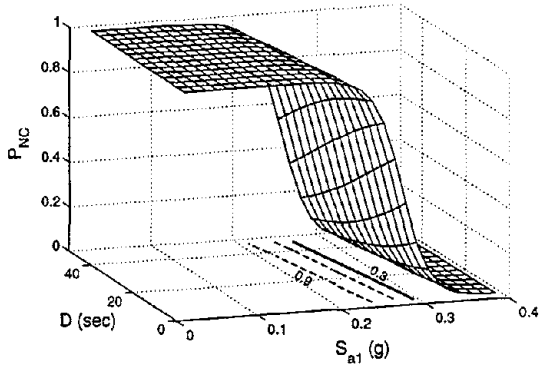

(d) $X_1 = D$

Figure 5.6: Variation of $P_{NC}(.)$ from logistic regression analysis with S_a and an additional parameter (X_1). Note that although we observe here that $P_{NC}(.)$ changes with the additional parameters, the prediction based only on S_a is not statistically significantly different.

this case, although the conditional story drift results (conditioned on S_a) are statistically significantly dependent on M or R, we do not find any practical difference in demand results based on S_a only. As Figures 3.10 and 4.15 showed, these additional parameters, M or R, do not change the median-damage prediction substantially. We will verify below whether this difference in results is statistically significantly different. If we find this difference is significant, then we will investigate further to explain this difference.

5.3.3 Verification of Difference in Demand Results from 1-D and 2-D PSDA

We have seen that the demand results for the 20-story building based on S_a and R appear to be different from the results based on S_a only. We need to verify whether this difference is due to limited sample size or is due to the seismological parameter R. This can be done by bootstrap replication of the seismic demand results. We calculate seismic demands based only on S_a (1-D PSDA) and based jointly on S_a and R (2-D PSDA) from the replicated bootstrap samples. The estimation of the mean and its one-sigma confidence band for the 20-story building are shown in Figure 5.8. We observe that the results from the 1-D and the 2-D PSDA are not statistically significantly different. Hence although the conditional responses (conditioned on S_a) are statistically significantly dependent on R, we do not get any difference in demand results that are based on these additional parameters. This is because this parameter does not substantially change the median drift prediction although the dependence of drift on R is statistically significant (see Figures 3.10 and 4.15). The observed difference may be due to the difference in the conditional distribution of distance, $f_{R|S_a}(r|s_a)$, between the data and the site. We will discuss this issue in detail in Section 5.5.2.

5.4 Additional Duration Dependency

We have seen in Table 3.7 that, given S_{a1}, the energy-based damage measure, NHE, is

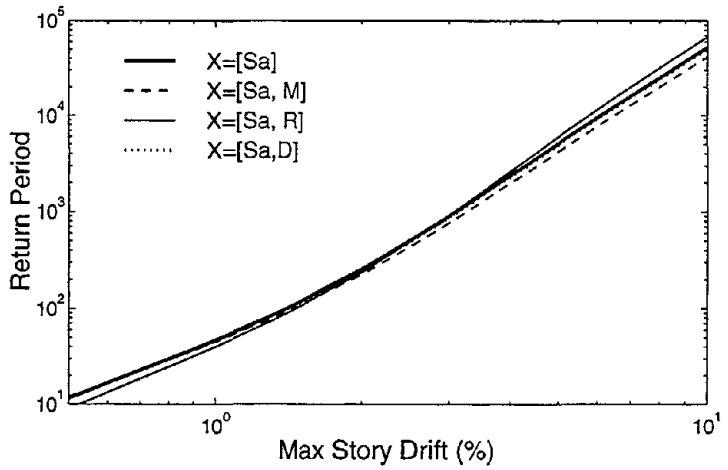

(a) 5-story SMRF

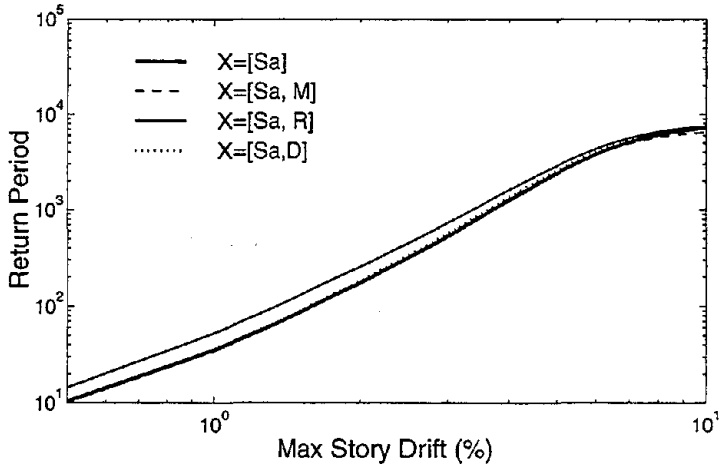

(b) 20-story SMRF

Figure 5.7: Variation of seismic drift demand hazards from 2-D PSDA when we consider different independent variables (X_1) in addition to S_{a1} in demand calculations for different buildings at a central Los Angeles site.

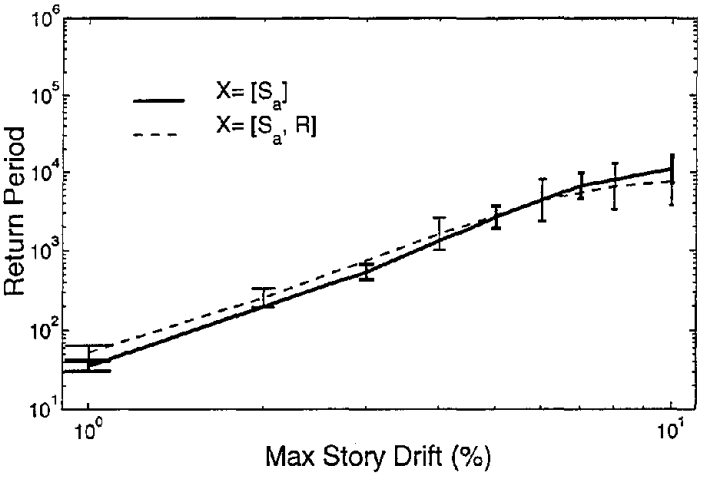

Figure 5.8: Story-drift demands from the 1-D (based on S_a) and from the 2-D (based on S_a and R) PSDA for a 20-story building at a central Los Angeles site. These results are obtained from bootstrap replication of the response results.

statistically significantly dependent on the duration (Trifunac and Brady, 1975) of ground-motion records. The mean frequency of exceedance of any damage measure Y of a level y can be calculated from Equation 5.2 as given in the following equation when the damage measures are dependent on duration (in addition to S_{a1}). The resulting expression is

$$\lambda_{Y>y} = \int\int G_{Y|S_a,D}(y|s_a,d)\cdot\lambda_{S_a,D}(s_a,d)\,ds_a\,dd \tag{5.10}$$

$$= \int\int G_{Y|S_a,D}(y|s_a,d)\cdot f_{D|S_a}(d|s_a)\cdot\lambda_{S_a,D}(s_a,d)\,ds_a\,dd \tag{5.11}$$

$$= \sum_i \int G_{Y|S_a,D}(y|s_a,d)\cdot p_{D|S_a}(d_i|s_a)\cdot\lambda_{S_a}(s_a)\,ds_a \tag{5.12}$$

where $\lambda_{[S_a,D]}(s_a,d)$ is the mean joint-rate density for $S_a = s_a$ and $D = d$, $p_{D|S_a}(d_i|s_a)$ is the probability mass function of duration D given S_a. The mean joint-rate density can be obtained from the following:

$$\lambda_{S_a,D}(s_a,d) = \int\int P(d \mid s_a,m,r)\cdot f(m,r \mid s_a)\cdot\lambda(s_a)\,dm\,dr \tag{5.13}$$

where $P(d \mid s_a,m,r)$ is the conditional probability that an earthquake of magnitude m

and distance r which generates a spectral acceleration s_a at a site will have duration of records d. This is obtained from the attenuation results of duration of records similar to the conventional spectral acceleration attenuation results (see, for example, Footnote 12 of Chapter 3). $f(m, r \mid s_a)$ is the conditional density of M and R conditioned on S_a. This is obtained from the deaggregation of conventional (1-D) seismic hazard results. It is observed that there is a low correlation between S_a and D (see Footnote 12 of Chapter 3; $\rho_{[S_a(0.25Hz),D]} = 0.27$, $\rho_{[S_a(1.0Hz),D]} = -0.10$). So we can assume, $f(d \mid s_a, m, r) \approx f(d \mid m, r)$. Hence to calculate the joint-rate density from Equation 5.13, we need the disaggregation of seismic hazard results for the calculation of $f(m, r \mid s_a)$ which we needed in the preceding section as well. Here we need *additionally* the attenuation of duration of records with M and R for the calculation of $f(d \mid m, r)$. This result, however, is not well documented in literature. Although Vanmarcke and Lai (1980) have made similar calculations, they adopted a different duration measure, one is not commonly used by structural engineers. We have shown in Equation 3.8 the attenuation results for the duration measure (Trifunac and Brady, 1975) that we have adopted in our study. The mean joint-rate mass function, $\tilde{\lambda}_{[S_a(0.25Hz),D]}(\cdot)$, from Equation 5.13 is shown in Figure 5.2 for a central Los Angeles site. The conditional probability mass function, $p_{D|S_a}(\cdot)$, shown in Figure 5.4, can be used to calculate the joint-rate density as well . We will use the regression results in Table 4.4 to calculate the conditional distribution in Equation 5.12. An equation similar to Equation 5.9 is used here to calculate the demand hazard at high damage levels. We will adopt here the logistic regression model for binary regression analysis due to the advantages described in the previous section. The binary regression results are given in Table 5.2. These binary regression results for P_{NC} against S_a and D are plotted in Figure 5.6. We find that P_{NC} conditioned on S_a is not statistically significantly dependent on D.

The seismic demand hazard results based on this S_a and D regression are shown in Figure 5.7. We find that the drift demand hazard results are virtually the same as the results based on S_a only. This is because the story drift conditioned on no collapse and also the probability of no collapse are not statistically significantly dependent on duration when first conditioned on S_a. We make similar observations for the 5-story building in

Figure 5.7. The results of these regression results are also given in Table 5.1. We can conclude that unless the story drift results are statistically dependent on duration, and the demand prediction, too, is changed substantially by D, we need not to consider this parameter in demand-hazard calculations.

5.5 Additional Dependency on Higher-Frequency Spectral Acceleration

5.5.1 2-D Demand Hazard Computation

For the 2-D demand-hazard calculations, we will calculate the performance of a structure when its responses are dependent on spectral accelerations at higher frequencies in addition to being dependent on the first-mode spectral acceleration. We have seen in Tables 3.7 and 4.4 that responses are statistically significantly dependent on both the first- and the second-mode spectral accelerations. We have seen in Figures 3.10 and 4.15 that only this additional parameter, S_{a2}, substantially changes the prediction of the responses from the prediction based on only S_{a1} (at least when one focuses on pairs of values that are likely to occur together in the records used). We want to incorporate this parameter in demand calculations, because doing so will reduce significantly the number of expensive nonlinear analyses (for example, see the last column in Table 4.4). We can calculate the mean annual frequency of exceedance of the damage variable Y of a level y from Equation 5.2 as follows:

$$\lambda_{Y>y} = \int \int G_{Y|S_{a1},S_{a2}}(y|s_{a1},s_{a2}) \cdot \lambda_{S_{a1},S_{a2}}(s_{a1},s_{a2})\, ds_{a1}\, ds_{a2} \tag{5.14}$$

where, $\lambda_{S_{a1},S_{a2}}(s_{a1},s_{a2})$ is the mean rate density of events for $S_{a1} = s_{a1}$ and $S_{a2} = s_{a2}$. Previously we have obtained the joint rate density $\lambda_{S_{a1},X_1}(\cdot)$ of S_{a1} and the additional parameter X_1 either directly from the disaggregation of seismic hazard results (see Section 5.3) or indirectly from the disaggregation results by assuming negligible correlation between S_{a1} and X_1 (see Section 5.4). It has been observed by Inoue (1990) that, conditional on M and R, there is a correlation between S_{a1} and S_{a2}. This correlation, however, depends on

the difference in frequencies at which those spectral accelerations are calculated: the higher the difference, the lower is the correlation[5]. In this case we need to carry out site-specific seismic hazard calculations *exclusively* for this structure. This joint-rate density can be obtained from the "vector"-valued or 2-D PSHA which is a methodology for for computing joint mean-frequency that spectral accelerations at two different frequencies equal specific levels at a site [e.g., $\lambda[S_{a1}(0.25Hz) = 0.30g, S_{a2}(0.67Hz) = 1.5g] = 0.119 \times (10^{-3})$ for a central Los Angeles site].

The mean annual frequency of two spectral accelerations $S_{a1}(f_1) = s_{a1,i}$ and $S_{a2}(f_2) = s_{a2,j}$ at two different frequencies f_1 and f_2 due to N sources located at different distances, R, from a site and capable of generating events of different magnitudes, M, is the following (see Bazzurro, 1998, for a detailed discussion on the calculation of 2-D PSHA):

$$\lambda_{s_{a1,i},s_{a2,j}} = \sum_{k=1}^{N} \nu_k \left\{ \int\int P(s_{a1,i}, s_{a2,j}|m,r) \cdot f_{M,R}(m,r)\, dm\, dr \right\}_k \tag{5.15}$$

where ν_k is the mean annual rate of occurrence of earthquakes generated by source k, $f_{M,R}(m,r)$ is the joint probability density function of magnitude M and distance R for source k, and $P(s_{a1,i}, s_{a2,j}|m,r)$ is the conditional probability that an earthquake of magnitude m and distance r causes a ground motion at a site of $S_{a1} = s_{a1,i}$ and $S_{a2} = s_{a2,j}$. This probability is obtained using the conventional attenuation results for spectral accelerations S_{a1} and S_{a2} and the correlation coefficients $\rho_{S_{a1},S_{a2}}$ between those spectral accelerations.

The results in this study were obtained by Bazzurro. The 2-D joint mean rate mass function, $\tilde{\lambda}_{[S_{a1},S_{a2}]}$, at a central Los Angeles site for the 5%-damped spectral accelerations at the 0.25Hz and 0.67Hz frequencies is shown in Figure 5.2(d). The correlation coefficient for spectral accelerations at these frequencies is 0.66. The contour plot of $\tilde{\lambda}_{S_{a1},S_{a2}}$ is shown is Figure 5.9(a). We observe that because of strong positive correlation between S_{a1} and

[5]The correlation coefficient ρ between the logarithm of S_{a1} and the logarithm of S_{a2} is estimated from the following equation (Inoue, 1990):

$$\rho_{\ln S_{a1},\ln S_{a2}} = max\{1 - 0.33|\ln \frac{f_2}{f_1}|; 0\}$$

where f_1 and f_2 are the frequencies at which the spectral accelerations S_{a1} and S_{a2} are calculated.

S_{a2}, the peaks of $\tilde{\lambda}_{[S_{a1},S_{a2}]}$ are along a diagonal of the S_{a1}-S_{a2} plane. Thus the fraction of hazard which comes from different S_{a2}'s changes substantially as S_{a1} changes, and this is illustrated in Figure 5.4(d). We observe that at higher S_{a1} the contribution of hazard comes from higher S_{a2}'s because of their positive correlation. Another way to present the same results may be to calculate the ratio of the spectral accelerations ($Z = S_{a2}/S_{a1}$) at each S_{a1}. This result is shown in Figure 5.10. This ratio is a measure of the shape of the response spectra. We observe that because the low-magnitude events contribute significantly at the low-intensity levels, the frequency of the higher Zs is high at these levels. We have shown in Figure 2.1 that the low-magnitude records are richer in high frequency content compared to the high-magnitude records when conditioned on the same S_a at a low frequency (i.e., the low-magnitude records have a higher ratio of spectral accelerations). We observe that the smooth nature of these curves [now like Figure 5.4(a)-(c)] implies that an approximate analytical solution (analogous to Equation 5.7) is now feasible for S_{a1} and Z. See Section 5.5.5 below.

Nonetheless, here we solve Equation 5.14 numerically to calculate the seismic demand of structures. Because we have not considered the likelihood of "collapse" of structures in the equation, this equation is applicable for the 5-story structure in Chapter 3 and also for the 20-structure at the low-demand levels. The probability of exceedance of 2.5% maximum story drift for the 20-story building from Equation 5.14 is 1.4×10^{-3} (or 700-year return period). The demand results at the same drift level from the conventional 1-D PSDA is $\lambda_{[Y \geq 2.5\%]} = 3.1 \times 10^{-3}$ or 320-year return period. Thus the difference in results is about a factor of two. Note that the demand hazard estimations for 1-D PSDA are also carried out numerically to avoid the approximation introduced by calculation of the hazard function from Equation 3.23. We observe significant difference between 1-D and 2-D demand-hazard results for other damage measures as well and also for even the single-frequency dominated 5-story building. We also indicate the demand-hazard results in Table 5.1. We need to verify whether this difference is due to the limited sample size or due to the improvement that we get in the demand results by adding information of the risk associated with S_{a2} conditioned on S_{a1}. Recall that we have observed in Figure 4.15 that the prediction of the

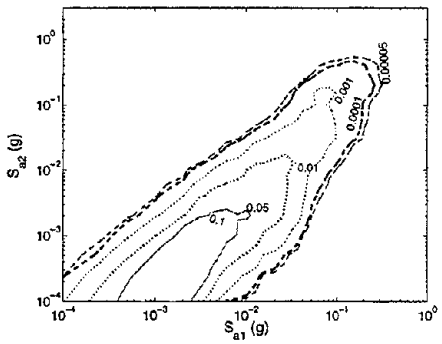

(a) 0.25Hz and 0.67Hz; ρ=0.66

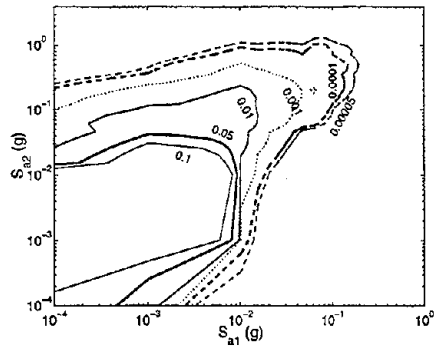

(b) 0.25Hz and 1.33Hz; ρ=0.45

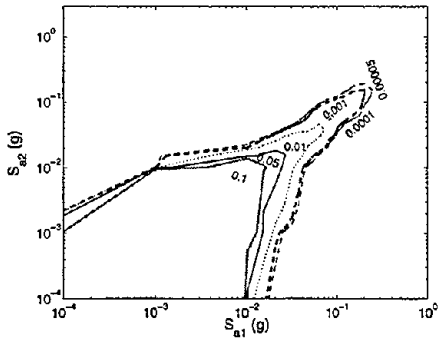

(c) 0.25Hz and 0.20Hz; ρ=0.93

Figure 5.9: Contour plot of the mean frequency rate of events, $\lambda_{S_{a1},S_{a2}}(s_{a1}, s_{a2})$, which is the frequency of events for $S_{a1} = s_{a1}$ and $S_{a2} = s_{a2}$, from the 2-D PSHA results for a central Los Angeles site. Note that the spectral accelerations are calculated at the frequencies indicated in the caption and ρ indicates the correlation coefficient of those spectral accelerations.

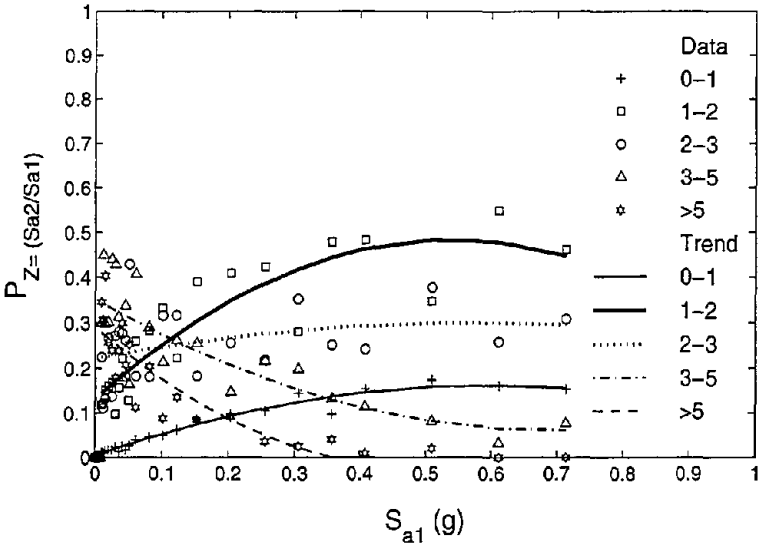

Figure 5.10: Conditional probability mass function of the ratio of spectral accelerations ($Z = S_{a2}/S_{a1}$) as a function of S_{a1} for a central Los Angeles site.

median damage measures changes substantially when based on S_{a1} and S_{a2} pairs that are likely at the site.

5.5.2 Verification of Difference in Demand Results from 1-D and 2-D PSDA

We want to verify that the seismic demands from the 2-D and the 1-D PSDA are statistically significantly different from one another rather than the difference being simply due to the limited sample size of the response data. In order to verify this, as we have done in Section 5.3, we will use a bootstrap resampling technique to generate a number of samples from the original sample of analysis results to calculate the mean (geometric) estimate of the drift demand hazards from the 1-D PSDA and its "one-sigma" confidence band (67% confidence). This calculation is shown in Figure 5.11 for the 5-story and the 20-story buildings. The same calculation from the 2-D PSDA is also shown in the same figure. (We show below the basis for the calculation of demand hazards from 2-D PSDA for the 20-story building at the high demand levels, where the likelihood of collapse is significant).

We focus our attention now only on the low drifts. We observe that in this case the seismic-demand-hazard results from the 2-D PSDA are apparently statistically significantly different from the 1-D PSDA. We observe additionally that the confidence band becomes wider with the increase in demand level. Because of correlation between the 1-D and 2-D estimates, we repeat the resampling to find the statistics of the estimate of the ratio. The mean of the estimator of the ratio of the return periods of drift demand from the 2-D and the 1-D PSDA and its one-sigma confidence band (67%) are shown in Figure 5.12. These results confirm that at low-drift levels the seismic drift demand results from the 2-D and the 1-D PSDA for the 5-story and the 20-story structures are indeed significantly different. We observe that at low drifts ($\leq 4\%$) the ratio of the return periods increases with drift. This trend is similar for both the structures; the 20-story structure, as expected, has a higher ratio, i.e., S_{a2} has a higher contribution to the demand results (e.g., at the 4% drift level the ratio of the return periods from 2-D and 1-D PSDA is 1.8 for the 5-story building, and the same for the 20-story building is 2.8). Next we will investigate in detail why we see this difference in results.

5.5.3 "Modified" 1-D PSDA: "Weighted" Regression Analysis

The difference between the 1-D and the 2-D PSDA results, as pointed out by Bazzurro (1998), is due to the difference in the conditional distribution $G_{Y|S_{a1}}(\cdot)$ which we get from Equations 3.19 and 5.14. We can appreciate this argument if we rewrite Equation 5.14 as follows:

$$\lambda_{Y>y} = \int \underbrace{\left[\int G_{Y|S_{a1},S_{a2}}(y|s_{a1},s_{a2}) \cdot f_{S_{a2}|S_{a1}}(s_{a2}|s_{a1}) ds_{a2}\right]}_{\text{Equal to } G_{Y|S_{a1}}(y|s_{a1}) \text{ in Equation 3.19}} \lambda_{S_{a1}}(s_{a1})\, ds_{a1} \qquad (5.16)$$

where $f_{S_{a2}|S_{a1}}(\cdot)$ is the "site-specific" conditional density function of S_{a2} conditioned on S_{a1}. We get this density function from the 2-D PSHA results. If the (conditional) dependency of response on S_{a2} is mild, then $G_{Y|S_{a1},S_{a2}}(.)$ will be approximately equal to $G_{Y|S_{a1}}(\cdot)$. [In this case, $\int G_{Y|S_{a1},S_{a2}}(y|s_{a1},s_{a2}) \cdot f_{S_{a2}|S_{a1}}(s_{a2}|s_{a1})\, ds_{a2} \approx G_{Y|S_{a1}}(s_{a1}) \int f_{S_{a2}|S_{a1}}(s_{a2}|s_{a1})\, ds_{a2} =$

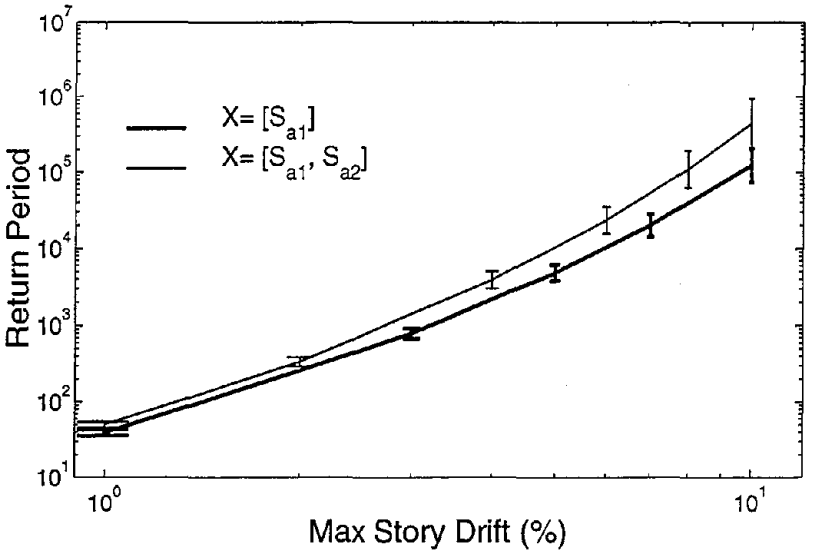

(a) 5-story SMRF building

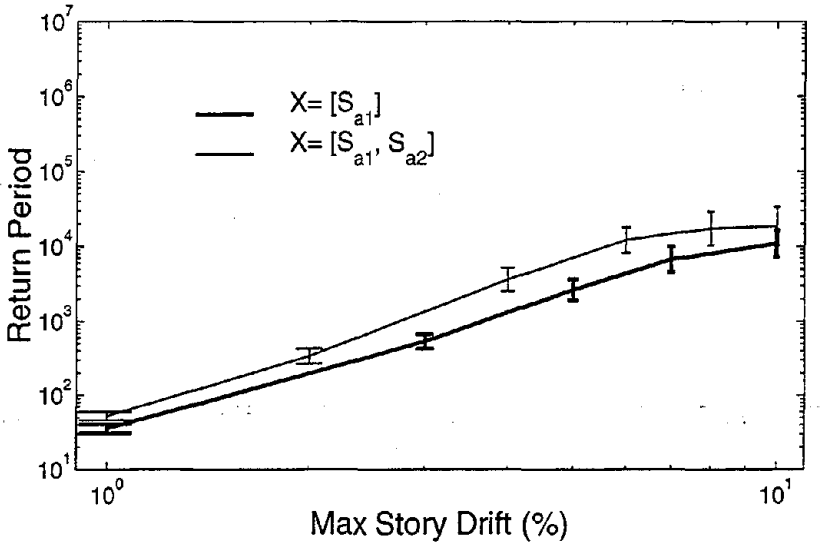

(b) 20-story SMRF building

Figure 5.11: The best estimate of story drift demand hazard and its one-sigma confidence band from the 1-D and the 2-D PSDA for different buildings at a central Los Angeles site. These results are obtained by bootstrap replication of the sample of results. Note that in demand calculations of the 20-story building we have considered the likelihood of collapse of the structure at high intensity levels.

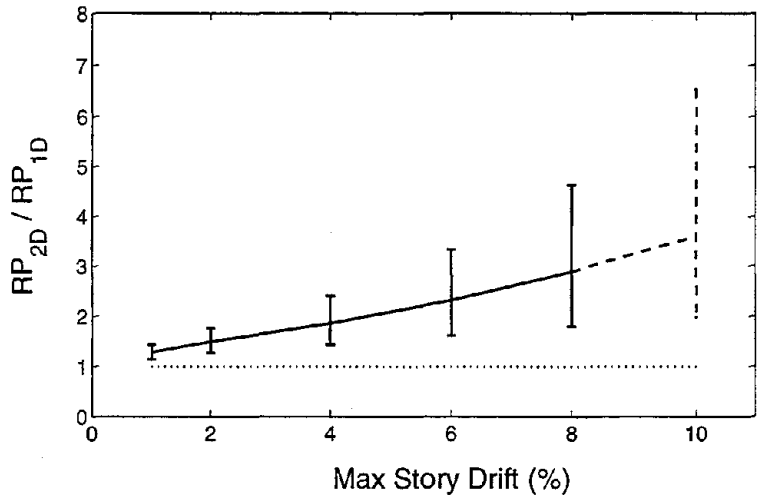

(a) 5-story SMRF building

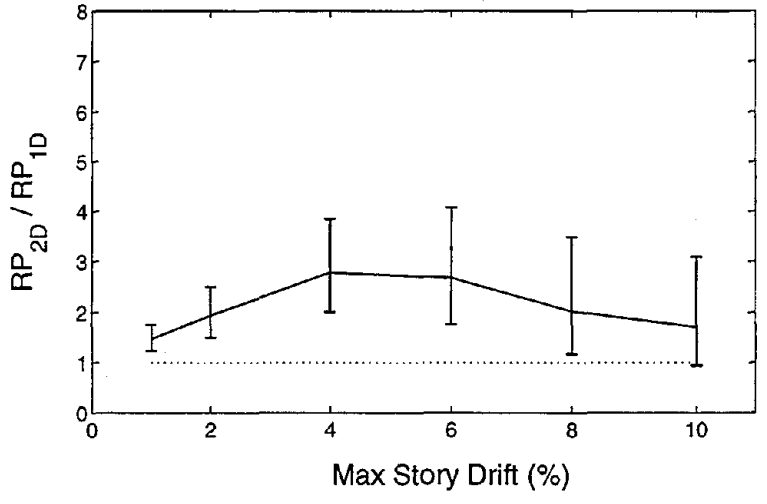

(b) 20-story SMRF building

Figure 5.12: The best estimate of the ratio of the return periods (RP) and its one-sigma confidence band for story-drift demand from the 1-D and the 2-D PSDA for different buildings at a central Los Angeles site. These results are obtained by bootstrap replication of the sample responses. The prediction of the same return periods from the 1-D and 2-D PSDA (i.e., $RP_{2D}/RP_{1D} = 1$) is indicated by the dotted lines. Note that in demand calculations of the 20-story building we have considered the likelihood of collapse of the structure at high intensity levels. The demand hazard results beyond 8% drift of the 5-story building are based on extrapolation of regression results in a large number of cases of bootstrap replications, hence the dashed line.

$G_{Y|S_{a1}}(s_{a1})$ for any $f_{S_{a2}|S_{a1}}$ distribution.] So from Equation 5.16 for 2-D PSDA we get Equation 3.19 for 1-D PSDA. On the other hand, if structural responses are statistically significantly dependent not only on S_{a1} but on the spectral accelerations at higher frequencies as well, then the resulting integrand inside the parenthesis of Equation 5.16, $G_{Y|S_{a1}}(s_{a1})$, may not be equal to what we get from the analysis of the response data via 1-D regression against S_{a1} only. That function will, in this case, depend on the relative frequency of S_{a1}-S_{a2} pairs in the data set of accelerograms used for the demand analysis. It will specifically depend on the relative frequency of S_{a2} values for each S_{a1} value: $f_{S_{a2}|S_{a1}}$. If the dependence of response on S_{a2} (given S_{a1}) is significant, then we can get the same $G_{Y|S_{a1}}(s_{a1})$ from these two approaches only when the conditional distribution $f_{S_{a2}|S_{a1}}(\cdot)$ for the data is the same as that of the site.[6]

The conditional density function at the site and that from the data used in the 20-story demand regression analyses are shown in Figure 5.13. We observe that there is a significant difference between these two sets of distributions. Further, the site-specific distribution varies significantly with S_{a1}. At the low intensity levels, we observe that the variability of conditional S_{a2} is higher. The contribution of comparatively higher S_{a2} is also higher at the low intensity levels. This is due to the low-magnitude records, which, compared to the high-magnitude records, have low spectral accelerations, but are relatively richer in high frequency content and likely to occur more frequently. In contrast, in Chapter 4, for the demand regression analysis we used the same set of records but scaled to different intensity levels. So we get the same conditional distribution shape at all the levels. This difference in conditional distributions most likely explains the difference between the results from the 2-D and the 1-D PSDA.

So if we can in effect "correct" the conditional density function $f_{S_{a2}|S_{a1}}(\cdot)$ of the data to get the "site-specific" conditional density function, then from 1-D PSDA we may get

[6]This observation emphasizes the desirability of selecting the records in such a way that the magnitude, or distance, or duration, or spectral shape of the records represents the hazard dominating events at least if structural responses are significantly dependent on these parameters in addition to on S_{a1}. In this process we will get in the data set itself approximately the "correct" (site-specific) conditional distribution of the additional parameters conditioned on S_{a1}. When we select records in that way (only), the 1-D demand regression $G_{Y|S_{a1}}$ will be equivalent to the site-specific one, obtained from $\int G_{Y|S_{a1},S_{a2}}(s_{a1},s_{a2})\cdot f_{S_{a2}|S_{a1}}(s_{a2}|s_{a1})\,ds_{a2}$.

results similar to the 2-D PSDA. In order to do this we carry out a "weighted" regression analysis of the response data. The weight (w_i) of each of the sample points is the ratio of the conditional PMF from the 2-D PSHA results to that of the data. (In conventional weighted regression analysis the weight is proportional to the regression error, hence the quote on "weight." See Neter, et al., 1996, for details.) This can be calculated from the following:

$$w_i \propto \left[\frac{p_{S_{a2}|S_{a1}}(s_{a2}|s_{a1})_{2\text{-}D\ PSHA}}{p_{S_{a2}|S_{a1}}(s_{a2}|s_{a1})_{data}} \right]_i \tag{5.17}$$

These two conditional PMFs (p) are obtained from Figure 5.13. Note that the weights from Equation 5.17 are renormalized so that the sum of all the weights is equal to one. The results of this weighted regression analysis of maximum story drift and maximum beam plastic rotation conditioned on no collapse are given in Table 5.3. We observe that these regression results are not very much different from the unweighted regression results in Table 4.4. But when we use these weighted regression results in 1-D PSDA (Equation 3.19), we observe in Figure 5.14 that the 1-D demand-hazard calculations improve significantly over the previous estimates of the 1-D results in Chapter 4. In this case the observed "error" is a factor of about 2 to 3 at return periods of 10^4 and less. This observation suggests that the difference between the results from the 2-D and the 1-D PSDA is due to the difference between the conditional distribution of S_{a2} of the site and of the data. This information of conditional distribution, however, can be obtained only from the 2-D PSHA. We conclude that the results of 2-D PSHA are important if any structural response of interest significantly depends on S_{a2} conditioned on S_{a1}. This is true whether the demand hazard is obtained by the direct 2-D analysis (Equation 5.16) or by 1-D analysis from properly "weighted" regressions.

The success of this weighted regression scheme suggests additionally that when we calculate the demand of a structure (even for primarily single-frequency dominated structures) at a specific ground-motion intensity, e.g., 475-year intensity, we should in principle use different sets of records at different intensity levels so that the conditional distribution of S_{a2} of the records matches that of the site. We have observed in Figure 5.13 that this

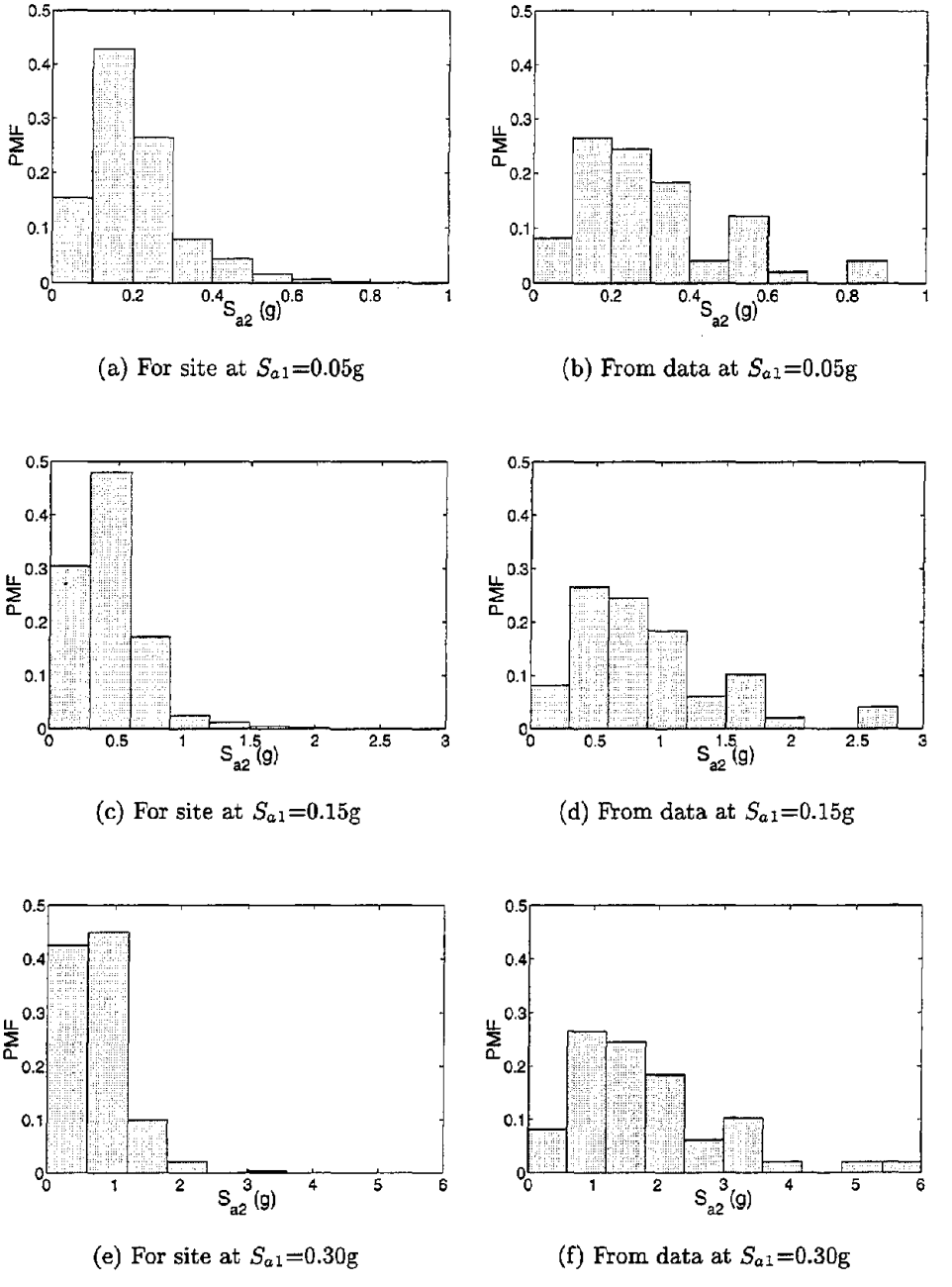

(a) For site at S_{a1}=0.05g

(b) From data at S_{a1}=0.05g

(c) For site at S_{a1}=0.15g

(d) From data at S_{a1}=0.15g

(e) For site at S_{a1}=0.30g

(f) From data at S_{a1}=0.30g

Figure 5.13: Conditional probability mass function (PMF) of S_{a2} conditioned on S_{a1} from the accelerogram data set used in Chapter 4 (44 records) and from the 2-D PSHA (specific for the 20-story building) for a central Los Angeles site. The spectral accelerations S_{a1} and S_{a2} are calculated at 0.25Hz and 0.67Hz respectively and at 5% damping.

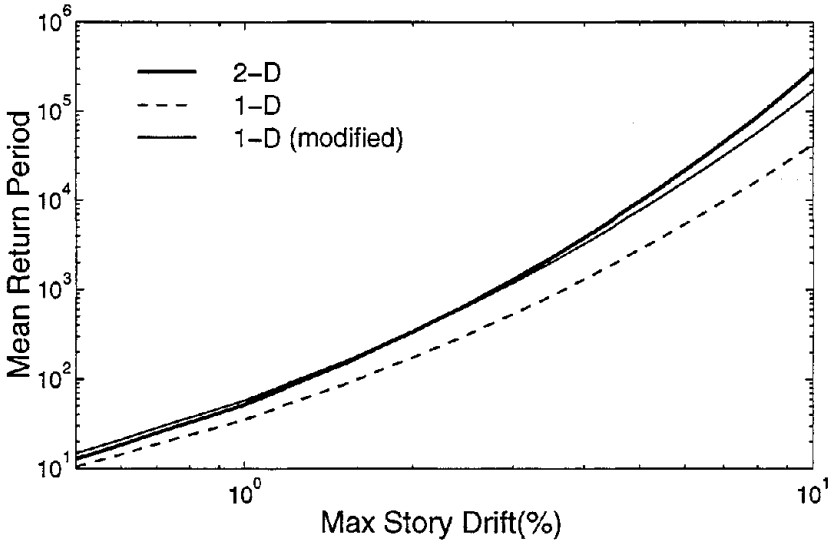

(a) Maximum story drift

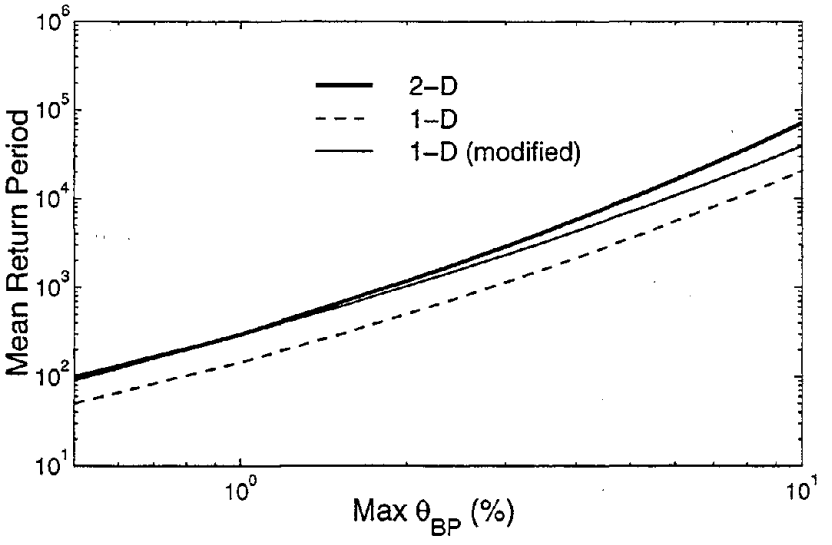

(b) Maximum beam plastic rotation

Figure 5.14: Seismic demand curves *conditioned on no collapse* of a 20-story SMRF at a central Los Angeles site. The results of the modified 1-D PSDA are obtained from the weighted regression results where the weights are calculated from Equation 5.17.

Damage Measure	Regression Function	δ_ε
Maximum Story Drift (D_{st})	$D_{st} = 0.14 \cdot (S_{a1})^{0.95}$	0.38
Maximum Beam θ_{CP}	$\theta_{CP} = 0.31 \cdot (S_{a1})^{1.64}$	0.60

Table 5.3: Results of weighted regression analysis of different damage measures of the 20-story building from the records scaled to the 0.30g, 0.15g, and 0.05g first-mode spectral accelerations. The weights are calculated from Equation 5.17. The independent variable S_{a1} is calculated at the 0.25Hz frequency and 5% damping. Note that the regression results are conditioned on no collapse of the structure.

distribution varies significantly with S_{a1}. By this record selection process we will get more accurate 1-D PSDA estimates of seismic-demand hazards at that intensity level. Alternatively, the weighted regression scheme proposed here appears to produce a significant 1-D PSDA improvement. Finally 2-D PSDA is always an option. No matter how the analysis is done, it is going to be more accurate if the data set includes records that "sample" the range of S_{a1}-S_{a2} pairs appropriate both to the site and to the intensity levels that dominate the response/demand levels important to the assessment of the structure (be that for immediate occupancy, life safety, collapse prevention, or all these levels).

5.5.4 2-D Demand-Hazard Computation When the Likelihood of Collapse of Structures is Significant

Note that Equation 5.14 for 2-D PSDA does not take into account the likelihood of collapse of structures, which is important for the 20-story structure at high demand levels. We have seen in Figure 4.23 that at high demand levels the difference between the demand-hazard results conditioned on no collapse and the results considering the likelihood of collapse at high intensity levels becomes significant. When we take into account the likelihood of collapse in demand calculations, then Equation 5.14 is modified as follows:

$$\lambda_{Y>y} = \int_0^{+\infty}\int_0^{\infty} P_C(s_{a1},s_{a2}) \cdot \lambda_{S_{a1},S_{a2}}(s_{a1},s_{a2})\, ds_{a1}\, ds_{a2} + \int_0^{+\infty}\int_0^{+\infty} P_{NC}(s_{a1},s_{a2}) \cdot G_{Y|S_{a1},S_{a2}}(y|s_{a1},s_{a2}) \cdot$$

$$\lambda_{S_{a1},S_{a2}}(s_{a1}, s_{a2})\, ds_{a1}\, ds_{a2} \tag{5.18}$$

where

$$P_{NC}(s_{a1}, s_{a2}) = \alpha_C \cdot (s_{a1})^{-\beta_{C1}} \cdot (s_{a2})^{-\beta_{C2}} \quad \text{such that,} \quad 0 \leq P_{NC}(s_{a1}, s_{a2}) \leq 1 \tag{5.19}$$

The binary regression coefficients, α_C, β_{C1}, and β_{C2}, can be obtained from Table 4.5. As we have mentioned in Section 4.3.4, that the likelihood function of the convenient binary-regression model in Equations 4.13 and 5.19 has sharp peaks and valleys compared to that of the logistic model in Equation 4.12. This makes it difficult to get a proper, optimized solution of Equation 4.15 from the convenient form. However when the explanatory variables are S_{a1} and S_{a2}, the optimized log-likelihood value $[L(\alpha, \beta)]$ from the convenient model is lower than what we get from the logistic model (compare this value in Tables 5.2 and 4.5). This indicates that the convenient form, although difficult to solve, works better in this case than the logistic model. So we find in Table 5.2 that although the probability of no collapse is not statistically significantly dependent on S_{a2}, the better fitted convenient model indicates the opposite. We also find in Figure 5.6 that P_{NC} from the logistic model depends mainly on S_{a1}. We adopt here the convenient model to calculate $P_{NC}(\cdot)$ from Equation 5.19.

The numerical integration of Equation 5.18 for maximum story drift of the 20-story building is shown in Figure 5.16. These results are compared with the results from 1-D PSDA. As we have observed before, we also find that the difference between the results from the 1-D and the 2-D PSDA is quite high at high-drift levels. We also observe in Figures 5.11 and 5.12 that this difference is statistically significant. We make a similar observation in Figure 5.15 for the 5-story building. Note that the demand-hazard results at high drifts ($\geq 8\%$) of the 5-story building are based on extrapolation of regression results in a large number of cases of bootstrap replication. Hence for the 5-story building at high drifts the results in the figure *may not be* accurate. We observe in Figure 5.12 that the best estimate of the ratio of the return periods from the 2-D and the 1-D PSDA increases with

drift at low drifts. This ratio, however, is higher for multi-frequency dominated 20-story structure. The best estimate of this ratio is 2.2 for the 5-story structure and 2.9 for the 20-story structure at the 5% story drift. At higher drifts the best estimate of this ratio and the variability of this estimate keep on increasing for the 5-story structure, whereas for the 20-story building at high drifts this ratio decreases again as the likelihood of collapse dominates the result, and the variability of the estimate of this ratio is practically constant. The best estimate of the ratio is 3.6 for the 5-story structure and 1.7 for the 20-story structure at the 10% story drift.

The results of other damage measures for the 5-story and the 20-story building are shown in Figure 5.15 and Figure 5.16 respectively. The results at 2.5% and 5% drifts are also shown in Table 5.1 for ready reference. We conclude here that it may be important to carry out 2-D PSDA (or, perhaps, 1-D PSDA based on "weighted" regressions) for both the single-frequency dominated 5-story structure and the multi-frequency dominated 20-story structure.

5.5.5 Direct Closed-Form 2-D PSDA

Explicit 2-D Results (No Collapse): We can simplify the 2-D demand calculation that is based on two spectral accelerations, S_{a1} and S_{a2}. We have seen in Equation 5.7 that we can get a closed form solution of the 2-D PSDA Equation 5.16 if we assume that the probability mass function $p_{(S_{a2}|S_{a1})}$ is approximately constant over S_{a1}. We observe, however, in Figure 5.4(d) that this is not valid. We, however, find in Figure 5.10 that the ratio of spectral accelerations, $\frac{S_{a2}}{S_{a1}}$, is much smooth over a wide range of spectral accelerations. This smoothness permits a coarse discretization over, say, three to five S_{a2} intervals. Hence for the 5-story building and, conditioned on no collapse, for the 20-story building, we can get the following closed-form solution of the equation for the calculation of the 2-D PSDA (Equation 5.16) from Equation 5.7:

$$\lambda_{Y>y} = \left[\sum_{i=1}^{N_Z} H(s_{a1y,i}) \cdot p_{[Z|S_{a1}]}(z_i|s_{a1} = s_{a1y,i})\right] \cdot e^{\frac{1}{2}\left[\frac{K_1 \cdot \sigma_{(\ln Y|Sa1,Sa2)}}{(\beta_1+\beta_2)}\right]^2} \quad (5.20)$$

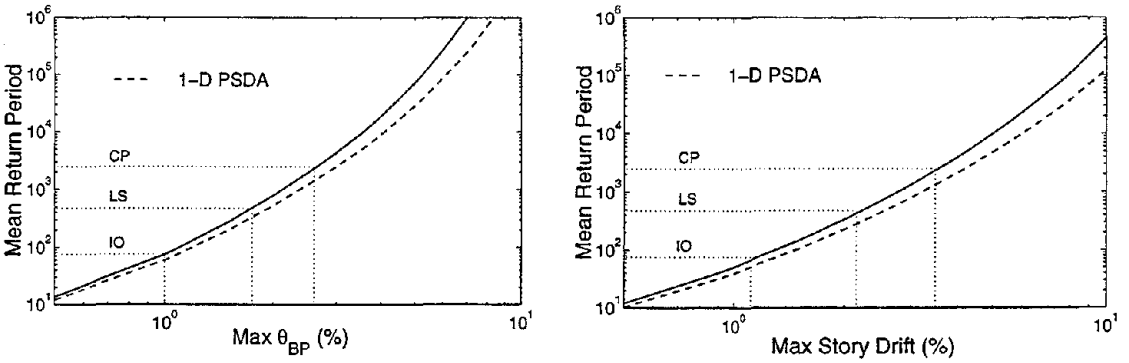

(a) System drift

(b) Maximum story drift

(c) Maximum story NHE

(d) Maximum beam plastic rotation (θ_{BP})

Notation: CP=Collapse Prevention, LS=Life Safety, IO=Immediate Occupancy

Figure 5.15: Seismic demand hazard curves of a 5-story SMRF buildings at a central Los Angeles site from 2-D and 1-D PSDA.

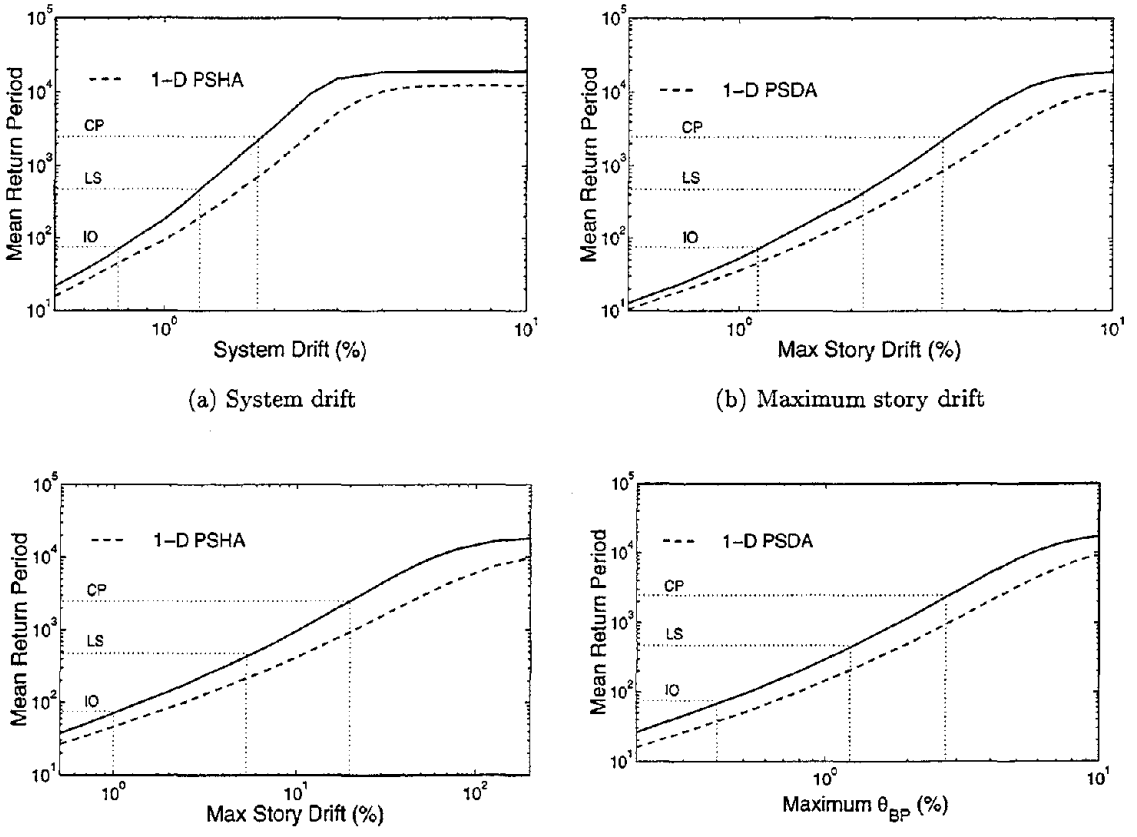

(a) System drift

(b) Maximum story drift

(c) Maximum story NHE

(d) Maximum beam plastic rotation (θ_{BP})

Notation: CP=Collapse Prevention, LS=Life Safety, IO=Immediate Occupancy

Figure 5.16: Seismic demand curves of a 20-story SMRF building at a central Los Angeles site from 2-D and 1-D PSDA.

where

Z is equal to $\frac{S_{a2}}{S_{a1}}$.

N_Z is the number of ranges of the ratio of the spectral accelerations.

s_{a1y} is the spectral acceleration, S_{a1}, required to induce a median damage $\hat{y} = y$ in the structure at the ratio of spectral accelerations, $Z = z_i$. This can be obtained from the following equation:

$$s_{a1y,i} = \left[\frac{\hat{y}}{\alpha \cdot z_i^{\beta_2}}\right]^{\frac{1}{\beta_1+\beta_2}} \tag{5.21}$$

Note that we have used here the inverse of the regression model given in Equation 3.2 for fitting the response results, namely:

$$\begin{aligned} \hat{y} &= \alpha \cdot S_{a1}^{\beta_1} \cdot S_{a2}^{\beta_2} \\ &= \alpha \cdot S_{a1}^{\beta_1+\beta_2} \cdot \left[\frac{S_{a2}}{S_{a1}}\right]^{\beta_2} \\ &= \alpha \cdot S_{a1}^{\beta_1+\beta_2} \cdot Z^{\beta_2} \end{aligned} \tag{5.22}$$

$p_{[Z|S_{a1}]}(\cdot)$ is the probability that the ratio of spectral accelerations is equal to z_i given $S_{a1} = s_{a1}$. We get this information from Figure 5.10.

The other terms in the equation are defined in Equation 3.25. We can use this equation directly to calculate the seismic demand of the 20-story structure. These demand results are conditioned on no collapse of the structure and are shown in Figure 5.17. We observe that this procedure gives the same result at low drift levels that we have obtained before from the numerical integration of Equation 5.18. We also anticipate that for the 5-story structure we will get a close match at all drift levels.

Including Collapses: Upper-Bound of Return Period (RP_{UB}): This simplified calculation, however, differs significantly at high drift levels when the likelihood of collapse of the structure becomes significant. On the other hand, we have seen in Section 4.4 that if we consider only the lower return periods from (1) the results conditioned on no collapse and (2) the upper-bound return period from Equation 4.25, we can get a quite satisfactory

result from this approach even at high drifts (see, for example, Figure 4.23). This upper-bound of return period is similar to Equation 4.25 and is calculated from the following equation:

$$\begin{aligned} 1/RP_{UB} &= \int_0^{+\infty} P_C(s_a, z) \cdot p_{Z|S_a}(z|s_a) \cdot \lambda(s_a)\, ds_a\, dz \\ &= \sum_{i=1}^{N_Z} p_{Z|S_a}(z_i|s_a = s_{ao,i}) \left[H(s_{ao,i}) \frac{\beta_{C1} + \beta_{C2}}{K_1^1 + \beta_{C1} + \beta_{C2}} \right] \end{aligned} \tag{5.23}$$

Here we are using Equation 5.19 to predict the probability of no collapse of the structure. We calculate $s_{ao,i}$ from the following:

$$s_{ao,i} = \left[\frac{\alpha_C}{z_i^{\beta_{C2}}} \right]^{\frac{1}{\beta_{C1}+\beta_{C2}}} \tag{5.24}$$

The results of the upper-bound return period from the above equation are shown in Figure 5.17. We observe that as we have seen in Section 4.4, the prediction of demand from Equations 5.20 and 5.23 works quite satisfactorily. The demand at the intermediate drift levels can be improved by fitting a smooth transition curve between the results at the low and high drift levels. The advantage of this approach is that we can calculate the 2-D seismic demand from simple explicit equations.

5.5.6 Importance of Selection of Two Spectral Acceleration Frequencies

We have found that in PSHA practice spectral attenuation results and hence PSHA results are available only at a limited number of frequencies. We will investigate here how much importance one should give to selection of the precise frequencies for the calculations of spectral accelerations that are used in PSDA as intermediate or explanatory variables. Because the structure is nonlinear in the region of response/demand interest, we do not expect the use of precisely the first and second-mode frequencies to be critical. For the 20-story structure we consider the additional S_a frequencies at 1.33Hz and at 0.2Hz that are respectively higher and lower than the elastic first-mode frequency. Note that, although

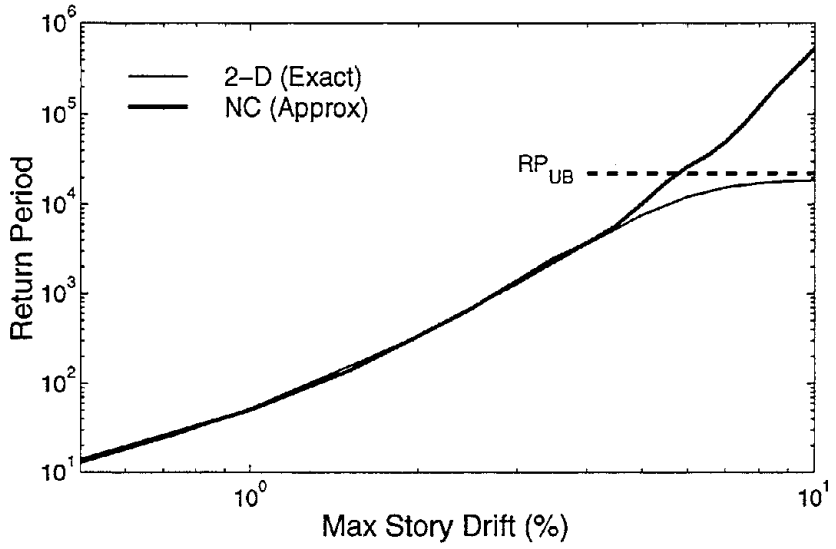

Figure 5.17: Seismic story-drift demand curves for the 20-story SMRF building at a central Los Angeles site. Here, $2-D(Exact)$ indicates the numerical integration results from Equation 5.18; $NC(Approx)$ indicates the approximate solution conditioned on no collapse from Equation 5.20; RP_{UP} is the upper-bound return period from Equation 5.23.

0.20Hz is very close to the first-mode frequency (0.25Hz), it is the lowest frequency at which the attenuation results are available (see Abrahamson and Silva, 1997). We first carry out the 2-D regression analysis of the story drift results of the 20-story building conditioned on no collapse. The regression results are in given in Table 5.4. We find that the (conditional) dependence of the maximum story drift on $S_{a3}(f = 1.33Hz)$ is as high as S_{a2} (compare the δ_ϵ or R_a^2 values) and it is statistically significantly dependent on S_{a3}. the story drift, however, does not depend on $S'_a(f = 0.20Hz)$ given S_{a1}. The binary regression results for the convenient model (Equation 4.13) for these additional explanatory variables are given in Table 5.5. We find that the probability of no collapse conditioned on S_{a1} is statistically significantly dependent on these variables; to our surprise the conditional dependence on $S'_a(0.20Hz)$ given S_{a1} is even higher than the conditional dependence on S_{a2} given S_{a1}.

The contour plot of the 2-D PSHA results for $\lambda_{S_{a1},S_{a2}}(\cdot)$ for spectral accelerations at 0.2Hz and at 1.33Hz along with the first-mode frequency (0.25Hz) are shown in Figure 5.9. The correlation coefficients of the spectral accelerations at these frequencies are

Damage Measure	Independent Variable	Regression Function	R_a^2	δ_ε	n_{req}
Maximum Story Drift (D_{st})	S_{a1}	$\boldsymbol{D_{st} = 0.16 \cdot (S_{a1})^{0.95}}$	0.70	0.44	20
	S_{a1}, S_{a2}	$\boldsymbol{D_{st} = 0.09 \cdot (S_{a1})^{0.56} \cdot (S_{a2})^{0.40}}$	0.80	0.36	13
	S_{a1}, S_{a3}	$\boldsymbol{D_{st} = 0.07 \cdot (S_{a1})^{0.60} \cdot (S_{a3})^{0.36}}$	0.80	0.36	13
	$S_{a1}, S'_a(0.20Hz)$	$D_{st} = 0.18 \cdot (S_{a1})^{0.78} \cdot (S'_a)^{0.17}$	0.71	0.44	20
Maximum Column Plastic Rotation	S_{a1}	$\boldsymbol{\theta_{CP} = 0.29 \cdot (S_{a1})^{1.46}}$	0.67	0.66	43
	S_{a1}, S_{a2}	$\boldsymbol{\theta_{CP} = 0.16 \cdot (S_{a1})^{1.05} \cdot (S_{a2})^{0.55}}$	0.76	0.56	32
	S_{a1}, S_{a3}	$\boldsymbol{\theta_{CP} = 0.11 \cdot (S_{a1})^{1.08} \cdot \cdot (S_{a3})^{0.52}}$	0.77	0.56	32
	$S_{a1}, S'_a(0.20Hz)$	$\theta_{CP} = 0.30 \cdot (S_{a1})^{1.37} \cdot (S'_a)^{0.09}$	0.67	0.66	43

Table 5.4: Results of regression analysis of different damage measures for a 20-story building conditioned on no collapse. The independent variables S_{a1}, S_{a2},, S_{a3}, and S'_a are calculated at 0.25, 0.67, 1.33 and 0.20Hz respectively and at 5% damping. The sample size requirement ($n_{req} = [\delta_\varepsilon/0.10]^2$) is obtained for a target one-sigma confidence bandwidth of ±10%. The bold letters indicate that the addition of an independent variable makes the result statistically significantly different from the result without that independent variable at the 1%-significance level.

$\rho_{0.25Hz,0.20Hz} = 0.93$ and $\rho_{0.25Hz,1.33Hz} = 0.45$. We observe in the plot that the contour lines of the spectral accelerations at 0.25Hz and 0.20Hz are concentrated along a line of the S_{a1}-S'_a plane, signifying high correlation of spectral accelerations at these frequencies, whereas the contour lines of the spectral accelerations at 0.25Hz and 1.33Hz are spread out on the S_{a1}-S_{a3} plane because of low correlation.

The seismic drift demands of the 20-story building from the 2-D PSDA for spectral

Explanatory Variable	Regression Function ($P_{NC}(X) \leq 1$)	$L(\alpha, \beta)$
S_{a1}	$P_{NC} = 0.015 \cdot (S_{a1})^{-2.78}$	23.7
S_{a1}, S_{a2}	$P_{NC} = 0.008 \cdot (S_{a1})^{-3.33} \cdot (S_{a2})^{-0.57}$	19.7
S_{a1}, S_{a3}	$P_{NC} = 0.005 \cdot (S_{a1})^{-3.75} \cdot (S_{a3})^{-0.32}$	21.0
S_{a1}, S'_a	$P_{NC} = 0.001 \cdot (S_{a1})^{-4.02} \cdot (S_{a2})^{-1.71}$	17.8

Table 5.5: Results of regression analysis of the probability of no collapse (P_{NC}) against spectral accelerations for a 20-story building. The independent variables S_{a1}, S_{a2},, S_{a3}, and S'_a are calculated at 0.25, 0.67, 1.33 and 0.20Hz frequencies respectively and at 5% damping. $L(\alpha, \beta)$ is the optimized log-likelihood value.

accelerations at 0.25 and 1.33Hz and at 0.25 and 0.20Hz are shown in Figure 5.18. We observe that as the story drift does not depend on the spectral acceleration at 0.20Hz, the results of the 2-D PSDA for spectral accelerations at frequencies 0.25Hz and 0.20Hz are the same as those of the 1-D PSDA, which we obtained in Chapter 4 based on 0.25Hz spectral acceleration. On the other hand, story drift is (conditionally) dependent on the spectral acceleration at 1.33Hz (close to the elastic third mode). The results from the 2-D PSDA based on spectral accelerations at 0.25Hz and 1.33Hz are close to what we got precisely based on spectral accelerations at 0.25Hz and 0.67Hz. We find that although P_{NC} is statistically significantly dependent on $S'_a(f = 0.20Hz)$, there is no difference in results even at high drift levels between the 1-D and the 2-D PSDA for spectral accelerations at 0.25Hz and 0.20Hz. We can, however, explain this (apparent) inconsistency when we look into the variation of P_{NC} with S_{a1} at the conditional mean of these additional variables (e.g., $\hat{S}_{a2}|S_{a1}$). This is shown in Figure 5.19. (We described in Footnote 12 of Chapter 3 the procedure for calculating these conditional mean values.) We observe that P_{NC} conditioned on S_{a2} or S_{a3} given S_{a1} is much higher than the prediction conditioned on only S_{a1} for $S_{a1} \leq 0.4$. The probability of exceeding these low spectral accelerations is very high; we get in the end a lower probability of exceedance and thus a higher return period at high damage levels. Based on S_{a1} and S'_a, P_{NC} is much lower than the prediction based on only S_{a1} for $S_{a1} \geq 0.3$; for $S_{a1} \leq 0.3$ it is slightly higher. The much lower values of P_{NC}, coupled with the low probability of occurrence of high spectral accelerations, somewhat balances the slightly higher P_{NC} at the low spectral accelerations, which have a higher probability of occurrence. As a result we get practically the same result from the 1-D and the 2-D PSDA for spectral accelerations at 0.25Hz and 0.20Hz.

We also calculate drift demand of the 5-story building from spectral acceleration at 0.25Hz and 1.33Hz. The results are shown in Figure 5.18. We find that the results are very close to the 2-D PSDA results based on spectral accelerations at the first and second-mode frequency. We can conclude here that for 2-D PSDA we can select spectral accelerations at any two frequencies that will be able to represent the shape of the ground-motion spectrum in the region important for the structure. Because 0.20Hz is very close to the first-mode

frequency of the 20-story structure, the spectral accelerations at those two frequencies cannot predict the shape of the spectrum properly; hence we do not find any improvement of demand hazard prediction from S_{a1}-S'_a pairs.

5.6 Low-Corner Frequency: Shortcomings of Current Methodology

Recall that in Chapter 4 we calculated the damage measures conditioned on records qualified by having an appropriate low-corner filter frequency (f_{LC}). This is a necessity because these corner frequencies reflect that the records have lower signal-to-noise ratios at still lower frequencies, and these frequencies may be of importance to the structures (especially the 20-story structure). We introduce here an indicator variable, LCF, where $LCF = 1$ if a record satisfies the criterion of low-corner frequency (which we have considered in Chapter 4 as $f_{LC} \leq 0.10Hz$ for the 20-story building), or $LCF = 0$ otherwise. We can calculate the probability of a low-corner frequency of ground-motion records conditioned on M and R by binary-regression analysis. A typical binary-regression result of $P(LCF = 1|M, R)$ is shown in Figure 5.20. This result demonstrates that the low-magnitude, high-distance records have low probability of qualifying for analysis, whereas the high-magnitude, long-distance records have relatively much higher probability. Hence as we will see below, when we incorporate this information in PSHA, the net effect is to reduce the hazard results (i.e., a lower probability of exceedance of spectral accelerations). This reduction may not be substantial at high spectral acceleration levels in California where the contribution of high-magnitude records is high at high spectral accelerations (see, for example, Figure 5.3), but it may be significant for some sites in the Eastern United States where a significant contribution to seismic hazard comes from low to moderate magnitude earthquakes at fairly large distances. Our objective is to calculate the seismic demand hazard accurately. We will demonstrate here how we can incorporate in demand hazard calculations the subset of results from the records that do not qualify. Note that so far we have neglected those results.

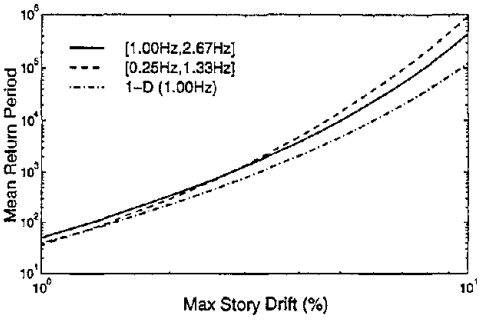

(a) Maximum story drift; 5-Story SMRF

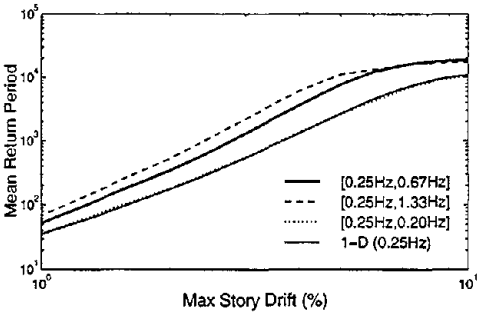

(b) Maximum story drift; 20-Story SMRF

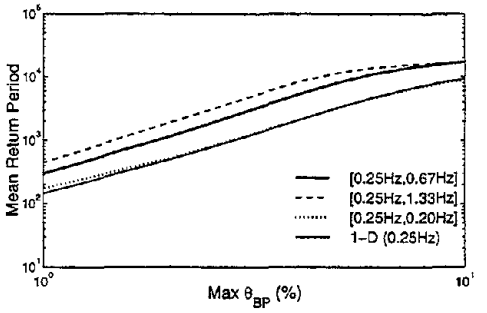

(c) Maximum beam plastic rotation (θ_{BP}); 20-story SMRF

Figure 5.18: Seismic demand curves for different damage measures of different structures at a central LA site from different 2-D and the 1-D PSDA results. The results from the 2-D PSDA for the 5-story building are based on spectral accelerations for two combination of frequencies: 1.0Hz and 2.67Hz, and 0.25Hz and 1.33Hz. For the 20-story building, the results are based on three combinations of frequencies: 0.25Hz and 0.20Hz, 0.25Hz and 0.67Hz, and 0.25Hz and 1.33Hz. The 1-D PSDA results are based on the spectral acceleration at 1.0Hz for the 5-story building and at 0.25Hz for the 20-story building.

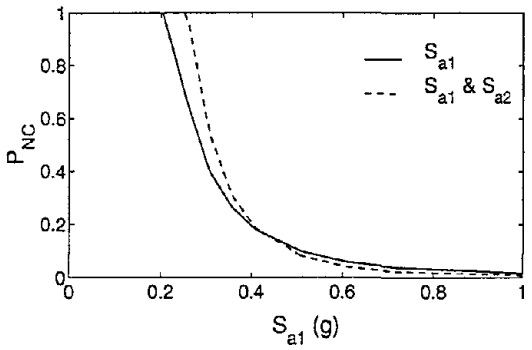

(a) $S_{a1}(0.25Hz)$ and $S_{a2}(0.67Hz)$

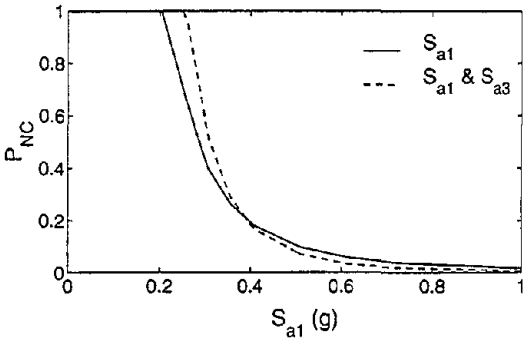

(b) $S_{a1}(0.25Hz)$ and $S_{a3}(1.44Hz)$

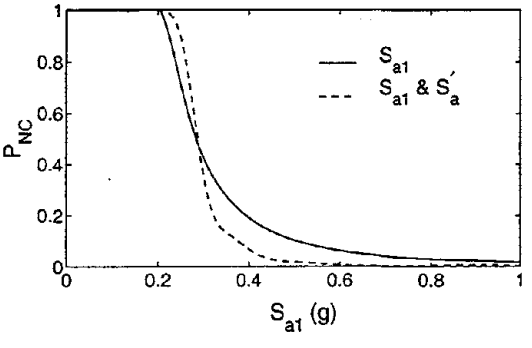

(c) $S_{a1}(0.25Hz)$ and $S'_a(0.20Hz)$

Figure 5.19: Comparison of binary regression results for the probability of no collapse (P_{NC}) against spectral acceleration in addition to S_{a1} for a 20-story building. The values of the additional spectral accelerations used in these calculations are the mean values conditional on S_{a1} (from the record data set).

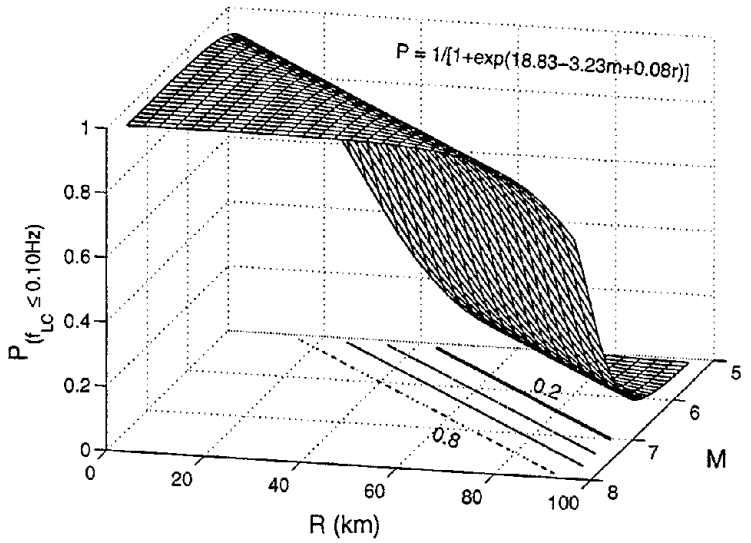

Figure 5.20: Variation of the conditional probability, $P(LCF = 1|m, r)$, that a record has the effective low-corner frequency ($f_{LC} \leq 0.10Hz$) conditioned on magnitude, m, and distance, r. The records are obtained from the record set provided by Dr. Walt Silva.

The probability of exceedance of any damage measure Y of a level y can be written from Equation 5.2 as follows:

$$\begin{aligned} \lambda_{Y>y} &= \int G_{[Y|S_a,LCF=0]}(y|s_a) \cdot \lambda_{[S_a,LCF=0]}(s_a)\, ds_a + \\ &\quad \int G_{[Y|S_a,LCF=1]}(y|s_a) \cdot \lambda_{[S_a,LCF=1]}(s_a)\, ds_a \end{aligned} \tag{5.25}$$

Note that for the demand calculations in Chapter 4 we a priori rejected those records that do not have an effective low-corner frequency ($LCF = 0$) based on the assumption that these records have a weak S_{a1} and therefore cannot cause significant damage to properly designed structures. Hence, we have in effect assumed, $G_{[Y|S_a,LCF=0]}(y|s_a) = 0$. So Equation 5.25 simplifies as follows:

$$\begin{aligned} \lambda_{Y>y} &= \int G_{[Y|S_a,LCF=1]}(y|s_a) \cdot \lambda_{[S_a,LCF=1]}(s_a)\, ds_a \\ &= \sum_i G_{[Y|S_a,LCF=1]}(y|s_{a,i}) \cdot \lambda_{[S_a,LCF=1]}(S_a = s_{a,i}) \end{aligned} \tag{5.26}$$

Note that the attenuation results what we and others have used in PSHA are based on the ground-motion records whose low-corner-filter frequency is at least lower than the frequency of the elastic oscillator used to calculate the response spectrum (see, for example, Abramhamson and Silva, 1997). While selecting a record for attenuation study, the low-corner frequency is introduced because the signal-to-noise ratio below that corner frequency is too low to get a reliable result. The conventional-hazard results are conditioned on only those records that have a reliable signal at the frequency of the structure. Hence we get a conditional hazard result which is $\lambda_{[S_a|LCF=1]}(s_a)$.[7] In the previous chapters while combining the seismic-hazard results and the nonlinear structural analysis results, we got the following conditional probability of exceedance:

$$\lambda_{Y>y|LCF=1} = \sum_i G_{[Y|S_a,LCF=1]}(y|s_{a,i}) \cdot \lambda_{[S_a|LCF=1]}(s_a = s_{a,i}) \tag{5.28}$$

On the other hand, if we get $\lambda_{[S_a,LCF=1]}(s_a)$ by modifying the hazard calculations as per Footnote 7, we will directly get $\lambda_{Y>y}$ instead of the conditional probability.

We can also rewrite Equation 5.26 as follows:

$$\lambda_{Y>y} = \int G_{[Y|S_a,LCF=1]}(y|s_a) \cdot \lambda_{[S_a|LCF=1]}(s_a) \cdot P_{[LCF=1|S_a]}(s_a)\, ds_a \tag{5.29}$$

where the conditional probability, $P(LCF = 1|S_a)$, can be obtained from the following:

$$P(LCF = 1|s_a) = \int\int P(LCF = 1|m, r, s_a) \cdot f_{[M,R|S_a]}(m, r|s_a)\, dm\, dr \tag{5.30}$$

---

[7] We can get the joint distribution by modifying the conventional PSHA calculations as follows:

$$\lambda_{S_a}(s_a) = \lambda_{S_a}(s_a, LCF = 1) = \sum_{i=1}^{N} \left\{ \int\int P(S_a = s_a|LCF = 1, m, r) \cdot P(LCF = 1|M = m, R = r) \cdot f_{M,R}(m, r)\, dm\, dr \right\}_i \tag{5.27}$$

where $P(LCF = 1|M, R)(m, r)$ is the probability that a record from an event of magnitude m and distance r has the effective low-corner frequency. See Equation 3.16 for a description of other notations. We are assuming here $P(S_a = s_a|LCF = 0, m, r) = 0$. In the conventional PSHA calculations we have not considered the conditional probability, $P(LCF = 1|M, R)(m, r)$, and thus we get finally a conditional hazard result, $\lambda_{[S_a|LCF=1]}(s_a)$.

where the conditional distribution, $f_{M,R|S_a}(.)$, can be obtained from the disaggregation of seismic-hazard results; the conditional probability of the low-corner frequency, $P(LCF = 1|m, r, s_a)$, can be obtained from Figure 5.20 by assuming a negligible correlation between LCF and S_a. The conditional probability can be plotted like those in Figure 5.4. This will help to decide whether we need to correct additionally the demand hazard results or whether the results based on the previously discussed procedure are sufficiently accurate. At present we cannot calculate the conditional probability, $P(LCF = 1|S_a)$, because we do not get $f_{[M,R|S_a]}(.)$ from the disaggregation of conventional hazard results (we need to modify PSHA calculations as suggested in Footnote 7 to get this information.).

5.7 Summary

In this chapter we have investigated whether the demand calculations are dependent on the seismological parameters (M and R) or the record parameters (S_{a2} and D) *in addition to the first-mode spectral acceleration.* These parameters for the two example problems only sometimes statistically significantly change the response prediction conditioned on S_{a1}, but for illustration we have considered all the parameters for demand calculations. The advantage of considering these additional parameters, if they are significant, is that we then need fewer number of expensive nonlinear structural analyses to obtain reliable median demand estimates. We also find that 2-D PSDA may improve the accuracy of the demand estimations.

We have observed in Figures 3.10 and 4.15 that although the response of a structure is statistically significantly dependent on M, R, or D, the median response does not change substantially with these additional parameters. The binary regression results also indicate that the probability of no collapse of the 20-story structure is not statistically significantly dependent on those parameters. So we find that for the 5-story as well as the 20-story structures the 2-D PSDA results based on S_{a1} and the additional parameter M, or R, or D, are not different from the 1-D PSDA results based on S_{a1}. If, for some other structures,

these parameters change the damage prediction substantially, we will get improved estimation of seismic demand based on these additional parameters. Note that the calculation of seismic demand for these additional parameters requires additional PSHA information, namely disaggregation analysis of conventional seismic hazard results. Today, this is readily available.

In contrast, we have found in the previous chapters that the median damage prediction conditioned on S_{a1} and on a high frequency spectral acceleration, S_{a2}, is statistically significantly different from the prediction based on S_{a1} for both the 5-story and the 20-story structures. The difference in median estimates can also be substantial (see Figures 3.10 and 4.15). We have also found that the probability of no collapse conditioned on S_{a1} is statistically significantly dependent on S_{a2}. Hence the 2-D PSDA results based on S_{a1} and S_{a2} may be rather different (by a factor of two or more) at the high as well as at the low intensity levels from the 1-D PSDA results. This is true for both the "single-frequency dominated" 5-story structure and the "multi-frequency dominated" tall 20-story structure. This conclusion implies that in contrast to M, R, and D the spectral shape is *at least* a second-order problem (a factor of three is second order; a factor of ten is first order).

We have shown that this difference in the 1-D and 2-D demand hazard results is due to the "mismatch" of the statistical characteristics of the spectral shape of the ground-motion records that we have used in structural analysis and those that we will get at the site. We have also shown through an example that when we rectify this mismatch of ground-motion characteristics between the site and the data, we can obtain the same demand result from the 2-D PSDA and the 1-D PSDA. In particular we need to have the relative frequencies of different (S_{a1}, S_{a2}) pairs to be consistent with the site threat.

The procedure of demand calculations by 2-D PSDA may look complicated at first sight. We have shown that the 2-D PSDA results can be approximated by two simple explicit equations. The seismic demand at low damage levels can be simplified to the demand calculation conditioned on no collapse and this calculation can be obtained from the explicit expression given by Equation 5.20. On the other hand, the demand at high damage levels can be obtained from the explicit expression given by Equation 5.23. The

results from these two simple explicit equations match very well with the results from numerical integration of Equation 5.18 at the high and at the low drift levels. The demand prediction at the intermediate damage levels can be improved by fitting a smooth transition curve between the demand results at the high and low damage levels.

We have also investigated the importance of selection of spectral accelerations for 2-D PSDA. We have found essentially the same demand results from the following combinations of spectral accelerations at two different frequencies: 1.0 and 2.67Hz, and 0.25 and 1.33Hz for the 5-story building; 0.25 and 0.67Hz, and 0.25 and 1.33Hz for the 20-story building. We find that for all the buildings the story drift results conditioned on S_{a1} are statistically significantly dependent on all the additional spectral accelerations. For the 20-story building the probability of collapse is also statistically significantly dependent on these spectral accelerations. Hence we find that although the spectral accelerations are calculated at quite different frequencies, we essentially get the same demand results from the 2-D PSDA. In short these different pairs of spectral accelerations effectively predict the same spectral shape in the region of full response spectrum that is important for these structures. Therefore it is not extremely critical exactly which pair of frequencies is used in the 2-D PSDA.

We have also found that the current state of the art of PSHA calculations is essentially conditioned on the records that have an effective low corner frequency. Hence the PSDA results we get from these hazard results are also conditioned on the records that have an effective low-corner frequency. We propose here a procedure to carry out PSHA calculations "correctly." This is specially important for low-frequency tall buildings. This improvement will reduce the spectral ordinate at low frequencies of the uniform hazard spectrum (UHS). When we combine these correct PSHA results in the demand calculations we have proposed in this dissertation, we will get the correct demand result.

Chapter 6

Recommended Practice for the Estimation of Seismic Demand

The objective of the present study is to estimate seismic demand hazard *accurately* and *efficiently*. By accurate we mean here that the estimation should be unbiased. In Chapters 2 to 5 we have investigated how to estimate demand hazard in such a way that we get an unbiased estimate from the smallest number of structural analyses, i.e., how to get an efficient as well as an unbiased estimate. In this chapter we will first recommend efficient and accurate procedures for demand calculations at a given intensity of ground motion. These recommendations will be applicable for the performance evaluation of structures according to a code procedure. We will determine the uncertainties in demand calculations. On the basis of our results we will recommend the number of structural analyses required for a certain accuracy of demand estimation. Second, we will address the broader issue of uncertainty in the estimation of the probability of exceedance of a given allowable demand (or demand hazard) to recommend the required number of analyses. In determining the uncertainties in the estimation of the demand or the demand hazard, we will consider the uncertainty in the estimation of the ground-motion hazard, in structural response, in material properties, and in mathematical representation of structures. The recommendations we

will be making may be quite general, but it must be remembered that those recommendations are based on a limited number of case studies. Further studies may reveal exceptions and limitations to the range of the conclusions.

The recommendations we will be making here are based on the results of the following cases: three SDOF structures that have three distinct frequencies which are low (0.25Hz), medium (1.0Hz), and high (4Hz) (presented in Appendix E), stick model representations of three MDOF structures that have the first-mode frequencies close to the SDOF frequencies (presented in Chapter 2 and Appendix E), and 2-D representations of two steel moment resisting frames that have low and medium frequencies (presented in Chapters 3 and 4). The conclusions we will be drawing are bound to limitations in the modeling of structures and the specific ground-motion characteristics that have been considered in this study. The limitations are as follows:

Modeling of Structure: We have made the following simplifications of 2-D modeling of structures:

- We have considered only the center-line model of the moment resisting frames. We have not considered here the effects of panel zone shear strength and deformation on lateral strength and stiffness of the frames. The consideration of these parameters for the 20-story building at a Los Angeles site considered in Chapter 4 reduces the maximum story-drift-demand prediction on an average by 5% at the 2500-year intensity level (see Gupta, 1999).

- In the nonlinear analysis we *have not* considered any strength or stiffness degradation of the structural members. We have assumed a bilinear force-displacement model for all the beam and column elements. We *have* considered the P-Δ effect which reduces the stiffness of structures. This effect is, however, significant only for the 20-story structure, and as a result we get negative effective stiffness at high deformations for some of the stories of the 20-story structure (as reflected in the static-pushover results in Chapter 4). So although the structural elements are not modeled with stiffness

degrading elements, we get, due to the P-Δ effect, negative stiffness, which leads to "collapse" of the 20-story structure at high-intensity levels. The collapse at high intensity levels is frequent for the mathematical model considered in this study. It was observed by Gupta (1999) that at the 2500-year intensity level although he got only 5% collapse for the center-line model that is adopted in this study, he did not observe any collapse of the structure when he considered the additional stiffness of the interior simple frames, joint panels, and the floor slabs.

- We have assumed that all the structures are fixed at the base except the 20-story structure, which is pinned at the base. The effect of soil-structure interaction has been neglected for all the cases.

- We model the steel frames here without taking into account the composite action of floor slabs and floor girders. Consideration of this effect increases the stiffness of beam sections. We have not considered any additional strength and stiffness due to the interior simple frames and the non-structural elements. It has been observed by Gupta (1999) that for the 20-story building at a Los Angeles site the consideration of additional strength and stiffness for (1) the interior simple frames, (2) panel zones, and (3) floor slabs reduces the median maximum story drift demand by 30% at the 2500-year intensity level compared to the results from the center-line model that has been adopted in this study.

Ground motion characteristics: While selecting the ground-motion records we have considered only those accelerograms which are recorded in California at stiff soil sites (soil type S_2 as defined in UBC, 1994, or site class D as per FEMA-273, 1996). Further studies of the ground-motion characteristics must be made before one can generalize the conclusions in this study. The characteristics that must be considered are:

- Near-source ground motion whose major energy comes from a small number of high-energy pulses. In contrast, the energy is spread over a wide range of frequencies for the records considered in this study.

- Large subduction-zone type ground motion, which has the characteristic of very long duration and/or has comparatively stationary (constant root mean square) acceleration.
- Soft-soil ground motion, which has significant amplification at the frequency of vibration of soil deposit and hence has a characteristically narrow spectrum. This ground motion is also poorer in high-frequency content.
- Rock ground motion, which has in general lower intensity compared to the ground motion at a stiff-soil site.

6.1 Demand Estimations for Scenario Earthquakes

In the case of scenario earthquakes one has the seismic threat, which can be either the M-R of an event or a spectrum. Given this information, a code procedure (for example, in FEMA-273) requires us to calculate the median response or demand of a structure. We have considered here several efficient procedures to calculate the median demand of different types of structures. The types of structures considered in this study are broadly speaking single-frequency-dominated and multi-frequency-dominated steel structures. We have addressed several key issues of demand estimation for scenario earthquakes (presented mainly in Chapter 2 and later verified in the other chapters). These issues are how to select the records, how many records are to be used, the legitimacy of the scaling of records, etc. Finally, in Sections 6.1.5 and 6.1.6 below, we will recommend an efficient procedure for estimating the demand for each type of structure. These recommendations may, however, be subject to the limitations which we have described in the previous section.

6.1.1 An Efficient Intensity Measure

We have concluded that a convenient and efficient intensity measure for single-frequency dominated structures (e.g., the 5-story building in Chapter 3, the 5-DOF stick model in Chapter 2, etc.) is the elastic-first-mode spectral acceleration at 5% or higher damping.

The response of tall buildings (e.g., the 20-story building in Chapter 4 and the 20-DOF stick model in Appendix E) depends significantly on the higher-frequency spectral accelerations in addition to the first-mode spectral acceleration. We have observed in Chapter 4 that this dependency on higher frequencies is mainly due to the higher relative spectral ordinates at higher frequencies because the fundamental period of the tall building is in the strongly decaying part of the spectrum. Hence although the 5-story and the 20-story structures have quite similar modal participation factors, the higher relative spectral ordinates at frequencies near those of the higher elastic modes of the 20-story structure contribute significantly to the response of the structure. Therefore, for tall buildings an efficient intensity measure is the modal-participation-factor-based, weighted-average spectral acceleration. We conclude that for longer-periods and/or taller buildings we should scale the records to the weighted-average spectral acceleration before we do the analysis. Consideration of higher than 5% damping for ground-motion intensity calculations (in Chapter 2, Chapter 3, and Appendix E) shows some additonal reduction in variance of structural response, and hence more efficient; this, however, is not very substantial. We need to investigate further to determine the most efficient intensity measure for different types of structures.

6.1.2 Scaling–Selection of Records

We have found that it is possible to select a comparatively small number of records from a catalogue provided we scale the selected records to the target intensity level. For single-frequency-dominated structures, for example, we scale them to the elastic first-mode spectral acceleration at 5% damping of the specified design spectrum or of the spectrum predicted by an appropriate attenuation law for the M-R of an event. Proper scaling of ground-motion records reduces the sample size requirements by about 75% compared to the requirement for unscaled records if the damage measure of interest is displacement based; this percentage reduction is even higher for the energy-based damage measure. Without scaling of records, the sample size requirements may be very large (Section 2.5.1).

Thus scaling is an effective tool to improve the efficiency of estimation of seismic demand because it reduces the required number of records, and as we have seen in Chapters 2, 3,

and 4, it is legitimate. We have verified the legitimacy of scaling by comparing the results from scaled records with the results from the as-recorded ground motion (direct results) for a given M-R bin. We have used the direct results as a bench mark for all the results that we have obtained by scaling the records in different ways. We conclude that proper scaling (i.e., scaling to the first-mode spectral acceleration for single-frequency dominated structures and to the weighted-average acceleration for multi-frequency dominated structures) does not introduce any significant bias in damage estimation, and that the dispersion of damage results from scaled records is in general about 50% lower than that of the direct analysis. We have considered the damage results from different M-R bins. Normalization of these bin of records indicates that the results are unbiased and the dispersion is around 50% of the direct results. Also scaling of one bin of records to the median intensity of another bin indicates that the results from scaled records are essentially unbiased compared to the direct results of that bin. Therefore the scaling of records is legitimate. The similarity of results from different bins also indicates that the nonlinear displacement damage measures are not very sensitive to the bin parameters (i.e., magnitude, distance, and duration). We conclude that for all practical purposes we can select records from a wide range of magnitudes and distances without introducing any bias in displacement-damage estimation. Precise information about the M-R of records is therefore not very important in seismic demand calculations.

6.1.3 Bin-to-Bin Scaling versus Regression Analysis

Although comparing the results from different bins of records is an easy and effective way to verify the legitimacy of scaling, we have found (in sections 3.4 and 4.3) that regression analysis is an even more effective way to study these issues. Regression results indicate that structural responses are primarily dependent on spectral acceleration at the (approximate) first-mode frequency. This finding again supports the conclusion that we can scale ground-motion records to the first-mode spectral acceleration without biasing the structural response. Regression results indicate that conditioned on the first-mode spectral acceleration, structural responses do not depend substantially on the magnitude, distance,

or duration of records. We can also determine from the regression results which parameter is more important than the others. The regression results give us the functional relationship between any damage measure and the explanatory variables, e.g., spectral acceleration at the first mode. We need this information for demand-hazard calculations.

6.1.4 Number of Records

We can determine the required minimum number of records, n, once we have the required standard error of estimation of the median demand. We denote the standard error due to the limited sample size by $\delta_{U,\hat{Y}|X}$. This is the epistemic uncertainty (U) in the estimation of median demand $\hat{Y}$. There are additional sources of uncertainties in the estimation of the seismic demand of structures. We have focused only on the uncertainty in the demand estimation that is introduced by the limited number of analyses. For perspective we will consider here in addition the uncertainties in demand estimation due to the variabilities in the properties of a structure and the variabilities in the mathematical representation or modeling of a structure. We will recommend here a practical number of analyses based on the typical levels of these uncertainties. There is no reason to use a large number of records to reduce the uncertainty introduced by the limited sample size if the other uncertainties become dominant.

Uncertainties due to Limited Sample Size: As described before (see Chapter 2), the standard error of estimation of the median damage measure $\hat{Y}$ due to limited sample size is approximately equal to $\delta_{R,Y|X}/\sqrt{n}$, where $\delta_{R,Y|X}$ is the random (R) record-to-record dispersion of that damage measure Y given an intensity of ground motion X, such as S_{a1}. For the 5-story building example, if the required standard error of estimation of the median maximum story drift is 15%, the regression error (Table 3.7) indicates that we need 7 nonlinear analyses because $\delta_{R,Y|S_{a1}}$ is found to be close to 0.40 (i.e., $0.40/\sqrt{7} \cong 0.15$). For the 20-story building, the regression error of maximum story drift in Table 4.4 (for no-collapse results) indicates that we require a higher number of records if we follow the simple first-mode spectral-acceleration-based scaling scheme (i.e, $X = S_{a1}$). On the other

hand if we follow a modal-participation-factor-based-weighted-average scaling scheme (i.e, $X = S_a^\star$), regardless of the building type–tall or short–we need a number of records similar to that required for the 5-story building, i.e., around 7 for 15% standard error of estimation of the median drift (based on the no-collapse results of the 20-story building). The latter scaling scheme reduces the dispersion of damage measures ($\delta_{R,Y|S_a} > \delta_{R,Y|S_a^\star}$), and hence we need a smaller number of analyses. Additionally it reduces the bias in demand calculations.

We have also investigated possibilities to reduce the sample size requirements that have been reported by other researchers. These are scaling to spectral acceleration at higher damping and scaling to an average spectral acceleration over a range of frequencies. Although we get (somewhat) lower dispersion in response from these schemes for the structures considered in this study, we have concluded that this further reduction is in general not important for most practical purposes. Although we have observed in Appendix E that we get quite a significant reduction by using 20% damped spectral acceleration, this observation deserves more study for different practical structures. The highly damped spectral accelerations might be a practical intensity measure if the attenuation results were available at higher dampings as well. Additional studies will help to determine whether the proposed schemes or other as yet unknown schemes for scaling improve substantially the estimation of the median damage measure. We have shown that $\delta_{R,Y|X}$ is an approximate way to measure the effectiveness of the above proposals (provided always the proposed scheme has been shown to be unbiased). We have addressed these questions in detail in Chapter 2 and in Appendix E.

Additional Uncertainties in Physical Properties of Structures: So far we have calculated the seismic demand of structures using the mean (or "best estimate") structural properties. There are additional uncertainties in the estimation of demand due to the uncertainties in structural properties. We denote this uncertainty by $\delta_{U,Y|X-prop}$. This problem has been looked at by several investigators using Monte-Carlo studies. We cite here some recent examples for nonlinear cases. Song (1998) considered the uncertainties in Young's modulus, shear modulus, yield strength of beams and columns, shear strength in panel

zones and structural damping in nonlinear seismic analysis of ductile frame structures. He observed no substantial increase in the variabilities of global drift or maximum interstory drift (at a given spectral acceleration X) compared to the same results based on simply the mean value of those member properties (i.e., $\delta_{U,Y|X-prop}$ is small compared to $\delta_{R,Y|X}$). Cornell and Luco (1998) also made a similar observation for the uncertainty in the fracture model of connection elements in non-ductile SMRF's. Sues et al. (1985), however, observed a significant increase in the variabilities of story drift of a 4-story steel frame and a 7-story concrete building from records generated from a filtered Gaussian random process. The variabilities of local damage measures due to the uncertainties in physical properties need to be investigated in future. Wen (1993) also included variabilities in live load on structures for response calculations and he observed that compared to the randomness in structural response due to seismic loading, the additional variability in response due to the variability of other loadings is not important. If we expect a substantial increase in the uncertainty of damage measures for any specific structure, we can relatively easily include that effect in demand calculations.

Effect of Modeling Uncertainties: In this study we have considered a simple center-line model to represent the 2-D moment-resisting frames. We can improve representation of structures by introducing a more realistic model such as that reported elsewhere (Gupta, 1999 and Attalla, et al., 1994). This model will imply at least a certain bias in the demand results that are reported in this study. It is, however, reported by Gupta (1999) that the improved representations he considered did not necessarily change the dispersion of damage measures for a 3-story, a 9-story and a 20-story structure at a Los Angeles site. The required number of analyses predicted in this study may therefore be equally valid for better representations of structures. Nonetheless the facts that the results depend systematically on the model and that we are unsure about the "exact model" mean we must admit to a resulting uncertainty, $\delta_{U,Y|X-model}$, in our results.

Studies of the sensitivity of results to models help to quantify this uncertainty. It depends of course on how much we "push" the models; for example, most of the models

become less reliable as the displacements become larger. Studies of seismic safety of nuclear power plants and offshore structures have used quantitative estimates of such modeling uncertainties in practice. See, for example, DOE-1020 (1994), Kennedy, et al. (1980), Kennedy and Ravindra (1984), ISO 13819 (1997), Sues, et al. (1985), and Bea (1996). Numbers such as, for example, 15 to 20% are suggested in those cited documents for drift levels in the range prior to major strength degradation.

The total (epistemic) uncertainty in the estimation of demand of a structure is

$$\delta_{U,Y|X} = \sqrt{\frac{\delta^2_{R,Y|X}}{n} + \delta^2_{U,Y|X-prop} + \delta^2_{U,Y|X-model}} \tag{6.1}$$

Suppose that the total uncertainty in the estimation of nonlinear demand due to uncertainty in modeling and physical properties is around 30% (as suggested in ISO 13919, 1997, for offshore structures, or in DOE-1020, 1994, and EPRI, 1991, for nuclear structures). In that case if we accept the 15% uncertainty in the estimation of median demand introduced by limited sample size ($\delta_{U,\hat{Y}|X} = 0.15$), the total (epistemic) uncertainty, $\delta_{U,Y|X}$, in the estimation of demand is $\sqrt{0.30^2 + 0.15^2}$ or 0.34. Hence if we use the first-mode-spectral-acceleration-based scaling scheme for single-frequency dominated structures and the modal-participation-factor-based, weighted-average-spectral-acceleration scaling scheme for multi-frequency dominated structures, the total uncertainty in the estimation of demand is around 34% if we carry out structural analyses for seven different records at the target intensity level. The total uncertainty is around 36% if we carry out only five analyses (when $\delta_{U,\hat{Y}|X}$ has been permitted to increase to 0.20).

We will recommend below a number of procedures for demand calculations for different cases of scenario earthquakes and for different types of structures. These recommendations should be accepted subject to the reservations described at the beginning of this chapter.

6.1.5 Recommended Procedure for M-R Scenario Earthquake Case

In the case of M-R scenario earthquake we have been given information about the

magnitude M and the distance R of the design earthquake (e.g., the MCE in FEMA-273). As shown in Chapters 2 and 3, if we carry out nonlinear analysis of a structure by selecting the as-recorded accelerograms from an M-R bin ("direct analysis"), we will get a very large dispersion in nonlinear demand results, e.g., higher than 70%. Therefore we will need a large number of analyses to estimate the median demand with a specified accuracy ($\delta_{U,\hat{Y}|X} \approx 0.15$). We have concluded that an efficient and accurate (unbiased) method of the estimation of median damage is to scale the records to the median intensity level of the selected bin of records. We have concluded in Chapters 2, 3, and 4 that the spectral acceleration at or near the first-mode frequency is an efficient intensity measure for single-frequency dominated structures, and that an efficient intensity measure for multi-frequency dominated structures is a weighted-average spectral acceleration. The median spectral acceleration for a given M and R can be accurately predicted from the conventional attenuation results. In this procedure we will require less than 25% of the number of records and nonlinear analyses as required for direct analysis.

6.1.6 Recommended Procedures for the Case of Response-Spectrum-Based Scenario Earthquake

In the case of response-spectrum-based scenario earthquake, the design ground motion is characterized by a response spectrum spectrum, for example, a spectrum based on a particular M-R earthquake, or a uniform hazard spectrum (UHS) obtained from PSHA. The former case can be treated as above in Section 6.1.5. The latter case is more challenging because we do not have a unique M and R of the earthquake. In the latter case, one needs to decide which M-R records one should select from any catalogue of records for nonlinear analysis. We have observed that, conditioned on the first-mode spectral acceleration, nonlinear structural displacement-based responses do not depend substantially on the magnitude, distance, or duration of records. (Note that we have not considered any degrading system in the case studies. The response of this system might show some dependence on duration of records as well.) We conclude therefore that for most nonlinear structural analyses one can select records from a wide range of magnitude and distance events without

much concern (a few exceptions are reported in Appendix E). For example we have observed that the median maximum story drift of the 5-story building changes only about 10% per unit magnitude. Hence although a wide range of magnitude and distance pairs may contribute to the total risk, we can safely select records from any reasonable magnitude and distance pairs to get the structural response characteristics due to all possible events at a site. Nonetheless one may well want to use for guidance (in selecting the magnitude range) the disaggregated hazard results (McGuire, 1995 and Bazzurro and Cornell, 1999). These are strictly appropriate only for linear oscillators of course. To the degree that a structure is single frequency dominated and to the degree the "equal-displacement" rule applies, these linear-oscillator-based disaggregation remain useful.

Before analysis we have to scale the selected records to the intensity level as specified by the design spectrum to get the median response given that intensity level. As discussed before, we should scale the records to the elastic-first-mode spectral acceleration for single-frequency dominated structures and to the modal-participation-factor-based, weighted-average spectral acceleration for multi-frequency dominated structures.

Further investigation is needed to determine whether the above observations are valid for other building types (e.g., concrete frame, braced frame) and other framing types (e.g., irregular in plan and in elevation).

Although current building code procedures require only that one estimate the demand at a given specified intensity level, one might also be concerned about the variability of response at that intensity level. In that case one typically calculates the 84% response (as specified, for example, in DOE-1020). We have shown in Chapter 2 two procedures–a simple procedure, and a more accurate and involved procedure–for the calculation of 84% response from the information of the variability of structural response given an intensity level and the variability of that intensity.

6.2 Demand-Hazard Estimations

In most current code procedures we calculate the seismic demand of a structure at a

given spectrum or a scenario earthquake, and compare the demand results with an allowable limit specified in the guidelines. But this procedure ignores the record-to-record variability ($\delta_{R,Y|S_a}$) in structural response. In this study (described in Chapters 3 and 4) we have combined the variabilities in structural response and ground motion. We calculate in this process the probability of exceedance of any damage level, i.e., the demand hazard. We will recommend here a number of efficient and accurate procedures for the calculation of the demand hazard. First we will recommend the procedure for the simple case when the likelihood of the collapse of structures is negligible, and subsequently we will consider the case when the likelihood of the collapse of structures is high at the target damage level. We will additionally calculate the variability of the estimation of the demand hazard. This calculation will help to determine the number of analyses required for a certain accuracy in the estimation of demand hazard.

6.2.1 Recommended Procedure When the Likelihood of Collapse is Negligible

As described in Chapter 3, we estimate the demand hazard of a structure by combining the information from PSHA and nonlinear structural analysis. We have considered a 5-story building for illustration of the procedure when the likelihood of the collapse of structures is negligible at the demand level of interest. Recall that collapse is defined in Chapter 4 as the non-convergence of the numerical algorithm at high levels of deformation. This non-convergence implies an excessive deformations in structures. The demand hazard in this case can be estimated from a simple, explicit equation (Equation 3.25). It is

$$P(Y > y) \;=\; H[(y/\alpha)^{\frac{1}{\beta}}] \cdot e^{\frac{1}{2}\left(\frac{K_1 \cdot \delta_{R,Y|Sa}}{\beta}\right)^2} \tag{6.2}$$

where α and β are the regression coefficients in the regression equation, $Y = \alpha \cdot (S_a)^{\beta} \cdot \delta_{R,Y|Sa}$, which relates a damage measure to S_a, $\delta_{R,Y|Sa}$ is the dispersion of response (i.e., damage or demand) given S_a, $H(\cdot)$ is the seismic hazard function, K_1 is the (local) slope of the hazard function in log-log space, and $\delta_{R,Y|Sa}$ is the dispersion of response given S_a.

We follow the steps given below to calculate the parameters of the above equation for demand-hazard calculations:

1. Select randomly a number of records, n. By "randomly" we mean here that this selection need not be a formal exercise; one does not need to preselect records based on some criterion such as the shape of the record's response spectrum. Some of the limitations of this random selection process are indicated in Section 6.1.6. The selected records can be scaled to two different intensity levels so that the results bracket the allowable damage y. Alternatively, we can consider a number of as-recorded accelerograms from a catalogue in such a way that on average the structural damage is close to the target allowable damage y (these are called "direct" results). In this case, for large values of y one may need to scale upward some or all the records. Studies in Chapters 2, 3, and 4, and also in Appendix E have demonstrated the validity of scaling records to higher S_a levels. The appropriate range of S_a for a desired range of y values, however, requires some judgment and/or some trial analyses. For reasons discussed above (Section 6.1.6) one does no need be too concerned about the magnitudes and distances of events causing these records. This conclusion, which is based on the magnitude and distance sensitivity studies in Chapters 2, 3, and 4, and Appendix E, and on the fact that site hazard is seldom dominated by a single M-R pair, is not necessarily consistent with the current practice. It therefore deserves more verification for other structural systems in the future.

   If one is interested in evaluating the performance of a structure at multiple levels (e.g., the immediate-occupancy and the collapse-prevention performance level), then the range of response measures should be wide enough to cover all the performance levels. This can be achieved by scaling the records to a number of intensity levels or by choosing the range of as-recorded ground motion to be broad enough to cover the entire demand range.

2. Calculate the regression coefficients α and β by fitting a regression model ($Y = \alpha S_a^{\beta} \varepsilon_R$) to the results we have obtained in the previous step from nonlinear analysis of a

structure. The regression error gives us an estimate of the conditional dispersion of the damage measure, $\delta_{R,Y|Sa}$. This is the record-to-record variability of the nonlinear structural response, i.e., the randomness (or "aleatory uncertainty") of the nonlinear response conditioned on the first-mode spectral acceleration.

3. Obtain the spectral acceleration hazard, $H(s_a)$, from the conventional PSHA results (e.g., from a site-specific study or from a map such as those at the USGS web site http://geohazards.cr.usgs.gov/eq/).

4. Obtain the slope of the hazard curve in log-log space, K_1, by fitting a function, $H(s_a) = K_0 \cdot (s_a)^{-K_1}$, to the hazard results in the neighborhood of the required spectral acceleration, $s_{a,y} = (y/\alpha)^{\frac{1}{\beta}}$.

5. Calculate the probability of exceedance of any damage level, $P(Y > y)$, from Equation 6.2 or by numerical integration of Equation 3.19 for one or multiple levels of y. Examples can be found in Chapters 3 and 4 (e.g., Figure 3.15).

We have also found in Chapter 3 that at low-intensity levels (for example, at the immediate-occupancy performance level) for normalized hysteretic energy (NHE) and for beam plastic rotation, a polynomial regression model ($Y = \alpha + \beta_1 S_a + \beta_2 S_a^2 + \varepsilon_R$) works somewhat better than the power-law fit adopted in this study. If we adopt this model or any other functional form, we have to do a simple numerical integration for demand-hazard calculations instead of using the explicit Equation 6.2.

The steps and conclusions above are strictly valid for displacement-based demands and displacement-dominated damage indices, such as the Park-Ang damage index (Section 2.3), when the typically reported values of the parameter β of 0.20 or less are used. As we have seen in Chapter 5 strongly cumulative measures such as NHE may require consideration of, for example, magnitude or duration dependence in addition to the spectral acceleration at about the elastic-first-mode frequency.

Required Number of Analyses–Consideration of Uncertainties in the Demand Hazard

As discussed before, we have focused on the randomness (or record-to-record variability) of the nonlinear response in demand hazard calculations. Up to now we have calculated approximately the required number of analyses for demand calculations using as a basis simply the (epistemic) uncertainty in the estimation of the median demand ($\delta_{U,\hat{Y}|S_a}$) introduced by limited sample size. To put the choice of the number of records in a better perspective we now want to go further and determine the uncertainty in the estimation of the *annual probability of exceedance of a damage measure*, P_{exc}, (or demand hazard) introduced by the limited number of analyses, n. We denote this uncertainty here by $\delta^{P_{exc}}_{U,\hat{Y}|S_a}$. This uncertainty is a function of the level of S_a and n; it increases with the level of S_a and decreases in general with $\sqrt{n}$. One cannot, however, answer the question, "how large should n be" without considering the other epistemic uncertainties. To answer the question of the number of analyses one must consider how large the uncertainty, $\delta^{P_{exc}}_{U,\hat{Y}|S_a}$, may be and how it compares with the other sources of (epistemic) uncertainties. Here we will consider the uncertainties in the estimation of structural response and of ground-motion intensity.

We have found that for the 5-story building if the required standard error of estimation of median story drift (given S_a) is 15%, we need 7 records (e.g., Table 3.7). If, on the other hand, we want to estimate the *story-drift-demand hazard* with a certain accuracy recognizing *only* the uncertainty in the estimation of the (conditional) median demand, $\hat{Y}|S_a$, the required number of analyses can be obtained from Table 6.1. We have denoted this uncertainty in the estimation of demand hazard by $\delta^{P_{exc}}_{U,\hat{Y}|S_a}$. Note that for demand-hazard estimations from Equation 6.2 we have considered the randomness in structural response, but in Table 6.1 we have considered additionally the uncertainty in the estimation of median story drift introduced by limited number of analyses (i.e., considered the effect of $\delta_{U,\hat{Y}|S_a}$ on demand hazard). We have calculated the results in the table by bootstrap replication of the results from Chapter 3 for 66 records, which are scaled to two different intensity levels. In calculating the confidence band of the estimation of P_{exc} we have assumed that

% error in P_{exc} due to limited sample size ($\delta^{P_{exc}}_{U,\hat{Y}\|S_a}$)	65% confidence band of P_{exc} ($\times \hat{P}_{exc}$)	95% confidence band of P_{exc} ($\times \hat{P}_{exc}$)	No. of analyses at the following drift levels			
			5-story		20-story	
			2.5%	5.0%	2.5%	5.0%
10	0.9 - 1.1	0.8 - 1.2	322	471	531	662
25	0.8 - 1.2	0.6 - 1.6	52	76	85	106
50	0.6 - 1.6	0.4 - 2.7	13	19	21	27
100	0.4 - 2.7	0.1 - 7.4	4	5	6	7

Table 6.1: Requirements of the number of nonlinear analyses for the demand-hazard calculation versus the specified tolerable standard error of estimation of the probability of exceedance (P_{exc}) due to (only) uncertainty in the estimation of median demand for limited sample size. We have assumed that P_{exc} is lognormally distributed and the standard error of estimation of P_{exc} decreases with $\sqrt{n}$. We have verified the latter assumption in Figure 6.1. In these examples we have used the same set of records scaled to two different intensity levels to calculate the variability in the estimation of P_{exc} (Sections 3.4 and 4.3). Therefore the number of different records we used was only half the number of analyses.

the distribution of the estimation of P_{exc} is lognormal. So the 65% confidence band of the estimation of P_{exc} is $\hat{P}_{exc} \cdot e^{-\delta} \leq P_{exc} \leq \hat{P}_{exc} \cdot e^{+\delta}$. Table 6.1 implies that for a typical practical sample size of order 10 one must tolerate "one-sigma" uncertainty, which is a factor of about two in the estimation of the demand hazard.

The number of analyses required for the 20-story building at different values of the tolerable standard error of estimation of the demand hazard at the 2.5% story-drift level are indicated in Table 6.1. We observe that the required number of analyses at the same standard error of estimation of P_{exc} is much higher ($1\frac{1}{2}$ to 2 times) for the 20-story building than for the 5-story building. This high value is due to the fact that the slope of the hazard curve is steeper (45% higher) at the site at 0.25Hz than at 1.0Hz and to some extent due to the higher (20%) uncertainty in estimating $\hat{Y}|S_a$ for the 20-story building. Since the required number of analyses we recommend for demand hazard are specific for a central LA site, these conclusions should not be generalized. In particular it is common for hazard curves for lower oscillator frequencies to have lower slopes. The significance of this lower slope will be obvious in the following section.

The variation in the standard error of estimation of the probability of exceedance of maximum story drift (P_{exc}) with the number of analyses at the life-safety and the collapse-prevention performance level are shown in Figures 6.1(a) and 6.1(b). We confirm there that the standard error of estimation of P_{exc} decreases with $\sqrt{n}$. We can also calculate explicitly the uncertainty in the demand hazard due to the uncertainty in the estimation of the median demand, and it is approximately equal to the following (see Jalayer et al., 1999):

$$\begin{aligned} \delta_{U,\hat{Y}|S_a}^{P_{exc}} &= \frac{\delta_{R,Y|S_a}}{\sqrt{n}} \cdot \frac{K_1}{\beta} \\ &= \delta_{U,\hat{Y}|S_a} \cdot \frac{K_1}{\beta} \end{aligned} \tag{6.3}$$

If we use the above relationship to calculate the number of analyses required for the 5-story building at the 2.5% story-drift level for 10% standard error of estimation of P_{exc}, we find that we need 342 records. This result is very close to the results in Table 6.1, which are obtained by the bootstrap resampling technique.

We observe in Equation 6.3 that the uncertainty in demand-hazard estimation introduced by limited sample size is dependent on the slope of the hazard curve as well. Hence unlike in median demand estimations, where the uncertainty ($\delta_{U,\hat{Y}|S_a}$) is dependent on the characteristics of the structural response ($\delta_{R,Y|S_a}$), the uncertainty in demand-hazard estimations ($\delta_{U,\hat{Y}|S_a}^{P_{exc}}$) is dependent on the characteristics of structural response ($\delta_{R,Y|S_a}$ and β) and on the slope of the hazard curve (K_1). So the number of analyses we recommend here is very much specific to the site. For example, if we use DOE-1020 (1994) suggested hazard slopes, we find that if the structural response characteristics are the same at Eastern US and at Western US sites, then we will require around 50% higher sample size for the demand-hazard estimation of structures at Western U.S. sites because of the steeper hazard slope at those sites.

Figure 6.1 and Equation 6.3 indicate the uncertainty in the estimate of the demand hazard ($\delta_{U,P_{exc}}$) due to only the limited sample size of nonlinear results. We have mentioned in Section 6.1.4 that there are other uncertainties, e.g., uncertainty in physical properties

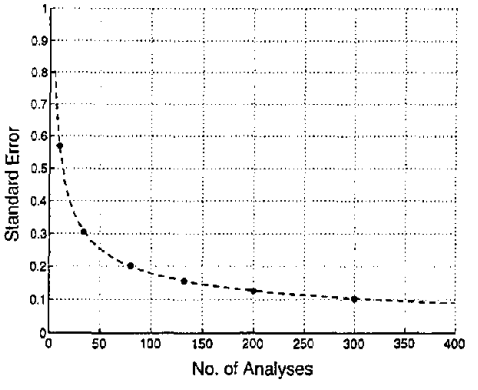

(a) 5-story SMRF at the life safety performance level (2.5% maximum interstory drift)

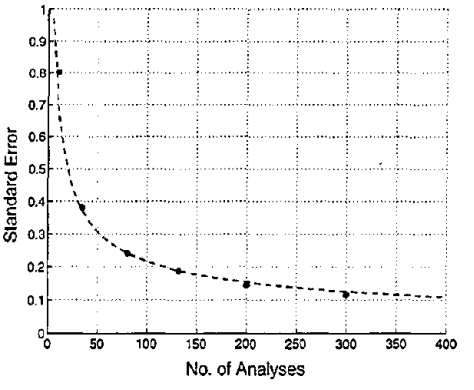

(b) 5-story SMRF at the collapse prevention performance level (5% maximum interstory drift)

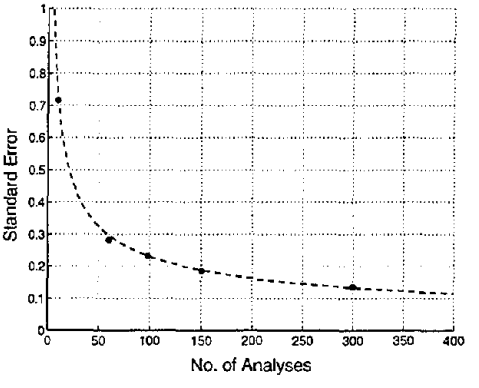

(c) 20-story SMRF at the life safety performance level (2.5% maximum interstory drift)

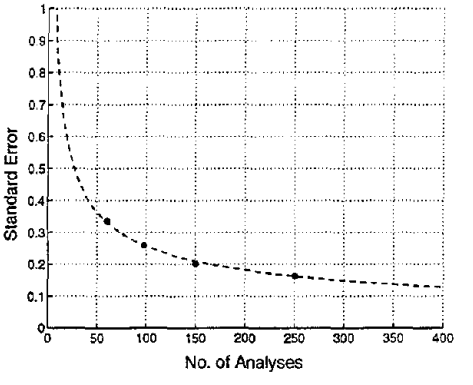

(d) 20-story SMRF at the collapse prevention performance level (5% maximum interstory drift)

Figure 6.1: Variation of the standard error of estimation of the demand hazard ($\delta^{P_{exc}}_{U,\hat{Y}|S_a}$) with number of analyses (or nonlinear runs), n, at different performance levels. We have calculated these results by bootstrap resampling of the sample of results in Chapter 3 for the 5-story building and in Chapter 4 for the 20-story building. These resampling results are shown by the dots. We have drawn the dotted lines by assuming that demand hazard decreases with $\sqrt{n}$. These lines are drawn in such a way that they match the results at the original sample size. The number of records in the original sample is 66 for the 5-story building and 50 for the 20-story building. Because in these applications the records were scaled to two different intensity levels in order to estimate the variation of damage with spectral acceleration, the required number of records is half the number we predict from this figure.

of structures, uncertainty in modeling of structures, etc., in the estimation of drift and the uncertainty has been estimated in Equation 6.1. In addition to those uncertainties in the demand-hazard calculations, there is also uncertainty in the PSHA results ($\delta_{U,H(s_a)}$). When we consider all the (epistemic) uncertainties in demand hazard calculations, we get the following (see Jalayer et al., 1999, for details):

$$
\begin{aligned}
(\delta_{U,P_{exc}})^2 &= \left(\frac{K_1}{\beta}\right)^2 \cdot \left(\delta^2_{U,\hat{Y}|S_a} + \delta^2_{U,Y|S_a-prop} + \delta^2_{U,Y|S_a-model}\right) + \delta^2_{U,H(S_a)} \\
&= \left(\frac{K_1 \cdot \delta_{U,Y|S_a}}{\beta}\right)^2 + \delta^2_{U,H(S_a)} \qquad (6.4) \\
&= (\delta^{P_{exc}}_{U,Y|S_a})^2 + (\delta_{U,H(S_a)})^2 \qquad (6.5)
\end{aligned}
$$

A typical value of $\delta_{U,H(s_a)}$ for a site in California is about 1.0 as suggested in IS0 13819, 1997. A typical value of uncertainty in the estimation of $\hat{Y}|S_a$ due to uncertainties in modeling and physical properties ($\delta_{U,Y|S_a-M+P}$) is about 0.30 (see Section 6.1.4). Note that engineers in nuclear industry consider the randomness (R) and uncertainty (U) in demand-hazard estimations (see, for example, Kennedy, et al., 1980, where randomness and uncertainty are considered to estimate the conditional probability of failure). Recently in HAZUS (1997) researchers also considered uncertainty and randomness in earthquake loss estimations. We can determine from Equation 6.5 the total uncertainty in the estimation of P_{exc} due to uncertainty in the estimation of hazard, in the modeling of structures, and in the physical properties of structures. It is

$$
\begin{aligned}
\delta^2_{U,P_{exc}} &= \left[\frac{K_1 \cdot \delta_{U,Y|S_a-M+P}}{\beta}\right]^2 + \left[\delta_{U,H(S_a)}\right]^2 \\
&= \left(\frac{3.5 \cdot 0.3}{1.0}\right)^2 + 1 \;=\; (1+1) \;=\; (1.4)^2
\end{aligned}
$$

If there were no uncertainty in the estimation of the median $\hat{Y}|S_a$ due to the limited sample size, i.e., $\delta_{U,\hat{Y}|S_a} = 0$, then the one-sigma confidence band of P_{exc} would be $\hat{P}_{exc} \cdot e^{\pm\delta_{U,H(s_a)}}$ or $\hat{P}_{exc} \cdot e^{\pm 1.4}$, or $\{0.2\hat{P}_{exc}\ ;\ 4\hat{P}_{exc}\}$. But if we adopt for example $\delta^{P_{exc}}_{U,\hat{Y}|S_a} = 0.50$, then the confidence band of P_{exc} will change to $\hat{P}_{exc} \cdot e^{\pm\sqrt{(\delta_{U,H(s_a)})^2+(\delta^{P_{exc}}_{U,Y|S_a-M+P})^2+(\delta^{P_{exc}}_{U,\hat{Y}|S_a})^2}}$ or

% Error ($\delta_{U,\hat{Y}\|S_a}^{P_{exc}}$)	65% confidence band ($\times \hat{P}_{exc}$) $\hat{P}_{exc} \cdot e^{\pm[(\delta_{U,H(S_a)})^2+(\delta_{U,\hat{Y}\|S_a-M+P}^{P_{exc}})^2+(\delta_{U,\hat{Y}\|S_a}^{P_{exc}})^2]^{\frac{1}{2}}}$	Required sample size for different values of $\delta_{R,Y\|S_a}$		
		0.3	0.4	0.5
0	0.23 - 4.26	∞	∞	∞
10	0.24 - 4.19	111	196	307
25	0.23 - 4.26	18	32	49
50	0.22 - 4.54	5	8	13

Table 6.2: 65% confidence-band width in the estimation of P_{exc} due to different values of $\delta_{U,\hat{Y}\|S_a}^{P_{exc}}$ and the representative required sample sizes to meet these objectives of error. We have assumed here that the standard error of estimation of $H(s_a)$ is 1.0, which is a typical value for a site in California. We have also assumed that the uncertainty in the estimation of $Y|S_a$ due to uncertainties in modeling and physical properties ($\delta_{Y|S_a-M+P}$) is 30% and that $\frac{K_1}{\beta}$ is 3.5.

$\hat{P}_{exc} \cdot e^{\pm\sqrt{1.43^2+0.5^2}}$, or $\hat{P}_{exc} \cdot e^{\pm 1.51}$ or $\{0.2\hat{P}_{exc}\ ;\ 4.5\hat{P}_{exc}\}$. Therefore because of the large uncertainty in the PSHA, in the modeling and in the physical properties of structures, the change in the 65% confidence band width of the estimation of P_{exc} is negligible ($< 10\%$) due to 50% uncertainty in the estimation of P_{exc} introduced by the limited sample size. In Table 6.2 we show the confidence-band width in the estimation of P_{exc} for different values of uncertainties of $\delta_{U,\hat{Y}\|S_a}^{P_{exc}}$. Note that for the 5-story building ($\frac{K_1}{\beta} \cong 3.4$) if $\delta_{U,\hat{Y}\|S_a}^{P_{exc}}$ is equal to 50% at the 2.5%-drift level, then we have 15% uncertainty in the estimation of the median drift demand ($\delta_{U,\hat{Y}\|S_a} = 0.15$) due to limited sample size (from Equation 6.5). We conclude that one can conservatively adopt for the required number of analyses the numbers indicated in the third row of Table 6.1 (implying an increase in the demand-hazard confidence band by 10%). Values in the fourth column of Table 6.1, i.e., values of about 5 or 6, imply quite reasonably an increase in the confidence band. Again we point out that this recommendation is specific to the site we have considered in our case studies via K_1.

We observe in Table 6.1 the increase in sample size at the higher drift-demand level. But we have higher uncertainties in the estimation of $H(s_a)$ at the lower probability of exceedance of the intensity of ground motion. We can, therefore, consider higher uncertainties in the estimation of $\hat{Y}|S_a$ at high demand levels. This will give similar total (epistemic)

uncertainties in the estimation of P_{exc} (i.e., a similar $\delta_{U,P_{exc}}$) at all the demand levels. This allowance of higher uncertainties at higher demand levels will make possible to use a very similar number of analyses at all the demand levels.

6.2.2 Recommended Procedure When the Likelihood of "Collapse" of Structures is High

The demand-hazard calculations are somewhat complicated when the likelihood of "collapse" of structures is high. Here we will recommend a procedure for demand hazard calculations based on the experience gained in Chapter 4. We will also recommend some simplified procedures for demand-hazard calculations. We have illustrated those procedures through an example problem of a 20-story building for a central Los Angeles site in Chapter 4. We will also recommend the number of analyses required to estimate the demand hazard within a certain confidence band.

We can calculate the demand-hazard of a structure when the likelihood of collapse of that structure is high from the closed-form solution given in Appendix F. We can, however, easily carry out numerical integration of Equation 4.21 for the demand-hazard calculations. We have introduced a three-parameter distribution model of response results to consider the collapse results in demand-hazard calculations (Section 4.2.6). The parameters of this model are obtained from regression analysis of the no-collapse results and from binary-regression analysis for all the response results. Regression analysis of the no-collapse results indicates that conditioned on the first-mode spectral acceleration, the response of the 20-story building depends to some extent on the second-mode spectral acceleration as well. We make a similar observation in estimating the probability of collapse of the structure using binary-regression analysis.

The demand-hazard calculation in this case is based on the following steps:

1. Select "randomly" a number of ground-motion records for nonlinear structural analysis. Carry out analysis of the structure for the as-recorded accelerograms or for the accelerograms scaled to certain intensity levels by appropriate scalar factors. The

intensity of the records should be such that the results bracket the target damage measure, y. This step is very similar to the first step of the procedure recommended in Section 6.1.6. See that section for a detailed description of this step.

2. Separate the results into two sets, those that converge (do not "collapse") and those that do not converge (to a "reasonable" response). The latter we term "collapse".

3. Carry out the conventional regression analysis (e.g., maximum story drift on S_a, or better on $S_a^\star$; see below for a description of the latter) of the no-collapse results to estimate α, β and δ_ε.

4. Carry out binary-regression analysis of all the response results to estimate β_C and s_{a0} (defined in Section 4.3.4).

5. Get $H(s_a)$ from the PSHA results.

6. Calculate the demand hazard by numerical integration of Equation 4.21 or from the explicit equation in Appendix F.

We will outline below some simplified procedures for demand hazard calculations when the likelihood of collapse is significant. Note that the demand-hazard results from Equation 4.21 or from Appendix F consider only the randomness (or aleatory uncertainty) of the structural response.

Number of Analyses–Consideration of Uncertainties in Demand Hazard

We are interested in giving guidance on the number of nonlinear analyses required for demand-hazard calculations. Hence we need to calculate the (epistemic) uncertainty of the demand-hazard results due to the uncertainty in estimating $\hat{Y}|S_a$ due to a limited number of analyses. The number of analyses of the 20-story building at 5% interstory drift for different standard errors of estimation of the probability of exceedance ($\delta^{P_{exc}}_{U,\hat{Y}|S_a}$) is indicated in Table 6.1. We have calculated these results by bootstrap replication of the response results from Chapter 4 for 50 records, which are scaled to two different intensity levels. For the

20-story structure we observe that the uncertainty in estimating P_{exc} due to limited sample size at the 5% interstory drift is very close the results predicted by Equation 6.3. This is because the likelihood of collapse of the 20-story structure is low at that drift level. But the uncertainty in estimating the demand hazard at high-drift levels, at which the likelihood of collapse of a structure is very high, is approximately equal to $\delta_{U,P_{C|S_a}}$. Note that at high-drift levels the (epistemic) uncertainty of the demand-hazard estimations of the 20-story building depends only on the characteristics of the structure ($\delta_{U,P_{C|S_a}}$), but for the 5-story structure it depends both on the characteristics of the structure ($\delta_{U,Y|S_a}$) and also on the slope of the hazard curve (K_1). Hence when the likelihood of the collapse of structures is very high, the uncertainty in the estimation of the demand hazard is the following:

$$\delta^2_{U,P_{exc}} = \delta^2_{U,\hat{P}_{C|S_a}} + \delta^2_{U,P_{C|S_a-prop}} + \delta^2_{U,P_{C|S_a-model}} + \delta^2_{U,H(S_a)} \tag{6.6}$$

where $\delta_{U,\hat{P}_C}$ is the uncertainty in the estimation of the conditional median probability of collapse ($\hat{P}_{C|S_a}$) due to limited sample size, $\delta_{U,P_{C|S_a-prop}}$ is the uncertainty in the estimation of $P_{C|S_a}$ due to uncertainties in the physical properties of a structure, and $\delta_{U,P_{C|S_a-model}}$ is the uncertainty in the estimation of $P_{C|S_a}$ due to uncertainties in the modeling of a structure.

As we suggested before for the 5-story building, we suggest here as well that for all practical purposes we can use the number of analyses in the third (or fourth if a lower confidence or higher $\delta_{U,P_{exc}}$ is acceptable) row of Table 6.1 if the standard error of estimation of the seismic hazard is of the order of one ($\delta_{U,H(s_a)} = 1$). We also point out here that these numbers are to some degree site dependent; these conclusions cannot yet be generalized.

Simplified Demand-Hazard Calculation

The demand-hazard calculation from Equation 4.21 or from Appendix F is somewhat complicated. We have, however, shown in Section 4.4 that we can simplify this calculation procedure and still get a quite accurate solution. This simplification is based on the following simple calculations:

- Calculate the demand hazard from Equation 6.2 based on no-collapse results only.
- Calculate the lower-bound of the demand hazard based on only the probability of collapse (Equation 4.25). This requires the results of binary-regression analysis (described in Section 4.3.4).
- If the first result is lower than the lower-bound probability, use the lower-bound probability.

The advantage of this procedure is that it is based on two simple, explicit equations (Equations 6.2 and 4.25) and also gives us quite accurate results.

Another Simplified Procedure for Demand-Hazard Calculation

We have also shown (Section 4.4.1) that we can use Equation 6.2 directly for demand-hazard calculations at all damage levels. In this case we need to calculate the parameters of the equation from the following results by scaling the records to two intensity levels close to the region of interest:

- Calculate the slope, β, which in this case is an equivalent slope. We calculate the slope from the median damages at two intensity levels in the region of interest.

$$\beta_{eq} = \frac{(\hat{y}_1 - \hat{y}_2)}{(s_{a,1} - s_{a,2})}$$

  The median damage in this case can be estimated by counted median (Section 4.2.3) or by fitting the parameter distribution model introduced in Section 4.2.6.

- The dispersion of conditional damage, $\delta_{R,Y|S_a}$, is the average of the equivalent dispersions (Equation 4.2) at those intensity levels. Note that we have obtained the equivalent dispersions of the sample of results at those intensity levels by bootstrap replication of the sample of results (described in Section 4.2.3).
- Calculate the other parameters as recommended in Section 6.2.1.

The results from this approach also match quite well the more accurate numerical integration results.

6.3 More Efficient Demand-Hazard Calculations for Multi-Frequency Dominated Structures

We have also observed in Chapter 4 that for longer period, taller structures the (epistemic) uncertainty in the estimation of median damage at a given intensity is reduced significantly when the intensity measure of ground motion is based on a weighted-average spectral acceleration ($S_a^\star$). This is because we found that for the 20-story building the uncertainty in estimating the median story drift based on the weighted-average spectral acceleration, $\hat{Y}|S_a^\star$, is around 20% lower than the estimation of median story drift based on the first-mode spectral acceleration (i.e., $\delta_{Y|S_a^\star} = 0.8\delta_{Y|S_a}$). This implies a 35% reduction in the required number of nonlinear analyses. We have in addition found in Section 4.4.2 that the demand-hazard results based on the weighted-average spectral acceleration are also *more accurate* (closer to the 2-D PSDA results in Chapter 5) than the results based on the first-mode spectral acceleration. The only drawback in this approach is that the weighted-average-spectral-acceleration-seismic-hazard results strictly speaking are structure specific and are at present not as readily available. However seismologists can easily generate these results with the current PSHA software and with attenuation results if structural engineers request it.

6.4 2-D versus 1-D PSDA

We have seen in Chapters 3 and 4 that conditioned on spectral acceleration close to the first-mode frequency the demands of the 5-story and the 20-story structures may depend on some additional parameters. These additional parameters may be seismological parameters, e.g., M and R, and/or record parameters, e.g., duration (T) and higher frequency spectral

acceleration (S_{a2}). In Chapter 5 we have considered those additional parameters in *demand-hazard* calculations. This calculation requires the joint-hazard results from 2-D PSHA for spectral acceleration close to the first-mode frequency and the additional parameter. Although at present the joint-hazard results are not readily available, we have shown in Chapter 5 how we can generate those results. The advantages of this calculation are that sometimes we can get more accurate results and that we may require a smaller number of expensive nonlinear analyses for demand hazard estimations with a certain accuracy.

We observed in Chapters 3 and 4 that considering M, R, and T, in addition to S_{a1}, does not reduce significantly the required number of analyses. These additional parameters do not change substantially the demand prediction based on regression results against S_{a1} alone. We found in Chapter 5 that consideration of M, R, or T in addition to S_{a1} does not change the estimation of the demand hazard with respect to that obtained from the regression results against only S_{a1}. The calculation of the demand hazard based on those additional parameters requires extra effort, but can be computed from the available informations. We need 2-D regression results of structural responses against those additional parameters and the disaggregation of the conventional PSHA results for the calculation of the 2-D mean-rate density function. This density function for M or R and S_{a1} can be calculated directly from the standard disaggregation of hazard results. The calculation of the mean-rate density function for T and S_{a1} requires the disaggregation results as well as the attenuation results for the duration of records.

We observed in Chapter 4 that the number of analyses required for a target accuracy of median drift demand is much higher for the 20-story building than for the 5-story building when demand prediction is based on S_{a1} only; the required number of analyses is, however, similar for both the buildings when the demand prediction is based on S_{a1} and S_{a2} (here we are considering only the regression results conditioned on no collapse of the 20-story building). We take advantage of this more accurate demand estimation through the 2-D demand-hazard calculation. The calculation of demand-hazard based on S_{a1} and S_{a2} needs a separate 2-D PSHA calculation (disaggregation results are not sufficient because of the correlation between S_{a1} and S_{a2}). The practical drawback of this approach is that

the 2-D PSHA results are not yet readily available. We have shown that if the likelihood of collapse of a structure is negligible at the spectral acceleration required to induce the allowable drift, we can calculate the 2-D demand hazard from a simple, explicit solution. We find that the 2-D demand-hazard results are somewhat different from the 1-D (based on regression results against only S_{a1}) results. We conclude that if structural responses depend also on S_{a2} (conditioned on S_{a1}), we may not get the same results from 1-D and 2-D PSDA unless the conditional distribution of $S_{a2}|S_{a1}$ within the data set used to calculate response and regressions matches that expected at the site.

6.4.1 Demand Hazard Based on Weighted-Regression Results

We have seen in Chapter 5 that the 1-D PSDA results can be improved significantly if one considers the effect of the additional parameter, S_{a2}, by using the weighted-regression results instead of the conventional 1-D regression results (based on S_{a1}). In using the weighted-regression results in demand-hazard calculations we do need, however, the 2-D PSHA results to calculate the weights, although we do not need to carry out the 2-D PSDA integrations. This procedure thus allows us to use Equation 6.2 (if the probability of collapse of a structure is low), or the previously described simplified procedures. In this procedure we have to make the following calculations from the weighted-regression analysis. The rest of the procedure for demand-hazard calculations is similar to the procedures recommended in Section 6.2.1.

- Calculate the conditional distribution of $S_{a2}|S_{a1}$ for a site from the 2-D PSHA results ($f_{S_{a2}|S_{a1}}$).
- Depending on the S_{a1} and S_{a2} values of each record, calculate a weight to apply to the result from that record based on the site-specific $f_{S_{a2}|S_{a1}}$ (Equation 5.17).
- Evaluate α, β, and δ_ε from weighted-regression analysis.

An alternative to this might be consideration of different sets of records at different

intensity levels so that the conditional distribution $f_{S_{a2}|S_{a1}}$ of the records matches approximately that of the site. The success of the weighted regression analysis suggests that, even for a demand calculation at a specific intensity level (which is the calculation we do in the current code approach), we should select records in such a way that the conditional distribution $f_{S_{a2}|S_{a1}}$ is satisfied at each intensity level. This implies that the sets of records we should use for demand calculation at the collapse-prevention level should be different from those we use for the demand calculation at the immediate-occupancy performance level; the records for demand calculation at the immediate-occupancy performance level will be richer in high-frequency content because at low-intensity levels the contribution to the hazard from the relatively high-frequency rich low-magnitude events is usually higher.

6.5 Future Studies

The recommendations in this chapter and elsewhere in this dissertation are based on results from a number of steel moment resisting building frames that were analyzed for ground-motion records at only stiff soil sites in California. We need the following further studies, which may reveal the exceptions and limitations of the recommendations made in this chapter.

1. For case studies, we have considered only steel SMRF structures. Other building types, such as, shear-wall structures, base-isolated structures, braced-frame structures, etc., should be studied in the future.

2. In this study we have investigated the results from 2-D center-line representation of steel building frames. We also compared those results with the results from some improved representation of structures which consider the effect of (1) shear strength and deformation of joint panel zones, (2) additional stiffness of interior simple frames, (3) additional stiffness of girders due to floor slabs, and (4) additional stiffness from partition walls. The results we have reported in this study are biased compared to

those obtained from those improved representations of structures, but there is not much difference in the dispersion of results. Hence the sample size predicted in this study based on the dispersion of responses from the center-line model does not change much even if we use an improved representation of structures. The professionals in this area, however, have to decide which mathematical representation of structures is more appropriate.

We have to improve further the mathematical representation of structures to get more accurate (unbiased) results. For example, a 3-D model even for regular structures may improve the accuracy of our estimation of nonlinear response. In this case we can use as-recorded ground motion or scale up/down all the components of ground-motion records by a single factor at a site. We can carry out regression analysis of any damage measure against a (geometric) average of the spectral accelerations for the two horizontal components. Because the PSHA results are also in general for a (geometric) average of spectral accelerations, these regression results can be used conveniently to estimate the demand hazard from the conventional hazard results.

3. In this study we have only considered accelerograms recorded in California at stiff-soil sites. The characteristics of near-source records are quite different from those considered in this study, e.g., the major energy of near-source records comes from a small number of pulses, whereas the energy is spread over a wide range frequencies for the records considered in this study. Hence we need further study to verify whether the recommendations are valid for near-source records (see Krawinkler and Alavi, 1998, for some preliminary results from near-source records).

Appendix A

Definitions of Two Sample Statistics: Median and Dispersion

Median

In this study we refer the best estimate or "central value" as the median. We define this estimator as the *geometric mean* which is the exponential of the average of the natural logarithms of the observed values, x_i, of the sample. This can be written as

$$\hat{x} = \exp\left[\frac{\sum_{i=1}^{n} \ln x_i}{n}\right] \tag{A.1}$$

where n is the number of observations.

The geometric mean is a logical estimator of the median, especially if the data are sampled from lognormal distribution (see Benjamin and Cornell, 1970). It is observed that the data in general have asymmetry of their histogram, displaying a longer right-hand tail. The consideration of lognormal distribution for right skewed data is the first choice in science and engineering. For ground-motion estimations, lognormal distribution is nearly a universal choice and we have verified in Appendix C that the nonlinear response of a structure is also lognormally distributed. The other advantage of considering the above estimator of median is that the estimate is "robust" with respect to the estimator of mean for a data

point which is much higher than the others. This characteristic of response data is very common in nonlinear seismic response analysis.

Dispersion

In this study the dispersion measure δ is the standard deviation of the natural logarithms of the data.

$$\delta = \left[\frac{\sum_{i=1}^{n} (\ln x_i - \ln \hat{x})^2}{n-1} \right]^{\frac{1}{2}} \tag{A.2}$$

For smaller values, e.g., 0.3 or less, the above dispersion measure is approximately equal to the coefficient of variation. Under the lognormality assumptions, it is the natural dispersion measure (see Benjamin and Cornell, 1970). The above estimator of dispersion is almost universally used in ground-motion estimation, and because of the advantages described before of considering natural logarithm of data we have adopted in this study the above dispersion measure. We loosely use the term "dispersion" when referring to this parameter in the in the main body of the text.

Appendix B

Details of the 5-Story Structure in Chapter 2 and Its Mathematical Model

We have considered a 5-story, 4-bay steel moment-resisting frame (SMRF) in Chapter 2 (see Searer, 1994, for details). The structure has been designed for A36 steel using LRFD specifications (AISC,1986) and NEHRP provisions for a Los Angeles site. The geometry of the structure is shown in Figure B.1. The size of the members are given in Table B.1. The member properties and loading on the structure are given below.

Modulus of elasticity, E = 29,000 ksi
Modulus of plasticity, E_p = 290 ksi
Yield stress, F_y = 41.6 ksi
Ultimate stress, F_u = 49.9 ksi
Damping ratio = 2%
Roof Load : DL=0.625 kip/ft LL=1.125 kip/ft
Floor Load: DL=1.875 kip/ft LL=1.250 kip/ft
While calculating earthquake loading on the structure, 25% of the design LL was considered

Ext. Column (below col. spl.)	Ext. Column (above col. spl.)	Int. Column (below col. spl.)	Int. Column (above col. spl.)	Roof Girder	Floor Girder
W 14x61	W 14x43	W 18x97	W 18x60	W 24x55	W 18x35

Table B.1: Member Sizes

in the analysis.

Initially, we have developed a 2D-nonlinear finite element model of the structure. We have used a nonlinear beam-column element to model the structural members. The structure has been considered fixed at base. In order to understand the overall behavior of the structure, we have carried out a step-by-step static-nonlinear analysis ("pushover analysis") with the help of the commercial software package CAP (PMB, 1996). In this analysis we have not considered any P-Δ effect. The equivalent static lateral-force pattern on the structure was according to the NEHRP provisions. The results of the pushover analysis are shown in Figure B.2. From these results, we have calculated the equivalent lateral stiffness of each story to develop a simplified spring-mass model of the 2-D structure. The 5-DOF spring-mass model of the structure is shown in FigureB.3. The spring at each floor is idealized by a multi-linear spring as shown in FigureB.3, and the properties of springs are given in Table B.2. These properties are obtained from the results of "pushover analysis" given in Fig B.2. We have used the yield displacements, d_y, which are given Table B.2 to normalize the displacement and energy results. Finally, we have adopted the simplified spring-mass model of the structure for nonlinear dynamic analyses in Chapter 2. This relatively simple model made possible to carry out a large number of nonlinear dynamic analyses with comparatively little computing time.

Story	d_y (in)	St. Drift(%) at Yield	K_1 (k/in)	d_1 (in)	K_2 (k/in)	d_2 (in)	K_3 (k/in)	d_3 (in)	K_p (k/in)
1	1.2	0.8	302	0.8	116	1.2	64	2.2	24
2	1.8	1.2	182	1.2	110	1.8	72	2.7	19
3	1.7	1.1	169	1.1	88	1.7	71	2.4	15
4	1.6	1.0	148	0.9	117	1.6	51	2.4	10
5	1.6	1.0	112	0.9	53	2.2	18	4.0	8

Table B.2: Properties of the equivalent story spring elements

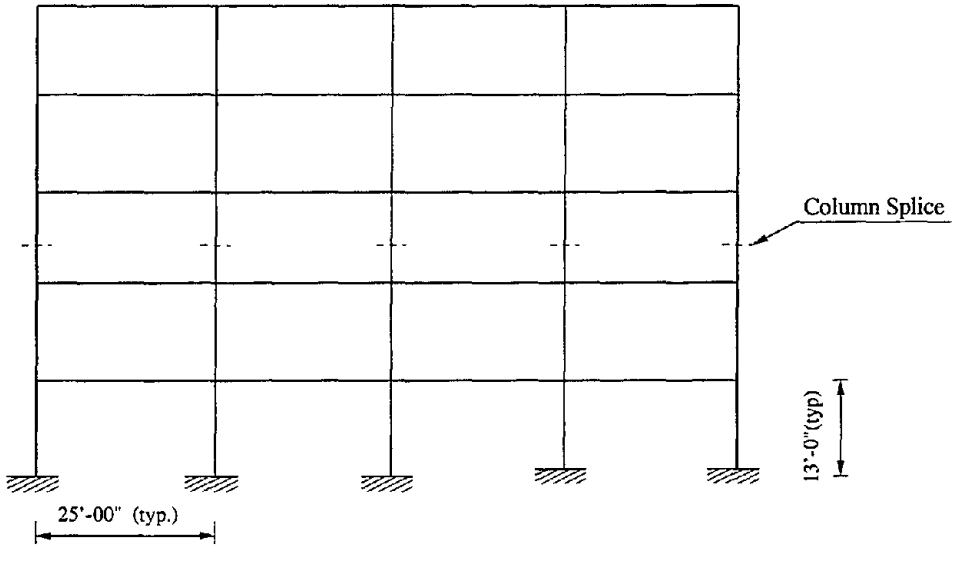

Figure B.1: Geometry of the structure

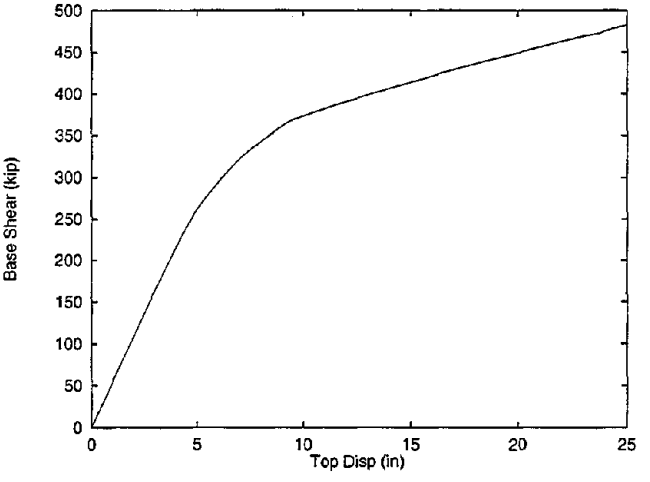

(a) Global

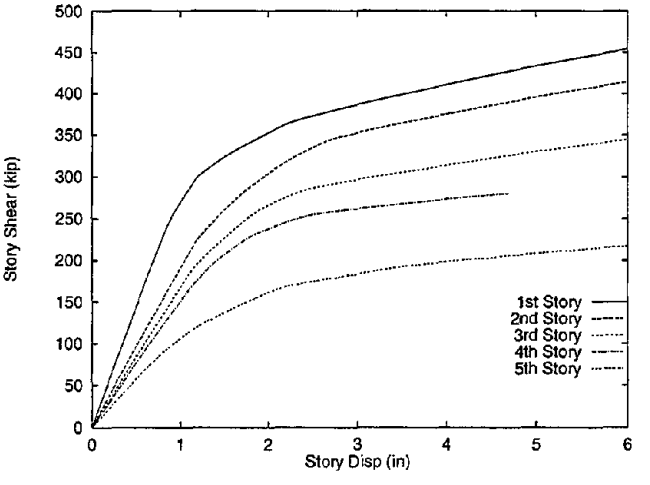

(b) Story

Figure B.2: Load-deformation from pushover analysis

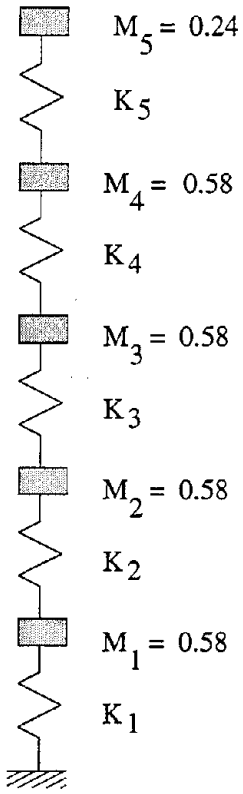

Spring-Mass Model

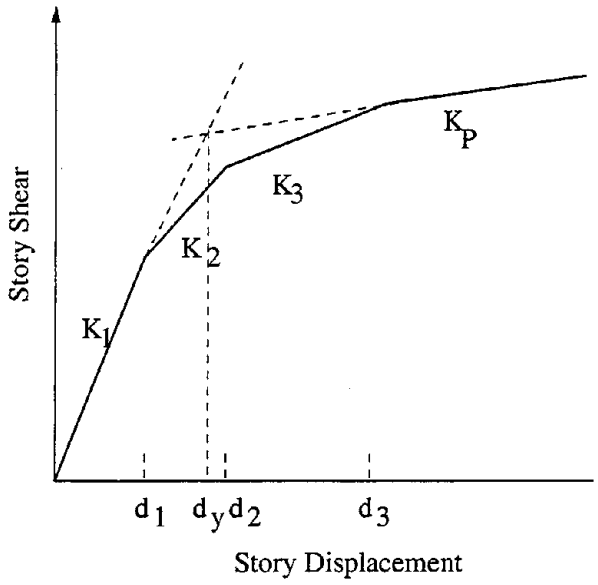

Backbone Curve of a typical story

Figure B.3: Spring-mass model

Appendix C

Probability Distribution of Maximum Inter-Story Ductility Given M and R

It is well established that the distribution of spectral acceleration given M and R is lognormal. However, not much work has been done to verify that the response of a nonlinear structure also follows the same distribution. An underlying distribution is necessary, for example, for the calculations of the 84^{th} percentile demand or for the probabilistic seismic demand-hazard analysis of structures.

A popular way to verify a distribution assumption is to plot the results on probability paper and observe how closely the cumulative frequency curve of the data fits a straight line. The direct and normalized results of the maximum inter-story ductility are plotted on lognormal probability papers (Figure C.1) along with the fitted lognormal distribution. It is observed that the data fit quite well to a straight line, but there appears to be a systematic deviation in the upper tail of the distribution. The lognormal distribution has a narrower upper tail than the data and under predicts the values there. The lognormal assumption, however, appear still to be satisfactory for the estimation of fractiles as high as the 84^{th} percentile to be used for demand calculation.

Results				Critical Statistic		
Analysis type	Bin			α		
	I	II	III	0.10	0.05	0.01
Direct	0.10	0.11	0.15	0.26	0.29	0.35
Normalized	0.12	0.12	0.20			

Table C.1: Kolmogorov-Smirnov goodness-of-fit test results and critical statistics for a sample size of 20 for various levels of significance, α.

In order to quantify how well the data fit the distribution models, a Kolmogorov-Smirnov goodness-of-fit test has been carried out on the maximum inter-story ductility results. In this method, the maximum of the deviations between the hypothesized cumulative lognormal distribution and the observed cumulative distribution is calculated by the following expression:

$$D = max_{i=1}^{n}[\mid F^*(X_i) - F_X(X_i) \mid] \tag{C.1}$$

where, $F^*(X_i) = \frac{i}{n}$; n= number of sample points; $F_X(X_i)$= CDF of the fitted lognormal distribution.

The results of the test along with the critical statistics for the Kolmogorov-Smirnov goodness-of-fit test are given in Table C.1. Since the test statistic (D) is less than the critical value, the assumption of lognormal distribution of the maximum inter-story ductility cannot be rejected at the 10% or lower significance level.

Because of the systematic deviation at the upper tail where each single bin has only a very limited number of data points, a larger sample is created by pooling data from Bins I, II, and IV. The records from these bins are scaled to the Bin-IV median spectral acceleration (0.24g). This level of ground-motion induces higher levels of nonlinearity in the structure compared to the previous case. The plot of the computed maximum inter-story ductility values is shown in Figure C.2 on a lognormal probability paper. The conclusions drawn above appears to be supported by these larger sample of results as well. Fitting of the data to other standard distributions remains to be investigated.

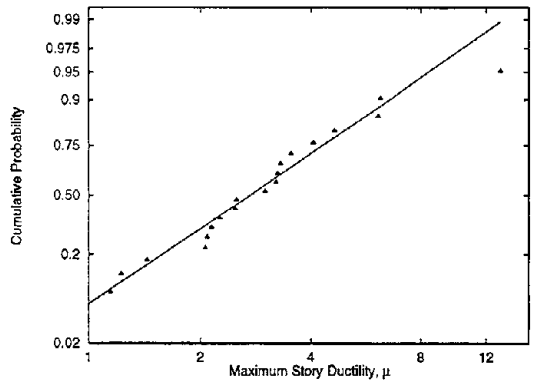

(a) Direct Results of Bin-I and Structure I

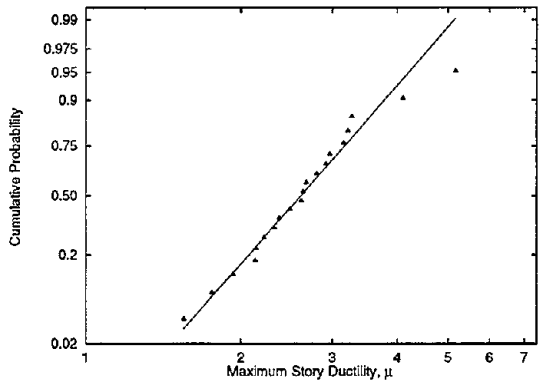

(b) Normalized Results of Bin-I and Structure I

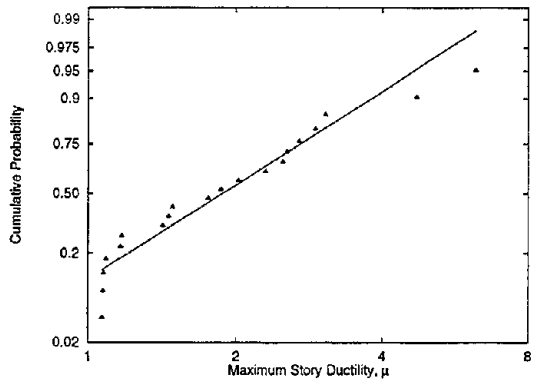

(c) Direct Results of Bin-II and Structure I

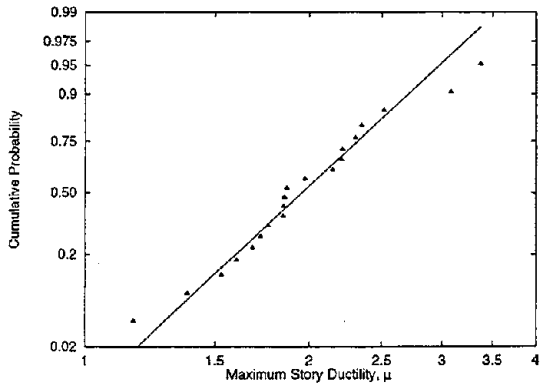

(d) Normalized Results of Bin-II and Structure I

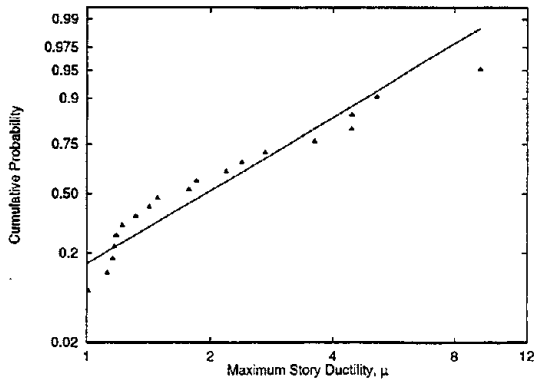

(e) Direct Results of Bin-III and Structure II

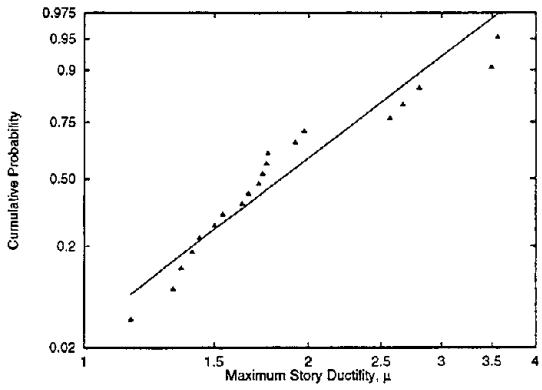

(f) Normalized Results of Bin-III and Structure II

Figure C.1: Maximum inter-story ductility values shown on lognormal probability paper.

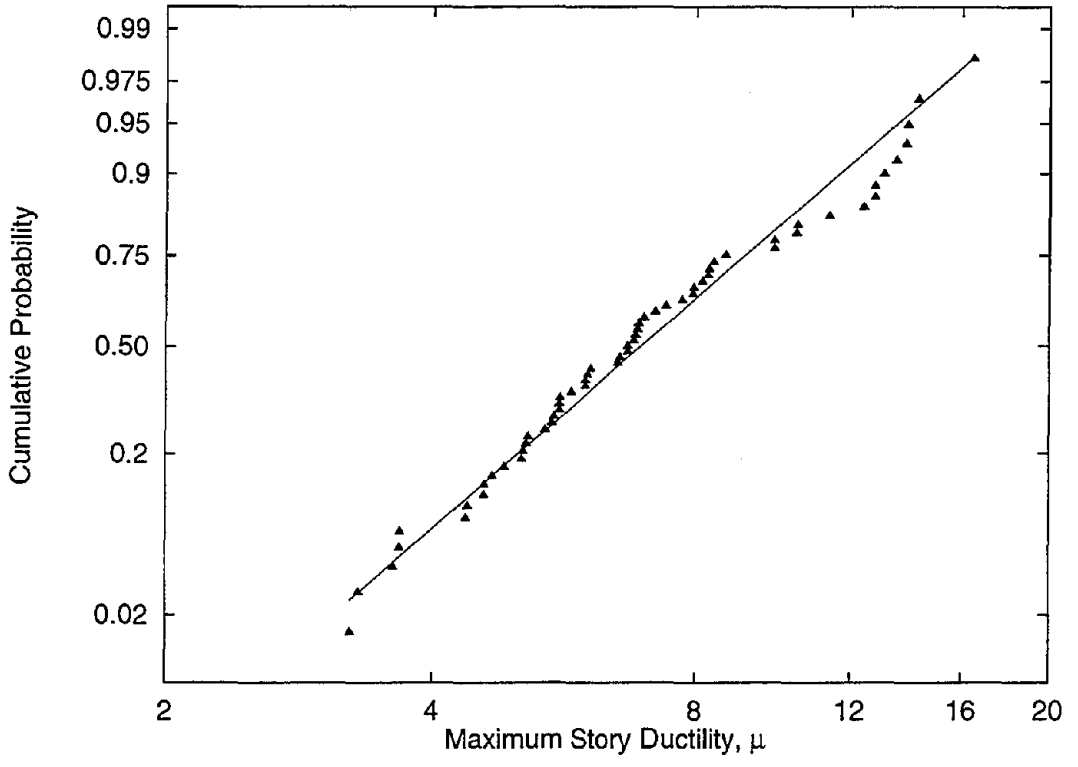

Figure C.2: Maximum inter-story ductility values (Structure-I) from Bin-I, Bin-II, and Bin-IV records, scaled to S_a=0.24g, displayed on lognormal probability paper.

Appendix D

Different Computational Procedures for the Estimation of $S^R_{a_{\mu'}}$ and $\mu \mid S_a$

For a particular set of ground-motion records, there are different possible approaches to the calculation of required spectral acceleration to induce a specified ductility level, μ'. For the purpose of demonstration, we consider here two methods for the estimation of a target ductility in a structure given S_a, denoted as $\mu \mid S_a$, and three methods for the calculation of the spectral accelerations required to induce a level of ductility, $S^R_{a_{\mu'}}$. For brevity, we limit ourselves to maximum inter-story ductility only.

D.1 Estimation of $\mu \mid S_a$

D.1.1 Direct Method

The estimation of the statistics of μ for a given S_a requires only scaling the records to the specified spectral ordinate. For example, for Bin-I records, when the target acceleration is 0.12g, we find that the median and "dispersion", δ, of maximum inter-story ductility are

2.6 and 0.28 respectively (Table 2.3).

D.1.2 Regression Analysis

If the scaled results of μ are available at least two different levels of spectral acceleration, we can perform a regression analysis to estimate the statistics of μ as a function of S_a. The statistics of $\mu \mid S_a$ are needed, for example, when we need to carry out the Probabilistic Seismic Demand Analysis, PSDA (see Section 3.5).

A suggested relation for the dependence of μ (or other damage measure) on S_a is the following:

$$\mu = \beta_0 \cdot S_a^{\beta_1} \cdot \varepsilon \tag{D.1}$$

where β_0 and β_1 are the regression parameters and ε is a random error term with median, $\hat{\varepsilon}$=1, and with dispersion $\delta_\varepsilon = \sigma_{\ln \mu | S_a}$. The model is a linear in $\ln \mu$ and $\ln S_a$. β_1=1 corresponds to simple proportionality.

The model can be fit to response data obtained from direct (unscaled) records, as done in Figure 2.3 both for individual bins or pooled bins. The same model, however, can also be used to fit the response data obtained from normalized records (e.g., from Bin-I records normalized to the median spectral acceleration of the bin (Table 2.3), or scaled to a specified spectral acceleration 0.24g (Table 2.7)). As an illustration, the direct Bin-I response values fit by this model yield β_0=0.17, β_1=0.73 and "$\delta_{\mu|S_a}$=0.33. For the spectral acceleration level S_a =0.12g, we estimate the median of μ to be equal to 2.8. The corresponding median of μ for normalized results is 2.6 with a δ of 0.28 (Table 2.3).

D.2 Calculation of $S^R_{a_{\mu'}}$

D.2.1 Iterative Method

In this approach each ground-motion record is scaled to the level necessary to induce the target level of damage measure, μ'. Because the problem is nonlinear in nature, the

scaling has to be carried out by trial and error, until the specified damage is observed within a desired tolerance. Although this method can give accurate results, it is also time consuming. In the case of Bin-I records, for a target maximum inter-story ductility of 4, the median and δ of $S^R_{a_{\mu'}}$ are 0.17g and 0.28 respectively. We will use these results as a benchmark to find the accuracy of other simplified but more efficient methods.

D.2.2 Interpolation Method

In this approach a structure is analyzed for each ground-motion record at multiple, arbitrary levels of spectral acceleration. Then for each record the estimate of S_a required to produce the target level of ductility, μ', is obtained by linear interpolation. The statistics of $S^R_{a_{\mu'}}$ can be obtained for any level of μ' by running a suite of records. For Bin-I records we have found that the median and δ of $S^R_{a_{\mu'}}$ at μ'=4 are 0.18g and $(0.25^2+0.10^2)^{1/2}$=0.27 respectively (where, 0.25=δ_{F_μ} and 0.10=$\delta_{S_{a,ref}}$). These results are in good agreement with those obtained by the "iterative method" (0.17g and 0.28 respectively).

D.2.3 Regression Analysis

If the results of $S^R_{a_{\mu'}}$ are available at least for two different levels of μ, then a regression analysis of $S^R_{a_{\mu'}}$ on μ can be performed. In the regression analysis, we used the following model for the estimation of the statistics of $S^R_{a_{\mu'}}$ as a function of μ.

$$S^R_{a_{\mu'}} = \gamma_0 \cdot (\mu')^{\gamma_1} \cdot \varepsilon \tag{D.2}$$

(D.3)

where the parameters are analogous to those in Equation D.1.

If the records have been preliminary scaled to a specified S_a levels (e.g., within-bin medians, etc.), then a data manipulation is needed before carrying out the regression. More precisely, for each record the scaled results have to be interpolated to first estimate $S^R_{a_{\mu'}}$ for two or more values of μ' and, finally, the $(S^R_{a_{\mu'}}, \mu')$ pairs can be used to fit this regression model.

Finally, it is worth noting that, if of interest, the variability of $\mu \mid M,R$ or $S^R_{a_{\mu'}} \mid M,R$ can be recovered from these results. For this purpose, a simplified method and also an improved but slightly more complex procedure is described in Section 2.5.2.

Appendix E

Normalization and Scaling Accelerograms for Nonlinear Structural Analysis[1]

E.1 Introduction

Both seismologists and engineers often question the legitimacy of scaling accelerograms up (or down) before using them to predict the non-linear structural behavior. The duration and spectral shape issues are voiced in this context. We interpret this concern formally as: do records scaled to some appropriate reference or "intensity" level give the same non-linear response as unscaled records? We define intensity as the spectral acceleration at the lowest structural frequency for 2% elastic damping. We will focus primarily on the calculation of a best estimate of the damage measure. For this purpose, we calculate the *median* value which is the geometric mean (see Equation A.1). We will also calculate the "dispersion" of the damage measure, δ, which is defined as the standard deviation of the natural logarithms of the data (see Equation A.2). We will compare these statistics of nonlinear response from

[1]This is an extended version of the paper published in 6th U. S. National Conference on Earthquake Engineering, Seattle, 1998. In particular we have included more results for a 4sec SDOF and a 4sec MDOF structures.

two sets of 20 recorded accelerograms, where each set is chosen from a specific magnitude-distance (*M-R*) "bin" (i.e., from a specific scenario or design earthquake). We will first consider SDOF structures of different frequencies to verify several aspects of scaling, and subsequently we will examine whether those observations are valid for MDOF structures.

We distinguish generally between "normalization", where the records within a specific bin are adjusted to have the same intensity level, and "scaling", where records from one bin are adjusted systematically up (or down) to the intensity level of other bin. This can be done with or without prior normalization within the bin. The parameters of normalization are the structure-specific "intensity" or linear SDOF response for a record such that it is a helpful predictor of nonlinear behavior of SDOF or MDOF structures, i.e., nonlinear responses are highly correlated to the parameter giving lowest "dispersion", but unbiased.

One of our main objectives is to attempt to reduce the "dispersion" of damage calculations without biasing them. We will focus on estimation of an "efficient" structure-specific intensity measure so that we get minimum variance of damage measure. The minimum variance insures the narrowest possible confidence band which in turn reduces the number of nonlinear analyses required to achieve a desired level of accuracy. We will examine different procedures for normalization of records, e.g., normalization to the common choice PGA, normalization to the spectral acceleration at the lowest structural frequency, frequency-averaged normalization, etc. We shall see that the advantage of normalization of records prior to their use in structural analysis is that the dispersion of the damage calculations is reduced compared to the non-normalized or direct results.

In order to verify the issue of scaling, the records from one bin are scaled to represent intensities from a different bin and the response statistics are compared with those of the unscaled set. This also helps to answer the question of dependency of nonlinear responses on M and R of ground-motions.

Note that we will draw conclusions based on the other studies as well as on the results that we will present here. We will show in the tables only a sampling of some of the interesting results.

E.2 Ground Motion

The ground-motions considered in this study belong to two scenario events, i.e., to two narrow magnitude and distance intervals or "bins":

Bin-I: M = 5.25-5.75 and R = 5-25km.

Bin-II: M = 6.7-7.3 and R = 10-30km.

In this context, M is the moment magnitude and R is the closest distance to the rupture zone.

We consider 20 recorded accelerograms in California on stiff soil (soil type S_2 as per UBC, 1994) for each bin. We select these records so that the median intensity and dispersion of the records are similar to the Abramhamson and Silva (1997) attenuation results. Thus the response results of a bin should be representative of a scenario event corresponding to the M-R of that bin. See Shome et al. (1997) for a detailed description of the records.

We consider Bin-I and Bin-II as they represent low- and high-magnitude events respectively. These two bins have different response spectra characteristics. Compared to Bin-II, the Bin-I response spectrum is richer in high frequency content, but poorer in low frequency content (see Figure 2.1). Note that between these two bins, the difference in central magnitude is one and half units which implies a factor of 175 in energy release. Further the Bin-II records typically have larger duration. Many believe that the nonlinear responses from these two bins will be substantially different because of these quite different ground-motion characteristics. Hence the comparison of the results between these two bins will help to confirm or deny the issue of scaling of ground-motion records. In order to reinforce the observations, in the same cases we consider additionally a larger number of records in each bin. In this case, the number of records in each bin is the maximum records available from our catalogue (see Silva, 1995), 36 records in Bin-I and 63 records in Bin-II.

E.3 Structures

We consider both SDOF and MDOF structures to verify the issues of normalization and

scaling. We consider three SDOF structures. The frequencies of these structures are 0.25, 0.95, and 4.0Hz. The ratio of plastic to elastic stiffness (α) is 3% for the 0.25Hz and the 4.0Hz structures, whereas, for the 0.95Hz structure this is about 10%. The viscous damping of all these structures is 2%. All the SDOF structures are modeled by a simple bilinear-spring. Note that for the 0.25Hz structure we will use two different yield-displacement capacities for analyses at the low- and high-intensity levels, those are respectively Bin-I and Bin-II intensity levels. We will see below that the median spectral acceleration at 0.25Hz of Bin-II records is about 9 times higher than that of the Bin-I records, and the use different capacities of the 0.25Hz structures helps us in getting nonlinear results within a bound that is of interest to the engineering community.

For the MDOF structures, we consider simple stick-models with 1-DOF per node representing the horizontal displacement of each story. This simple model takes very little computer time to carry out the nonlinear dynamic analyses. Thus we are able to make multiple runs to confirm whether the observations of SDOF results are also valid for the MDOF structures. We consider three structures of 4, 5, and 20 stories. The fundamental frequencies of these structures are 4.1, 0.95, and 0.26Hz respectively. The α value of the 4.1Hz structure is 3% for each of the bilinear springs representing each story. The modal mass participation at the fundamental mode is 87%. The 5-DOF 0.95Hz structure is a simplified model of a 5-story UBC Zone-4 SMRF structure (see Searer, 1994). The yield capacity of this structure is scaled down by $\frac{1}{10}$ to insure interesting levels of nonlinear behavior under the unscaled recordings. We have represented this structure by a multi-linear spring (see Shome et al., 1997, for details). The modal mass participation at the fundamental mode is 82%. The 20-DOF 0.26Hz structure is a modified 20-story building in UBC Zone-4. See Gupta (1999) for a detailed description of the original structure. The yield capacity of each story in this structure is also reduced for the same reason as discussed before for the 5-story structure. Each story of this structure is represented by a bilinear spring-mass model. The α values of the springs are, however, similar to the original 20-story building for no P-Δ effect. The damping of all these structures is 2%. Note that we have not considered any P-Δ effect in the nonlinear analysis of these structures.

E.4 SDOF Results

The damage measures, we have considered, are ductility and normalized hysteresis energy (NHE). Although the damage index (Park and Ang, 1985) is a popular damage measure, for typically reported values of the weighting coefficient (0.10-0.20), we find that it just reflects the characteristics of the ductility measure. We do not report the damage index calculations; however for the SDOF case, one can calculate them from the reported ductility and NHE results for any value of the weighting coefficient. Although NHE is seldom used alone as a damage measure, we report it here for completeness.

E.4.1 Direct (Non-Normalized) Results

In this case the structure is analyzed for the recorded ground-motion intensity, i.e., unscaled. These results provide the benchmark for the normalized and scaled results. See Figure E.1(a) for typical results. The scatter is large. The statistics of damage results of the 0.95 Hz structure for the two bins are given in Tables E.1 and E.2. It is observed that the dispersion (δ) of ductility is quite similar to the dispersion of intensity (spectral acceleration) of ground-motion; the dispersion of normalized hysteresis energy (NHE) is still higher. This wide scatter in damage calculations implies that we need to analyze the structure for large number of unscaled records in order to estimate the median damage measures for a reasonably narrow-target-confidence-band width. The uncertainty of the estimate of the median is equal to the δ divided by the square root of the sample size. If the acceptable "one-sigma" (i.e., 65% confidence) confidence-band width is $\pm$15% for the median ductility, then we need a minimum of 20 Bin-I records ($=[0.66/0.15]^2$). Whereas, if the one-sigma target confidence-band width is the same for NHE, we need 44 records. These numbers are much higher than the numbers being used or recommended in current practice (e.g., 3 to 7 by SEAOC, 1996).

We make similar observations for the 0.25Hz (low-frequency) and 4.0Hz (high-frequency) structures. See Tables E.3, E.4, E.5, and E.6. In the following paragraphs, we will look into different methods to reduce the variance of damage calculations. This will reduce the

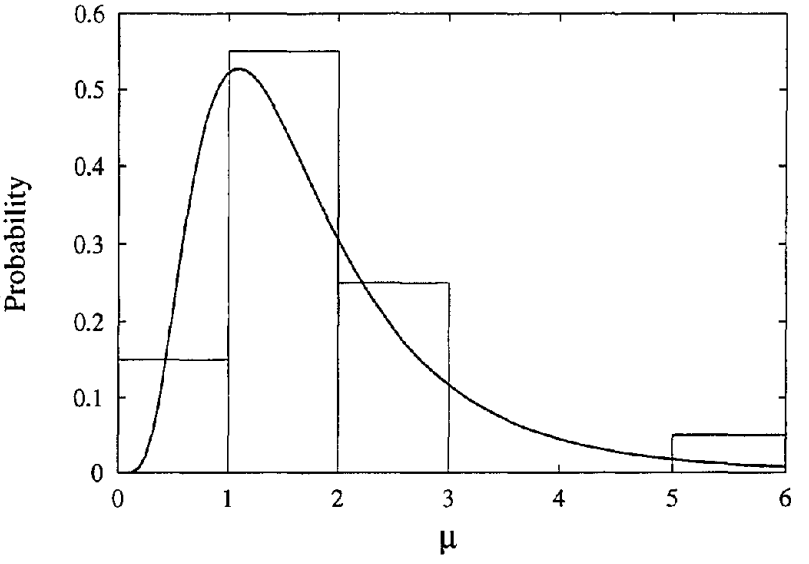

(a) Histogram and moment-fit lognormal distribution function of ductility

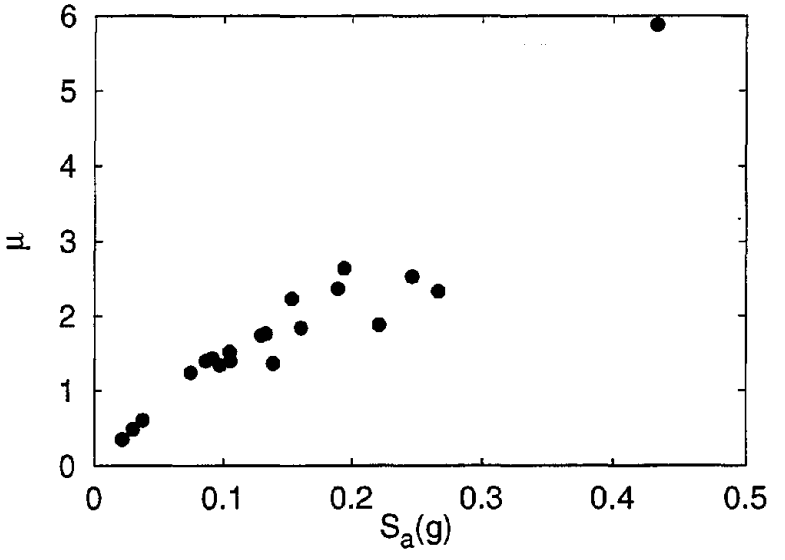

(b) Variation of ductility with spectral acceleration, S_a(0.95Hz,2%)

Figure E.1: Results of 0.95Hz structure for Bin-I records

Case	$S_a(g)$	δ_{S_a}	$\hat{\mu}$	δ_μ	$\widehat{NHE}$	δ_{NHE}
Direct (unnormalized)	0.12	0.75	1.5	0.66	2.1	0.99
Normalized to a Single Freq. at 2% Damping						
a. Simple Structure Specific Intensity, $S_a(f_0)$	0.12	0.00	1.5	0.13	1.5	0.34
b. PGA ($f = \infty$)	0.12	0.75	1.5	0.63	2.1	1.17
c. Lower Frequency (0.25Hz)	0.12	0.60	1.5	0.49	1.0	0.78
Normalized to a High Damping Level						
a. Damping=5%	0.12	0.12	1.5	0.13	1.5	0.49
b. Damping=20%	0.12	0.29	1.5	0.19	1.3	0.88
Normalized Over a Freq. Range at 2% Damping						
a. Spectral Acceleration ($f_0 - 12.5\%$)	0.12	0.13	1.5	0.18	1.4	0.44
b. Spectral Acceleration ($f_0 - 75\%$)	0.12	0.22	1.5	0.22	1.2	0.68
c. Spectral Velocity ($f_0 - 12.5\%$)	0.12	0.22	1.5	0.17	1.3	0.73
d. Spectral Velocity ($f_0 - 75\%$)	0.12	0.22	1.5	0.17	1.3	0.79
e. Method of Least Squares	0.12	0.92	1.5	0.81	2.4	1.15
Scaled to Bin-II Median Intensity	0.31	0.00	3.2	0.21	10.9	0.44
Larger Set (36 Records), Bin-II Median Intensity	0.31	0.00	3.0	0.20	11.8	0.45

Table E.1: Nonlinear response results of the 0.95Hz SDOF structure from Bin-I ($M \approx 5.5$, $R \approx 15$km) for alternative normalizing parameters, and for bin-to-bin scaling. The sample size is 20 unless otherwise indicated.

Case	$S_a(g)$	δ_{S_a}	$\hat{\mu}$	δ_μ	$\widehat{NHE}$	δ_{NHE}
Direct	0.31	0.43	4.0	0.66	16.9	0.92
Normalized to a Single Freq. at 2% Damping						
a. Simple Structure Specific Intensity, $S_a(f_0)$	0.31	0.00	4.0	0.40	18.6	0.58
b. PGA ($f = \infty$)	0.31	0.49	4.1	0.66	17.6	1.25
c. Lower Frequency ($f = 0.25Hz$)	0.31	0.83	3.6	0.62	14.3	1.51
Normalized to High Damping Level						
a. Damping=5%	0.31	0.14	3.9	0.31	18.7	0.57
b. Damping=20%	0.31	0.30	3.9	0.29	18.6	0.64
Normalized over a Freq. Range at 2% Damping						
a. Spectral Acceleration ($f_0 - 12.5\%$)	0.31	0.19	3.9	0.38	18.8	0.44
b. Spectral Acceleration ($f_0 - 75\%$)	0.31	0.27	3.7	0.27	18.1	0.33
c. Spectral Velocity ($f_0 - 12.5\%$)	0.31	0.18	3.9	0.38	18.8	0.53
d. Spectral Velocity ($f_0 - 75\%$)	0.31	0.28	3.8	0.27	18.1	0.36
e. Method of Least Squares	0.31	0.59	4.2	0.87	16.3	1.37
Scaled to the Bin-I median intensity	0.12	0.00	1.7	0.18	1.9	0.45
Larger Set (63 Records), Bin-II Median Intensity	0.31	0.00	3.9	0.36	17.1	0.53

Table E.2: Nonlinear response results of the 0.95Hz SDOF structure from Bin-II ($M \approx 7.0$, $R \approx 20$km) records for alternative normalizing parameters, and for bin-to-bin scaling. The sample size is 20 unless otherwise indicated.

Case	$S_a(g)$	δ_{S_a}	$\hat{\mu}$	δ_μ	$\widehat{NHE}$	δ_{NHE}
Direct	0.005	0.97	2.7	0.87	7.1	1.01
Normalized to a Single Freq. at 2% Damping						
a. Simple Structure Specific Intensity, $S_a(f_0)$	0.005	0.00	3.0	0.17	7.1	0.51
b. PGA ($f = \infty$)	0.005	1.09	2.7	0.87	5.3	1.75
Normalized to a High Damping Level						
a. Damping= 5%	0.005	0.08	3.0	0.17	7.0	0.45
b. Damping=20%	0.005	0.24	3.0	0.21	6.8	0.41
Normalized Over a Freq. Range at 2% Damping						
a. Spectral Acceleration ($f - 12.5\%$)	0.005	0.05	3.0	0.19	7.0	0.47
b. Spectral Acceleration ($f - 75\%$)	0.005	0.11	3.0	0.21	7.0	0.42
c. Spectral Displacement ($f - 12.5\%$)	0.005	0.05	3.0	0.19	7.0	0.47
d. Spectral Displacement ($f - 75\%$)	0.005	0.13	3.0	0.22	6.9	0.40
e. Method of Least Squares	0.005	1.17	2.8	1.03	7.6	1.30
Scaled to Bin-II Median Intensity	0.043	0.00	7.1	0.20	40.2	0.51
Larger Set (36 Records), Bin-II Median Intensity	0.043	0.00	7.2	0.26	55.1	0.70

Table E.3: Nonlinear response results of the 0.25Hz SDOF structure from Bin-I ($M \approx 5.5$, $R \approx 15$km) records for alternative normalizing parameters, and for bin-to-bin scaling. The sample size is 20 unless otherwise indicated.

number of runs required to estimate the median within a reasonable permissible error.

E.4.2 (Within Bin) Normalization at a Single Frequency

Structural Frequency

For the 0.95Hz SDOF structure, the plot of the Bin-I direct results of ductility versus spectral acceleration at 0.95Hz for each record is shown in Figure E.1(b). This plot suggests that the ductility is strongly correlated with this (structure-specific) ground-motion "intensity" measure. In particular, the linear trend between this intensity measure and ductility suggests that there will be a substantial reduction in dispersion if we first normalize the records of a bin to the median spectral acceleration of that bin at the structural frequency of interest and then analyze the structure for these normalized records. We refer this obvious choice of normalization parameter, the structure-specific "intensity", $S_a(f_0, 2\%)$, as "simple" normalization. In this case, we will not get any dispersion of responses for the linear dynamic analyses, but we do observe a finite dispersion in the damage calculations for nonlinear dynamic analyses. The reduction in dispersion, however, is quite significant

Case	$S_a(g)$	δ_{S_a}	$\hat{\mu}$	δ_μ	$\widehat{NHE}$	δ_{NHE}
Direct	0.043	0.90	7.4	0.87	25.9	1.39
Normalized to a Single Freq. at 2% Damping						
a. Simple Structure Specific Intensity, $S_a(f_0)$	0.043	0.00	7.4	0.45	33.1	0.58
b. PGA ($f = \infty$)	0.043	1.00	6.8	1.02	25.4	1.56
Normalized to a High Damping Level						
a. Damping= 5%	0.043	0.11	7.3	0.46	33.2	0.52
b. Damping=20%	0.043	0.30	7.4	0.46	32.8	0.47
Normalized Over a Freq. Range at 2% Damping						
a. Spectral Acceleration ($f - 12.5\%$)	0.043	0.15	7.4	0.41	33.4	0.53
b. Spectral Acceleration ($f - 75\%$)	0.043	0.33	7.1	0.30	32.9	0.54
c. Spectral Displacement ($f - 12.5\%$)	0.043	0.17	7.4	0.41	33.4	0.53
d. Spectral Displacement ($f - 75\%$)	0.043	0.31	7.0	0.30	32.5	0.65
e. Method of Least Squares	0.043	1.15	7.3	1.10	23.0	1.89
Scaled to Bin-II Median Intensity	0.005	0.00	2.8	0.31	5.9	0.46
Larger Set (63 Records), Bin-II Median Intensity	0.043	0.00	6.5	0.37	28.9	0.53

Table E.4: Nonlinear response results of the 0.25Hz SDOF structure from Bin-II ($M \approx 7.0$, $R \approx 20$km) records for alternative normalizing parameters, and for bin-to-bin scaling. The sample size is 20 unless otherwise indicated.

Case	$S_a(g)$	δ_{S_a}	$\hat{\mu}$	δ_μ	$\widehat{NHE}$	δ_{NHE}
Direct	0.42	0.62	2.5	0.68	4.4	1.33
Normalized to a Single Freq. at 2% Damping						
a. Simple Structure Specific Intensity, $S_a(f_0)$	0.42	0.00	2.6	0.34	4.8	0.49
b. PGA ($f = \infty$)	0.42	0.27	2.3	0.31	4.4	0.68
Normalized to a High Damping Level						
a. Damping= 5%	0.42	0.11	2.5	0.30	4.8	0.38
b. Damping=20%	0.42	0.25	2.3	0.29	4.4	0.62
Normalized Over a Frequency Range						
a. Spec. Acceleration ($f - 75\%$) at 2% Damping	0.42	0.31	2.3	0.23	4.1	0.48
b. Spec. Acceleration ($f - 75\%$) at 20% damping	0.42	0.35	2.2	0.31	3.7	0.85
Scaled to Bin-II Median Intensity	0.80	0.00	5.7	0.64	20.6	0.67
Larger Set (36 Records), Bin-II Median Intensity	0.80	0.00	5.4	0.52	22.4	0.71

Table E.5: Nonlinear response results of the 4.0Hz SDOF structure from Bin-I ($M \approx 5.5$, $R \approx 15$km) records for alternative normalizing parameters, and for bin-to-bin scaling. The sample size is 20 unless otherwise indicated.

Case	$S_a(g)$	δ_{S_a}	$\hat{\mu}$	δ_μ	$\widehat{NHE}$	δ_{NHE}
Direct	0.80	0.58	6.0	0.82	31.5	1.22
Normalized to a Single Freq. at 2% Damping						
a. Simple Structure Specific Intensity, $S_a(f_0)$	0.80	0.00	7.2	0.62	42.7	0.77
b. PGA ($f = \infty$)	0.80	0.33	6.4	0.40	39.4	0.52
Normalized to High Damping Level						
a. Damping= 5%	0.80	0.09	6.9	0.55	42.3	0.68
b. Damping=20%	0.80	0.22	6.9	0.49	42.1	0.48
Normalized over a Frequency Range						
a. Spec. Acceleration ($f - 75\%$) at 2% Damping	0.80	0.26	6.7	0.41	41.2	0.34
b. Spec. Acceleration ($f - 75\%$) at 20% Damping	0.80	0.32	6.3	0.34	38.9	0.44
Scaled to Bin-I Median Intensity	0.42	0.00	2.7	0.34	6.8	0.70
Larger Set (63 Records), Bin-II Median Intensity	0.80	0.00	6.6	0.69	39.2	0.83

Table E.6: Nonlinear response results of the 4.0Hz SDOF structure from Bin-II ($M \approx 7.0$, $R \approx 20$km) records for alternative normalizing parameters, and for bin-to-bin scaling. The sample size is 20 unless otherwise indicated.

compared to the direct calculations, and very importantly, this "simple" normalization parameter does not introduce bias in the median estimations. Statistics of the normalized damage results of the three SDOF structures for Bins I and II are given in Tables E.1 to E.6. The small difference between the normalized and direct median results is not statistically significant. The standard error of estimation of the ratio of the medians from the direct and normalized results is equal to the square root of the sum of the squared dispersions (δ) divided by $\sqrt{n}$. For example, the one sigma confidence band on the ratio of the estimator of the median NHE from the direct and normalized results for the 0.95Hz structure from Bin-II records is equal to 18.6/16.9 $\pm(\sqrt{(0.92^2 + 0.58^2)/20})\%$ or 1.10 $\pm$0.27; this implies that the ratio is not statistically significantly different from unity.

Note that the reduction in dispersions provided by this normalization is about half, however, this reduction reduces as the level of ductility increases (compare the Bin-I versus Bin-II results). This reduction in dispersion reduces the number of records required for a given confidence bandwidth by a factor of four. For the high frequency oscillator the reduction in dispersion is, however, less (approximately $\frac{2}{3}$), which we will confirm below

using a larger sample of results[2]. Note that since higher median ductilities are associated with higher dispersions, we need more records when the nonlinearity is higher if the same confidence bandwidth is to be maintained. We can conclude that the normalization of ground-motion records to the median spectral acceleration at the structural frequency is an efficient method to reduce the variance of the damage calculations and that this does not introduce any bias in the median estimations.

By this procedure, however, we have lost the information on actual dispersions of the damage measures given a bin of records (M and R). This information is needed if the design basis calls for "84^{th}-percentile" demand calculations. The dispersion can be recovered approximately by taking the square root of the sum of squares of the dispersion of spectral acceleration and that of the ductility of normalized results. For example, for the 0.95Hz structure, the dispersion of ductility given the Bin-II records is equal to $\sqrt{0.43^2 + 0.40^2}$ or 0.59 (note the corresponding value from the direct results is 0.66). However, this error in estimation does not significantly affect the calculation of the "84^{th}-percentile" ductility (the ratio of this quantity from the direct and normalized results is $\exp(0.66 - 0.59)$ or 1.1). See Section 2.5.2 for improved methods of estimation of this quantity.

PGA

Among the different normalization parameters being used by the practicing engineers, the most conventional one is normalization to the peak ground acceleration (PGA) level.

[2]The mean square response of any SDOF elastic oscillator can be written as follows (see Newland, 1993):

$$E(y^2) = \int_{-\infty}^{\infty} |H(\omega)|^2 \cdot S_X(\omega) d\omega \qquad \text{(E.1)}$$

where y is the response of a structure, $H(\omega)$ is complex frequency response function, and $S_X(\omega)$ is the spectral density of any forcing function, X. In seismic analysis of low-frequency structures we find that most of the contribution to the above integration comes from forcing function at $\omega = \omega_0$, where ω_0 is the frequency of the structure. On the other hand, for high frequency structures a significant contribution comes from forcing function at $\omega < \omega_0$ as well. Hence by normalizing although we match the spectral acceleration at the frequency of structure, because of contribution of low-frequency accelerations to the structural response we do not get as high reduction in dispersion of response as the low frequency structures. Hence we will propose afterwards normalizing to an average spectral acceleration over a range of frequencies to get higher reduction in dispersion of response.

This method is equivalent to normalization at a very high frequency ($f = \infty$). The advantage of this method is that we do not need any information about structure. The results of normalization to PGA for all the structures are given in Tables E.1 to E.6. We observe that the medians are essentially the same as those estimated from the direct results; results are unbiased. We also observe for the 0.25 and 0.95Hz structures that the dispersion of damage measures is of the same or higher order as the direct results. On the other hand, for the high frequency 4.0Hz structure we get a substantial reduction in dispersion over the previously described simple normalization at the structural frequency. So for the low frequency building structures, this method is to be discouraged strongly. Although we are getting some reduction in dispersion for the high frequency structure, we will discuss other methods to further reduce the dispersion.

Low Frequency

Since the frequency of a structure reduces when the structure is in the inelastic range, we want to examine whether we can get an additional benefit over the "simple" normalization by scaling the ground-motion records at a frequency lower than the frequency of structure. The results of normalizing the records to a spectral acceleration at 0.25Hz and applying them to the 0.95Hz structure are given in Tables E.1 and E.2. We find although there is no significant bias in the results, we do not get any significant reduction in dispersion of the response results over those from the direct results.

Higher Damping

It was concluded by Kennedy et al. (1984) that the inelastic response of a SDOF structure can be better predicted by spectral acceleration at a lower frequency and higher damping compared to its elastic counterpart. A similar argument is also implicit in the "capacity spectrum method" (Freeman, 1978). From the results of normalization of records to the median spectral acceleration at the structural frequency and at a higher dampings, it is observed that we do not any significant bias in the results and only for medium- (0.95Hz) and for high-frequency (4.0Hz) structures we get additional reduction in dispersion over the

previously described simple normalization at the structural frequency and 2% damping. See Tables E.1 to E.6. However, this reduction at a low ductility level is not very significant. In general, we can say that instead of normalizing the records at the elastic damping level, we should normalize the records at a higher damping level to get additional reduction in dispersion.

E.4.3 (Within Bin) Normalization Over a Frequency Range

Spectral Acceleration Based

It was also concluded by Kennedy et al. (1984) that the dispersion in the nonlinear responses is reduced when each of the ground-motion records is scaled with respect to a spectral acceleration found by averaging spectral acceleration over range of frequencies varying from the frequency of the structure to an equivalent reduced frequency which depends on the level of nonlinearity in the structure. It is to be noted here that the above observation is mainly from experience with higher frequency nuclear power plant structures. Hence, we need to verify whether the above observation is also true at lower frequencies which are of interest to the building community. In order to normalize the records, we first calculate the average spectral acceleration over a frequency range and then scale each of the records to the median of that averaged spectral acceleration obtained from 20 records. First we observe that we do not get any significant bias in the damage results. We observe also that for the 0.25 and 0.95Hz structures we get a substantial (more than 30%) reduction in dispersion over the simple normalization only at high ductility (compare the results of Bin-I and Bin-II in Tables E.1 to E.4). However, for the high frequency structure (4.0Hz), there is a substantial reduction in dispersion of the damage measures for both at low and high ductilities (see Tables E.5 and E.6). This is due to comparative ineffectiveness of simple normalization of for this oscillator, especially at higher ductilities (we will verify this observation below from larger sample size results). We also observe in those tables that the normalization by frequency averaging at a higher damping do not necessarily reduce the dispersions of the damage calculations.

Spectral Velocity or Displacement Based

One of the possible alternatives to the above frequency-averaged normalization procedure is that, depending on the frequency of structure, we can normalize the records to the median displacement or velocity level instead of always normalizing the records to the median spectral acceleration level. For example, if the structural frequency is in the "constant-displacement" region of response spectra, we can normalize the ground-motion records to the frequency-averaged displacement level. Hence, for the 0.25Hz, 0.95Hz, and 4.0Hz structure, we need to normalize the ground-motion records to the frequency-averaged median spectral displacement, velocity, and acceleration level respectively. We have already observed for the 4.0Hz structure, the advantage of normalization to the frequency-averaged spectral acceleration. For the other structures, although we do not get any bias in response results, the reduction in dispersion is not higher than the same from the normalization to the frequency-averaged spectral acceleration. Compare the results of Bin-I and Bin-II for the 0.95Hz and 0.25 structure in Tables E.1 to E.4. So it can be concluded that this method of normalization is not better than the previously described frequency-averaged spectral acceleration. The advantage of the former method is that the same approach is applicable at all the structural frequencies.

Method of Multi-Frequency Least Squares

In this method we match the recorded-ground-motion spectrum to the target spectrum by multiplying the ground-motion record with a single scaling factor which will minimize the sum of the weighted squared error over some suite of frequencies. We are interested in the ratios, so we will minimize the sum of the squared differences between the logarithms of the target spectrum and the ground-motion spectrum. The target spectrum is the median spectrum of a bin. We match the target spectrum at only four frequencies. The frequencies are 0.25, 0.50, 1.0, and 3.33Hz and the corresponding weighting factors are 0.3, 0.3, 0.3, and 0.1 respectively. These values are the same as has been adopted in the SAC Phase-II project (see Somerville, et al., 1998) for use with different MDOF structures with natural

frequencies in the 1.0 to 4.0Hz range (in that project the two horizontal components were scaled simultaneously so that the "fit" of either single component was less good than we obtain here). The results of this normalization are given in Tables E.1 to E.4 for the 0.95Hz and 0.25Hz structure. We see that although the results are not biased, we do not get any advantage from this method over the previously described "simple" normalization scheme. Indeed the dispersions are all greater than those of the direct results.

E.4.4 Scaling of Ground-Motion Records

We have already found that normalization of the ground-motion records to the median spectral acceleration at the natural frequency of the structure reduces the dispersion of damage results significantly without introducing bias in the median estimation. Hence within-bin scaling ("normalization") is acceptable and desirable. Now we go one step further and ask a more general question, can we scale the records of one bin to the median intensity level of another bin? More precisely, we are trying to find out whether the nonlinear response of structure depends on M and R for reasons beyond simply intensity-level differences. It should be remembered (e.g., Figure E.1) that the intensity of ground-motion within a bin itself varies by a factor of 10. So the common belief that the scaling of ground-motion records to a higher or lower intensity level will necessarily represent different M-R characteristics, is not true.

By *scaling* of ground-motion records, we mean to increase or decrease each of the ground-motion records by a constant factor so that the spectral acceleration at a given frequency and damping is equal to the target spectral acceleration. In this process, the spectral shape, relative phases, and duration of the ground-motion remain unchanged. We scale-up the Bin-I records to the median-intensity of Bin-II and scale-down the Bin-II records to the Bin-I median-intensity level. Now the question is: is scaling legitimate? We have to compare these scaled results to the results of the target bin, and check whether the difference is statistically significant. But the answer is not obvious because of the high dispersion of the direct results. Given our conclusions above (Section E.4.3), it is more effective to compare the normalized results rather than the direct results.

The advantage of scaling of records (i.e., of assuming M and R independence of response) is that when we are given a target ground-motion intensity, typically from probabilistic seismic hazard analysis (PSHA), we need not be overly concerned with what is the M and R of the ground-motion records that we use for structural analysis. In seismic hazard analysis, a wide range of M and R pairs contribute in different proportions to the total risk of exceeding a particular level of spectral acceleration. So a single scenario earthquake of a particular M and R will not be able to represent the risk from different M and R combinations of earthquakes. If the nonlinear response of structure is strongly dependent on the M and R, then we would have to calculate the response for each of the M and R combinations for a given intensity to calculate the probability of exceeding a damage level. Thus, if, for example, the permissible error requires us to analyze for a minimum of 5 records to estimate the median damage, then the total number of analyses required are 5 times the number of magnitude-distance bins. (This number, however, can be reduced to some extent by interpolating the results.) On the other hand, if the responses are independent of M and R, this reduces to the calculation of responses for a given intensity to only 5 records. The calculation of probability of exceedance of a given ductility also becomes simpler if the nonlinear response is independent of M and R (see, for example, Section 3.5).

The scaled results are given in Tables E.1 to E.6. We see, for example, for the 0.95Hz structure when the Bin-I records are scaled-up to the Bin-II intensity level, the one-sigma confidence band on the ratio of the median ductilities from these two bin of records is equal to $4.0/3.2 \pm (\sqrt{(0.21^2 + 0.40^2)/20})\%$ or 1.25 ± 0.10. So in this case the difference between the scaled results is statistically significant (i.e., 1.3 is 30% greater than unity, and this difference represents a deviation of 30%/10% or three standard deviations, implying less than 1% likelihood that the difference is random). When the level of ductility is low, e.g., results at the Bin-I intensity level, similar calculations show that the results are not statistically significant (see Table E.1). The results of 0.25 and 4.0Hz structures show that although the higher magnitude events induce higher ductilities in a structure, the differences are not statistically significant at even the 10% significance level. So, typically (5 out of 6 cases) for ductility response scaling is legitimate. The difference of NHE results is, however,

statistically significant for all the structures. (Perhaps because duration as well as intensity is important for NHE response.) We observe that the trend for the 0.25Hz structure is different from the other structures; the low magnitude records induce higher NHE in the 0.25Hz structure (we observe also similar trend for the MDOF structure in Chapter 4).

In order to confirm the legitimacy of scaling, we need to investigate the issue of dependency of nonlinear response on bin properties. First we compare the scaled results with the direct results from the same set of records. For case study we scale the Bin-I records to several intensity levels, and then compare the characteristics of direct results of the 0.95Hz structure with the results from scaled records for the same structure by regression analysis of those results (see Chapter 3 for a detailed discussion on regression analysis). The regression results for 0.95Hz structure are shown in Figure E.2(a). From these regression results we get median response not only at the median intensity levels (as we obtained before), but also at several other intensity levels. We observe in Figure E.2(a) that there is virtually no difference between these two regression results. So scaling of a bin of records to different intensity levels does not introduce any bias in response results compared to the results from the as-recorded ground motion; *intra-bin scaling is legitimate.* Now we want to find out whether scaling of one bin of records to the intensity level of another bin can represent the response characteristics of that bin. In order to verify this we scale all the records of one bin by a single multiplying factor so that the median intensity of that bin of records matches that of another bin (recall that this type of scaling is referred in Chapter 3 as "cloud scaling"). Thus the relative nature of the intensities of the records remains unchanged, but the median intensity is exactly the same for both the bins. Response results for the 0.95Hz structure from the "cloud-scaled" Bin-I records and from the as-recorded Bin-II records are shown in Figure E.2(b), and the regression results for these two sets of data are also plotted in the same figure. So we observe in this case that the regression results are not quite the same. The regression results for all the three structures at two different intensity levels which correspond to Bin-I and Bin-II intensity levels are given in Table E.7. All these results indicate that when we scale the records of one bin to the intensity level of another bin, we may introduce some bias in the results (here we observe only one in six different

f_0	Records	Type of Analysis	Median Intensity	Regression Results	Error (δ_ϵ)	One SCB of $(\hat{\mu}_{-II}/\hat{\mu}_{-I})_{\hat{s}_a}$
0.25Hz	Bin-I	Direct	0.005	$\mu = 217.2(S_a)^{0.83}$	0.23	
	Bin-II	C.S.	0.005	$\mu = 249.1(S_a)^{0.85}$	0.19	0.9 - 1.1
	Bin-I	C.S.	0.043	$\mu = 66.4(S_a)^{0.74}$	0.25	
	Bin-II	Direct	0.043	$\mu = 90.1(S_a)^{0.80}$	0.43	1.0 - 1.3
0.95Hz	Bin-I	Direct	0.12	$\mu = 8.94(S_a)^{0.81}$	0.16	
	Bin-II	C.S.	0.12	$\mu = 11.11(S_a)^{0.86}$	0.26	1.0 - 1.2
	Bin-I	C.S.	0.31	$\mu = \mathbf{7.63(S_a)^{0.74}}$	0.20	
	Bin-II	Direct	0.31	$\mu = \mathbf{15.71(S_a)^{1.15}}$	0.42	1.1 - 1.4
4.0Hz	Bin-I	Direct	0.42	$\mu = 5.25(S_a)^{0.85}$	0.40	
	Bin-II	C.S.	0.42	$\mu = 7.25(S_a)^{1.2}$	0.35	0.9 - 1.1
	Bin-I	C.S.	0.80	$\mu = 7.11(S_a)^{1.00}$	0.64	
	Bin-II	Direct	0.80	$\mu = 7.62(S_a)^{1.12}$	0.47	0.9 - 1.2

Table E.7: Regression results from direct results and results from "cloud-scaled" (C.S.) records for the three SDOF structures. In each case one set of records are "cloud scaled" to the intensity level of the other bin, and the regression results from these two sets of response results are compared. For each structure we have scaled up the Bin-I records in one case and in the other case we have scaled down the Bin-II records. The last column indicates the one-sigma confidence bandwidth (one SCB) of the ratio of the medians calculated from the regression results for Bin-I and Bin-II results at the median intensity level ($[\hat{\mu}_{-II}/\hat{\mu}_{-I}]_{\hat{s}_a}$). Note that we have considered here two 0.25Hz structures those have different yield displacements for analysis at the high- and the low-intensity levels. Only the regression results for the 0.95Hz structure at the high-intensity level are statistically significantly different from each other at the 5% or lower significance level and the results are highlighted with bold letters.

cases). This bias in results is statistically significant. Later on we will confirm this bias on the basis of larger sample of results; this bias is, however, quite small.

In order to find out what explains the difference among different structures in the results between two bins scaled to the same intensity level, we look into the shape of the normalized spectra. The median spectra from Bin-I and Bin-II records normalized at 0.25, 0.95, and 4.0Hz frequencies are shown in Figure E.3. We observe that there is a difference between the two spectra at low frequencies when normalized at 0.95Hz. When a structure goes to the nonlinear range, it "samples" spectral accelerations at frequencies lower than the elastic frequency. The difference in median spectra may explain the difference between the Bin-II and scaled Bin-I ductility damage measure of the 0.95Hz structure. Similar plots

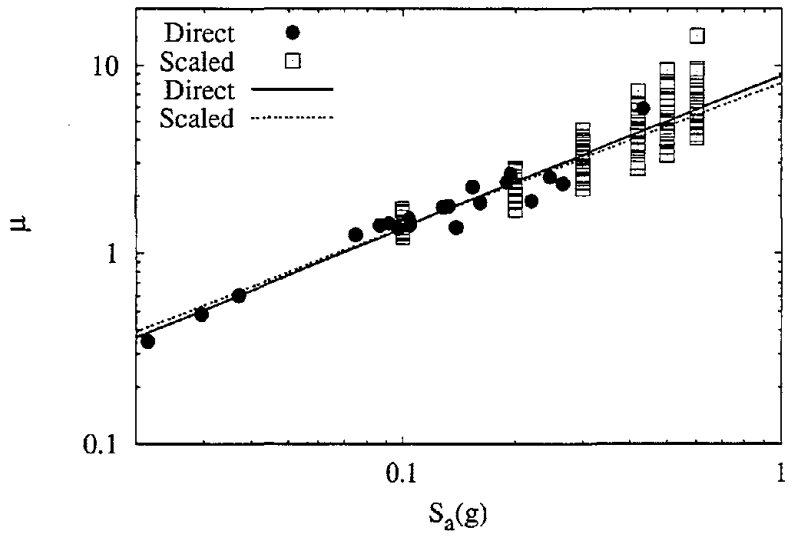

(a) Intra-bin scaling (Bin-I)

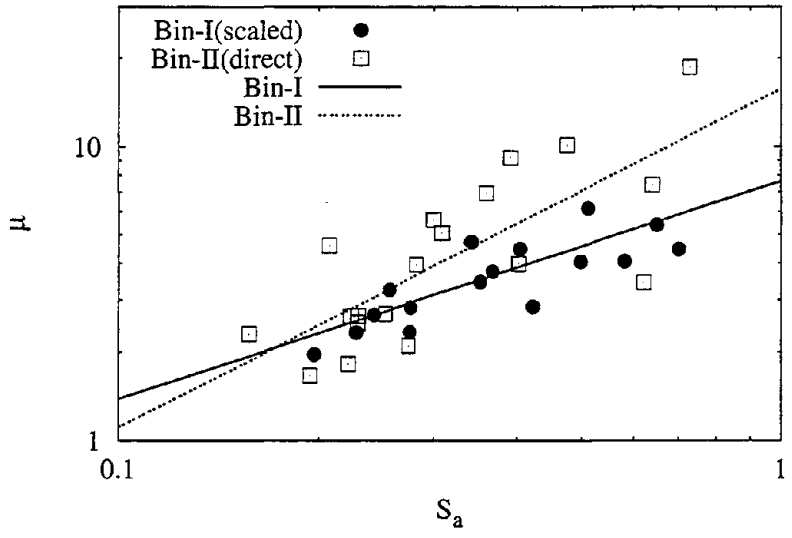

(b) Inter-bin scaling (Bin-I to Bin-II)

Figure E.2: Variation of ductility (μ) of 0.95Hz structure with spectral acceleration, $S_a(0.95Hz, 2\%)$, for different cases of scaling. Regression results are for μ against S_a.

for normalization at 0.25Hz and 4.0Hz in Figure E.3 show that the difference in spectra at the frequencies lower than the frequency of the structure is not very significant; the higher difference is observed for normalization at 4.0Hz. So we do not observe statistically significantly different results from Bin-I and Bin-II records for the 0.25 structure; the observed difference for the 4.0Hz structure is, however, mild and not statistically significant at the 5% significance level (the one-sigma confidence band width of the ratio of the results from these bins is 1.26 ± 0.20). Note that the normalized spectra for the 4.0Hz structure are close to each other up to 1Hz frequency. This indicates (Kennedy at al., 1984) that like the 0.95Hz structure the 4.0Hz structure typically does not see much different ground motion for these two bins of records as long as the ductility is less[3] than 16. Recall that for the 4.0Hz structure the "one-sigma" band on estimation of the median ductility from Bin-II results is 7.2 ± 2.5; the ductility is well below 16. All these results indicate that there may be some systematic dependency of ductility on the spectral shape, and hence to some degree on the magnitude of the ground-motion records.

Considering all the cases together we observed above we can conclude that the higher magnitude events are apparently somewhat correlated with higher ductilities of SDOF structures, but it is hard to establish this trend because of high natural dispersion of the results. The number of records we have considered is 20. Although this number is quite high by conventional practical standards, but still the results remain inconclusive. Therefore we increase the number of records further to improve the statistical significance of the difference in results between the high- and low-magnitude events. Recall in this case we have 36 records for Bin-I and 63 records for Bin-II. The larger sets of Bin-I and Bin-II records are scaled to the Bin-II median intensity level, and the results are given in Tables E.1 to E.6. These results confirm a mild dependency of the nonlinear response (ductility) on magnitude. Since R is kept constant, it can be stated from these results that for medium

---

[3] $\frac{f_{\mu=16}}{f_{\mu=1}} = \left[\frac{K_{\mu=16}}{K_{\mu=1}}\right]^{1/2} = \frac{1}{4}$
where K is the secant stiffness of a oscillator deformed to ductility μ and f is the "equivalent" frequency of the oscillator based on that stiffness. See Kennedy, et al. (1984) for details on this calculation.

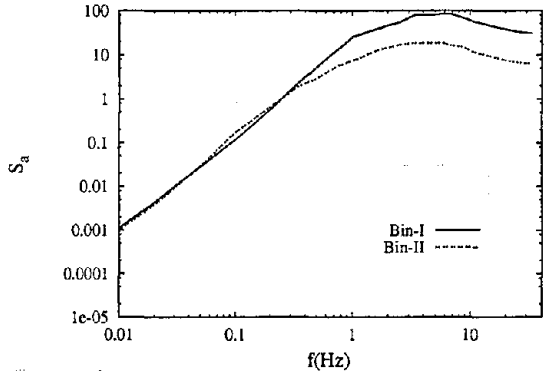

(a) Normalized at 0.25Hz

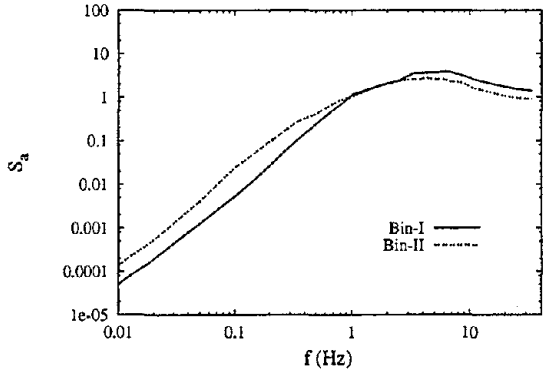

(b) Normalized at 0.95Hz

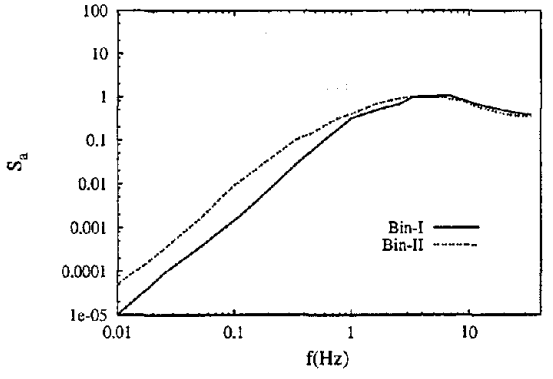

(c) Normalized at 4.0Hz

Figure E.3: Variation of shape of the spectra normalized at different frequencies to 1.0g spectral acceleration.

frequency (SDOF) structures (approximately 1.0Hz) at ductility approximately 4.0, the estimated percentage change in median ductility is $20\%/\Delta M$ (the ratio of the medians for Bin-II and Bin-I results is equal to $\frac{3.9}{3.0} \pm (\sqrt{\frac{0.36^2}{63} + \frac{0.20^2}{36}})\%$ or 1.3±0.1, and the difference in magnitude, ΔM, is 1.5). Similarly we can state that for the high-frequency (SDOF) structures (approximately 4.0Hz) at ductility around 6.0, the estimated percentage change in median ductility is $10\%/\Delta M$ (the ratio of the medians for Bin-II and Bin-I results is equal to $\frac{6.6}{5.4} \pm (\sqrt{\frac{0.69^2}{63} + \frac{0.52^2}{36}})\%$ or 1.2±0.1, and the difference in magnitude, ΔM, is 1.5). We do not observe any practical dependency of response on magnitude for the low-frequency oscillators (approximately 0.25Hz). The one-sigma confidence bandwidth of the ratio of the medians at ductility around 7.0 is 0.9±0.1 which is not statistically significantly different from unity. Based on SDOF systems, at least, we can conclude that if we keep the magnitude of records within about 0.5 to 1.0 of the "target" magnitude, then scaling is apparently legitimate for nonlinear structural analysis.

E.5 MDOF Results

Some of the interesting results of the 0.95Hz MDOF structure are given in Table E.8. See Chapter 2 for a detailed discussion on the results of this structure. The results of analyses of the 0.26Hz and 4.1Hz MDOF structures are given in Tables E.9 and E.10. As before we investigate now different normalization and scaling schemes for MDOF structures. We observe in general that those schemes we considered do not introduce any bias in damage results, but we get different dispersions of damage measures from those schemes. So in our discussions we will mainly point out the difference in dispersions.

E.5.1 Normalization at a Single Frequency

Fundamental Frequency

In all the cases we have carried out normalization at the lowest or fundamental frequency of the structure and at 2% damping. By normalizing the ground-motion records, we get a reduction of around half in dispersion calculations compared to the direct results for

Case	$S_a(g)$	δ_{S_a}	$\hat{\mu}$	δ_μ	$\widehat{NHE}$	δ_{NHE}
Bin-I (M≈5.5, R≈15km)						
Scaled to 0.24g	0.24	0.00	6.2	0.36	27.6	0.52
Larger Set (36 records), Scaled to 0.24g	0.24	0.00	5.5	0.43	29.5	0.63
Bin-II (M≈7.0, R≈20km)						
Scaled to 0.24g	0.24	0.00	7.7	0.41	48.7	0.55
Normalized to High Damping at 0.95Hz						
a. Damping=5%	0.24	0.14	7.5	0.31	48.9	0.57
b. Damping=20%	0.24	0.30	7.6	0.32	48.7	0.65
Normalized Over a Freq. Range at 2% Damping						
a. Spectral Acceleration ($f_0 \pm 12.5\%$)	0.24	0.16	7.7	0.37	48.4	0.47
b. Spectral Acceleration ($f_0 \pm 75\%$)	0.24	0.26	7.3	0.41	47.1	0.55
Larger Set (63 records), Scaled to Bin-II intensity	0.24	0.00	7.9	0.40	43.4	0.50

Table E.8: Results of maximum interstory damage measures of the 0.95Hz MDOF structure from Bin-I and Bin-II records for alternative normalizing parameters, and for bin-to-bin scaling. The sample size is 20 unless otherwise indicated.

Case	$S_a(g)$	δ_{S_a}	$\hat{\mu}$	δ_μ	$\widehat{NHE}$	δ_{NHE}
Bin-I (M≈5.5, R≈15km)						
Direct	0.005	0.97	2.0	0.67	2.2	1.43
Normalized to a Single Frequency at 2% Damping						
a. Simple Structure Specific Intensity, S_a(4.1Hz)	0.005	0.00	1.8	0.78	2.5	1.18
Larger Set (36 records), "Direct" Bin-II Intensity	0.043	1.30	13.7	0.91	117.2	1.23
Larger Set (36 records), Scaled Bin-II Intensity	0.043	0.00	12.6	0.68	107.9	1.08
Modified Set (18 records), Scaled Bin-II Intensity	0.043	0.00	6.0	0.60	25.1	0.80
Bin-II (M≈7.0, R≈20km)						
Direct	0.043	0.90	6.7	0.85	26.5	0.80
Normalized to a Single Frequency at 2% Damping						
a. Simple Structure Specific Intensity, S_a(0.26Hz)	0.043	0.00	4.8	0.52	21.1	1.05
Normalized to a High Damping Level at 0.26Hz						
a. Damping=5%	0.043	0.10	4.7	0.49	21.7	0.99
b. Damping=20%	0.043	0.28	4.5	0.33	21.4	0.93
Normalized Over a Freq. Range at 2% Damping						
a. Spectral Acceleration ($f_0 \pm 12.5\%$)	0.043	0.14	4.7	0.49	20.8	1.03
b. Spectral Acceleration ($f_0 \pm 75\%$)	0.043	0.26	4.5	0.43	21.0	0.92
c. Weighted Normalization Scheme	0.043	0.45	5.0	0.34	24.5	0.56
Larger Set (63 records), "Direct" Bin-I Intensity	0.005	0.73	0.8	0.60	0.6	1.30
Larger Set (63 records), Scaled Bin-I Intensity	0.005	0.00	0.7	0.63	0.9	0.91
Larger Set (63 records), Scaled Bin-II Intensity	0.043	0.00	5.2	0.52	23.7	0.88

Table E.9: Results of maximum interstory damage measures of the 0.26Hz MDOF structure from Bin-I and Bin-II records for alternative normalizing parameters, and for bin-to-bin scaling. The sample size is 20 unless otherwise indicated.

Case	$S_a(g)$	δ_{S_a}	$\hat{\mu}$	δ_μ	$\widehat{NHE}$	δ_{NHE}
Bin-I (M≈5.5, R≈15km)						
Direct	0.42	0.66	2.2	0.88	2.5	1.60
Normalized to a Single Frequency at 2% Damping						
a. Simple Structure Specific Intensity, S_a(4.1Hz)	0.42	0.00	2.3	0.39	2.7	0.56
Larger Set (36 records),Scaled Bin-II Median Intensity	0.84	0.00	5.4	0.53	19.0	0.63
Bin-II (M≈7.0, R≈20km)						
Direct	0.84	0.60	5.7	0.90	19.8	1.6
Normalized to a Single Frequency at 2% Damping						
a. Simple Structure Specific Intensity, S_a(4.1Hz)	0.84	0.00	6.0	0.50	29.2	0.71
b. Normalized to the Median PGA ($f = \infty$)	0.84	0.30	5.7	0.42	25.3	0.74
Normalized to a High Damping Level						
a. Damping=5%	0.84	0.11	6.0	0.43	28.7	0.67
b. Damping=20%	0.84	0.24	6.2	0.35	27.3	0.56
Normalized Over a Freq. Range at 2% Damping						
a. Spectral Acceleration ($f_0 \pm 75\%$)	0.84	0.23	5.9	0.39	26.6	0.54
Larger Set (63 records), Scaled Bin-II Median Intensity	0.84	0.00	6.2	0.58	30.3	0.77

Table E.10: Results of maximum interstory damage measures of the 4.1Hz MDOF structure from Bin-I and Bin-II records for alternative normalizing parameters, and for bin-to-bin scaling. The sample size is 20 unless otherwise indicated.

the 0.95 structure, and for the 4Hz structure the same is around 66%. For the 0.26Hz structure the reduction is around 40% at high ductilities, but we do not get any reduction at low ductilities. Note that in all the previous cases the reduction in dispersion was very high (higher than 50%) at low ductilities. We will explain this variation afterwards. We observe in general this percentage of reduction reduces somewhat as the ductility increases. Compare the results of Bin-I and Bin-II in Table E.10. The general observations are similar as those made before for the SDOF structures.

PGA

It is observed, that although for the 0.26 and 0.95Hz MDOF structures normalization to the median PGA does not reduce the dispersion of the damage measures compared to the direct analyses, we do get some reduction in dispersion for the 4.1Hz MDOF structure. This observation also follows the SDOF results.

E.5.2 Normalization Over a Frequency Range

Spectral Acceleration Based

We want to verify whether the observations made for the normalization to the spectral acceleration averaged over a frequency band of the SDOF structures are also valid for the MDOF structures. However, instead of considering only the lower frequencies, as we did before for the SDOF structures, we consider the frequencies symmetric about the fundamental frequency. This helps to factor in the differences of spectral acceleration at the higher frequencies that certainly affect these MDOF systems when those structures are linear and probably also nonlinear. A limited comparative study of the normalization of one-sided and symmetric frequency-averaging indicated that the symmetric averaging reduces the dispersion of damage measures more than the one-sided averaging. So for the MDOF structures, we consider only the symmetric averaging about the fundamental frequency.

We first consider the 4.1Hz structure. The reduction in dispersion is higher than the normalization at the fundamental frequency when the median ductility is high (see Bin-II results in Table E.10), however, this reduction is not significant at the lower ductility. We have made similar observations for the 4.0Hz SDOF structure. Note that the normalized (at the fundamental frequency) elastic analysis has shown that the dispersions of global and story displacements are close to zero, signifying little dependency on higher mode effects in this structure. This fact appears to encourage the very similar trend between the SDOF and MDOF nonlinear results. When a structure goes into nonlinear domain, the notion of elastic modes in explaining response is questionable. They do prove, however, a good indicator to understand the effect of accelerations at frequencies higher than the first-mode frequency on MDOF nonlinear structural response.

For the 0.95Hz structure, we scale the Bin-II records to the 0.24g intensity to get global ductility values similar to the SDOF results; this will make a fair comparison between the SDOF and MDOF results. See Table E.8. When we compare these results to the simple normalization at the fundamental frequency, we observe that for both the ductility and NHE results we get a reduction in dispersion at the low as well as at the high ductility

level when the frequency-band width is small. The dispersion, however, increases at the low ductility level as the frequency band-width increases. These results are in variance with the SDOF results where at a lower ductility we do not get any reduction. From the normalized *elastic* analysis of the Bin-II records (not shown), we find that the dispersion of the maximum interstory displacements is close to 0.20, signifying a considerable higher-mode effect (or more appropriately higher-frequency effect) on the response results, perhaps explaining these differences.

For the 0.25Hz structure, the reduction in dispersion by frequency-averaged normalization is higher than the reduction by "simple" normalization at the fundamental frequency. See Table E.9. We have made a similar observation for the 0.25Hz SDOF structure; the reduction for the MDOF structure is, however, significantly higher. The normalized *elastic* analysis of this structure for the Bin-II records indicates that the dispersion of maximum story drift is 60%. Note that this value is much higher than the results those we have obtained before for the predominantly single-mode dominated 0.95Hz structure. This shows that the structural response has significant higher-frequency effect which can possibly explain the difference in reduction of response dispersion by this method between the SDOF and the MDOF structures.

Weighted Average Spectral Acceleration

The results of the 0.25Hz structure suggest that the contribution of higher frequencies is significant in overall response of the structure. So instead of normalizing the records to the first-mode spectral acceleration, we will normalize the records to the weighted average spectral accelerations at different higher frequencies. We consider here the spectral accelerations at the first three modes. The weights of these spectral accelerations are calculated from the modal participation factors which are 0.80, 0.10, and 0.05 at the first, second, and third mode respectively. The results of these weighted-average-normalization scheme is shown in Table E.9. We observe that by this scheme we get a substantial reduction in dispersion over the "simple" normalization at the first-mode spectral acceleration. This result and also the normalized elastic analysis result suggest that the 0.25Hz structure is indeed

a multi-frequency dominated structure and for this structure we should give "appropriate" weight to the higher frequency spectral accelerations.

E.5.3 Normalization at High Damping

The results of normalization at high dampings are found to be as good as the frequency-averaged normalization for structures. This is true also both at low and high ductility. The advantage of this method is that it permits us to use the structure-independent, conventional (5% damped) attenuation laws and hazard results. Whereas the adoption of the frequency-averaged normalization procedure requires development of new attenuation laws and new hazard maps (20%-damped spectral acceleration attenuation laws could be easily provided). So this method can be recommended for the normalization of ground-motion records for the single-mode dominated MDOF structures. Note that this method is also effective for the multi-frequency dominated 0.26Hz structure.

E.5.4 Scaling of Ground-Motion Records

As discussed before, when we scale the records, we observe in Tables E.8, and E.10 that for the two higher frequency structures somewhat higher ductilities are associated with higher-magnitude events. This observation is in close agreement with the SDOF results. This observation is again verified from the results of larger number of records. We get similar estimates of percentage change of inter-story ductilities with magnitude from the larger data set as we have obtained before for the SDOF structures, namely 20% change in ductility per unit magnitude for the 0.95Hz structure at ductility about eight and 10% change in ductility per unit magnitude at ductility about six.

For the 0.26Hz structure we observe that the ductility decreases with the increase of magnitude when the records are scaled to the same intensity level. Compare the Bin-I results when scaled to the Bin-II intensity level with the normalized Bin-II results in Table E.9. This observation is also confirmed from the larger set results. This trend is completely different from the trend that we have seen for the SDOF structure. For the SDOF

structure we did not find any statistically significantly different result between Bin-I and Bin-II. Because this lower-frequency structure is dependent on the spectral accelerations at higher (than 0.25Hz) frequencies and the low-magnitude events are relatively richer at high frequencies (see Figure E.3(a)), we expect that the ductility of this tall, higher-frequency-effected structure will be somewhat negatively correlated with magnitude[4]. We observe 100% increase in ductility from low-magnitude events compared to the results from high-magnitude events. The "direct" or "cloud-scaled" results of these bins also indicate similar results.

When we look into the Bin-I records more carefully, we find that most of the low-magnitude records (more than 90%) do not have any energy at low frequencies which are important for this 0.26Hz MDOF structure. The low-corner frequency of the filter used to process the large sub-set of the records is higher than the elastic frequency (0.26Hz), leaving little or no energy at the frequency band important for this structure. So when we scale these records to the Bin-II intensity level, because of the very low spectral acceleration at the structural frequency we have to scale up these records by large factors. Therefore these originally "weak" records (little or no energy at low frequencies) have very high spectral accelerations at high frequencies. As a result we get high response from these scaled "weak" records for the high-frequency dominated 0.26Hz structure. When we select a set of records from the magnitude 5 to 6 range that have 0.10Hz or lower low-corner frequency (we refer to this as the "modified" set), we observe in Table E.9 that the median ductility from these records is quite close to the Bin-II results. The plot of predicted normalized spectra from Bin-I and Bin-II M and R based on Abrahamson and Silva attenuation results (1997) and the median spectrum[5] from the larger set of records are shown in Figure E.4. We observe

[4]We do not observe any significant magnitude or spectral-shape dependency for the 0.25Hz SDOF structure, because the SDOF structural response do not depend on the accelerations at frequencies higher than the structural frequency. Figure E.3(a) indicates that the normalized Bin-I and Bin-II records have similar shape at frequencies lower than 0.25Hz. So we get similar response statistics from these two bins.

[5]Note that here the spectral ordinates of each of the records are adjusted by a correction factor to the center of the magnitude and distance range of a bin. The correction factor is the ratio of the spectral ordinates calculated from the attenuation results for the magnitude and distance at the center of a bin and the same for the magnitude and distance of the record. The spectral ordinates of a record are then adjusted to the center of the bin by this factor.

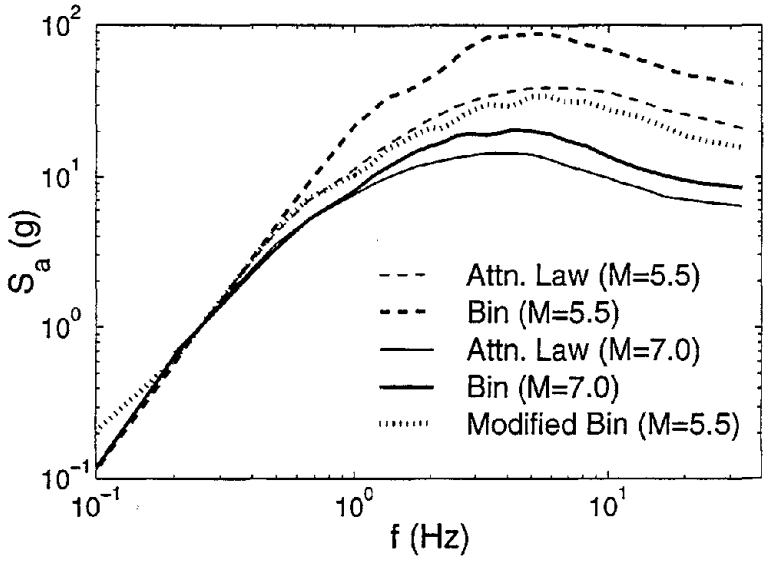

Figure E.4: Acceleration spectrum normalized to unity at 0.25Hz.

that there is a difference between the spectral ordinates from these two bins at higher frequencies[6]; the difference for the low magnitude Bin-I records is specially noticeable. The very high spectral ordinates of Bin-I records at high frequencies can explain the higher response from Bin-I records. On the other hand we observe in Figure E.4, the "modified" Bin-I records have spectral ordinates much lower than the original Bin-I records, and much closer to the Bin-II records. Therefore we get lower median damage results and these results are close to Bin-II results. This observation indicates that if we neglect the "weak" records in Bin-I considering that these records cannot generate Bin-II-like intensity, then the ductility of the 0.25Hz structure, like the high (4.0Hz) and medium (1.0Hz) frequency structures, is mildly dependent on the magnitude of the events (conditioned on scaled to the same spectral acceleration). The ductility, unlike those structures, decreases with the increase of magnitude of events.

[6]Note that the frequencies at the first three modes of the 0.26Hz MDOF structure are 0.26, 0.70, and 1.13Hz.

E.6 Conclusion

We have addressed mainly two issues: the effect of normalization and scaling of ground-motion records on nonlinear SDOF and MDOF responses. With some exceptions (notably for the lowest-frequency structure that is sensitive to higher than the first-mode frequency spectral accelerations) the conclusions are quite similar for both the SDOF and MDOF representations of three structures. We summarize here only the (more realistic) MDOF results.

It is observed that the nonlinear MDOF responses from a suite of 20 records of a particular M-R "bin" display a wide dispersion. The dispersion of NHE is much higher than that of ductility. In order to reduce the dispersion, we consider first normalizing the records to the within-bin median "intensity" level and then analyzing the structure. We examined effectiveness of several different normalization or "intensity" parameters to reduce the dispersion (without, hopefully, introducing any bias in the median response), e.g, normalization to the median PGA level, normalization to the median spectral acceleration at the structural frequency and at higher dampings, frequency-averaged normalization, etc. In all the cases, we find that the bias of the damage estimation caused by normalization is not statistically significant. We conclude that the uncritical use of PGA is to be discouraged especially for low frequency building structures. We find that the normalization to the spectral acceleration at the fundamental frequency and at a higher damping is most convenient to use and best among the alternatives. The advantage of normalization of records is that we can estimate the median damage measures within a given confidence bandwidth from a smaller number of records than otherwise. Typically the reduction in standard deviation compared to the direct analysis is about half. This reduces by a factor of four the number of runs required for the given confidence band width. For the normalized results (normalization at a high damping for a single-frequency dominated structure and weighted-average normalization for a multi-frequency dominated structure) to estimate the one-sigma (65%) confidence band of the median ductility within $\pm 15\%$, it may typically require about 4 to 6 records; for the unnormalized records, the same accuracy would require 20 to 35 records.

When we scale the records from one bin to the intensity level of another bins, especially one based on a different magnitude where systematic spectral shape differences are expected, we estimate a mild dependency of ductility on the magnitude of event. This is statistically significant (at 5% or lower significance level) only at the medium frequency (approximately 1.0Hz) and higher ductility level. The median ductility may vary about 10 to 15% for one unit change in magnitude (this is determined by scaling magnitude 5.5 records to the magnitude 7.0 intensity level). The high-frequency MDOF structure in our case study is essentially a first-mode dominated structure; response characteristics are very similar to the high-frequency SDOF structure. On the other hand, the ductility of the low-frequency structure decreases with the increase of magnitude; this is opposite to what we have seen for the other structures (care must be taken in this case to insure that the low-magnitude records have a valid signal in the low-frequency range). However, the dependency of NHE on magnitude is substantial.

Finally, we have found that it is quite easy to recover an estimate of the dispersion of the damage measures for a given intensity and M-R from the normalized or scaled results. We need this information to estimate the 84% demand or to evaluate the performance of a structure probabilistically.

We conclude that, subject perhaps to further confirmation by more structural cases, this may well value in the future in (1) obtaining attenuation laws and conducting PSHA for still higher (more than 5%) damped spectral acceleration, and (2) using higher damped (5 to 20%) S_a at the first natural frequency as the scaling and or intensity parameter for efficient and accurate nonlinear structural response estimation.

Appendix F

Demand-Hazard Calculation including Collapse of Structures: Closed-Form Solution

The annual probability of exceedance of a level y of any damage measure Y which is dependent on only a single spectral acceleration, S_a, can be written from Equation 4.21 as follows:

$$P(Y > y) \cong \lambda_{Y>y} = \underbrace{\int_0^{+\infty} P_{C|S_a}(s_a) \cdot \lambda_{S_a}(s_a)\, ds_a}_{\text{Term-C}} + \underbrace{\int_0^{+\infty} G_{Y|NC,S_a}(y|NC, s_a) \cdot P_{NC|S_a}(NC|s_a) \cdot \lambda_{S_a}(s_a)\, ds_a}_{\text{Term-NC}} \quad \text{(F.1)}$$

where

$\lambda_{Y>y}$ is the mean annual rate of events exceeding y.

$P_{NC|S_a}(NC|s_a)$ is the conditional probability of no collapse given that S_a equals level s_a. This can be obtained from Equation 4.22. The functional relationship between P_{NC} and S_a is assumed to be of the form $P_{NC|S_a}(NC|s_a) = (s_a/s_{a0})^{-\beta_C}$ for $s_a \geq s_{a0}$, where s_{a0} is the minimum spectral acceleration required to cause collapse in a structure.

$P_{C|S_a}(C|s_a)$ is the probability of collapse which can be written as $P_{C|S_a}(C|s_a) = 1 - P_{NC|S_a}(NC|s_a)$.

$\lambda_{S_a}(s_a)$ is the mean rate density of events for $S_a = s_a$. We assume here that the seismic hazard function $H(s_a)$ can be represented by Equation 3.23. The functional form of seismic hazard is given below.

$$H(s_a) = K_0 \cdot (s_a)^{-K_1}$$

We can calculate the rate density (with the approximation described in Footnote 2 of Chapter 5) from the above functional relationship as given below.

$$\lambda_{S_a}(s_a) = \left|\frac{dH(s_a)}{ds_a}\right| = K_0 K_1 (s_a)^{-(K_1+1)}$$

$G_{Y|NC,S_a}(y|NC, s_a)$ is the complementary cumulative distribution function of drift Y given no collapse (NC) at spectral acceleration level s_a. We assume that the function is lognormally distributed. The parameters of this distribution can be obtained from regression analysis of no-collapse results of Y against S_a as described in Section 4.3.1.

Term C of Equation F.1: This term calculates the contribution of the probability of collapse of a structure to the annual rate of damage exceeding y. Substituting the functional form of $\lambda_{S_a}(s_a)$ and $P_{C|S_a}(s_a)$

$$\begin{aligned} \text{Term C} &= \int_{s_{a0}}^{+\infty} K_0 K_1 (s_a)^{-(K_1+1)}\, ds_a - \\ &\quad \int_{s_{a0}}^{+\infty} \left(\frac{s_a}{s_{a0}}\right)^{-\beta_C} \cdot K_0 K_1 (s_a)^{-(K_1+1)}\, ds_a \\ &= H(s_{a0}) \cdot \left[\frac{\beta_C}{K_1 + \beta_C}\right] \end{aligned} \tag{F.2}$$

where $H(s_{a0})$ is the probability that spectral acceleration exceeds s_{a0}.

Term NC of Equation F.1: This term calculates the contribution of the probability of no collapse of a structure to the overall probability of exceeding y.

$$\text{Term NC} = \underbrace{\int_0^{s_{a0}} G_{Y|NC,S_a}(y \mid NC, s_a) \cdot P_{NC|S_a}(\not{NC}^1|s_a) \cdot \lambda_{S_a}(s_a)\, ds_a}_{\text{Term NC1}} + \underbrace{\int_{s_{a0}}^{+\infty} G_{Y|NC,S_a}(y \mid NC, s_a) \cdot P_{NC|S_a}(NC|s_a) \cdot \lambda_{S_a}(s_a)\, ds_a}_{\text{Term NC2}} \quad \text{(F.3)}$$

Term NC1 of Equation F.3: After integration by parts,

$$\text{Term NC1} = -G_{Y|NC,S_a}(y|NC, s_{a0}) \cdot H(s_{a0}) + \int_0^{s_{a0}} \left| \frac{\partial G_{Y|NC,S_a}(y \mid NC, s_a)}{\partial S_a} \right| \cdot H(s_a)\, ds_a \quad \text{(F.4)}$$

where $G_{Y|NC,S_a}(y|NC, s_{a0})$ is the probability exceedance of damage level y of a structure due to spectral acceleration s_{a0}. The density function of $Y|NC, S_a$ is the partial derivative of $G_{Y|NC,S_a}(\cdot)$ with respect to S_a and it is given in the following:

$$\frac{\partial G_{Y|NC,S_a}(y \mid NC, s_a)}{\partial S_a} = \phi\left[\frac{\ln(y/\alpha s_a^{\beta})}{\delta_{\varepsilon}}\right] \times \frac{1}{s_a \cdot (\delta_{\varepsilon}/\beta)} \quad \text{(F.5)}$$

Recognizing $\phi(u) = \phi(-u)$, the above equation can be rearranged as follows:

$$\frac{\partial G_{Y|NC,S_a}(y \mid NC, s_a)}{\partial S_a} = \phi\left[\frac{\ln(s_a/s_{a,y})}{\delta_{\varepsilon}/\beta}\right] \times \frac{1}{s_a \cdot (\delta_{\varepsilon}/\beta)} \quad \text{(F.6)}$$

where $\phi(.)$ is the standardized normal probability density function and $s_{a,y}$ that is equal to $(y/\alpha)^{1/\beta}$ is the spectral acceleration required to induce a median damage y in a structure. We are assuming here the functional relationship between S_a and Y given in Equation 3.2 which is $Y = \alpha S_a^{\beta}\varepsilon$. Note that $\phi\left[\frac{\ln(s_a/s_{a,y})}{\delta_{\varepsilon}/\beta}\right] \times \frac{1}{s_a \cdot (\delta_{\varepsilon}/\beta)}$ can be interpreted as the probability density function of a lognormal variable with median equal to $(y/\alpha)^{1/\beta}$ and dispersion equal to $\delta_1 = \delta_{\varepsilon}/\beta$.

Hence we get the following:

$$\begin{aligned}\text{Term NC1} &= -G_{Y|NC,S_a}(y|NC,s_{a0})\cdot H(s_{a0}) + \\ &\quad K_0\int_0^{s_{a0}}(s_a)^{-K_1}\cdot\frac{1}{\sqrt{2\pi}\delta_1 s_a}\exp\left[-\frac{\ln(s_a/s_{a,y})^2}{2\delta_1^2}\right]ds_a \\ &= -G_{Y|NC,S_a}(y|NC,s_{a0})\cdot H(s_{a0}) + \\ &\quad H(s_{a,y})\cdot\exp\left[\frac{(K_1\delta_1)^2}{2}\right]\cdot\Phi\left\{\frac{\ln[(s_{a0}\cdot e^{K_1\delta_1^2})/(s_{a,y})]}{\delta_1}\right\} \qquad \text{(F.7)}\end{aligned}$$

In the above equation, we recognize (Equation 3.25) that $H(s_{a,y})\cdot\exp\left[\frac{(K_1\delta_1)^2}{2}\right]$ would represent the probability of exceedance of a damage level y if there were no collapse at any s_a, i.e., if $s_{a0}=\infty$. In Equation F.7 the function $\Phi(\cdot)$ corresponds to the probability that a lognormal variable with median equal to $s_{a,y}=(y/\alpha)^{1/\beta}$ and dispersion equal to $\delta_1=\delta_\varepsilon/\beta$ is less than $s_{a0}\cdot e^{K_1\delta_1^2}$.

Term NC2 of Equation F.3:

$$\text{Term NC2} = K_0K_1(s_{a0})^{\beta_C}\int_{s_{a0}}^{+\infty}G_{Y|NC,S_a}(y\mid NC,s_a)\cdot(s_a)^{-(\beta_C+K_1+1)}\,ds_a \qquad \text{(F.8)}$$

which after integration by parts and subsequent simplifications:

$$\begin{aligned}\text{Term NC2} &= \frac{K_1}{K_1+\beta_C}[G_{Y|NC,S_a}(y|NC,s_{a0})\cdot H(s_{a0})] + \\ &\quad K_0\cdot(s_{a0})^{\beta_C}\cdot\frac{K_1}{K_1+\beta_C}\int_{s_{a0}}^{+\infty}(s_a)^{-(\beta_C+K_1)}\cdot\frac{1}{\sqrt{2\pi}\delta_1 s_a}\exp\left[-\frac{\ln(s_a/s_{a,y})^2}{2\delta_1^2}\right]ds_a \\ &= \frac{K_1}{K_1+\beta_C}[G_{Y|NC,S_a}(y|NC,s_{a0})\cdot H(s_{a0})] + \\ &\quad \frac{K_1}{K_1+\beta_C}\left(\frac{s_{a,y}}{s_{a0}}\right)^{-\beta_C}\cdot H(s_{a,y})\cdot\exp\left[\frac{(K_1+\beta_C)^2\delta_1^2}{2}\right]\cdot \\ &\quad \Phi^C\left\{\frac{\ln[(s_{a0}\cdot e^{(K_1+\beta_C)\delta_1^2})/(s_{a,y})]}{\delta_1}\right\} \qquad \text{(F.9)}\end{aligned}$$

In this case although we have included the collapse results, the calculation of mean rate of exceedance of a damage level y is very similar to the calculation without the collapse

results. Compare the expression $H(s_{a,y}) \cdot \exp\left[\frac{(K_1+\beta_C)^2\delta_1^2}{2}\right]$ with Equation 3.25. In this case the probability of exceedance of a damage level depends on the seismic hazard function $H(s_a)$ and also on the no collapse function, $P_{NC|S_a}$. So the expression represents the probability exceedance of damage level y for the "combined" hazard from seismic load and collapse of structure. Therefore we have an additional term in the expression from the slope of the no-collapse function which is β_C. In Equation F.9 the function $\Phi^C(\cdot)$ corresponds to the probability that a lognormal variable with median equal to $(y/\alpha)^{1/\beta}$ and dispersion equal to $\delta_1 = \delta_\varepsilon/\beta$ is greater than $s_{a0} \cdot e^{(K_1+\beta_C)\delta_1^2}$.

We calculate the probability of no collapse at $s_{a,y}$ from the following:

$$P_{NC|S_a}(NC|s_{a,y}) = \left(\frac{s_{a,y}}{s_{a0}}\right)^{-\beta_C}$$

We can calculate the function $G_{Y|NC,S_a}(y|NC, s_{a0})$ from the following:

$$G_{Y|NC,S_a}(y|NC, s_{a0}) = \Phi\left[\frac{\ln(s_{a0}/s_{a,y})}{\delta_1}\right]$$

The above function can be interpreted as the probability that a lognormal variable with median equal to $s_{a,y} = (y/\alpha)^{1/\beta}$ and dispersion equal to $\delta_1 = \delta_\varepsilon/\beta$ is less than s_{a0}.

Now combining equations F.2, F.7, and F.9, and rearranging we get the following:

$$\begin{aligned} P(Y > y) = & \left[\frac{\beta_C}{K_1+\beta_C}\right] \cdot H(s_{a0}) \cdot \Phi^C\left[\frac{\ln(s_{a0}/s_{a,y})}{\delta_1}\right] + \\ & H(s_{a,y}) \cdot \exp\left[\frac{(K_1\delta_1)^2}{2}\right] \cdot \Phi\left\{\frac{\ln[(s_{a0} \cdot e^{K_1\delta_1^2})/(s_{a,y})]}{\delta_1}\right\} + \\ & \left[\frac{K_1}{K_1+\beta_C}\right] \cdot P_{NC|S_a}(NC|s_{a,y}) \cdot H(s_{a,y}) \cdot \exp\left[\frac{(K_1+\beta_C)^2\delta_1^2}{2}\right] \cdot \\ & \Phi^C\left\{\frac{\ln[(s_{a0} \cdot e^{(K_1+\beta_C)\delta_1^2})/(s_{a,y})]}{\delta_1}\right\} \end{aligned} \quad \text{(F.10)}$$

Note that if $s_{a0} = \infty$, i.e., if the likelihood of collapse of structures is negligible at the

intensity level of interest, $s_{a,y}$, we get the following from Equation F.10:

$$\begin{aligned} \Phi^C\left[\frac{\ln(s_{a0}/s_{a,y})}{\delta_1}\right] &= 0 \\ \Phi^C\left[\frac{\ln[(s_{a0}\cdot e^{(K_1+\beta_C)\delta_1^2})/(s_{a,y})]}{\delta_1}\right] &= 0 \\ \Phi\left[\frac{\ln[(s_{a0}\cdot e^{K_1\delta_1^2})/(s_{a,y})]}{\delta_1}\right] &= 1 \end{aligned}$$

$$\text{Then Equation F.10 simplifies to:} \quad P(Y>y) = H(s_{a,y})\cdot\exp\left[\frac{(K_1\delta_1)^2}{2}\right] \quad \text{(F.11)}$$

Equation F.11 is the same as Equation 3.25. Therefore Equation 3.25 is a special case of the generalized solution for demand calculation given in Equation F.10.

On the other hand, if $s_{a0} = 0$, i.e., if the likelihood of collapse of structures is very high at the intensity level of interest, we get the following from Equation F.10:

$$\begin{aligned} \Phi^C\left[\frac{\ln(s_{a0}/s_{a,y})}{\delta_1}\right] &= 1 \\ \Phi\left[\frac{\ln[(s_{a0}\cdot e^{K_1\delta_1^2})/(s_{a,y})]}{\delta_1}\right] &= 0 \\ P_{NC|S_a}(NC|s_{a,y}) &= 0 \end{aligned}$$

$$\text{Then Equation F.10 simplifies to:} \quad P(Y>y) = \left[\frac{\beta_C}{K_1+\beta_C}\right]\cdot H(s_{a0}) \quad \text{(F.12)}$$

Equation F.12 is the same as Equation F.2. Therefore when the likelihood of collapse of structures is very high, we can directly use Equation F.2 for demand-hazard calculations as we have done in Section 4.4.

The drift-demand-hazard results for a 20-story building at a central Los Angeles site is shown in Figure F.1. The contribution of each term in Equations F.1 and F.3 to the annual probability of drift exceeding a level of drift is also shown in the same figure. As we have discussed before, we observe in the figure that contribution of Term C (Equation F.1) to the probability of exceedance is significant only when the likelihood of collapse of the structure is high, otherwise the contribution from no-collapse terms, Term NC1 and Term NC2 (Equation F.3), is significant.

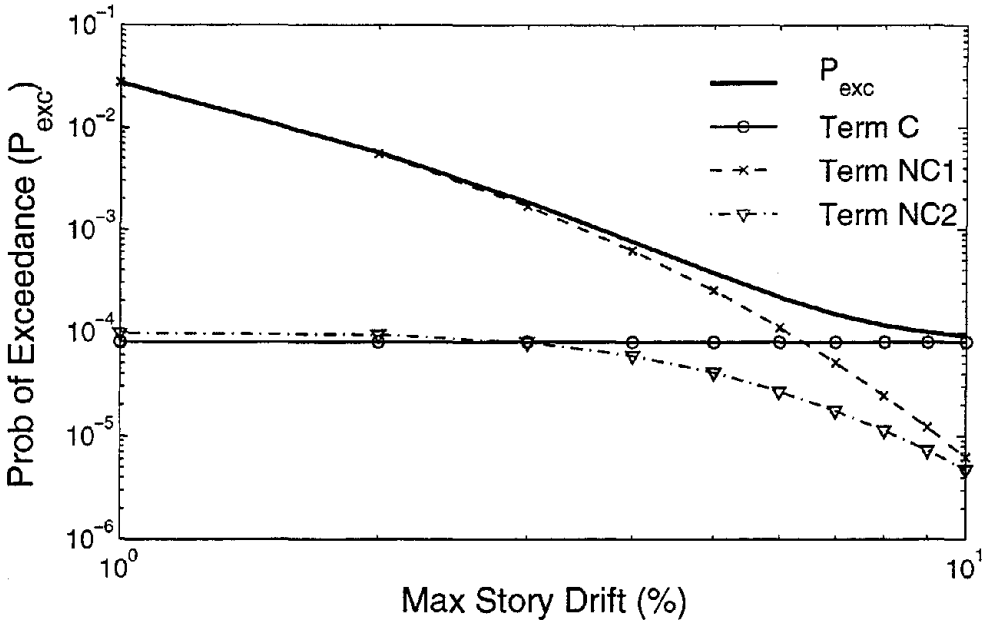

Figure F.1: Seismic drift-demand-hazard curves for a 20-story SMRF at a central Los Angeles site. The contribution of different terms in Equations F.1 and F.3 to the annual probability of exceedance of any drift level is also indicated the figure.

Bibliography

Abramhamson, N. A. and Silva, W. J. (1997), "Empirical Response Spectral Attenuation Relations for Shallow Crustal Earthquakes", *Seismological Research Letters*, Vol. 68, No. 1, 94-127.

ATC-19 (1995), "Structural Response Modification Factors", *Applied Technology Council*, Redwood City, CA.

ATC-32 (1996), "Improved Seismic Design Criteria for California Bridges: Provisional Recommendations", *Applied Technology Council* for California Department of Transportation, CA.

ATC-40 (1996), "Methodology for Seismic Evaluation and Retrofit of Existing Concrete Buildings", *Applied Technology Council*, Redwood City, CA.

Attalla, M. R., Deierlein, G. G., and McGuire, W. (1994), "Spread of Plasticity–A Quasi-Plastic Hinge Approach", *Journal of Structural Engineering*, Vol. 120, No. 8, 2451-2473.

Balopoulou, S. and Grigoriu, M. (1994), "Sensitivity of seismic response to uncertainties in restoring force model: a Monte Carlo simulation case study", *Engineering Structures*, Vol. 16, No. 7, 518-533.

Bazzurro, P. (1998), "Probabilistic Seismic Demand Analysis", *Ph.D. Thesis*, Dept. of Civil Eng., Stanford University, Stanford, CA.

Bazzurro, P., and C.A. Cornell (1999). "Disaggregation of Seismic Hazard", to appear in *Bulletin of Seismological Society of America.*

Bazzurro, P. and Cornell, C. A. (1994a), "Seismic Hazard Analysis of Nonlinear Structures. I: Methodology", *J. of Structural Eng.*, ASCE, Vol. 120, No. 11, 3320-3344.

Bazzurro, P. and Cornell, C. A. (1994b), "Seismic Hazard Analysis of Nonlinear Structures. II: Applications", *J. of Structural Engg.*, ASCE, Vol. 120, No. 11, 3345-3365.

Bazzurro, P., Cornell, C. A., Shome, N., and Carballo, J. E. (1998), "A Comparison of Three Proposals for Characterization of MDOF Non-linear Seismic Response", *J. of Structural Eng.*, ASCE (accepted for publication).

Bazzurro, P. and Cornell, C.A. (1998), "On Disaggregation of Seismic Hazard", *Bulletin of Seismological Society of America*, (to be published).

Bea, R. G. (1996), "Probability Based Earthquake Load and Resistance Factor Design Criteria for Offshore Platform", *Proceedings of Offshore Technology Conference*, OTC 8106, Society of Petroleum Engineers, Houston, Texas.

Benjamin, J. R. and Cornell, C. A. (1970), "Probability, Statistics and Decision for Civil Engineers", *McGraw-Hill, Inc.*, New York.

CAP (1996), "Capacity Analysis Program, CAP Technical Manual", *PMB Engineering Inc.*, San Francisco, CA.

Carballo, J. E., Cornell, C. A., Shome, N., and Bazzurro, P. (1999), "A Comparison of Four Hazard-Consistent Approaches to Nonlinear MDOF Structural Demands", Report (to be published), *Reliability of Marine Structures Program*, Dept of Civil Eng., Stanford University, Stanford, CA.

Carballo, J. E., and Cornell, C. A. (1998), "Input to Nonlinear Structural Analysis: Modification of Available Accelerograms for Different Source and Site Characteristics", *Proceedings of* 6^{th} *U.S. National Conference on Earthquake Engineering*, Seattle, WA, May 31-June 4.

CDMG (1992), "Peak Acceleration from Maximum Credible Earthquakes in California", CDMG Open File Report 92-1, *California Division of Mines and Geology*, Sacramento, CA.

Collins, K.R., Wen, Y.K., and D.A. Foutch (1996), "Dual-Level Design: a Reliability-Based Methodology", *Earthquake Engineering and Structural Dynamics*, Vol. 25, No. 12, pp. 1433-1467.

Cornell, C. A. and Luco, Nicolas (1998), "The Effect of Connection Fractures on Steel

Moment Resisting Frame Seismic Demands and Safety: A Report on SAC Phase II Task 5.4.6", *SAC Steel Project.*

Cornell, C. A. (1996a), "Calculating Building Seismic Performance Reliability: A Basis for Multi-level Design Norms", 11^{th} *World Conference on Earthquake Engineering*, Acapulco, Mexico, Paper No. 2122, Published by Elsevier Science Ltd, Oxford, U.K.

Cornell, C.A. (1996b). "Reliability-Based Earthquake-Resistant Design: the Future." *Proceedings of* 11^{th} *World Conference on Earthquake Engineering*, Paper No. 2166, Acapulco, Mexico, Published by Elsevier Science Ltd, Oxford, U.K.

Cornell, C. A. (1994), "Risk Based Structural Design", *Proc., Symposium on Risk Analysis*, Editor, Nowak, A., Dept. of Civil Engineering, Univ. of Michigan, Ann Arbor, MI.

Cornell, C. A. (1968), "Engineering Seismic Risk Analysis", *Bulletin of Seismological Society of America*, Vol. 58, No. 5, 1583-1606.

Cox, D. R. (1993), "Analysis of Binary Data", *Chapman & Hall*, New York, NY.

Diaz, O., Mendoza, E., and Esteva, L. (1994), "Seismic ductility demands predicted by alternate models of building frames", *Earthquake Spectra*, Vol. 10, No. 3, 466-487.

DRAIN-2DX (1993), "DRAIN-2DX: Basic Program Description and User Guide ", *Report No. UCB/SEMM-93/17*, by Prakash, V., Powell, G. H., and Campbell, S., University of California, Berkeley, CA.

Efron, B. and Tibshirani, R. J. (1993), "An Introduction to the Bootstrap", *Chapman & Hall*, New York, NY.

Eliopoulos, D. F. and Wen, Y. K. (1991), "Method of Seismic Reliability Evaluation for Moment Resisting Steel Frames", *Structural Research Series No. 562*, Dept. of Civil Eng., University of Illinois, Urbana, Illinois.

Ellingwood, B. R. (1994), "Probability-based codified design for earthquakes", *Engineering Structures*, Vol. 16, No. 7, 498-505.

Ellingwood, B. R., Galambos, T. V., MacGregor, J. G., and Cornell, C. A. (1980), "Development of a Probability Based Load Criterion for American National Standard", National Bureau of Standard, *NBS Special Publication 577*, Washington, DC.

Ellingwood, B. R., Galambos, T. V., MacGregor, J. G., and Cornell, C. A. (1980), "Probability Based Load Criteria–Load Factors and Load Combinations", *Journal of Structural Division*, ASCE, Vol. 108, No. ST5, 978-997.

EPRI NP-6041-1-SL (1991), "A Methodology for Assessment of Nuclear Power Plant Seismic Margin", *Electric Power Research Institute.*

FEMA 222 (1995), NEHRP Recommended Provisions for Seismic Regulations for New Buildings, *Building Seismic Safety Council*, Washington, D.C.

FEMA 273 (1996), NEHRP Guidelines for the Seismic Rehabilitation of Building, Building Seismic Safety Council, Washington, D.C.

Freeman, S. A. (1978), "Prediction of Response of Concrete Buildings to Severe Earthquake Motion", *Douglas McHenry International Symposium on Concrete and Concrete Structures*, SP-55, American Concrete Institute, 589-605.

Gupta, A. (1999), "Seismic Demands for Performance Evaluation of Steel Moment Resisting Frame Structures", *Ph. D. Thesis*, Stanford University, Stanford, CA.

Gupta, A. and Krawinkler, H. (1998), "Effect of Stiffness Degradation on Deformation Demands for SDOF and MDOF Structures", *Proceedings of the* 6^{th} *U.S. National Conference on Earthquake Engineering*, Seattle, WA.

Han, S.W., and Y.K. Wen (1997), "Method of Reliability-Based Seismic Design. I: Equivalent Nonlinear Systems. II: Calibration of Code Parameters", *Journal of Structural Engineering*, ASCE, Vol. 123. No. 3, pp. 256-270.

Hall, J. F., Heaton, T. H., Halling, M. W., and Wald, D. J. (1995), "Near-Source Ground Motion and its Effects on Flexible Buildings", *Earthquake Spectra*, Vol. 11, No. 4, 569-605.

Hensher, D. A. and Johnson, L. W. (1981), "Applied Discrete-Choice Modelling", *John Willey & Sons"*, New York, NY.

Hwang, H. and Huo, J. R. (1998), "Probabilistic Seismic Damage Assessment of Highway Bridges", *Proceedings of the* 6^{th} *U.S. National Conference on Earthquake Engineering*, Seattle, WA.

HAZUS (1997), "Earthquake loss estimation methodology", Technical manual, Vol. I-III,

Prepared by *Risk Management Solution, Inc.*, for National Institute of Building Sciences, Washington, D.C.

Inoue, T. and Cornell, C. A. (1991), "Seismic Hazard Analysis of MDOF Structures", *Proceedings, Sixth International Conference on Applications of Statistics and Probability in Civil Engineering (ICASP-6)*, Mexico City, Vol. I, 437-444.

Inoue, T. and Cornell, C. A. (1990). "Seismic Hazard Analysis of Multi-degree-of-freedom Structures", *RMS Rept No. 8*, Department of Civil Engineering, Stanford University, Stanford, CA.

Islam, M. S., Gupta, B., and Kunnath, S. (1998), "A Critical Review of State-of-the-Art Analytical Tools and Acceptance Criterion in Light of Observed response of an Instrumented Non-ductile Concrete Frame Building", *Proceedings of the* 6^{th} *U.S. National Conference on Earthquake Engineering*, Seattle, WA.

ISO 13819 (1997), "Seismic Loading and Response", International Standards Organization.

Jalayer, F. and Cornell, C. A. (1999), "Development of a probability-based demand and capacity factor design (DCFD) seismic format", *Draft Report (to be published).*

Joyner, W. B. and Boore, D. M. (1981), "Peak Horizontal Acceleration and Velocity from Strong-Motion Records including Records from the 1979 Imperial Valley, California, Earthquake", *Bulletin of Seismological Society of America*, Vol. 71, No. 6, 2011- 2038.

Kameda, H. (1994), "Probabilistic seismic hazard and stochastic ground motion", *Engineering Spectra*, Vol. 16, No. 7, 547-557.

Kennedy, R. P., Cornell, C. A., Campbell, R. D., Kaplan, S., and Perla, H. F. (1980), "Probabilistic Seismic Safety Study of an Existing Nuclear Power Plant", *Nuclear Engineering and Design*, Vol. 59, 315-338.

Kennedy, R. P. and Ravindra, M. K. (1984), "Seismic Fragilites for Nuclear Power Plant Risk Studies", *Nuclear Engineering and Design*, Vol. 79, 47-68.

Kennedy, R. P., Short, S. A., Merz, K. L., Tokarz, F. J., Idriss, I. M., Power, M. S., and Sadigh, K. (1984), "Engineering Characterization of Ground Motion - Task I: Effects of Characteristics of Free-Field Motion on Structural Response", NUREG/CR-3805, U.S. Nuclear Regulatory Commission, Washington, D.C.

Krawinkler, H. and Alavi, B. (1998), "Development of improved design procedures for near fault ground motions", *SMIP98 Seminar on Utilization of Strong-Motion Data*, Oakland, CA.

Krawinkler, H. and Seneviratna, G. D. P. K. (1997), "Pros and Cons of a Pushover Analysis of Seismic Performance Evaluation", *Engineering Structures*, Vol. 20, No. 4-6, 452- 464.

Krawinkler, H. (1996), "Pushover Analysis: Why, How, When and When Not to Use It", *Proceedings of the* 65^{th} *Annual Convention, Structural Engineers Association of California*, Maui, Hawaii.

LRFD, Load and Resistance Factor Design (1994), Manual of Steel Construction, *American Concrete Institute*, Chicago, IL.

Liao, S. S. C., Veneziano, D., and Whitman, R. V. (1988), "Regression Models for Evaluating Liquefaction Probability", *J. of Geotechnical Engineering*, Vol. 114, No. 4, 389- 411.

Liao, S. S. C. (1986), "Statistical Modeling of Earthquake-Induced Liquefaction", *Ph. D. Thesis*, Dept. of Civil Engineering, Massachusetts Institute of Technology, Cambridge, MA.

Luco, N. and Cornell, C. A. (1998), "Effects of Random Connection Fractures on the Demands and Reliability for a 3-Story Pre-Northridge SMRF Structures", *Proceedings of the* 6^{th} *U.S. National Conference on Earthquake Engineering*, Seattle, WA.

McGuire, R.K. (1995). "Probabilistic Seismic Hazard Analysis and Design Earthquakes: Closing the Loop", *Bulletin of Seismological Society of America*, Vol. 85, No. 5, pp. 1275-1284.

Miranda, E. and Bertero, V. V. (1994), "Reductions of Seismic Strength Demands due to Inelastic Behavior", *Proceedings,* 5^{th} *U.S. National Conference on Earthquake Engineering*, Chicago, Vol. II, 243-252.

Nassar, A. A. and Krawinkler, H. (1991), "Seismic Demands for SDOF and MDOF Systems", *Rept. No. 95, John A. Blume Earthquake Engr. Center*, Stanford University, Stanford, CA.

Neter, J., Kutner, H. K., Nachtsheim, C. J., and Wasserman, W. (1996), "Applied Linear Statistical Models", *Richard D. Irwin, Inc.*, Chicago, IL.

NUREG 1.165 (1997), "Identification and Characterization of Seismic Sources and Determination of Safe Shutdown Earthquake Ground Motion", U.S. Nuclear Regulatory Commission, Washington, D.C.

Park, Y. J. and Ang, A. H. S. (1985), "Mechanistic Seismic Damage Model for Reinforced Concrete", *Journal of Structural Division*, ASCE, Vol. 111, No. 4, 722-739.

Park, Y. J., Ang, A. H. S. and Wen, Y. K. (1985), "Seismic Damage Analysis for Reinforced Concrete Building", *Journal of Structural Division*, ASCE, Vol. 111, No. 4, 740-757.

Press, W. H., Teukolsky, S. A., Vetterling, W. T., and Flannery, B. P. (1992), "Numerical Recepies: The Art of Scientific Computing", *Cambridge University Press*, New York, USA.

Sasaki, K. K., Freeman, S. A., and Paret, T. (1998), " Multi-mode Pushover Procedure (MMP)- A Method to Identify the Effects of Higher Modes in a Pushover Analysis",6^{th} *U.S. National Conference on Earthquake Engineering*, Seattle, Washington.

SEAOC Blue Book (1996), "Recommended Lateral Force Requirements and Commentary", Seismology Committee, *Structural Engineers Association of California (SEAOC)*, Sacramento, CA.

SEAOC Vision 2000 (1995), "A Framework for Performance Based Design", Volumes I, II, and III, *Structural Engineers Association of California (SEAOC)*, Sacramento, CA.

Searer, G. R. (1994), "Inelastic Behavior and Seismic Design of Steel Moment Frames", *M.S. Thesis*, School of Civil& Environmental Engg., Cornell University, Ithaca, NY.

Seneviratna, G. D. P. K. and Krawinkler, H. (1996), "Modifications of Seismic Demands for MDOF Structures", 11^{th} *World Conference on Earthquake Engineering*, Acapulco, Mexico, Paper No. 2129.

Seneviratna, G.D.P.K., and H. Krawinkler (1994), "Strength and Displacement Demands for Seismic Design of Structural Walls", *Proceedings of* 5^{th} *U.S. National Conference on Earthquake Engineering*, Vol. II, pp. 181-190, Chicago, IL.

Sewell, R. T. and Cornell, C. A. (1987), "Seismic Hazard Analysis Based on Limit-State Structural Damage", *Proceedings, Fifth International Conference on Applications of Statistics and Probability in Civil Engineering (ICASP-5)*, Vancouver B.C., Canada.

Sewell, R. T. (1989), "Damage Effectiveness of Earthquake Ground Motions: Characterizations Based on the Performance of Structures and Equipment", *Ph. D. Thesis*, Dept. of Civil Engg., Stanford University, Stanford, CA.

Sewell, R. T. (1993), "Impacts of Earthquake Strong-Motion Duration on Inelastic Structural Response Factors and on Ground Motion Damage Potential", CSMIP Data Utilization Report, *California Department of Conservation, Division of Mines and Geology*, Sacramento, CA.

Shome, N., Cornell, C. A., Bazzurro, P., and Carballo, J. E. (1998), "Earthquake, Records and Nonlinear MDOF Responses", *Earthquake Spectra*, EERI, Vol. 14, No. 3, pp. 469-500.

Shome, N. and Cornell, C. A. (1998), "Normalization and Scaling Accelerograms for Nonlinear Structural Analysis", *Proceedings of the* 6^{th} *U.S. National Conference on Earthquake Engineering*, Seattle, Washington.

Shome, N., Cornell, C. A., Bazzurro, P., and Carballo, J. E. (1997), "Earthquake, Records and Nonlinear MDOF Responses", Report No. RMS-29, *Reliability of Marine Structures*, Dept. of Civil Engg., Stanford University, Stanford, CA.

Silva, W.J. (1995), "Strong-Motion Catalog", Pacific Engineering and Analysis, El Cerrito, CA.

Somerville, P. G., Smith, N. F., Graves, R. W., and Abrahamson, N. A. (1997), "Modification of Empirical Strong Ground Motion Attenuation Relations to Include the Amplitude and Duration Effects of Rupture Directivity", *Seismological Research Letters*, Vol. 68, No. 1, 199-222.

Song, J. (1998), "Seismic Reliability Evaluation of Steel Frames with Damaged Welded Structures", *Ph. D. Thesis*, The Johns Hopkins University, Department of Civil Eng., Baltimore, Maryland.

Spudich, P. (1997), "What Seismology May Be Able to Bring to Future Building Codes", *Proceedings of the ATC-35 Ground Motion Initiative Workshop*, Rancho Bernardo, CA.

Sues, R. H., Wen, Y. K., and Ang, A. H. S. (1985), "Stochastic evaluation of seismic structural performance", *Journal of Structural Division*, ASCE, Vol. 111, No. 6, 1204-1218.

Trifunac, M. D. and Brady, A. G. (1975), "A Study of the Duration of Strong Earthquake Ground Motion", *Bulletin of the Seismological Society of America*, Vol. 65, 581-626.

UBC (1994), "Uniform Building Code", *International Conference on Building Officials*, Whittier, CA.

U. S. DOE (1994), "Natural Phenomena Hazards design and Evaluation Criteria for DOE Facilities", DOE-STD-1020-94, Washington, D.C.

Vanmarcke, E. H. and Lai, S. S. P. (1980), "Strong-Motion Duration and RMS Amplitude of Earthquake Records", *Bulletin of the Seismological Society of America*, Vol. 70, No. 4, 1293-1307.

Wen, Y.K. (1995), "Building Reliability and Code Calibration", *Earthquake Spectra*, Vol. 11, No. 2, pp. 269-296.